



# Università degli Studi di Ferrara

DOTTORATO DI RICERCA IN  
"SCIENZE FARMACEUTICHE"

CICLO XXVI

COORDINATORE Prof. Stefano Manfredini

***"The developing of molecules to target  
the opioid receptors and to regulate the  
insulin gene."***

Settore Scientifico Disciplinare CHIM/08

**Dottorando**  
*Dott. Allegri Luisa*

**Tutore**  
*Prof. Salvadori Severo*

Anni 2011/2013

*Dear my family  
& my friends*

## ABSTRACT of THESIS

During my PhD I worked with the group of Professor Severo Salvadori, I have investigated opioid system involved in the pain transmission, in particular MOP and NOP receptors. Presently various external opiates are administered like morphine for analgesic therapy, but they have a limit for clinical usefulness, because their tendency is to produce tolerance and dependence. The main project aim is to synthesize peptides bivalent ligands characterized by a NOP and MOP substrate with the goal to reduce the typical side effects of the current therapy.

In order to obtain this peptide bivalent ligand was planned chemical strategies able to give them, in particular it was used Thio-Michael reaction and Thiol-ene reaction. Each reaction allows the introduction of the specific features into MOP pharmacophore and NOP pharmacophore involved in the reaction.

Thio-Michael has allowed to obtain two peptides bivalent ligands: the first is characterized by a MOP pharmacophore as dermorphin functionalized with a Lysin with a maleimide function in lateral chain in C-terminal portion able to interact with a NOP pharmacophore as N/OFQ functionalized with a Cysteine in position 18 in order to afford the bivalent ligand. The second one is represented by a MOP pharmacophore as hexapeptide N-terminal of dinorphin with a Lysin with a maleimide function in lateral chain in position 8 able to react with a NOP pharmacophore as N/OFQ functionalized like previously seen in order to yield the bivalent ligand. The requirement to afford a good bivalent ligand is to maintain *in vivo* an equipotency between the substrate MOP and NOP. Both are been tested *in vitro* through the analysis of the intracellular calcium mobilization, compared to standard endogenous ligands, to observe the activity of the two pharmacophores inside the ligand with receptors transfected in CHO cells. Currently studies are underway *in vitro* tissues. The tests are performed from the group of Dr Girolamo Calò of Ferrara University.

Thiol-ene reaction has not been successful to obtain peptide bivalent ligand, for these reasons it is decided to start an initial methodological study about Thiol-ene reaction. The aim was to understand the influence of the side chains of the aminoacids adjacent to the Cysteine, which aminoacid involved in the reaction.

It was synthesized pentapeptides prototype with the introduction in position 3 and 4 different aminoacids with side chains variable to assess whether some of these are involved in side reactions sequence dependent. As alkene substrate it was

used an olefin, such as the allyl-glucose. The peptides were analyzed by NMR in order to evaluate any changes of the chemical shift in the case of no success of reaction. Variable aminoacids are been investigated with characteristics hydrophilic, acidic and aromatic. All reactions tested have given the product of Thiol-ene and its byproduct sulfoxide.

I spent 11 months of my PhD at Aberdeen University in the group of Professor Matteo Zanda and I worked in collaboration with Dr John Barrow in a study regarding the analysis of change of conformation of particular promoters through gel-based assay (EMSA). In particular the attention was focused on insulin-linked polymorphic region (ILPR) that is a regulatory sequence located upstream of the human insulin gene. It is characterized by multiple repeats of consensus sequence rich in guanine residues able to assume a particular conformation called G-quadruplex. DNA complex is stabilized by some cations and small molecules. This peculiar structure is very important in the complex system of the activation of insulin gene expression.

Since insulin is directly related to the pathogenesis of diabetes, the potential regulatory role of the G-quadruplex in the insulin expression has received close attention.

The main project aim is to alter the functionality of the ILPR, and subsequently alter INS gene expression using small molecules as ligands that will bind to and regulate the ILPR.

The project was developed in different steps:

- Analysis of the appropriate concentration of oligonucleotides to proceed with the EMSA assay;
- Investigation of molecules known in literature and commercially available to have a good ability to stabilize G-quadruplex;
- Synthesis of a new compound triazine derivate to enhance the binding and stabilize the DNA complex.

The small molecules chosen have shown a stabilization of G-quadruplexes in line with the data in literature. These data are also confirmed by CD analysis did from Glasgow University. The new triazine synthetized was only tested with EMSA assay and it has shown a slight ability to interact with the G-quadruplex. CD analysis of the new compound are under study.

## RIASSUNTO della TESI

Durante il mio periodo di dottorato ho collaborato con il gruppo di ricerca del Professor Severo Salvadori e il mio progetto di ricerca si è svolto nell'ambito dei recettori oppioidi coinvolti nel sistema di trasmissione del dolore, in particolare i recettori NOP e MOP. Attualmente in terapia analgesica vengono somministrati oppiacei come la morfina, che presentano dei limiti dal punto di vista clinico in quanto a lungo termine inducono fenomeni di tolleranza e dipendenza. L'obiettivo del progetto di ricerca è di sviluppare molecole peptidiche bivalenti caratterizzate sia da un farmacoforo NOP sia da un farmacoforo MOP per poter ridurre questi effetti collaterali.

Per ottenere questo tipo di molecole peptidiche bivalenti sono state pianificate due strategie sintetiche in grado di permettere di legare i due substrati scelti, le reazioni utilizzate sono la reazione di Thio-Michael e la reazione di Thiol-ene.

La reazione di Thio-Michael ci ha permesso di ottenere due ligandi bivalenti: il primo è caratterizzato da un farmacoforo quale una dermorfina funzionalizzata al C-terminale con una Lisina modificata in catena laterale con una maleimmide in grado di poter reagire con il farmacoforo NOP, N/OFQ (1-17) modificata al C-terminale con l'introduzione di una Cisteina. Nel secondo ligando si è utilizzato come farmacoforo MOP l'esapeptide N-terminale della dinorfina funzionalizzata con una Lisina portante in catena laterale la funzione maleimmidica in grado di reagire con il substrato NOP di elezione descritto prima. Il requisito fondamentale per avere un buon ligando bivalente prevede che ci sia una potenza paragonabile *in vivo* tra i due recettori NOP/MOP. Entrambi sono stati testati *in vitro* con il test di mobilitazione del calcio intracellulare su cellule CHO in cui sono stati transfettati i recettori di interesse, attualmente sono in corso studi *in vitro* su tessuti. I test sono stati fatti presso il Dipartimento di Farmacologia del Dr. Girolamo Calò dell'Università di Ferrara.

La reazione di Thiol-ene ha portato a degli insuccessi nel raggiungere il nostro scopo di creare molecole bivalenti peptidiche. Per questo motivo è stato intrapreso uno studio metodologico più approfondito della reazione in campo peptidico.

Sono stati sintetizzati dei pentapeptidi prototipo modelli con sostituzioni puntiformi in posizioni 3 e 4 adiacenti alla Cisteina, quale aminoacido coinvolto nella reazione. In questo studio sono stati analizzati con la spettroscopia NMR pentapeptidi aventi aminoacidi aromatici, idrofilici ed acidi in modo da poter

identificare tutti i chemical shift dei protoni e dei carboni e in caso di insuccesso della reazione identificare le reazioni collaterali. Come substrato olefinico è stato utilizzato principalmente un allil-zucchero.

Tutti gli aminoacidi studiati hanno dato un esito positivo alla reazione formando sia il prodotto di tiolene sia un sottoprodotto rappresentato dal solfossido.

Successivamente ho trascorso 11 mesi del mio dottorato presso l'Università di Aberdeen nel gruppo di ricerca del Professor Matteo Zanda e sono stata coinvolta in un progetto di collaborazione con il Dr John Barrow. Il progetto ha riguardato lo studio dei cambiamenti di conformazione assunti da particolari promotori attraverso analisi di elettroforesi su gel (EMSA). In particolare il promotore di interesse è stato ILPR quale acronimo di insulin-linked polymorphic region che è una sequenza regolatoria collocata a monte del gene insulina umano. È caratterizzato da regioni ricche di guanina che sono in grado di formare particolari complessi conosciuti come G-quadruplex. Quest'ultimo è coinvolto nel complesso meccanismo di attivazione dell'espressione del gene insulina per cui in caso di sfaldamento di questa struttura si ha conseguentemente una irregolare attivazione del gene e correlato diabete. In letteratura è noto che questo complesso può essere stabilizzato e regolato da cationi e piccole molecole.

L'obiettivo principale del progetto è di poter regolare il promotore ILPR e conseguentemente l'espressione genica dell'insulina utilizzando ligandi in grado di poterlo stabilizzare.

Il progetto è stato sviluppato in diversi step:

- Studio di appropriate concentrazioni di oligonucleotidi per poterli analizzare con EMSA test;
- Studio di molecole commerciali note in letteratura come stabilizzanti di G-quadruplex;
- Sintesi di un composto derivato triazinico in grado di interagire con il complesso G-quadruplex e stabilizzarlo.

Le molecole commerciali investigate e le analisi CD (svolte presso l'Università di Glasgow) hanno confermato i dati presenti in letteratura. Il nuovo derivato triazinico ha mostrato leggera attività sul G-quadruplex, ma i dati CD sono in questo momento in corso di studio.

<b>CONTENTS</b>	
<b>ABBREVIATIONS</b>	<b>1</b>
<i>Chapter 1: Ferrara's project</i>	3
<b>INTRODUCTION</b>	<b>4</b>
1.1 Pain	4
1.2 Opioid receptor	5
<b>2. AIM OF THE PROJECT</b>	<b>14</b>
<b>3. DISCUSSION</b>	<b>19</b>
3.1 Thio-Michael strategy	21
3.2 Thiol-ene strategy	31
<b>4. CONCLUSION</b>	<b>46</b>
<i>Chapter 2: Aberdeen's project</i>	48
<b>1. INTRODUCTION</b>	<b>49</b>
1.1 G-quadruplex DNA	49
1.2 Important G-quadruplexes in the human genome	52
1.3 Small molecules binding to G-quadruplexes structures	55
<b>2. AIM OF THE PROJECT</b>	<b>59</b>
<b>3. DISCUSSION</b>	<b>62</b>
3.1 EMSA system approach and evaluation of different oligonucleotides	62
3.2 Investigation of interaction between G-quadruplexes and small-molecules ligands	63
3.3 Rational synthesis of the new compound	69
3.4 Circular dichroism analysis	72
<b>4. CONCLUSION</b>	<b>76</b>
<i>Chapter 3: Experimental Section</i>	78
<b>PART 1</b>	<b>79</b>
4.1 General Methods	79
4.2 Peptide synthesis	80
4.3 Purification and analytical control	85
4.4 Test of intracellular calcium mobilization	90
4.5 Synthesis and NMR spectra of the compounds	95
<b>PART 2</b>	<b>160</b>
4.1 General Methods	160
4.2 EMSA (electrophoretic mobility shift-assay)	161
4.3 Nucleic Acid Separation Applications	162
4.4 Biochemistry: EMSA	165
4.5 Synthesis of a new compound triazole derivate	173
4.6 Circular Dichroism	186
<b>REFERENCES</b>	<b>188</b>
<b>PUBLICATION &amp; COMMUNICATION</b>	<b>192</b>





## ABBREVIATIONS

Ac acetyl;

AVA 5-aminovaleric acid;

Bn benzyl;

Boc di-*tert*-butyl dicarbonate;

bp base pairs;

Cu-APC anionic copper phthalocyanine;

DCM or CH<sub>2</sub>Cl<sub>2</sub> dichloromethane;

Dde 1-(4,4-dimethyl-2,6-dioxacyclohexylidene)ethyl;

ddH<sub>2</sub>O double distilled water;

DIPCDI N,N'-diisopropylcarbodiimide;

DMEA dimethylethanolamine;

DMF dimethylformamide;

DMSO dimethyl sulfoxide;

DPAP 2,2-dimethoxy-2-phenylacetophenone;

EDTA ethylenediaminetetraacetic acid;

EMSA electromobility shift-assay;

Et ethyl;

Et<sub>3</sub>SiH triethylsilane;

Fmoc fluorenylmethyloxycarbonyl;

G4 G-quadruplex or G-tetraplex or G-tetrad;

h hour;

HEPES (4-(2-hydroxyethyl)-1-piperazineethanesulfonic acid);

HOBt hydroxybenzotriazole;

*i*-Pr isopropyl;

i.c.v. intracerebroventricular injection;

i.t. intrathecal injection;

ILPR insulin-linked polymorphic region;

INS insulin gene;

KMnO<sub>4</sub> potassium permanganate;

min. minutes;

N/OFQ nociceptin or orphanin FQ;

o.n. over night;

Oxyrna Pure ethyl 2-Cyano-2-(hydroxyimino)acetate;

Pmc 2,2,5,7,8-pentamethyl-chroman-6-sulphonyl;

Pt petroleum;

r.t. room temperature;

SPPS Solid Phase Peptide Synthesis;

TBE tris/Borate/EDTA;

<sup>t</sup>Bu *tert*- butyl;

TFA trifluoroacetic acid;

THF tetrahydrofuran;

TMS ethynyltrimethylsilane;

t<sub>r</sub> retention time;

Trt triphenylmethyl;

WSC 1-Ethyl-3-(3-dimethylaminopropyl)carbodiimide;

Y yield;

*Chapter 1*  
*Ferrara's project*

## INTRODUCTION

### 1.1 Pain

The prevalence and cost of pain is a major physical and mental health care problem from the past two decades. The pain is a symptom of suffering not classifiable and it has a degree of subjective effect due to variable human sensitivity. The pain can be assessed as *acute pain* or *chronic pain*.

*Acute pain* begins suddenly and is usually the individual feels a strong warning of disease or a threat to the body. It can be due to many events, like eg surgery, labor and childbirth, broken bones. Ordinarily acute pain may be mild or it may be more severe, but it does not last longer than six months and it disappears when the underlying cause of pain has been treated or has healed. Unrelieved acute pain, however, may lead to chronic pain.

*Chronic pain* persists longer than 3 months, often despite the fact that an injury has healed. Pain signals remain active in the nervous system for weeks, months, or years. It is characterized from physical effects like muscles problems, limited mobility, lack of energy and changes in appetite and/or emotional effects include depression, anger, anxiety, and fear of re-injury. Common chronic pain complaints include: headache, low back pain, cancer pain, arthritis pain, neurogenic pain, psychogenic pain. Chronic pain may have started from an initial trauma/injury or infection, however, some people suffer of this in the absence of any past injury or evidence of body damage<sup>1</sup>.

The pain appears to be a cause of social disability and for this reason there is a common scientific interest to assess the appropriate treatment for its resolution.

Endogenous opioids exhibit their activity through an interaction with specific receptors that play a crucial role in several physiological functions such as analgesia, respiratory depression, feeding, release of certain hormones (eg corticosterone and growth hormone) and mood elevation.

The introduction of drugs able to interact with the opioid receptor system may allow a physiological and multifunctional control. Various external opiates are administered like morphine for analgesic therapy, they interact with the complex system of endogenous opioids and unfortunately they also produce its side effects. The limit of the clinical usefulness of these drugs is their tendency to produce tolerance and dependence. The tolerance induces a need, during a chronic drug

---

<sup>1</sup> Pain Management Health Center, WebMD. <http://www.webmd.com/pain-management/>.

exposure, to increase the amounts of it to obtain the original effect. The related phenomenon of dependence arises like a physical or psychological withdrawal syndrome upon its removal and it is an important ability of these kinds of drugs.

The phenomena of opiate tolerance and dependence are intensively studied and the proposal, in this project, is to design a drug able to contain the specific characteristics inside one molecule and to decrease these fundamental problems<sup>2</sup>.

## 1.2 Opioid receptor

Opiates operate through specific receptors located in the CNS, first identified in 1973. They are used therapeutically to raise the threshold of perception of pain.

Pharmacological and biochemical evidence suggest the existence of four major classes of opioid receptors:  $\mu$ ,  $\delta$ ,  $\kappa$  and ORL-1, respectively called MOP, DOP, KOP and NOP. The opioid receptors are metabotropic receptors structurally correlated to rhodopsin, characterized by 7 domains transmembrane (TM) whose intracellular loops are coupled to proteins belonging to G-protein family.

Guanine nucleotide binding proteins (G proteins) are heterotrimers, made up of three distinct subunits ( $\alpha$ ,  $\beta$ ,  $\gamma$ ), which bind a large number of receptors to a variety of effects<sup>3</sup>.

There are many combinations of  $\alpha\beta\gamma$  with unique functional characteristics. The activity G-protein oligomer is attributed to the  $\alpha$  subunit, an enzyme having intrinsic GTPase capacity. Agonist binding to a receptor protein induces a series of events: dissociation of the  $\alpha$ -subunit, which is complexed to  $\beta\gamma$ , binding of GTP to the  $\alpha$ -subunit and its activation and separation of the G-protein from the subunits  $\beta\gamma$ . The link between GTP and  $G\alpha_i$  produces an inhibition of adenylyl cyclase to decrease a cAMP levels (Second Messenger), which produces a reduction in the cell voltage of the current dependent, which achieves negative values, increasing the excitability threshold neurons. Adenylyl cyclases are a family of enzymes, which modulates ATP to cyclic adenosine monophosphate (cAMP), an intracellular signalling molecule. Cyclic AMP activates several cAMP-dependent protein kinases, which control numerous events through phosphorylation. The reduction of cAMP also arouses a hypofunction of PKA (protein kinases cyclic AMP dependent) with a decrease in the release of excitatory neurotransmitters from nociceptive fibers (eg glutamate, substance P).

---

<sup>2</sup> L. M. Harrison, A. J. Kastin, J. E. Zadina, *Peptides*, (1998), 19, 1603–1630.

<sup>3</sup> K. M. Standifer, G. W. Pasternak, *Cell. Signal.*, (1997), 9, 237–248).

The cell hyperpolarization is also due to the action of  $G\beta\gamma$  subunits.

It seems that these are at the basis of the mechanism that leads to modulation of channel proteins of  $Ca^{2+}$  and  $K^+$ . The binding of the receptor with the agonist means the opening of potassium channels by inducing a hyperpolarization of membranes and inhibition of calcium conductance with the consequent reduction of neurotransmitter release at the synaptic level. This receptor status is usually reversible. When the biological action was explicated,  $G\alpha$ -GTP is hydrolyzed to GDP and  $G\alpha$ -subunit restores the initial trimer.

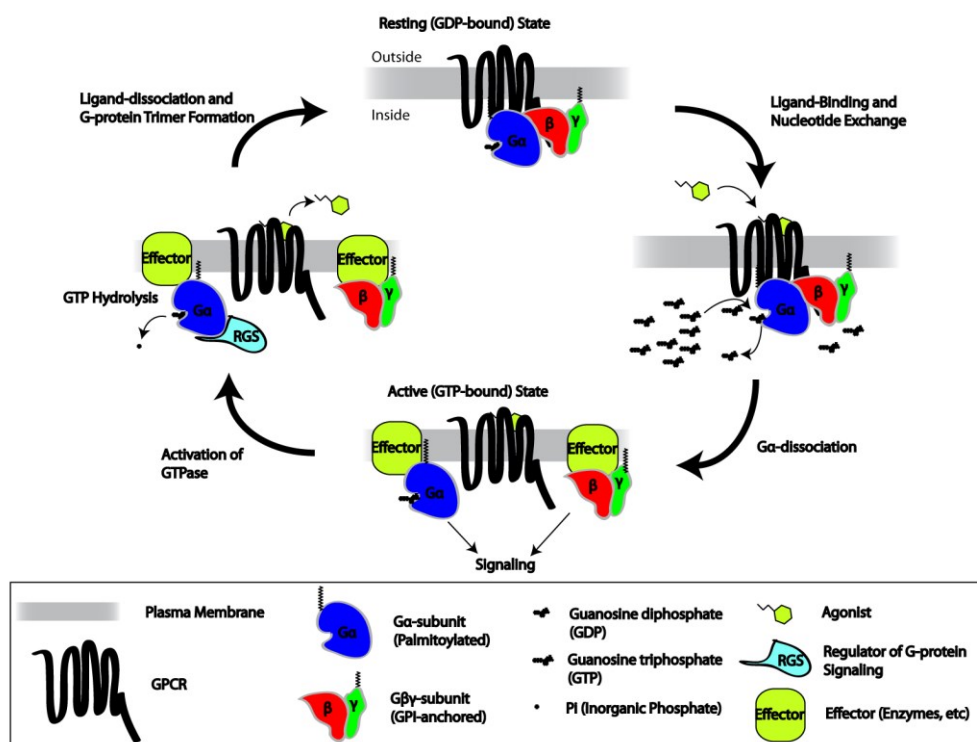


**Figure 1: Receptors coupled to G-proteins GPCR).**

When the receptor binds its ligand, stimulates the exchange of GDP for GTP by the  $\alpha$  subunit of the trimeric G protein, which moves away from the  $\beta\gamma$  complex and interacts with an effector, initiating the cascade of intracellular signals. Subsequently, the  $\alpha$  subunit hydrolyzes the GTP into GDP, returning to a non-active conformation, which is associated again to the  $\beta\gamma$  complex.

Studying the expression of mRNAs coding for the opioid receptors has been possible to identify the location of the various receptors. They are expressed at the level of the central nervous system (CNS) regions of the midbrain, diencephalon and telencephalon and spinal cord.

MOP and KOP receptor-like immunoreactivity is widely distributed across gastrointestinal regions: the stomach, duodenum, ileum, proximal and distal colon, these opioids may regulate gastrointestinal function<sup>4</sup>. The DOP receptor is

<sup>4</sup> D. Bagnol, A. Mansour, H. Akil, S. J. Watson, *Neuroscience*, (1997), 81, 579–591.

concentrated in neurons, myenteric and submucosal ganglia. NOP receptors are located in intestine, vas deferens, liver and spleen<sup>5</sup>. The endogenous ligands for these receptors are peptides of different lengths characterized by a N-terminal portion organized in a similar way.

In figure 2 there are the primary sequence of  $\beta$ -endorphin, a MOP endogenous ligand, the enkephalins, the DOP endogenous ligands, dynorphin, a KOP endogenous ligand and nociceptin/orphanin FQ (N/OFQ) a NOP receptor endogenous ligand.

**$\beta$ -Endorphin:** H-*Tyr-Gly-Gly-Phe*-Met-Thr-Ser-Glu-Lys-Ser-Gln-Thr-Pro-Leu-Val-Thr-Leu-Phe-Lys-Asn-Ala-Ile-Ile-Lys-Asn-Ala-Tyr-Lys-Lys-Gly-Glu-OH

**Met-Enkephalin:** H-*Tyr-Gly-Gly-Phe*-Met-OH

**Leu-Enkephalin:** H-*Tyr-Gly-Gly-Phe*-Leu-OH

**Dynorphin A:** H-*Tyr-Gly-Gly-Phe*-Leu-Arg-Arg-Ile-Arg-Pro-Lys-Leu-Lys-Trp-Asp-Asn-Gln-OH

**Nociceptin or orphanin FQ (N/OFQ):** H-*Phe-Gly-Gly-Phe*-Thr-Gly-Ala-Arg-Lys-Ser-Ala-Arg-Lys-Leu-Ala-Asn-Gln-OH

**Figure 2:** Primary aminoacid sequence of physiological ligands of opioid receptors MOP, DOP, KOP and NOP.

The N-terminal portion Tyr (or Phe)-Gly-Gly-Phe, highlighted in red, is the part defined message domain and it is responsible for the activation of the receptor while the C-terminal portion is involved in receptor selectivity and it is defined address domain. In 1997 two new peptides very selective against the MOP receptor were discovered: **Endomorphin I** (H-Tyr-Pro-Trp-Phe-NH<sub>2</sub>) and **Endomorphin II** (H-Tyr-Pro-Phe-Phe-NH<sub>2</sub>), whose precursor has not yet been identified<sup>6</sup>. From the point of view of the evolution gene, the nociceptin belongs to the same family of other opioid ligands, and also the NOP receptor has high sequence homology with the opioid receptors<sup>7</sup>, however from the functional point of view the NOP receptor does not bind opioid ligands with high affinity and in the same way the nociceptin does not interact with opioid receptors with high affinity. Drugs able to activate the MOP receptor are used from years for the pain therapy. MOP agonists have two important actions related to motivational systems:

<sup>5</sup> J. B. Wang, P. S. Johnson, Y. Imai, A. M. Persico, B. A. Ozenberger, C. M. Eppler, G. R. Uhl, *FEBS Letters*, (1994), 348, 75-79.

<sup>6</sup> J. E. Zadina, L. Hackler, L.-J. Ge, A. J. Kastin, *Nature*, (1997), 386, 499-502.

<sup>7</sup> C. W. Stevens, *Front Biosci*, (2009), 14, 1247-1269.

(1) suppress the pain and (2) promote the pursuit of pleasure.

Their most important clinical application is for pain relief. Indeed, the MOP agonists are the most powerful analgesics currently available. Their therapeutic efficacy undoubtedly derives from the fact that they have numerous inhibitory actions against the pain. They directly inhibit pain transmitted by neurons in the periphery and CNS.

They also act on the descending pain modulatory circuits that control pain transmission at the spinal cord level. In addition, MOP agonists induce significant positive motivational effects. A circuit that includes the dopaminergic neurons in the ventral tegmental area of the midbrain mediates these effects and their connections with the limbic regions, involving the sub-cortical areas taking the nucleus accumbens and the amygdala. For this reason the identification of new analgesic drugs without the side effects of opioids is the interest of today. It has recently been approved for intrathecal infusion a new analgesic drug called Ziconotide<sup>8</sup>. This molecule is a cyclic peptide derived from a shell of the genus *Conus Magus*<sup>9</sup>. Ziconotide is a peptide that blocks the entry of calcium in the neuronal voltage-gated calcium channels through N-type, preventing the conduction of nerve signals and decreasing the pain perception. However, Ziconotide is a small therapeutic window, because it has the considerable side effects in the CNS and for this the treatment is used for a small group of people with severe chronic pain. Also the peptidergic system NOP receptor/N/OFQ is implicated in the modulation of the painful stimulus and recent evidence suggests that this receptor system may be used to induce analgesia without causing dependence<sup>10</sup>. Furthermore, in vivo studies on non-human primate have shown that spinal administration of an analogue of N/OFQ 100-fold more potent called UFP-112 is able to evoke analgesic effects like those obtained with morphine<sup>11</sup> (Figure 3).

---

<sup>8</sup> J. E. Pope, T. R. Deer, *Expert Opinion on Pharmacotherapy*, (2013), 14, 957-966.

<sup>9</sup> D. R. Hillyard, V. D. Monje, I. M. Mintz, B. P. Bean, L. Nadasdi, J. Ramachandran, G. Miljanich, A. Azimi-Zoonooz, J. M. McIntosh, L. J. Cruz, J. S. Imperial, B. M. Olivera, *Neuron*, (1992), 9, 69-77).

<sup>10</sup> A. P. Lin, M.-C. Ko, *ACS Chem. Neurosci.*, (2013), 4, 214-224.

<sup>11</sup> E. Hu, G. Calò, R. Guerrini, M.-C. Ko, *Pain*, (2010), 148,107-113.



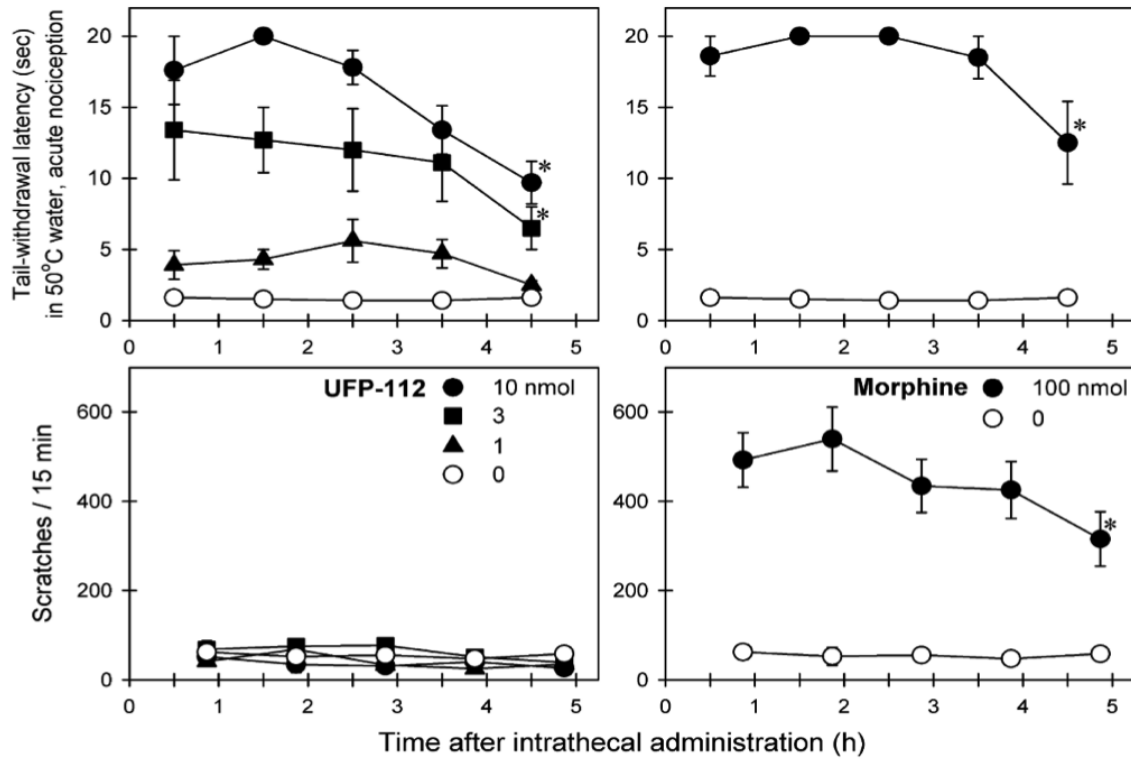


**Figure 3:** Comparison of analgesic effects produced by administration i.t. UFP-112 and morphine.

NOP agonist does not produce itching, typical side effect of MOP ligands regularly administered systemically. It has been shown that the co-administration of doses of intrathecal morphine (usually alone is an ineffective dose) and UFP-112 is capable of generating a robust analgesic effect (Figure 4).

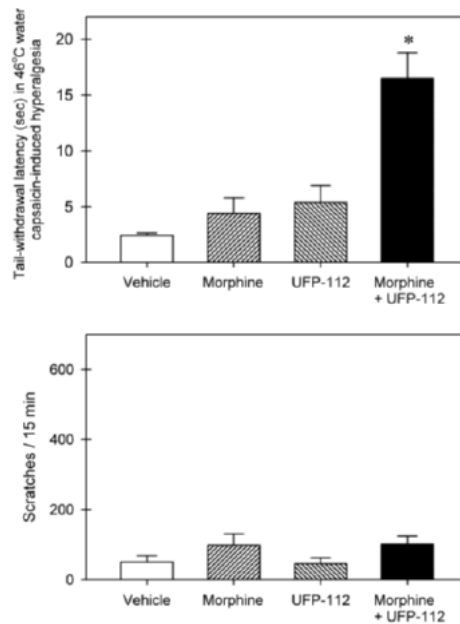


**Figure 4:** Analgesic effect due to co-administration i.t of UFP-112 and morphine.

These data suggest that a bivalent ligand is able to activate both NOP/ MOP receptors and it could be useful as analgesic cord. In the literature there are numerous examples of bivalent ligands capable of interacting with opioid receptors<sup>12</sup>. Furthermore, there are also extensive evidence on the existence of homo-and heterodimeric forms of GPCRs<sup>13</sup>. The dimerization appears to be important for the maturation of receptor<sup>14</sup>. Furthermore it was shown that dimerization could lead to the formation of new species potentially pharmacological target of innovative drugs. Recent observations highlight that the dimerization of receptors between different opioids or opioid and non-opioid is involved in the *in vivo* effects mediated from opioid and it plays an important role in evoking biological phenomena complexes such as the development of tolerance to morphine<sup>15</sup>. From scientific literature there are several examples of molecules able to interact with dimeric opioid receptors. One of the latest examples reported by Portoghese *et al.* proves that the compound MDAN-21 (MOP agonist/DOP antagonist) has a potent central analgesic activity without inducing tolerance<sup>12</sup>. This event could be due to lack of receptor internalization generated by co-stimulation of MOP and DOP heterodimeric receptors (Figure 5).

---

<sup>12</sup> A. S. Yekkiral, A. E. Kalyuzhny, P. S. Portoghese, *ACS Chem. Biol.*, (2010), 8, 1412–1416.

<sup>13</sup> V. Casadó, A. Cortés, J. Mallol, K. Pérez-Capote, S. Ferré, C. Lluís, R. Franco, E. I. Canela, *Pharmacology & Therapeutics*, (2009), 124, 248–257.

<sup>14</sup> S. Bulenger, S. Marullo, M. BouvierTrends, *Pharmacol. Sci.*, (2005), 26,131–137.

<sup>15</sup> R. Rozenfeld , N. S. Abul-Husn, I. Gomez, L. A. Devi, *Sci World J.*, (2007), 7, 64–73.

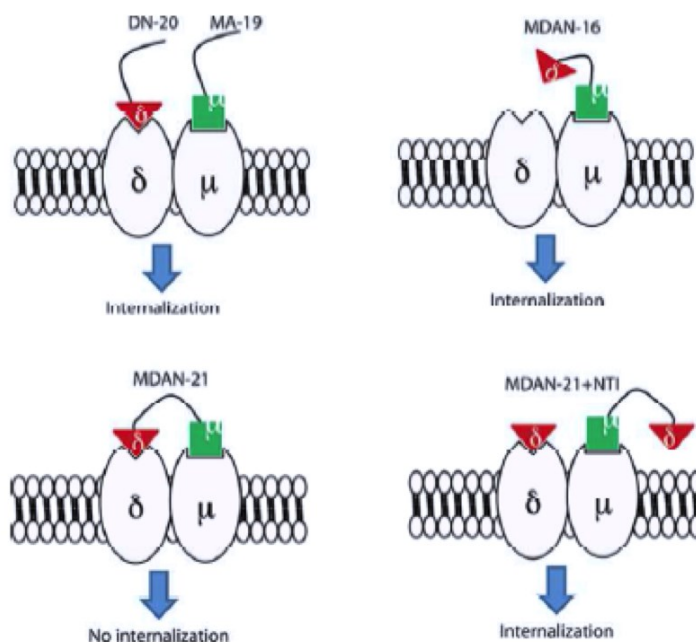


**Figure 5:** Scheme of the molecular mechanism proposed for the inhibition of internalization by a bivalent ligand opioid.

Thank to these knowledge homo- and heterodimers of opioid receptors could represent a novel therapeutic target for the pain therapy. In literature, there are some data that support the possible existence of MOP/NOP heteromeric receptor. For example, the i.c.v. administration of a selective NOP antagonist increases the analgesia induced by a MOP agonist and it produces an antinociceptive effect resistant to naloxone<sup>16</sup>. The contribution of these functional interactions in dimeric receptors was tested with recombinant receptors expressed in HEK293 cells<sup>17</sup>. Co-immunoprecipitation studies have shown that MOP and NOP receptors could be isolated in complexes that interact<sup>18 19</sup>. In cells that co-expressing MOP and NOP receptors, the treatment with the NOP agonist, nociceptin, stimulates the internalization of MOP. In a similar way the treatment with MOP agonist, DAMGO, due to the internalization of the NOP<sup>18</sup>. In vitro assays on cells who co-expressing MOP and NOP receptors show that the presence of the MOP receptor attenuates the inhibition of N channels of calcium induced by N/OFQ, while the activation of MOP receptor promotes the internalization of calcium channels only in the presence of the NOP receptor<sup>21</sup>.

In the figure below it is shown the schematic structure of a bivalent molecule.

<sup>16</sup> G. Calo', R. Guerrini, A. Rizzi, S. Salvadori, D.Regoli, *British Journal of Pharmacology* , (2000), 129, 1261- 1283.

<sup>17</sup> H.-L. Wang, C.-Y. Hsu, P.-C. Huang, Y.-L. Kuo, A. H. Li, T.-H. Yeh, A.-S. Tso, Y.-L. Chen, *Journal of Neurochemistry*, (2005), 92, 1285-1294.

<sup>18</sup> R. M. Evans, H. You, S. Hameed, C. Altier, A. Mezghrani, E. Bourinet, G. W. Zamponi, *J. Biol. Chem.*, (2010), 285, 1032-1040.

<sup>19</sup> Y. X. Pan, E. Bolan, G. W. Pasternak, *Biochem. Biophys. Res. Commun.*, (2002), 297, 659–663.

Ferrara's project

Introduction

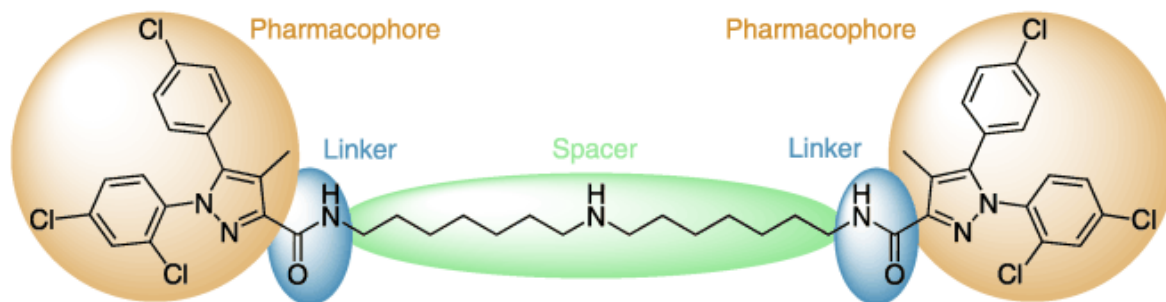
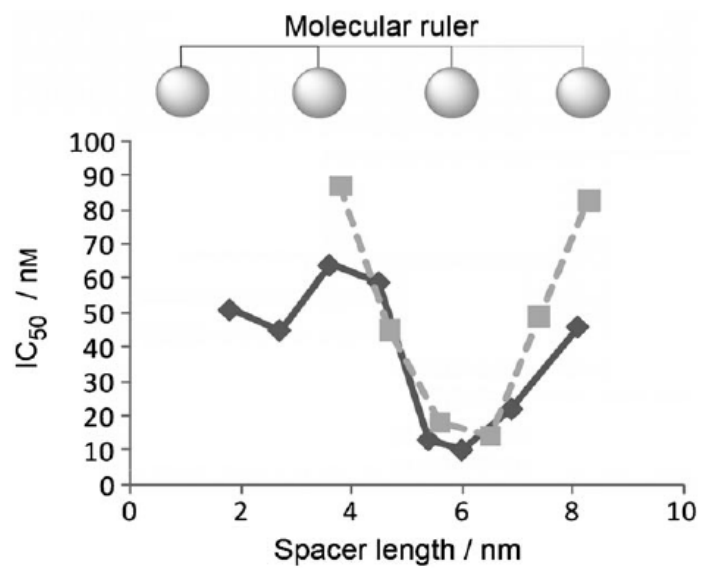


Figure 6: Scheme of a bivalent ligand.

For the design of this structure is essential to consider several parameters: the choice of the pharmacophore, the point of attachment of the linker and length of the spacer. The pharmacophore contains the structural information required for the binding and activation (or block) of the receptor and it must have an attachment point for the linker that do not compromise the desired biological activity. The spacer may have different length, several chemical compositions and it may be rigid or flexible. The possibility to modulate the length of the spacer makes possible the synthesis of bivalent molecules that they may have suitable characteristics to interact with dimeric receptor forms. At this regard, in literature there are many indications relative to the length of the spacer like a critical factor for the potency of the ligand<sup>20</sup> (Figure 7).

<sup>20</sup> J. Shonberg, P. J. Scammells, B. Capuano, *Chem. Med. Chem.*, (2011), 6, 963-974.



**Figure 7:** Graph that highlights the relationship between potency and length of the spacer that connect the two pharmacophores.

## 2. AIM OF THE PROJECT

In this project it has tried to develop bivalent ligands to use them as a spinal analgesic drugs. The project was created with the idea to introduce in a single molecule both a MOP pharmacophore and a NOP pharmacophore.

These ligands have as a NOP substrate N/OFQ and variable MOP substrate.



**Figure 8:** Scheme of a bivalent ligand design.

In order to exploit the synergism of enhancement analgesic highlighted with the co-administration in spinal cord in the non-human primate<sup>11</sup> of NOP agonist and a MOP agonist, one of the pharmacological characteristics desired for these bivalent ligands is NOP/MOP equipotency.

It was evaluated several possible MOP ligands, known in literature, to bind to the NOP ligand defined. It is planned to use the following substrates MOP: dermorphin changed in C-terminal with a Lysine (H-Tyr-D-Ala-Phe-Gly-Tyr-Pro-Ser-Lys-NH<sub>2</sub>), endomorphin I (H-Tyr-Pro-Trp-Phe-NH<sub>2</sub>), the endogenous opioid tetrapeptide (H-Tyr-Gly-Gly-Phe), the endogenous opioid tetrapeptide modified in C-terminal with a Lysine (H-Tyr-Gly-Gly-Phe-Lys) and finally the N-terminal hexapeptide of dynorphin (H-Tyr-Gly-Gly-Phe-Leu-Arg) (Figure 9).

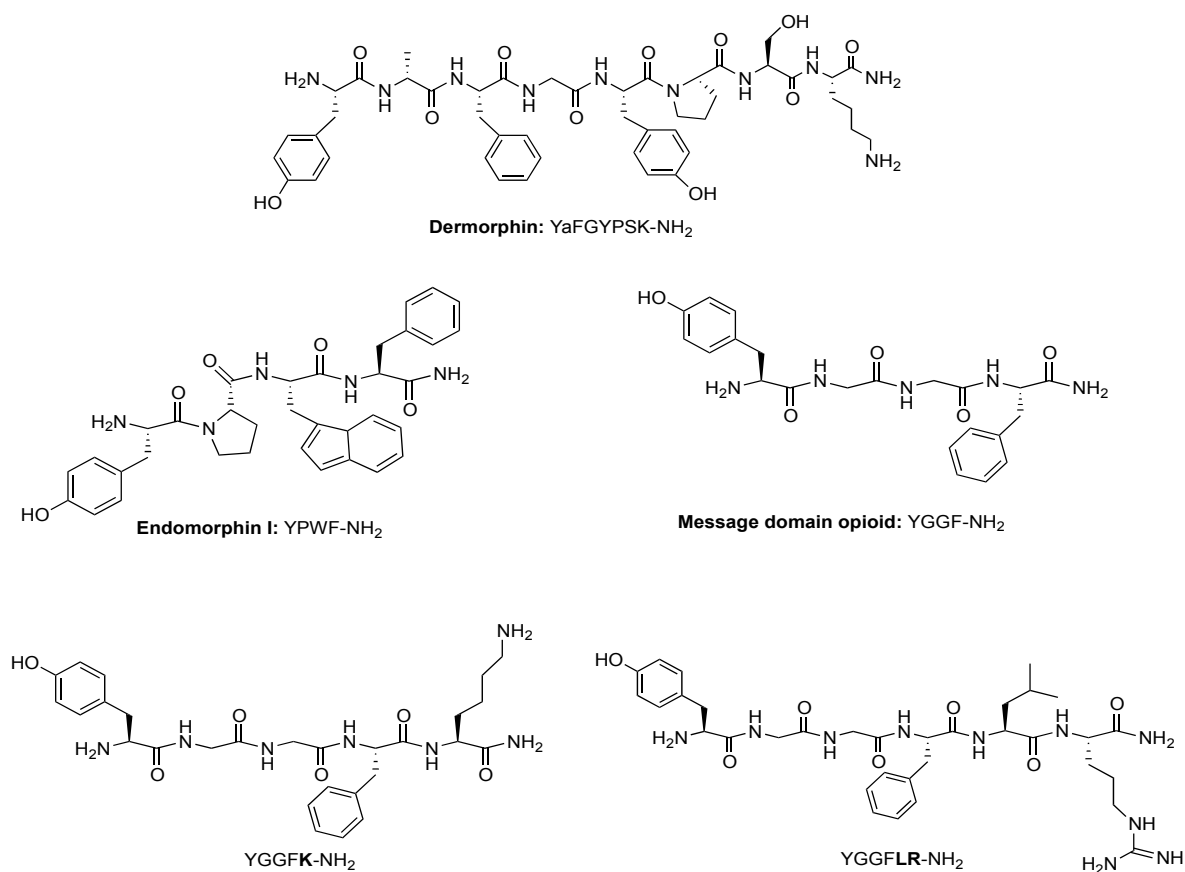


**Figure 9:** Opioid pharmacophores considered in this study.

These peptides prototype are functionalized to the carboxylic portion with spacer of different length and chemical composition having an acetylated Lysine side chain as the last amino acid of the sequence.

In particular, it is chosen a spacer consisting of glycine (Gly and Gly-Gly), amino valeric acid (AVA) and one spacer polyoxyethylene (O<sub>2</sub>Oc) (Figure 10).

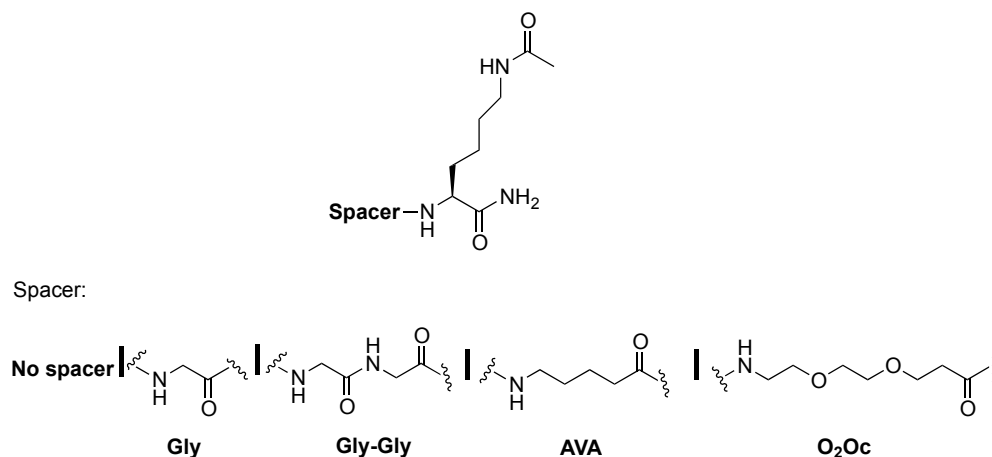


**Figure 10:** List of spacers and functionalization of pharmacophores in the C-terminal portion.

The acetyl group on the side chain of Lysine has the only aim to mimic the maleimide function that will be used to generate the bivalent ligands.

The chemistry strategy used to generate the bivalent ligands provides for the synthesis of the two NOP and MOP pharmacophores suitably functionalized, their purification and finally their conjugation through the use of a highly chemoselective reaction, such as Thio-Michael reaction<sup>21</sup>. My research group has already used this reaction for the synthesis of similar molecules and it is characterized by: high chemoselectivity, speed of reaction, almost quantitative yields and mild reaction conditions. The chemical strategy requires the functionalization of the C-terminal N/OFQ with a Cysteine residue [Cys<sup>18</sup>] N/OFQ-NH<sub>2</sub>, synthesis that was made of medium scale (hundreds of mg).

After pharmacological evaluation of the designed MOP pharmacophore, the compound that has showed the most suitable characteristics it was resynthesized and functionalized side chain of the Lysine with a maleimide group that allows the easy conjugation with [Cys<sup>18</sup>] N/OFQ-NH<sub>2</sub> according to the general pattern:

<sup>21</sup> D. P. Nair, M. Podgórski, S. Chatani, T. Gong, W. Xi, C. R. Fenoli, C. N. Bowman, *Chem. Mater.*, (2014), 26, 724–744.



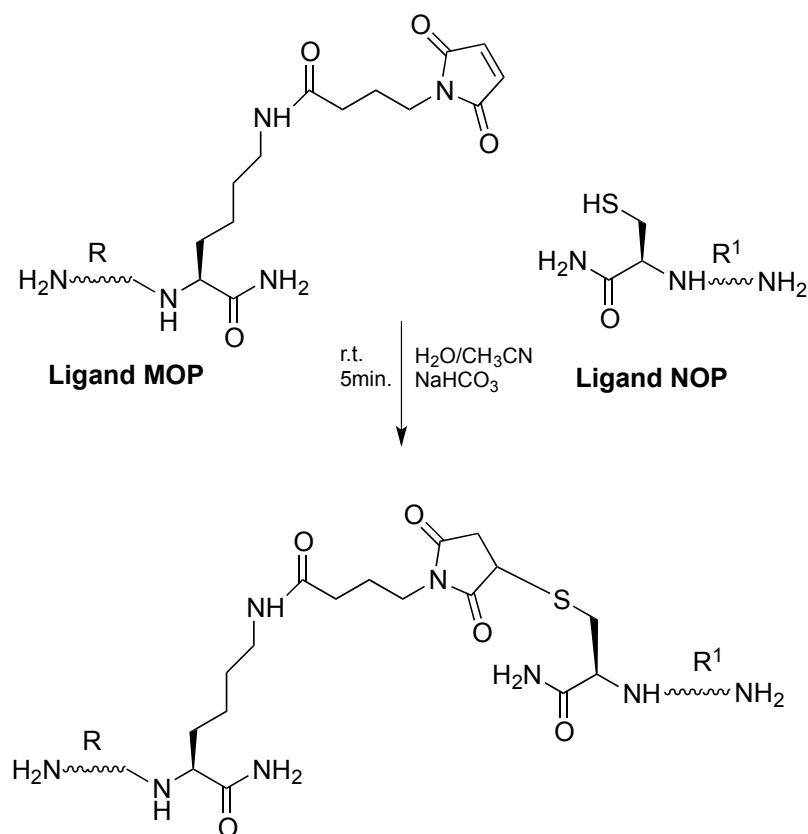


**Figure 11:** General scheme adopted for the synthesis of a bivalent ligand NOP/MOP.

To obtain bivalent ligands it was also planned to use a second synthetic strategy, such as the Thiol-ene reaction. There are many evidence in literature that confirm the availability of this reaction to connect two peptides<sup>22 23</sup>. It allows high efficiency and orthogonality of the reaction with bulky substrates. In this study Thiol-ene reaction provides to link two pharmacophores one MOP and one NOP suitably functionalized in C-terminal position.

<sup>22</sup> A. A. Aimetti, K. R. Feavera, K. S. Anseth, *Chem. Commun.*, (2010), 46, 5781–5783.

<sup>23</sup> A. Dondoni, A. Massi, P. Nanni, A. Roda, *Chem. Eur. J.*, (2009), 15, 11444 – 11449.

The chemical approach permits the introduction of thiols with a Cys in the C-terminal of NOP pharmacophore (N/OFQ) and a wide variety of unsaturated moiety in the C-terminal MOP pharmacophore. Below it is shown a scheme of Thiol-ene strategy (Figure 12).

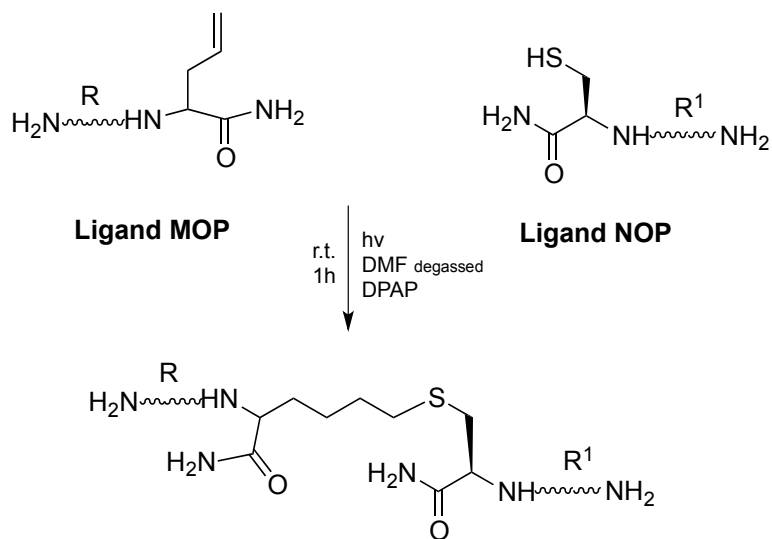


**Figure 12:** General scheme used for Thiol-ene strategy.

### 3. DISCUSSION

In this thesis the synthetic strategy to obtain NOP/MOP agonists bivalent ligands with natural peptides was investigated. These molecules were done applying a convergent synthetic approach. Firstly the NOP/MOP prototype peptides were synthesised, purified separately and then linked together using chemoselective reactions. Infact the presence in the peptides sequence of many functional groups as aminoacid side chains imposes the use of highly chemoselective reactions. The chemoselective reactions selected were Thio-Michael and Thiol-ene strategies.

The synthetic scheme adopted for the synthesis of bivalent ligand is reported in figure 13.

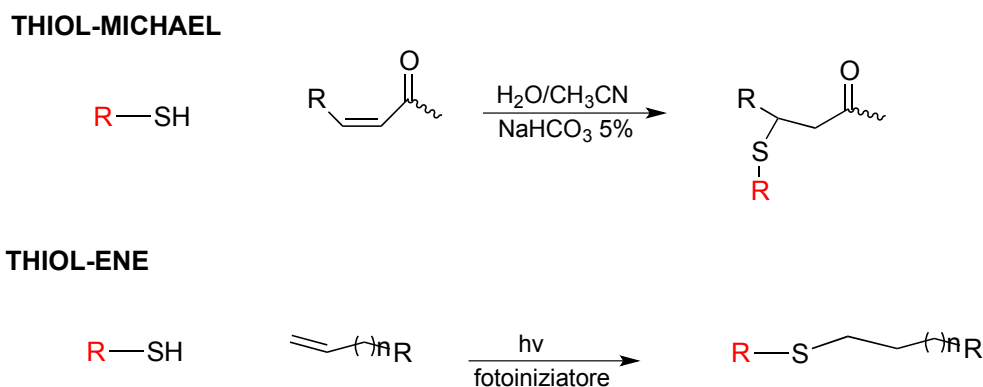


**Figure 13:** Chemical strategies to build bivalent ligand.

The strategies chosen have a peculiar characteristics, both belong from the “Click-chemistry” reaction family. In 2001, Sharpless *et al.* have described a new concept for conducting organic reactions with the introduction of reaction with highly selectivity, simple orthogonals that give not side products and that they form heteroatom-linked molecular systems with high efficiency under an assortment of mild conditions<sup>24</sup>. Many reactions belong to this class and they have in common the following characteristics:

- i. high yields and by-products (if any) are removed by nonchromatographic processes;
- ii. regioselectivity and stereoselectivity;
- iii. more or less insensible to oxygen or water;
- iv. mild reaction conditions (solventless or aqueous);
- v. orthogonality with other common organic synthesis reactions;
- vi. wide range of available starting compounds.

<sup>24</sup> C. E. Hoyle, C. N. Bowman, *Angew. Chem. Int. Ed.*, (2010), 49, 1540-1573.

All compounds were evaluated in tests carried out on intracellular calcium mobilization CHO<sub>hMOP</sub> + G<sub>αqi5</sub> cells and their activity was compared to standard MOP ligands as dermorphin, Leu-enkephalin and endomorphin 1.

The bivalent compounds (Figure 18 and 22) were also tested on cells CHO<sub>hNOP</sub> + G<sub>αqi5</sub> and their activity were compared to that of the endogenous ligand for the NOP N/OFQ. In these cells, thanks to the use of the chimeric G protein (see materials and methods), the activation of the receptor leads to increased levels of intracellular calcium.

**Standard ligands** - In CHO<sub>hMOP</sub> + cells G<sub>αqi5</sub> MOP receptor standard ligands dermorphin, Leu-enkephalin and endomorphin 1 have stimulated the release of intracellular calcium in a concentration-dependent effects producing maximum of  $177 \pm 24$ ,  $144 \pm 14$  and  $209 \pm 3$ .

For the ligand was calculated dermorphin a pEC<sub>50</sub> of 8.30 while for Leu-enkephalin and endomorphin 1 were estimated pEC<sub>50</sub> values of 7.26 and 8.00 (Table 1 and figure 14, left panel).

In cells CHO<sub>hNOP</sub> + G<sub>αqi5</sub> the natural peptide N/OFQ was able to increase the levels of intracellular calcium in a concentration-dependent, showing a maximal effect of  $224 \pm 1$  and a pEC<sub>50</sub> of 9.95 (Figure 14, right panel).

The results obtained with the standard ligands are similar with previously reported data in the literature.

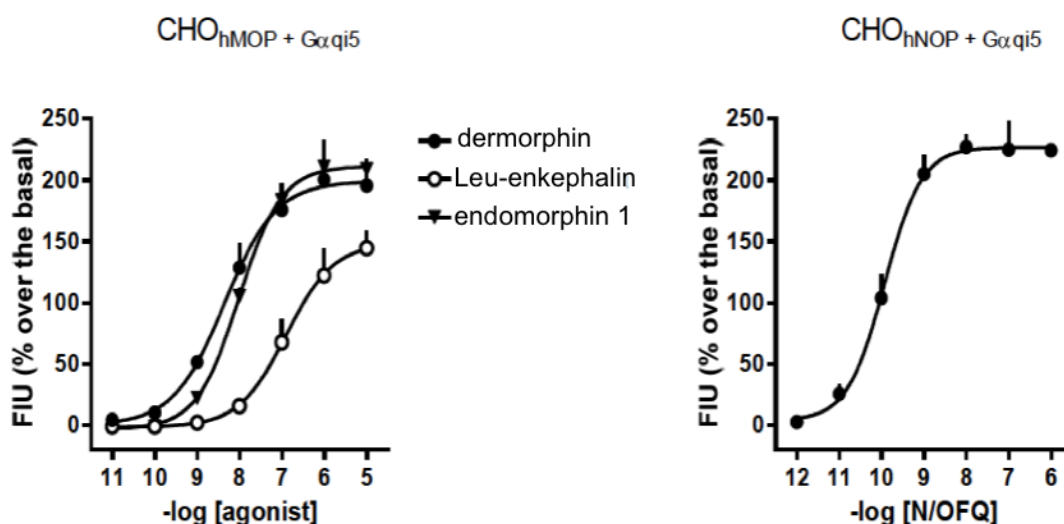


**Figure 14:** Test of intracellular calcium mobilization of cells CHO<sub>hMOP</sub> + G<sub>αqi5</sub> (left panel) and CHO<sub>hNOP</sub> + G<sub>αqi5</sub> (right panel). Effect of standard agonists dermorphin, Leu-enkephalin and endomorphin 1. Data are expressed as mean  $\pm$  e.s.m. of 4 experiments performed in duplicate.

### 3.1 Thio-Michael strategy

As first approach, in particular, it was used for the goal the Thiol-maleimide Michael addition reaction, because it has been widely exploited in biological systems, primarily due to high selectivity of the Thiol-maleimide reaction in aqueous environments, the rapid kinetics and the stability of the thiol-maleimide product<sup>21</sup>. The high reactivity of C=C bond in maleimide probably causes many factors: the bond angle distortion, the ring contortion and the carbonyl groups being in the *cis*-conformation<sup>25</sup>. The thiol function can be easily introduced in a peptide sequence as Cys side chain while the Michael acceptor group (in general is an  $\alpha$ - $\beta$  unsaturated carbonyl moiety) not present as an aminoacid side chain, but they can be ad hoc introduced in the peptide sequence to obtain the desired chemoselectivity of the linking reaction.

Like substrates were chosen a NOP pharmacophore N/OFQ (1-17) and a MOP pharmacophore dermorphin conveniently functionalized see figure 15.

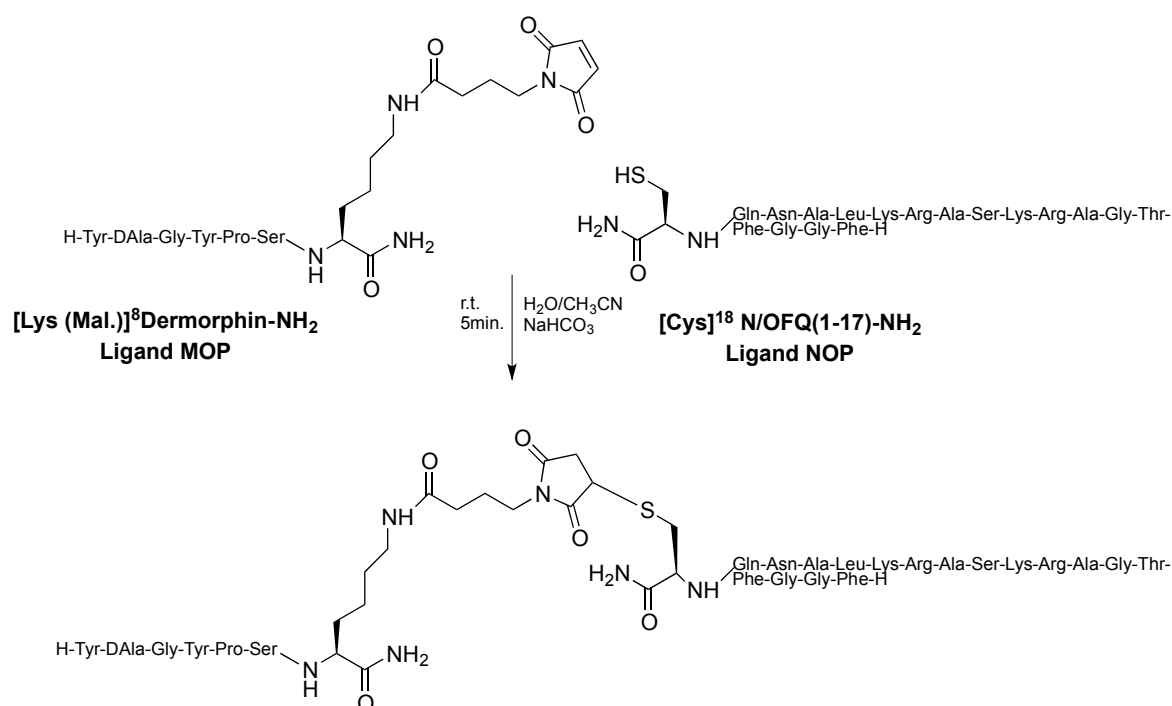


**Figure 15:** Synthetic scheme of Thio-Michael reaction to build a NOP/MOP bivalent ligand 23.

<sup>25</sup> M. Li, P. De, S. R. Gondi, B. S. Sumerlin, *Polym. Sci., Part A: Polym. Chem.*, (2008), 46, 5093-5100.

The first MOP pharmacophore (compound 1) synthesized is the dermorphin, a peptide isolated from the skin of amphibians)<sup>26</sup> functionalized at the C-terminal portion by a Lysine residue (acetylated in the side chain), while NOP pharmacophore is performed by N/OFQ modified in C-terminus with a Cys having a thiol function needed to reaction<sup>10</sup>.

Subsequently the Lysine acetate was substituted with a maleimide function see figure 16 and 17.

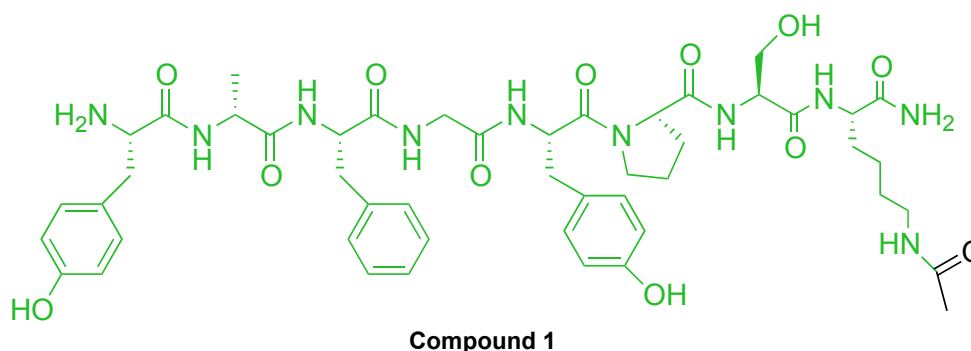


**Figure 16:** Structure of dermorphin sequence with Lysine acetylated in position 8.

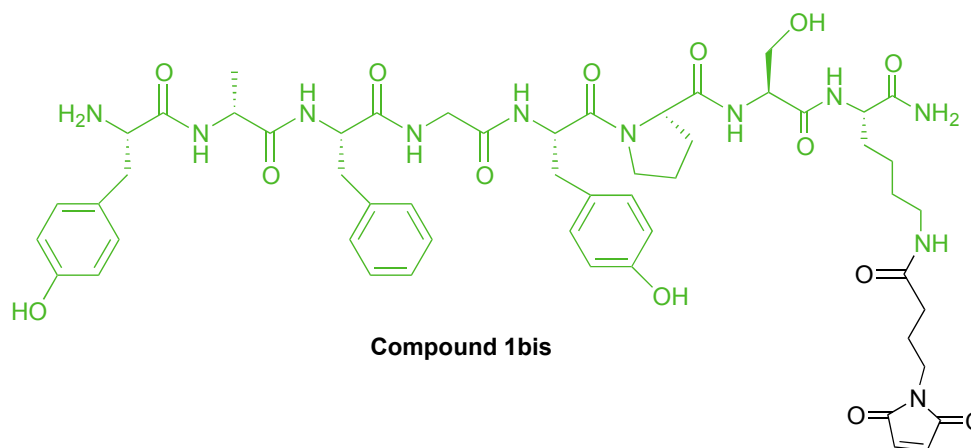
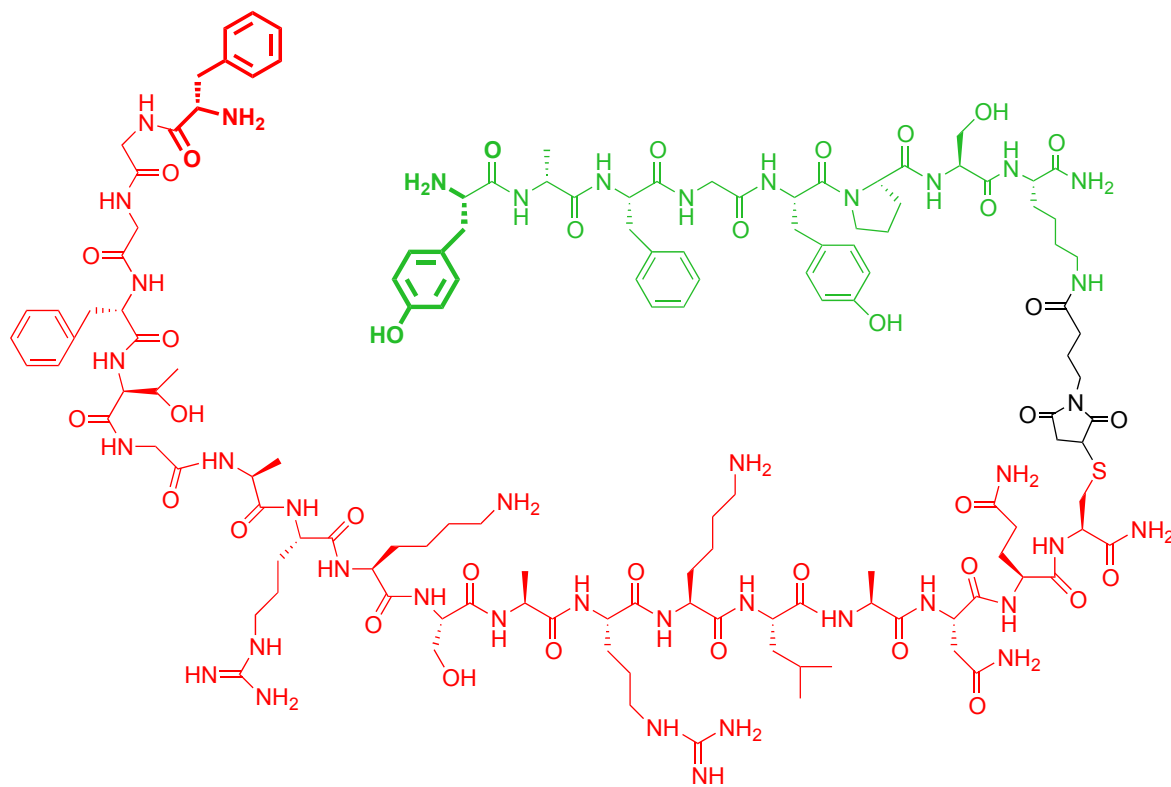


**Figure 17:** Structure of dermorphin peptide sequence modified in position 8 of the Lysine side chain with the introduction of maleimide function(see condition in material & methods).

The [Lys (Mal.)]<sup>8</sup>Dermorphin-NH<sub>2</sub> (compound 1bis) was purified and then linked with [Cys<sup>18</sup>] N/OFQ-NH<sub>2</sub> following the conditions described above.

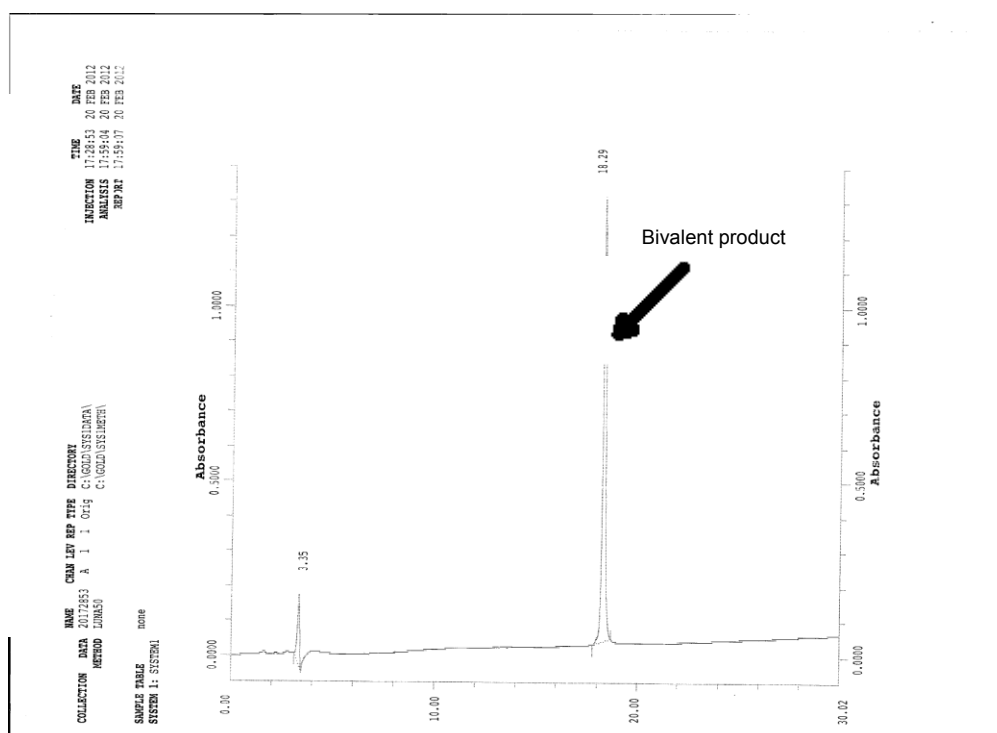
<sup>26</sup> L. Negri, G. F. Erspamer, C. Severini, R. L. Potenza, P. Melchiorri, V. Erspamer, *Proc. Natl. Acad. Sci. USA*, (1992), 89, 7203-7207.



Compound 24

**Figure 18:** Bivalent ligand NOP / MOP (compound 24) consists of the pharmacophore N / OFQ and compound 1 bis.

The conjugation reaction is practically complete after 5-min. In Figure 19 is shown the HPLC chromatogram of the final product purified and its mass spectrum.



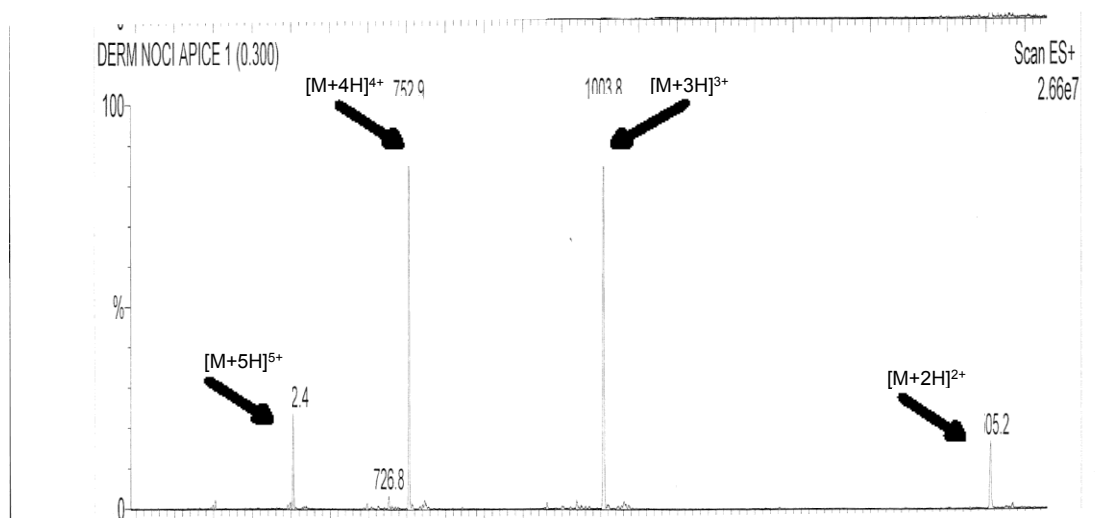


**Figure 19:** Analytical HPLC chromatogram and MS spectrum of the final compound 24.

**Bivalent ligand 24** – Compound 24 was tested in CHO cells stably expressing the MOP receptor. In these cells, compound 24 stimulates calcium mobilization in a concentration-dependent manner showing a  $pEC_{50}$  of 7.16. This value of potency is about 10-fold lower respect to the standard MOP reference agonist dermorphin ( $pEC_{50}$  8.30). On the contrary, in cells expressing NOP receptors, compound 24 stimulate intracellular calcium mobilization with a  $pEC_{50}$  of 9.58, only 2-fold less active respect the natural ligand N/OFQ ( $pEC_{50}$  9.95).

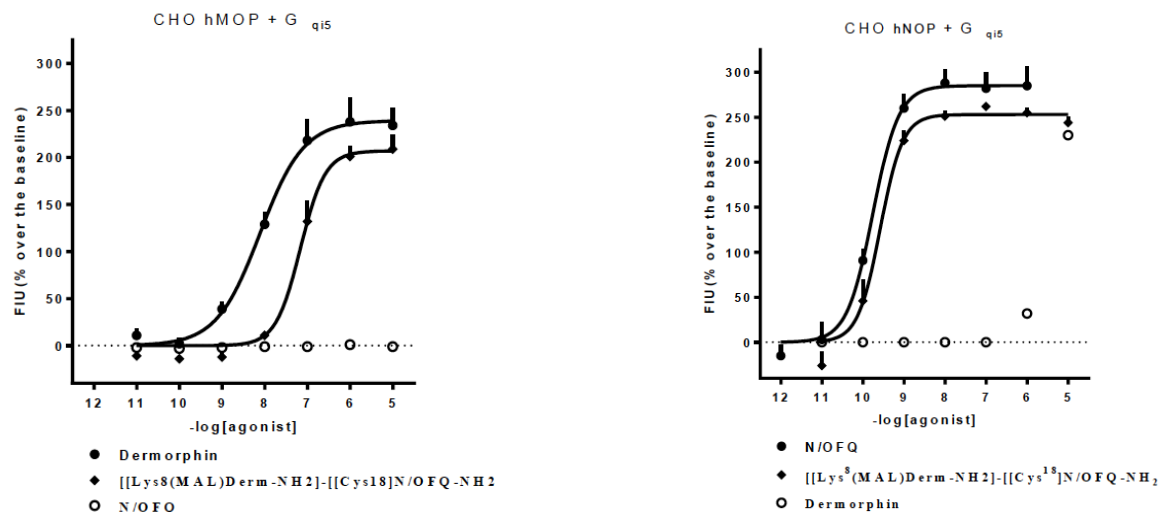


**Figure 20:** Test of intracellular calcium mobilization of cells  $CHO_{hMOP} + G_{\alpha q15}$  (left panel) and  $CHO_{hNOP} + G_{\alpha q15}$  (right panel). Effect of standard agonists dermorphin, N/OFQ and of the compound 24. Data are expressed as mean  $\pm$  e.s.m. of 4 experiments performed in duplicate.

The aim of this study was to identify NOP/MOP bivalent agonist ligands able to stimulate *in vivo* both receptors with the same potency. It is known in literature that *in vivo*, dermorphin stimulates the MOP receptor with an order of potency about



100-fold higher respect *in vitro* assays<sup>27</sup>. To cope with this trouble it is decided to recognize novel MOP ligands to be combined with N/OFQ and possibly to showing *in vivo* a potency comparable to that of N/OFQ.

As novel MOP ligands are studied the N-terminal of different MOP substrates like endomorphin I (H-Tyr-Pro-Trp-Phe-NH<sub>2</sub>), the endogenous opioid tetrapeptide (H-Tyr-Gly-Gly-Phe), the endogenous opioid tetrapeptide modified in C-terminal with a Lysine (H-Tyr-Gly-Gly-Phe-Lys) and finally the N-terminal hexapeptide of dynorphin (H-Tyr-Gly-Gly-Phe-Leu-Arg).

Compound	Sequence	pEC <sub>50</sub>	E <sub>max</sub>
Dermorphin	H-Tyr-DAla-Phe-Gly-Tyr-Pro-Ser-NH <sub>2</sub>	8.30 (8.09-8.52)	177±24
Leu-enkephalin	H-Tyr-Gly-Gly-Phe-Leu- NH <sub>2</sub>	7.26 (6.89-7.62)	144±14
Endomorphin 1	H-Tyr-Pro-Trp-Phe- NH <sub>2</sub>	8.00(7.91-8.09)	209±3
2	H-Tyr-Pro-Trp-Phe-Lys(Ac)- NH <sub>2</sub>	Crc incomplete: at 10µM 117±13	
3	H-Tyr-Pro-Trp-Phe- <b>Gly-Gly</b> -Lys(Ac)- NH <sub>2</sub>	Crc incomplete: at 10µM 81±1	
4	H-Tyr-Pro-Trp-Phe- <b>O<sub>2</sub>Oc</b> -Lys(Ac)- NH <sub>2</sub>	Crc incomplete: at 10µM 97±6	
5	H-Tyr-Pro-Trp-Phe- <b>AVA</b> -Lys(Ac)- NH <sub>2</sub>	Crc incomplete: at 10µM 43±8	
6	H-Tyr-Gly-Gly-Phe- NH <sub>2</sub>	6.29 (6.04-6.54)	179±15
7	H-Tyr-Gly-Gly-Phe-Lys(Ac)- NH <sub>2</sub>	5.98 (5.78-6.17)	152±28
8	H-Tyr-Gly-Gly-Phe- <b>Gly</b> -Lys(Ac)- NH <sub>2</sub>	Crc incomplete: at 10 µM 141±25	
9	H-Tyr-Gly-Gly-Phe- <b>Gly-Gly</b> -Lys(Ac)- NH <sub>2</sub>	Crc incomplete: at 10 µM 152±23	
10	H-Tyr-Gly-Gly-Phe- <b>O<sub>2</sub>Oc</b> -Lys(Ac)- NH <sub>2</sub>	Crc incomplete: at 10 µM 110±29	
11	H-Tyr-Gly-Gly-Phe- <b>AVA</b> -Lys(Ac)- NH <sub>2</sub>	Crc incomplete: at 10 µM 132±25	
12	H-Tyr-Gly-Gly-Phe-Lys- NH <sub>2</sub>	6.10 (5.94-6.26)	151±15
13	H-Tyr-Gly-Gly-Phe-Lys-Lys(Ac)- NH <sub>2</sub>	Crc incomplete: at 10 µM 97±27	
14	H-Tyr-Gly-Gly-Phe-Lys- <b>Gly</b> -Lys(Ac)- NH <sub>2</sub>	Crc incomplete: at 10 µM 88±13	
15	H-Tyr-Gly-Gly-Phe-Lys- <b>Gly-Gly</b> -Lys(Ac)- NH <sub>2</sub>	Crc incomplete: at 10 µM 80±14	
16	H-Tyr-Gly-Gly-Phe-Lys- <b>O<sub>2</sub>Oc</b> -Lys(Ac)- NH <sub>2</sub>	Crc incomplete: at 10 µM 65±25	
17	H-Tyr-Gly-Gly-Phe-Lys- <b>AVA</b> -Lys(Ac)- NH <sub>2</sub>	Crc incomplete: at 10 µM 67±17	
18	H-Tyr-Gly-Gly-Phe-Leu-Arg- NH <sub>2</sub>	7.12 (6.82-7.42)	175±25
19	H-Tyr-Gly-Gly-Phe-Leu-Arg-Lys(Ac)- NH <sub>2</sub>	6.52 (5.83-7.22)	168±28
20	H-Tyr-Gly-Gly-Phe-Leu-Arg- <b>Gly</b> -Lys(Ac)- NH <sub>2</sub>	6.84 (6.17-7.52)	187±39
21	H-Tyr-Gly-Gly-Phe-Leu-Arg- <b>Gly-Gly</b> -Lys(Ac)- NH <sub>2</sub>	6.89 (6.28-7.49)	167±21
22	H-Tyr-Gly-Gly-Phe-Leu-Arg- <b>O<sub>2</sub>Oc</b> -Lys(Ac)- NH <sub>2</sub>	6.52 (5.45-7.58)	181±29
23	H-Tyr-Gly-Gly-Phe-Leu-Arg- <b>AVA</b> -Lys(Ac)- NH <sub>2</sub>	6.81 (6.21-7.41)	143±17

**Table 1:** MOP pharmacological activity obtained in the assay of calcium mobilization.

*New pharmacophore MOP* - the activity in the test of intracellular calcium mobilization performed on cells CHO<sub>hMOP</sub> + G<sub>αq15</sub> of the new compounds synthesized in this thesis is shown in Table 1.

<sup>27</sup> R. Tomatis, M. Marastoni, G. Balboni, R. Guerrini, A. Capasso, L. Sorrentino, V. Santagada, G. Caltendo, L. H. Lazarus, S. Salvadori, *J. Med. Chem.*, (1997), 40, 2948-2952.

The functionalization of the C-terminal part of the endomorphin is not tolerated. It is sufficient to add a lysine residue (acetylated in side chain in compound 2) to completely lose its biological activity. This pharmacological data agrees with previous works in which the modification of the C-terminal of the endomorphin is not well admitted<sup>28 29</sup>. The insertion of spacers of different length between the MOP pharmacophore and the Lysine residue (compound 3-5) is not able to restore the binding to the MOP receptor. Even the MOP pharmacophore Tyr-Gly-Gly-Phe (compound 6) as itself or by insertion of a lysine residue (compound 12) shows to be very sensible to the C-terminal functionalization. In fact, the reference sequence Tyr-Gly-Gly-Phe-NH<sub>2</sub> has a pEC<sub>50</sub> of 6.29 little conditioned with the addition of a single acetylated lysine residue (compound 7; pEC<sub>50</sub> 5.98). The further functionalization with spacers investigated produces the loss of activity (compounds 8-11). The pharmacophore Tyr-Gly-Gly-Phe-Lys-NH<sub>2</sub> behaves in a similar way (compounds 13-17). The pharmacophore Tyr-Gly-Gly-Phe-Leu-Arg-NH<sub>2</sub> (compound 18), N-terminal portion of dynorphin, is found to be the most tolerant in changes in the C-terminal. Its replacement with Lys (Ac) (compound 19) resulted in a loss of potency of 7 times.

The further functionalization with the spacers produces molecules able to bind and activate the MOP receptor and it promotes (in the case of Gly (20) Gly-Gly (21) and Ava (23) a significant recovery of potency compared to Tyr-Gly-Gly-Phe-Leu-Arg-Lys (Ac)-NH<sub>2</sub> (compound 19). These data confirm that the endomorphin is a MOP pharmacophore that does not tolerate alterations in the C-terminal portion of the molecule. Moreover, even the simple opioid message domain Tyr-Gly-Gly-Phe cannot be replaced in the C-terminal with a residue of Lys (Ac). It seems to be better accepted a free lysine side chain (compound 12) even if the subsequent addition of Lys (Ac) drastically reduces the potency of the peptide (compound 13). The C-terminal hexapeptide of dynorphin become obvious be the one that best admits substitutions. In fact, this hexapeptide can be considered as a Leu-enkephalin (Tyr-Gly-Gly-Phe-Leu) with addition of Arg residue in the C-terminal. The further functionalization of this natural hexapeptide does not produce drastic loss potency suggesting that the minimum message opioid editable in the C-terminal may be represented by simple Leu (or Met) enkephalin. This hypothesis is under investigation in our laboratories.

---

<sup>28</sup> W. X. Liu, R. Wang, *Med. Res. Rev.*, (2012), 32, 536-580.

<sup>29</sup> C.-L. Wang, C. Guo, Y.-Q. Wang, Y. Zhou, Q. Li, J.-M. Ni, R. Wang, *Peptides*, (2011), 32, 293-299.

These results suggested that the peptide H-Tyr-Gly-Gly-Phe-Leu-Arg-Gly-Lys(Ac)-NH<sub>2</sub> (compound 20) it can be an efficient MOP pharmacophore to generate a new NOP/MOP bivalent ligand prototype. This peptide was resynthesized replacing the function of Lys acetylated in the side chain of C-terminal with a maleimide function (figure 21).

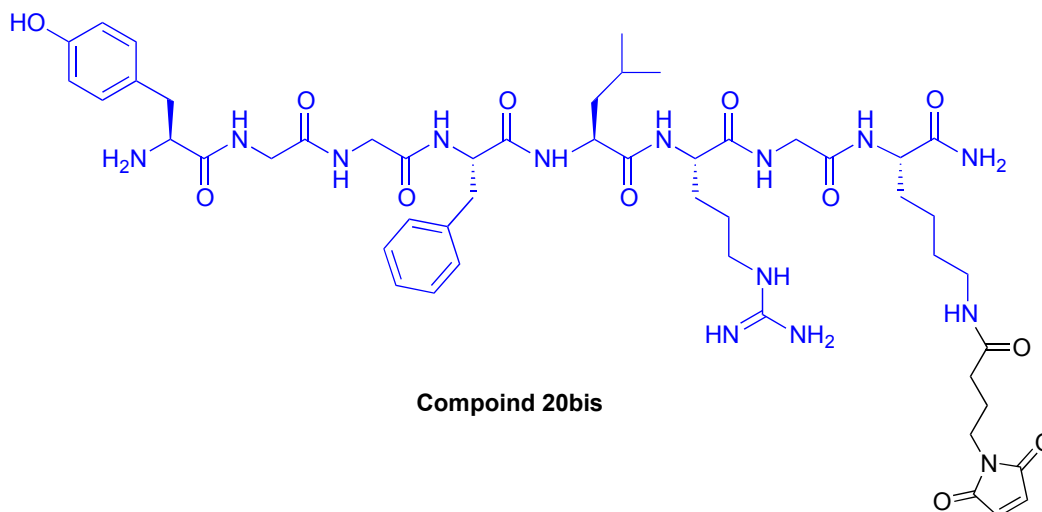


**Figure 21:** Compound 20bis with a maleimide function in the side chain.

Once purified, the peptide was conjugated with the [Cys<sup>18</sup>] N/OFQ-NH<sub>2</sub> using the Thio-Michael addition to yield (Figure 22) compound 25.

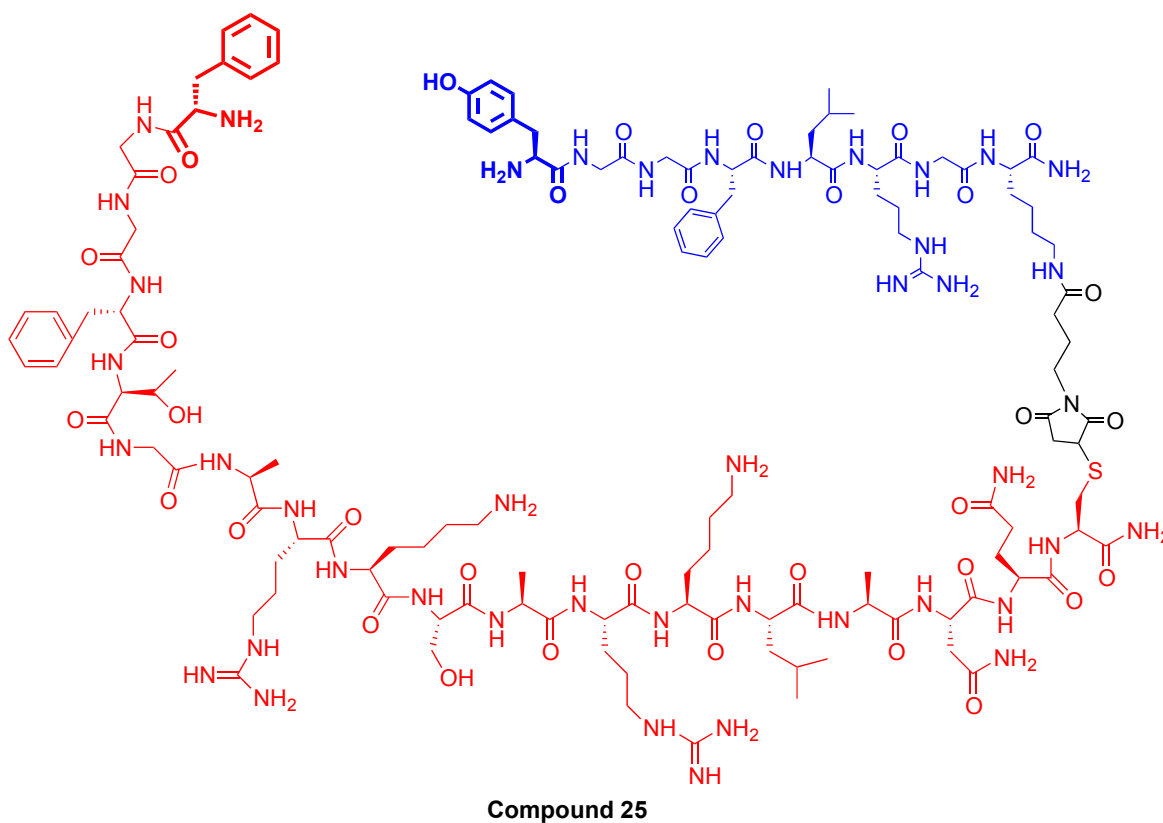


**Figure 22:** Bivalent ligand NOP / MOP (compound 25) consists of the pharmacophore **N / OFQ** and **compound 20bis**.

Also in this case the conjugation reaction is ended totally after 5-min. It is displayed the HPLC profile of the crude reaction as an example and you can see the full disappearance of Tyr-Gly-Gly-Phe-Leu-Arg-Gly-Lys(maleimide)-NH<sub>2</sub>, with only the formation of the desired product with a molar excess 10% of [Cys<sup>18</sup>] N/OFQ-NH<sub>2</sub> used to force the reaction to completeness.

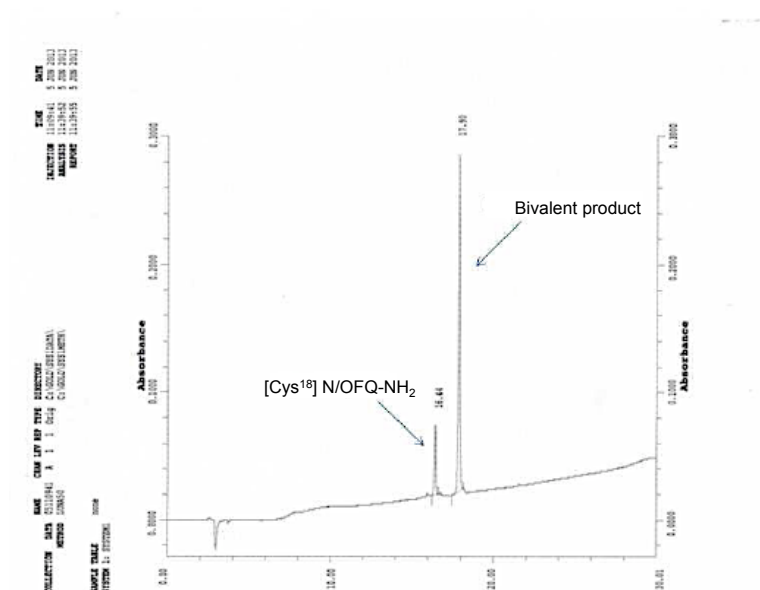


**Figure 23:** Analytical HPLC chromatogram of the reaction mixture [Cys<sup>18</sup>] N/OFQ-NH<sub>2</sub> and compound 20bis.

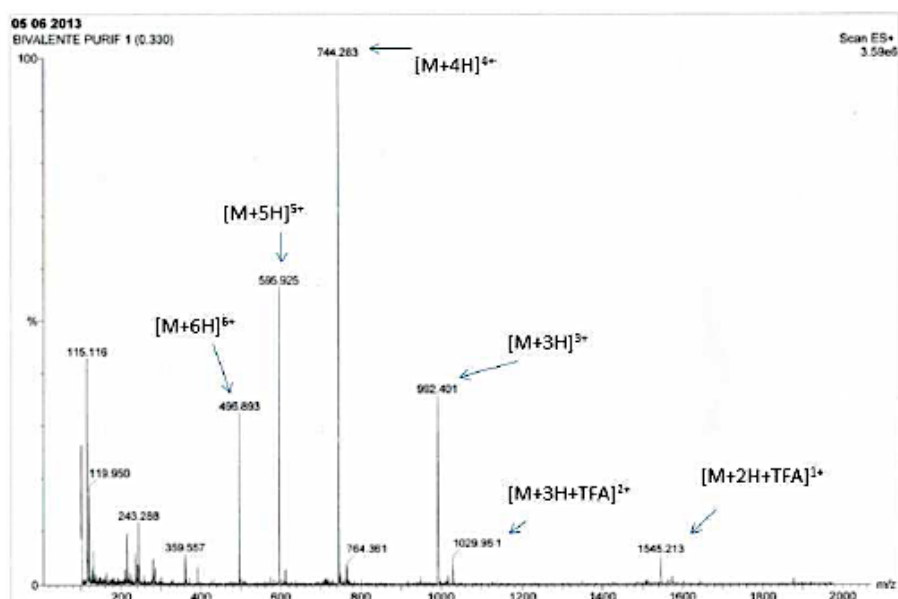
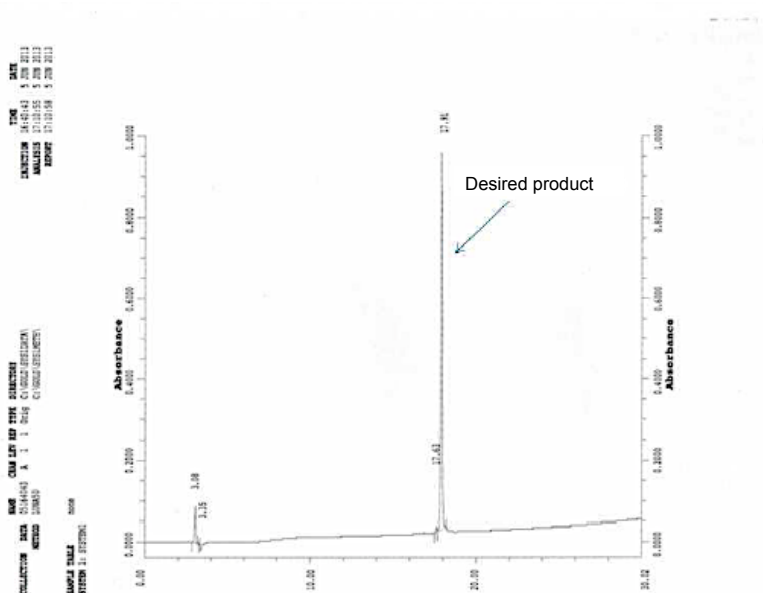
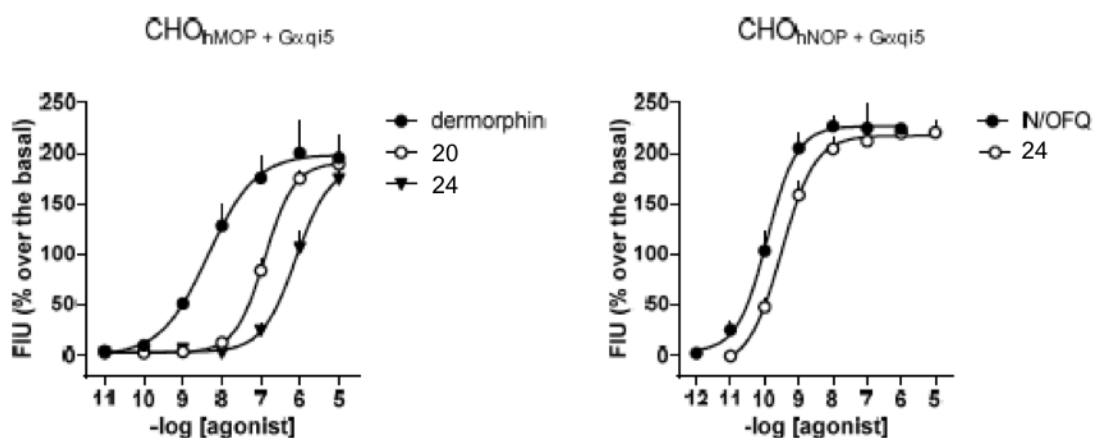


Figure 24: Analytical HPLC chromatogram and MS spectrum of the final compound 25.

**Bivalent ligand 25** – Compound 25 was tested on cells expressing the MOP receptor, compound 25 produced an increase in the levels of intracellular calcium in a concentration-dependent way with a potency of 6.15 and a maximum effect of  $174 \pm 28$ . This compound proves to be about 100 times less potent than the standard MOP agonist dermorphin ( $pEC_{50}$  8.30) and nearly 100-fold less potent than the starting compound 20 ( $pEC_{50}$  6.84). In cells expressing the NOP receptor the derivative 25 has stimulated intracellular calcium mobilization with  $pEC_{50}$  of 9.47 and a maximum effect of  $221 \pm 12$ , showing 3-fold less potent of the natural ligand N/OFQ ( $pEC_{50}$  9.95) (Figure 25).



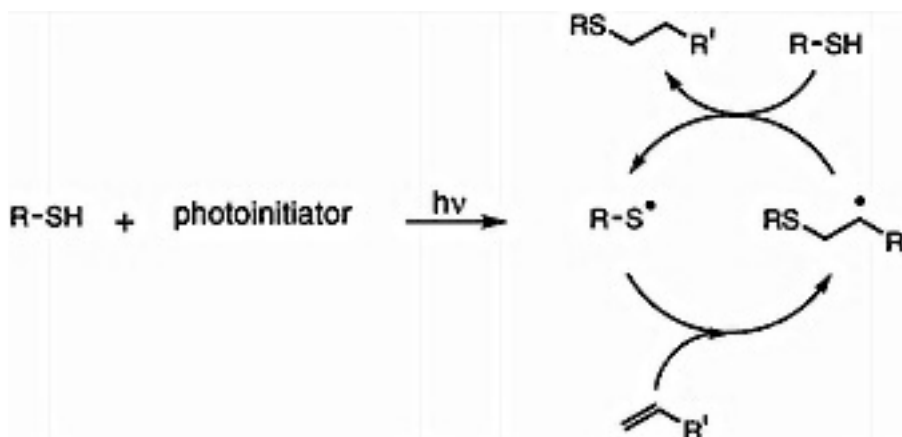
**Figure 25:** Test of intracellular calcium mobilization of cells CHO<sub>hMOP</sub> + G<sub>αqi5</sub> (left panel) and CHO<sub>hNOP</sub> + G<sub>αqi5</sub> (right panel). Effect of standard agonists dermorphin, N/OFQ and of the compound 20 and 25. Data are expressed as mean  $\pm$  e.s.m. of 4 experiments performed in duplicate.

The difference of potency between the two pharmacophores *in vitro* resulted to be about 1000 times and therefore at list in theory, not in line with the requirement of NOP/MOP equipotency recommended for the development of a potential spinal bivalent analgesic.

Compound 24 and 25 will be soon tested *in vitro* on tissues expressing the native NOP and MOP opioid receptors to determine the NOP and MOP potency.

### 3.2 Thiol-ene strategy

The second approach for the synthesis of bivalent ligands was Thiol-ene reaction. Thiol-ene chemistry takes advantages through the addition of thiols across virtually any terminal -ene double bond<sup>30</sup>. Below it is displayed the reaction mechanism of the Thiol-ene reaction (scheme 1).



**Scheme 1:** General Thiol-ene coupling mechanism.

In the 1938 M. S. Kharasch *et al.* demonstrated that the addition of thiols to alkenes proceeds via a free-radical chain mechanism. The reaction starts by radical formation UV excitation of a photoinitiator or the thiol itself. After sulfenyl radical product reacts with the unsaturated alkene substrate in an anti-Markovnikov fashion to give a new carbon radical. In a second propagation step, the new radical that is formed, interacts with another thiol molecule to yield the thioester product and a new sulfenyl radical, which propagates to carry on the radical cycle. A variety of termination pathways are possible through a crossing between sulfenyl or carbon radicals. The Thiol-ene coupling reaction can be described as a “click” reaction in agreement to the original definition explained by Sharpless *et al.*<sup>31</sup>.

However, despite the advantages that fit the “click” definition, there are limitations of this type of chemistry, which include its loss of stereospecificity, the developing of unwanted disulfide byproducts through radical recombination.

The Thiol-ene reaction may be carried out in batch or in flow<sup>32</sup>.

<sup>30</sup> C. E. Hoyle, *Polymer Preprints*, (2008), 49, 155-156.

<sup>31</sup> M. Kryger, *Chem. 535 Seminar*, (2008).

<sup>32</sup> C. Wiles, P. Watts, *Chem. Commun.*, (2011), 47, 6512–6535.

The difference between the two approaches are that the irradiation in batch can turn out to be not completely homogeneous throughout the sample.

In this study the flow reaction exploits the technique of photolithography that is a system in polydimethylsiloxane with an internal volume of 10 $\mu$ l and a size of the channels of 50 $\mu$ m. The photoinitiator is introduced in an amount equal to 10mol%, the allyl-compound in excess of 3 eq. compared to the peptide in a solution of degassed DMF (with molar concentration in thiol approximately 0.05M). A reaction solution of 20 $\mu$ l is injected every minute with a syringe in an anhydrous environment affected by UV light of  $\lambda$  365nm.

This technique allows to:

- radiate in a homogeneous solution;
- control the residence time, the time which needs the first molecule reaction to enter and exit from the microreactor according to this relation: **Vz / flow rate = reaction time** (Example 10 ( $\mu$ L) / 20 ( $\mu$ l / min) = 0.5 min = 30 seconds).

The system works in optimal conditions to 1  $\mu$ l/min, which corresponds to a residence time of 10 min.

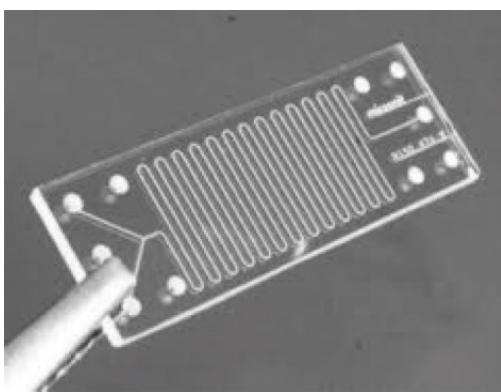


**Figure 26:** Image of a microreactor.

In order to exploit the characteristics of Thiol-ene coupling<sup>23</sup> it decided to carry on this reaction with the MOP substrate and NOP substrate fittingly functionalized as previously reported in our laboratory studies. An enkephalin (Tyr-Gly-Gly-Phe-Gly-NH<sub>2</sub>), functionalized at the C-terminus with a thiol function represented by Cys, was reacted with an olefin such as dodecene with a good outcome of the reaction.



Below you are illustrated spectra of analysis.

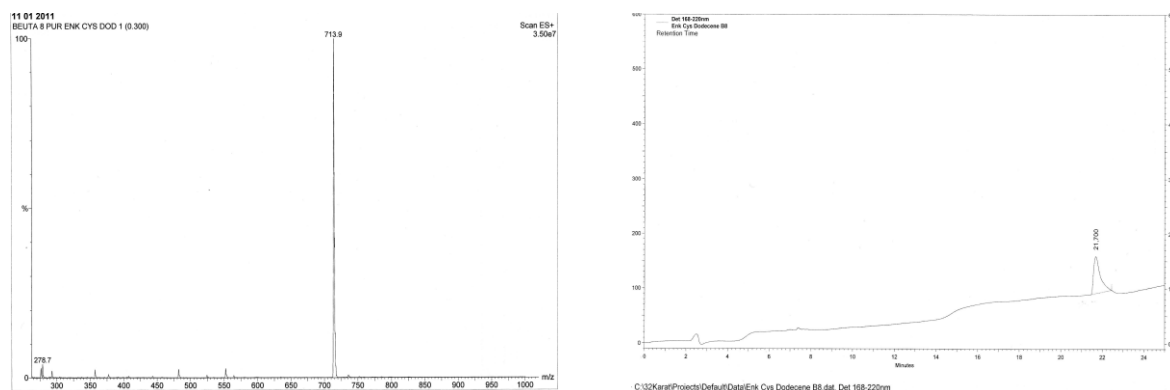


**Figure 27:** Mass spectrum (to the left) and HPLC profile (to the right) of the adduct purified.

Initially the reaction was tested using the elected pharmacophores: the bulky peptide NOP substrate [Cys<sup>18</sup>] N/OFQ-NH<sub>2</sub> and the MOP substrate dermorphin functionalized in position 8 of C-terminal with an allyl group such as allyl-Gly (purchased from Sigma-Aldrich) in different concentrations of solvent. The reaction was done in the following condition see figure 28.

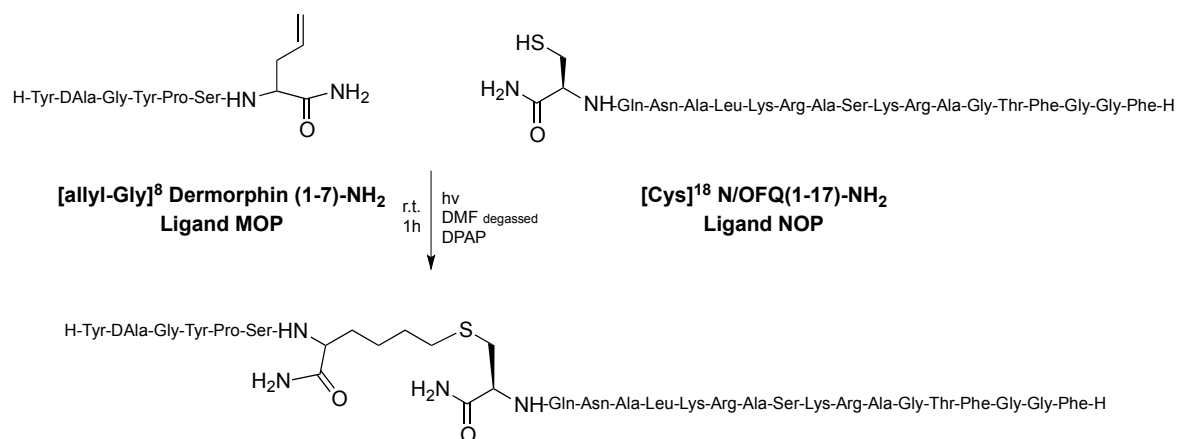


**Figure 28:** General scheme of Thiol-ene reaction to get a bivalent ligand.

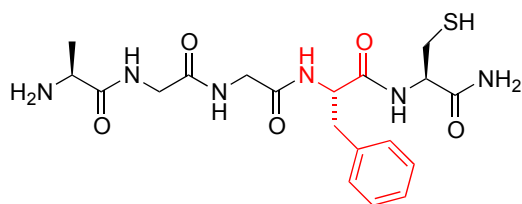
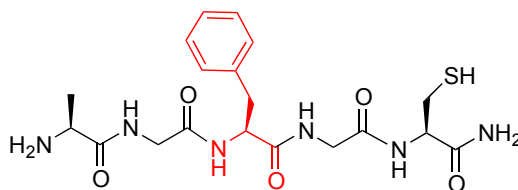
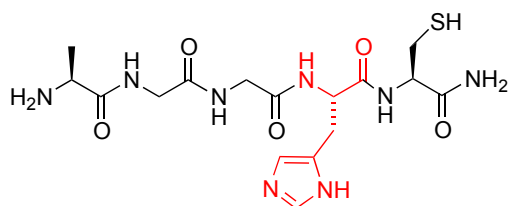
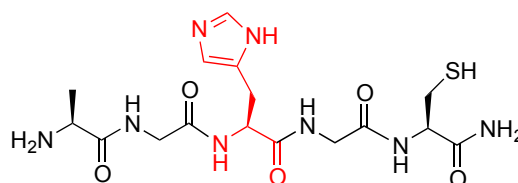
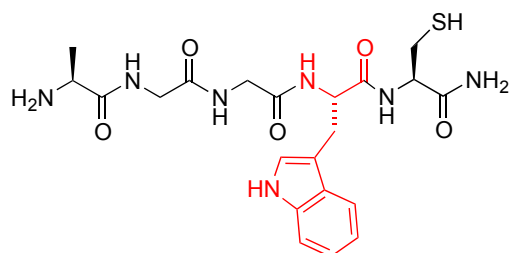
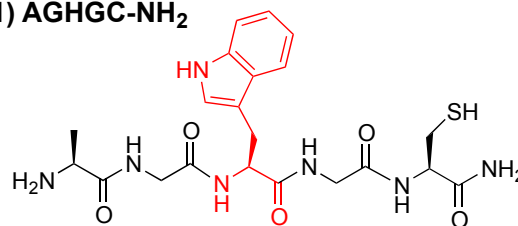
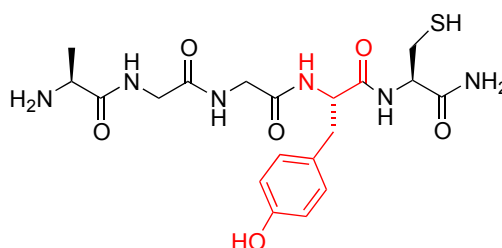
The tests are summarized in the table below.

Concentration	Amount		Wavelength	Photoinitiator	Time
Solvent	Peptide eq.	Alkene eq.			
0,5M DMF	1	1	365 nm	DPAP 10 mol %	1h
0,05M DMF	1	1	365 nm	DPAP 10 mol %	1h
0,05M DMF	1	1	365 nm	DPAP 10 mol %	1h
0,5M DMF	1	3	365 nm	DPAP 10 mol %	1h
0,5M DMF	1	4	365 nm	DPAP 10 mol %	1h
0,5M DMF	1	5	365 nm	DPAP 10 mol %	1h
0,5M DMF	3	1	365 nm	DPAP 10 mol %	1h

**Table 2:** Different reaction conditions tested.

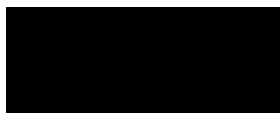
Unfortunately, the reaction has not been successful, the only product developed by this reaction appears to be the dimer of [Cys]<sup>18</sup> N/OFQ (1-17)-NH<sub>2</sub> with a formation of a disulfide bridge, so this assumption it has tried to investigate what were the causes. Moreover in literature there are not deepened studies in the field of the peptides Thiol-ene reaction.

For these reasons it was decided to start an initial methodological study about Thiol-ene reaction. The aim was to understand the influence of the side chains of the aminoacids adjacent to the Cysteine, which aminoacid involved in the reaction. Initially it was first synthesized a series of simple Pentapeptides model by introducing in position 3 and 4 aromatic aminoacids as you can see in the scheme below.

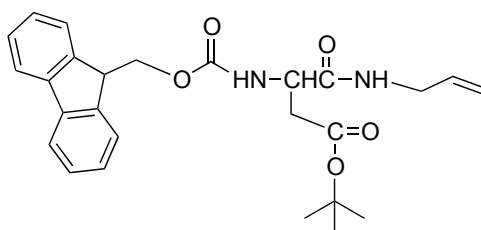
26) AGGFC-NH<sub>2</sub>27) AGFGC-NH<sub>2</sub>28) AGGHC-NH<sub>2</sub>29) AGHGC-NH<sub>2</sub>30) AGGWC-NH<sub>2</sub>31) AGHGC-NH<sub>2</sub>32) AGGYC-NH<sub>2</sub>**Scheme 2:** List of Pentapeptides of the first series.

Each peptide was subjected to a thorough analysis and identification NMR: <sup>1</sup>H, <sup>13</sup>C, DEPT, COSY, HMBC, HMQC before and after (in case of failure) the reaction in order to observe the variations in the spectra.

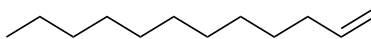
Each peptide was reacted with the allyl-sugar with this structure:



Some peptides were reacted well with Fmoc-allyl-Asp(O<sup>t</sup>Bu) whose structure follows:



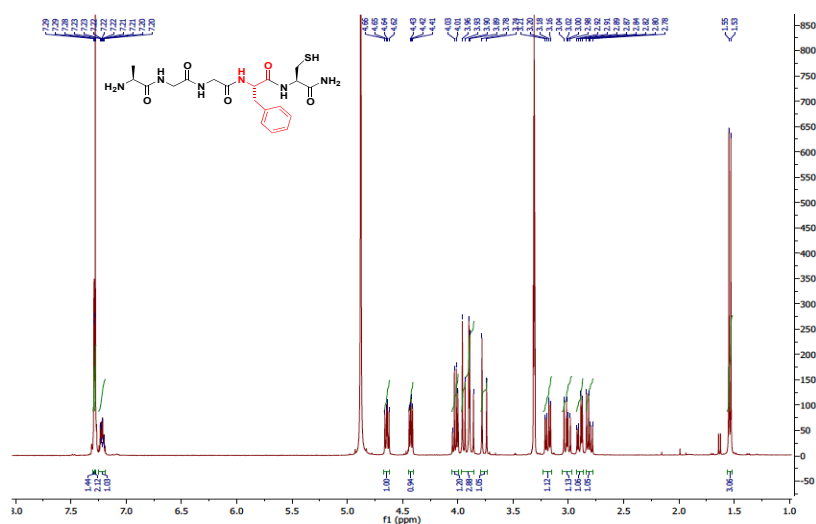
Finally for its commercial availability has been used in some cases the dodecene represented below:



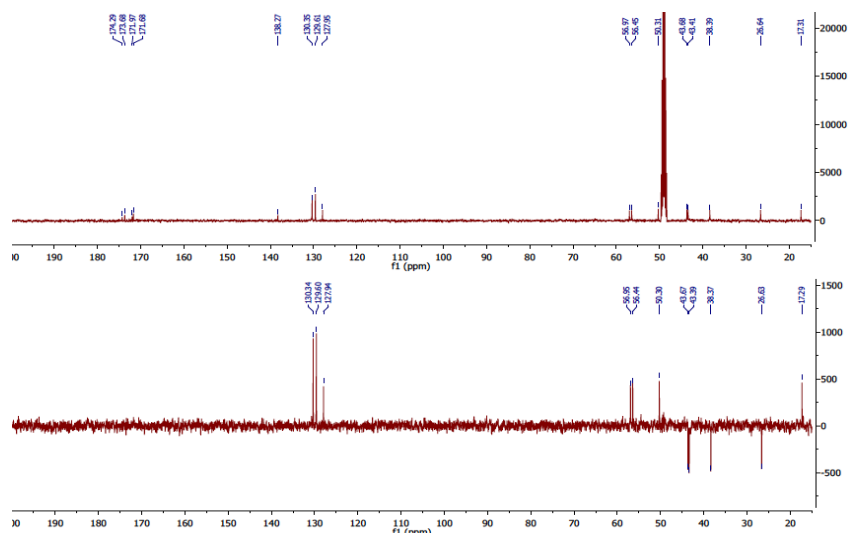
The methods of synthesis of allyl-glucose and Fmoc-allyl-Asp(O<sup>t</sup>Bu) are reported in the experimental part. The peptides are synthesized in solid phase using the Fmoc methodology and subsequently purified by preparative HPLC (see Experiment part).

In a specific way is explained an example of in-depth analysis that it was performed for each samples. Pentapeptide Ala-Gly-Gly-Phe-Cys-NH<sub>2</sub> (compound 26) has been studied as an individual and as conjugated to allyl-glucose in batch and in flow.

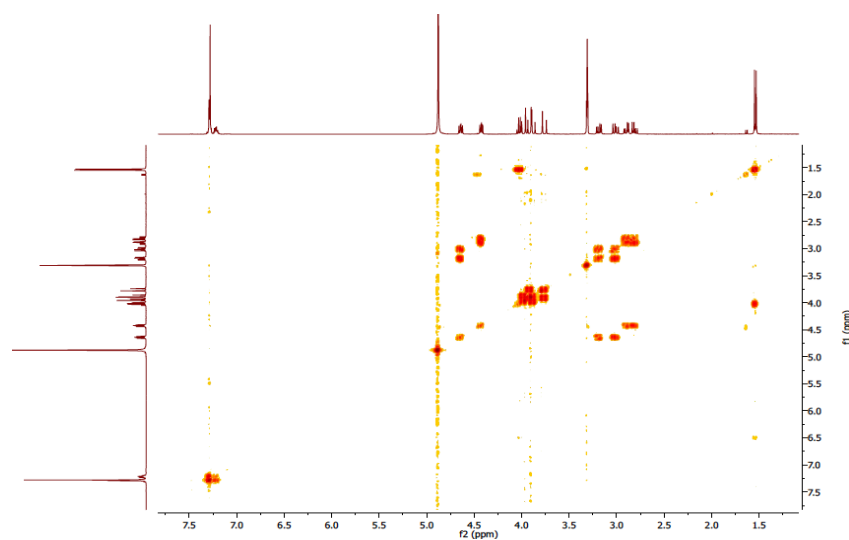
### <sup>1</sup>H AGGFC (26)



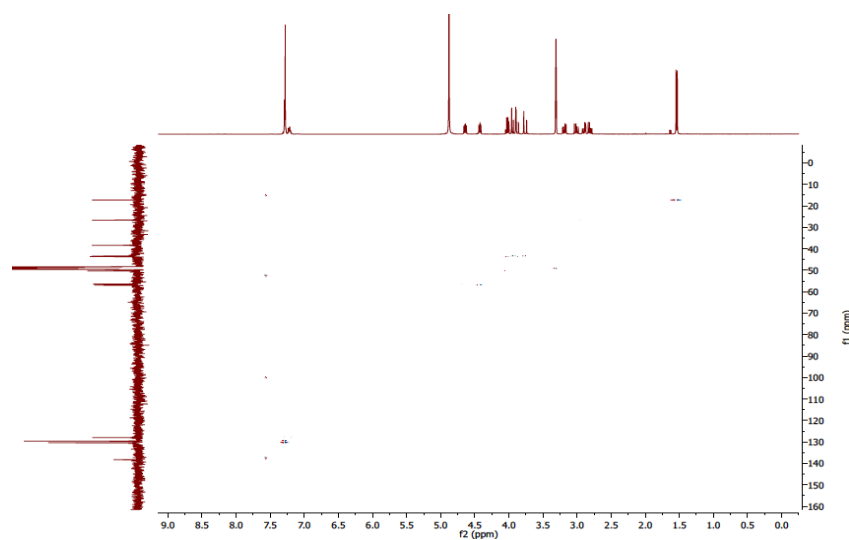
**<sup>13</sup>C-DEPT AGGFC (26)**



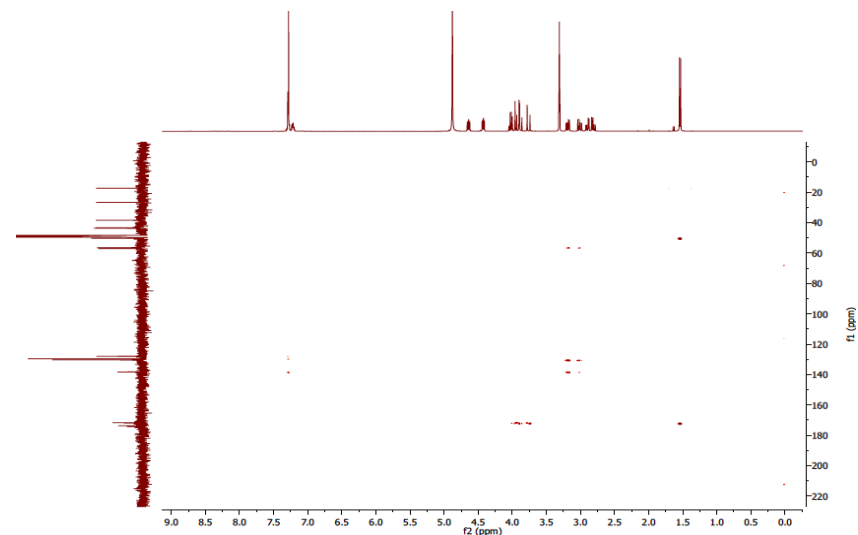
**COSY AGGFC (26)**



**HMBC AGGFC (26)**



## HMQC AGGFC (26)



The two-dimensional NMR analysis allowed the identification of the exact chemical shifts of all protons and carbons of the peptide.

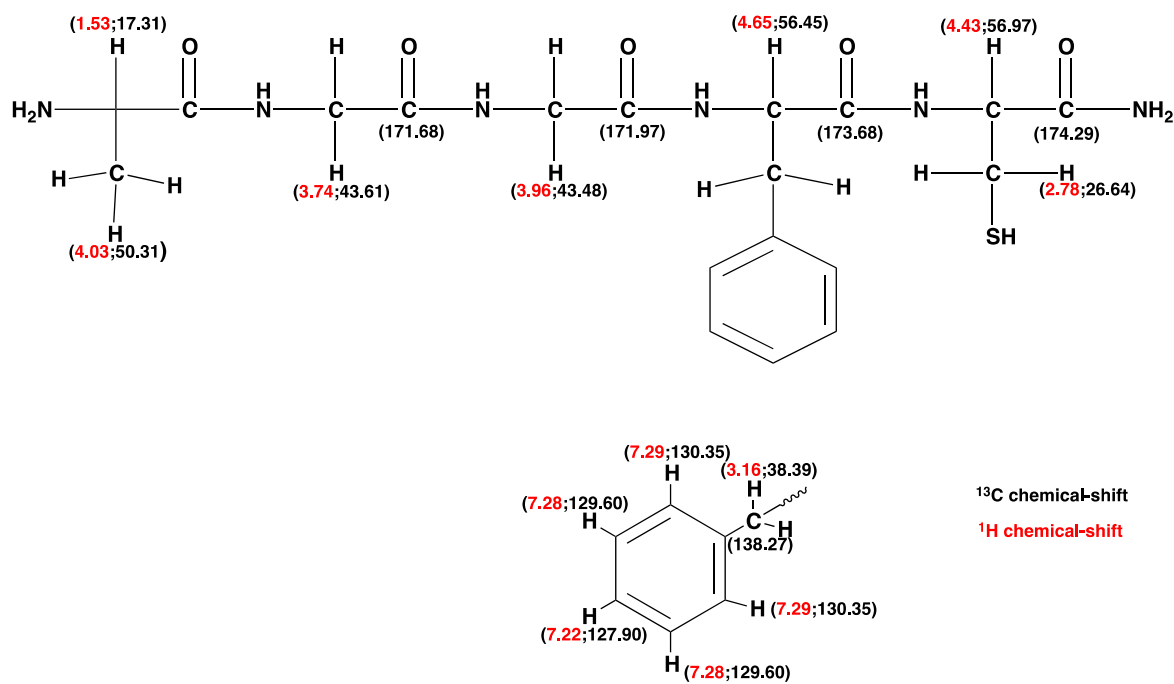


Figure 29: <sup>1</sup>H and <sup>13</sup>C chemical-shift of the peptide 26.

To understand better the reaction product and byproduct are shown the  $^1\text{H}$  NMR spectrum of the allyl-glucose.

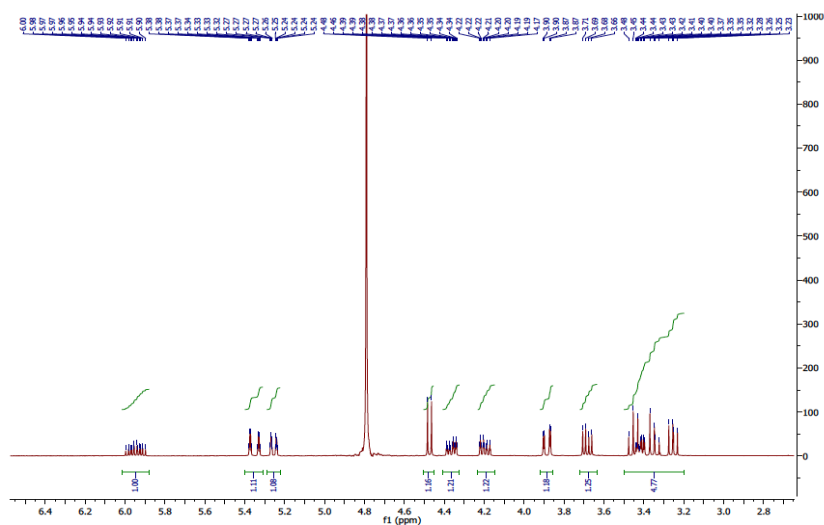


Figure 30:  $^1\text{H}$  NMR spectra of allyl-glucose.

This spectra puts in evidence the  $^1\text{H}$  chemical shifts of the two protons involved in the olefinic bond characteristic of allyl-sugar at 5.35 ppm and 5.26 ppm.

Below there are displayed the  $^1\text{H}$  NMR spectra of the reaction products.

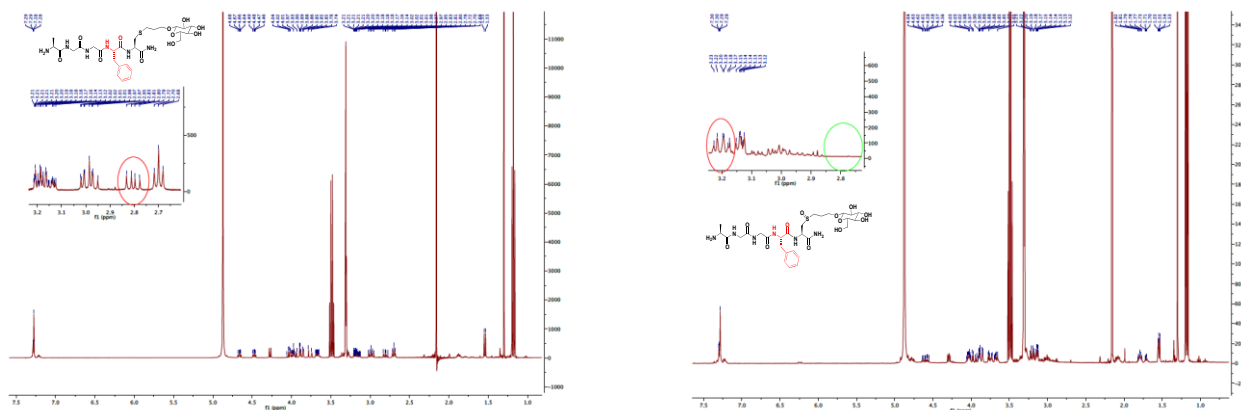
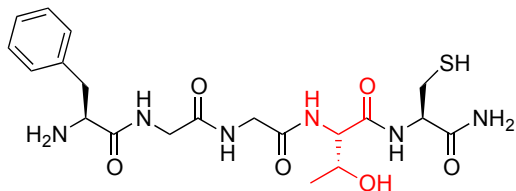
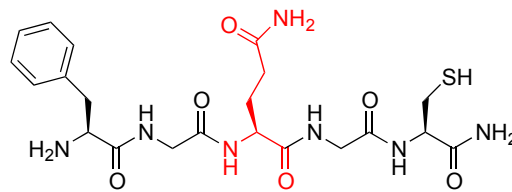
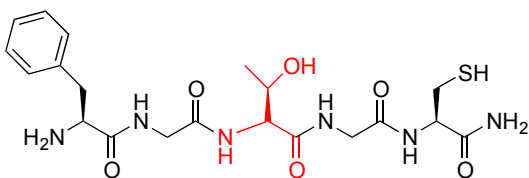
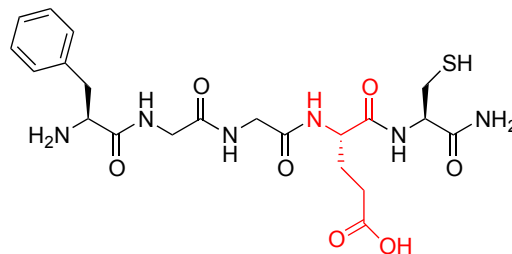
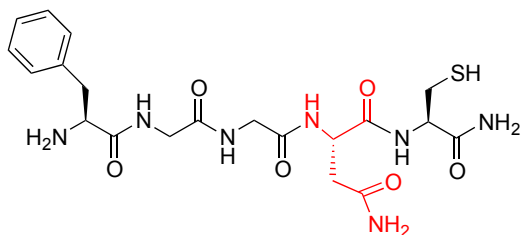
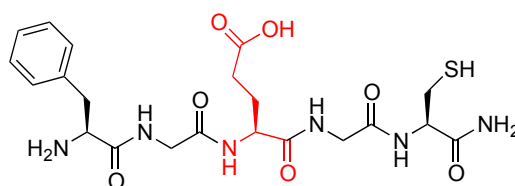
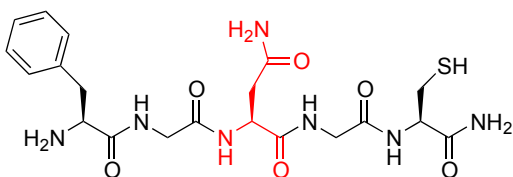
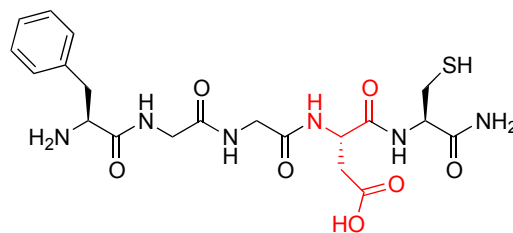
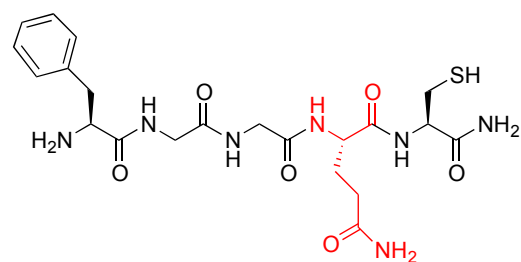
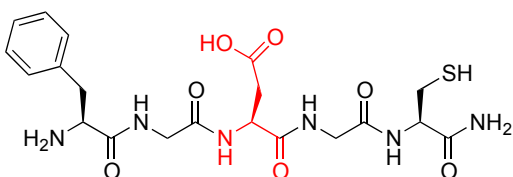


Figure 31: Left  $^1\text{H}$  NMR spectra of Thiol-ene product, right  $^1\text{H}$  NMR spectra of sulfoxide byproduct.

The left spectrum demonstrates that the reaction took place with good result and it is visible the disappearance of the signals of the two olefinic protons (5.26 ppm-5.35 ppm shown in the  $^1\text{H}$  spectra of allyl-glucose) with the appearance at 2.8 ppm of the signal indicative of the formation of thio-ether bond. The right spectrum exhibits the secondary product which is the corresponding sulfoxide. As proof of the two products there are also the exact masses (see experimental part).

Subsequently it was synthesized an other series of simple Pentapeptide model by inserting in position 3 and 4 aminoacids acidic, and neutral hydrophilic with in side chain amide or alcohol function in order to observe, possibly, which other conditions prevent the success of Thiol-ene reaction. In the scheme below there is the peptides sequence studied.

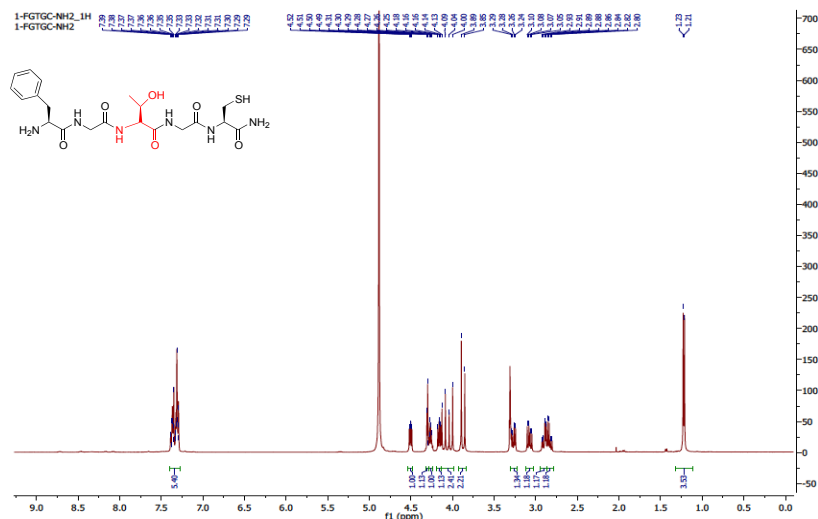
**33) FGGTC-NH<sub>2</sub>****38) FGQGC-NH<sub>2</sub>****34) FGTGC-NH<sub>2</sub>****39) FGGEC-NH<sub>2</sub>****35) FGGNC-NH<sub>2</sub>****40) FGEGC-NH<sub>2</sub>****36) FGNGC-NH<sub>2</sub>****41) FGGDC-NH<sub>2</sub>****37) FGGQC-NH<sub>2</sub>****42) FGDGC-NH<sub>2</sub>****Scheme 3:** List of Pentapeptides of the second series.



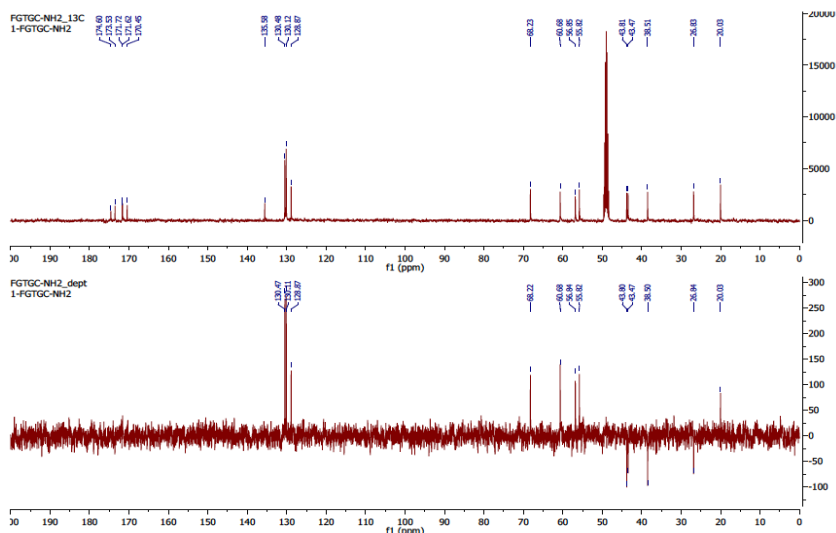
In this series for convenience of analysis has been introduced a Phe in position 1 as a chromophore that it has allowed a better purification.

All Pentapeptides were reacted with the allyl-glucose and like the previous ones were subjected to spectroscopic analysis. Here it reports the complete analysis carried out on the compound 34 for example (Phe-Gly-Thr-Gly-Cys-NH<sub>2</sub>).

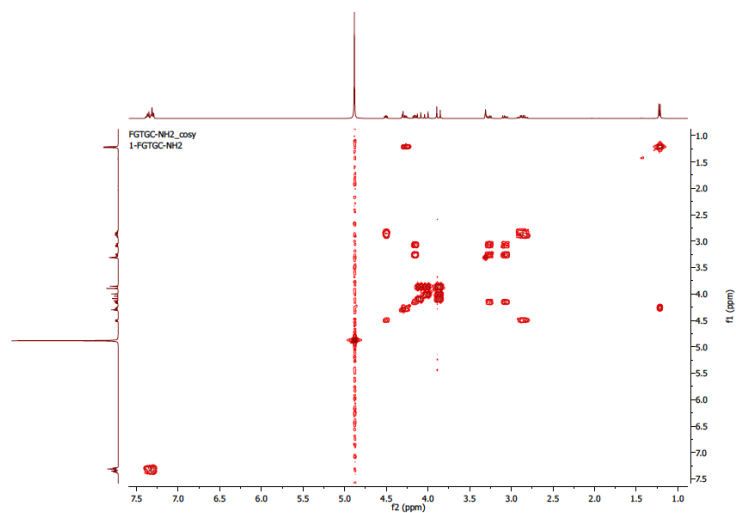
### <sup>1</sup>H FGTGC (34)



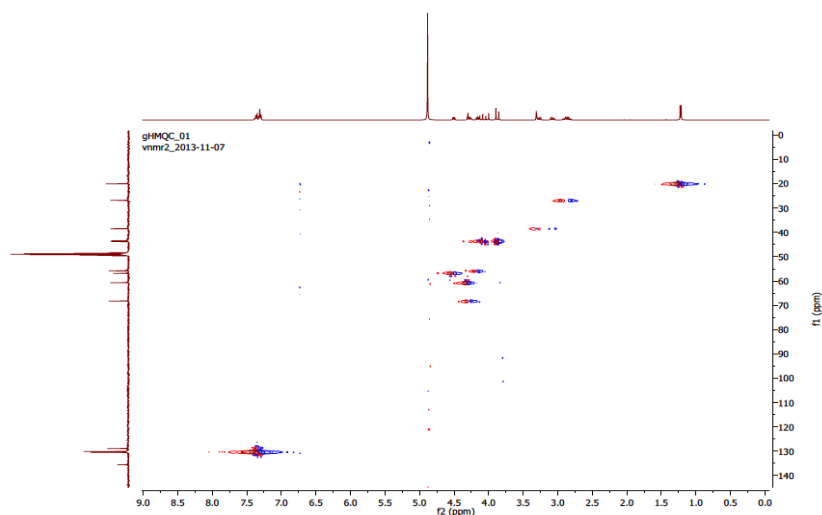
### <sup>13</sup>C-DEPT FGTGC (34)



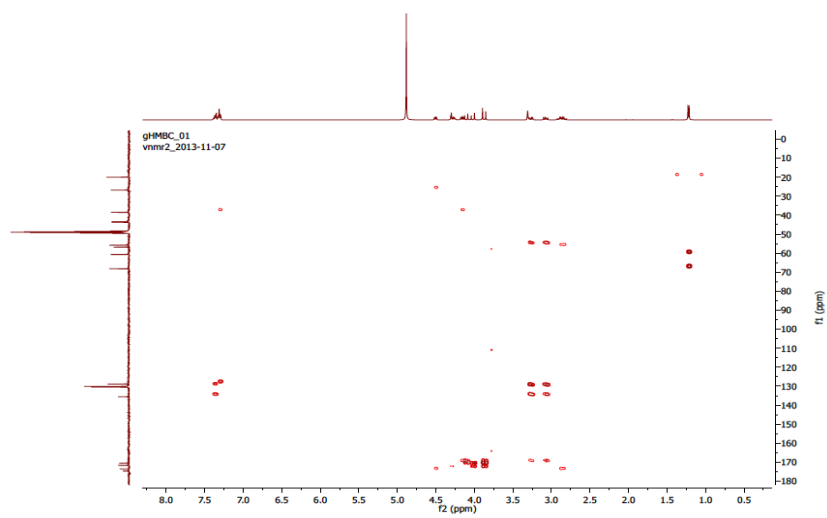
**COSY FGTGC (34)**



**HMBC FGTGC (34)**



**HMQC FGTGC (34)**



The two-dimensional analysis allowed to assign the various chemical shift of all the protons and carbons of the sequence.

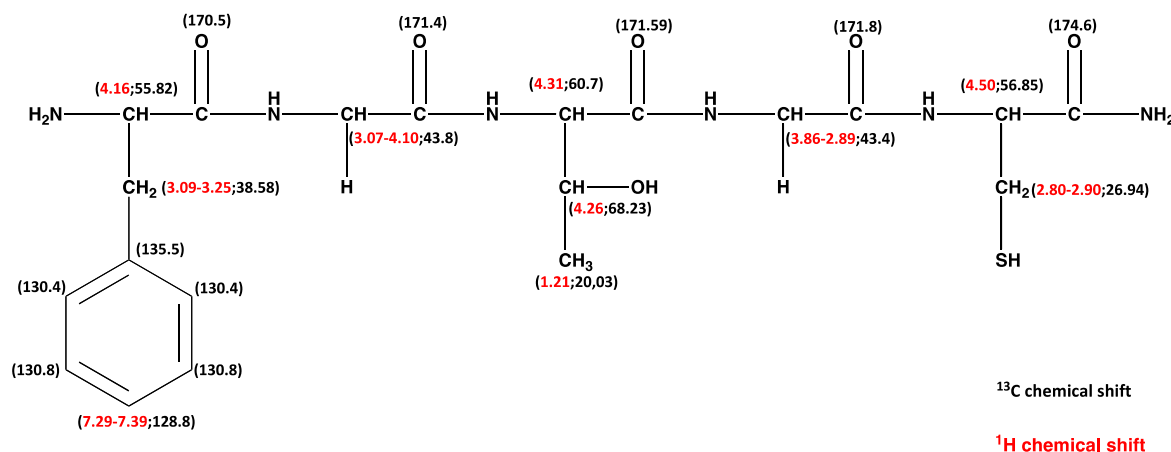
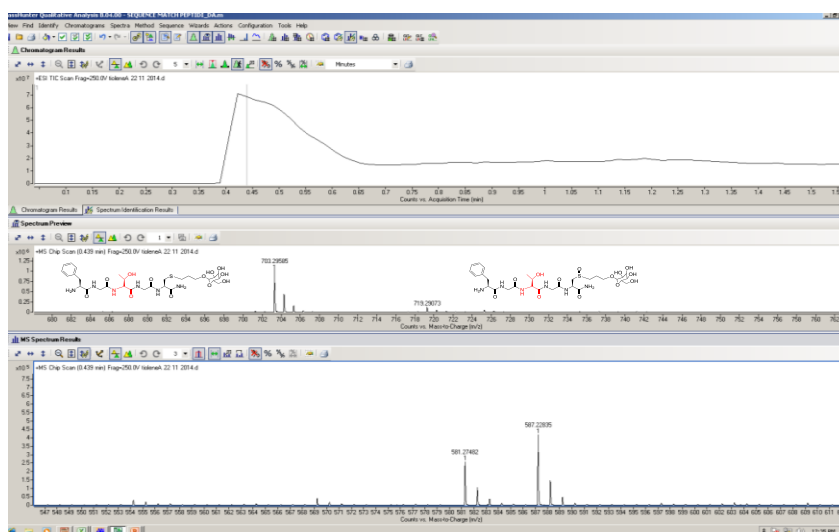


Figure 32: <sup>1</sup>H and <sup>13</sup>C chemical-shift of the peptide 34.

The NMR analysis of the reaction products has not been made because the exact mass spectrum confirmed the good outcome of the reaction.

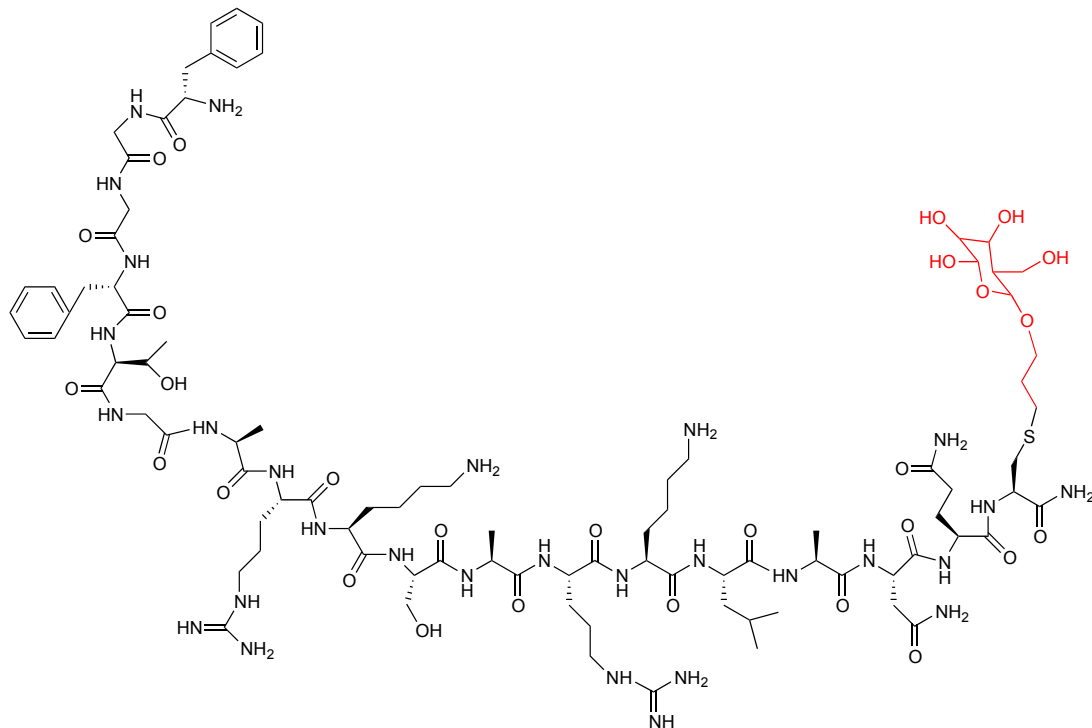
### HRMS THIOL-ENE COMPOUND (50)



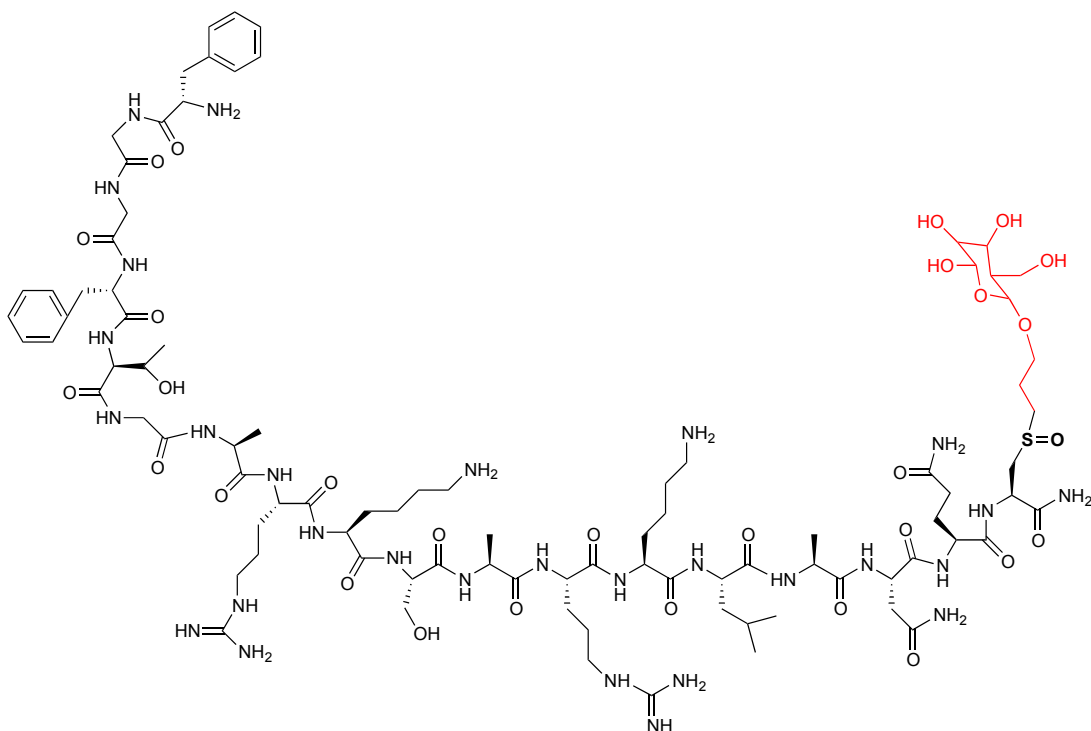
All peptides tested work successfully in Thiol-ene reaction. No difference it was observed in the reaction play in flow or in batch.

Following the good results obtained with the pentapeptide and the ally-sugar, the last reaction that it has been done was the ([Cys]<sup>18</sup> N/OFQ (1-17)-NH<sub>2</sub>) with the same allyl substrate. In this latter case, the Thiol-ene reaction was successfully and, as showed by HRMS it has been obtained both the thiol ether product and the corresponding sulfoxide.

The reaction condition was the same applied to all peptides seen before (it explained in experimental section).

**COMPOUND (60)**

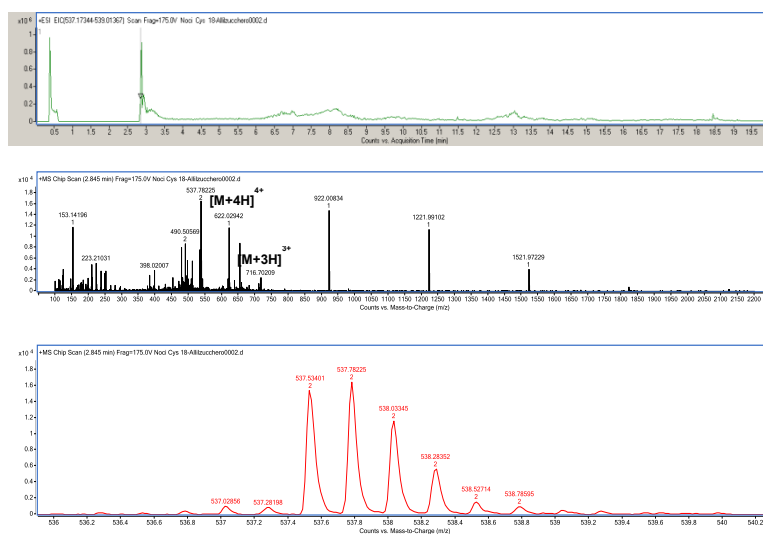
$C_{91}H_{151}N_{29}O_{28}S$   
Mw: 2131,4

**COMPOUND (60bis)**

$C_{91}H_{151}N_{29}O_{29}S$   
Mw: 2147,4

**Figure 33:** Structures of compound 60 and 60bis.

## HRMS THIOL-ENE COMPOUND (60-60bis)



Using the substrate like NOP pharmacophore with certain cluttered due to the presence of 18 aminoacids in the chain, the reaction of Thiol-ene has given positive results.

#### 4. CONCLUSION

In this work it was investigated the possibility to synthesize bivalent molecules able to activate the NOP and MOP opioid receptors. Molecules with this pharmacological profile may represent a new class of analgesic drugs with fewer side effects compared to classical opioids currently used in the treatment of pain.

The molecules investigated have a peptide structure for which the way suitable to administer should be intrathecally. It was studied the biological activity of MOP series of new pharmacophores drawn on the structure of MOP endogenous ligands and functionalized in the C-terminal portion with an appropriate way to be used in the synthesis of NOP/MOP bivalent molecules. It was planned to adopt two chemoselective reaction for this aim: Thio-Michael and Thiol-ene reaction.

The Thio-Michael reaction took place in mild conditions with extreme speed and high efficiency, confirming previous observations obtained in the research lab where I did my thesis work and that they had shown the Thio-Michael reaction as ideal for the synthesis of molecules of bivalent peptide type.

At the beginning was selected like MOP substrate a derivate of dermorphin H-Tyr-DAla-Phe-Gly-Tyr-Pro-Ser-Lys(Ac)-NH<sub>2</sub> (compound 1) to link with the NOP substrate [Cys<sup>18</sup>]N/OFQ-NH<sub>2</sub> through Thiol-Michael reaction. Each pharmacophores has been functionalized to obtain the first bivalent ligand (compound 24), the activity *in vitro* of the MOP substrate has shown 10-fold less potency respect to the standard opioid ligand and 2-fold less active respect the natural ligand N/OFQ; furthermore it is known that *in vivo* the potency of dermorphin is 100-fold higher. For this reason it was decided to find novel MOP pharmacophores able to bind to the standard NOP pharmacophore and to exhibit *in vivo* a potency comparable to that of N/OFQ. Between the new MOP ligands it was identified the sequence H-Tyr-Gly-Gly-Phe-Leu-Arg-Gly-Lys(Ac)-NH<sub>2</sub> (compound 20), which maintains a good ability to bind and activate the MOP receptor with a 100-fold less potency than endogenous ligand. This peptide was conjugated with the NOP ligand nociceptin exploiting the reaction of Thio-Michael like the bivalent ligand previously described. The bivalent ligand achieved, compound 25, is able to bind the MOP receptor with a potency 100-fold lower than the standard dermorphin ligand. Compound 25 activates the NOP receptor with a potency only 3-fold lower than the physiological ligand N/OFQ.

Afterwards compound 24 and 25 will be tested in vitro on tissues expressing the native NOP and MOP opioid receptors to assign the NOP and MOP potency.

Otherwise, Thiol-ene reaction is not been satisfying to produce a NOP/MOP bivalent ligand.

The first MOP substrate (compound 1), adequately functionalized in C-terminal portion with an olefinic group, is been reacted with the NOP substrate [Cys<sup>18</sup>] N/OFQ-NH<sub>2</sub> giving a failure data. In literature thiol-ene reaction is known as a good chemoselective and regioselective procedure for non peptide chemistry. In our hands, with functionalized peptide, this reaction showed some limitation; in order to better understand the chemical pathway involved in peptide thiol-ene chemistry it was planned an initial methodological study.

To reach the scope it has been chosen a pentapeptide prototype in order to deeply analyse its NMR features.

Every peptide is functionalized in C-terminal with a Cys, making available the thiol function involved in Thiol-ene reaction. As alkene substrate it was used an olefin, the substrate mainly elected was the allyl-glucose. In each prototype is been introduced a different aminoacid with side chains variable to assess whether some of these are involved in side reactions sequence dependent. The peptides were analyzed by NMR in order to assess any changes of the chemical shift in the case of no successfully of reaction. The introduction of aromatic aminoacids characterized by bulky side chains such as tryptophan, phenylalanine, tyrosine and histidine did not result alterations in the achievement of the reaction.

Similarly the introduction of hydrophilic aminoacids like threonine with an alcohol function in side chain, glutamine and asparagine with an amide function with variable length in side chains, do not change the Thiol-ene reaction.

Finally the introduction of aminoacid acid as aspartic and glutammic acid, identified from a carboxylic acid side chain of different length, do not modify the good success of the reaction. All reactions tested have given the product of Thiol-ene and its byproduct sulfoxide.

The same reaction was performed using the allyl-glucose substrate added to bulky substrate NOP [Cys<sup>18</sup>] N/OFQ-NH<sub>2</sub> and the reaction is gone successfully, generating the unexpected sulfoxide byproduct. In conclusion, it can say that the optimization of the reaction time and the maintainance of inert environment are necessary requirements to provide mainly the desired product.

*Chapter 2*  
*Aberdeen's project*



## 1. INTRODUCTION

### 1.1 G-quadruplex DNA

It is important to remember that the metabolically active form of DNA in its major activities like replication, transcription, repair and recombination is single-stranded; while the double helix is actually its inactive form<sup>33</sup>.

For DNA to become single-stranded it must overcome thermodynamic and kinetic barriers necessary for the dissociation of the double helix. Commonly, this could be achieved in the cell with small molecules or binding proteins that recognise single-stranded DNA (such as chaperone proteins). Polypurine–polypyrimidine and other repetitive sequences can form non duplex and/or higher-ordered chromatin structures easily, which relate to a wide variety of biological activities. One family of structures originating from guanosine-rich tracts is referred to as G-quadruplex or G-tetraplex (Figure 1), first reported by Davies *et al.* in 1962<sup>39 34</sup>.

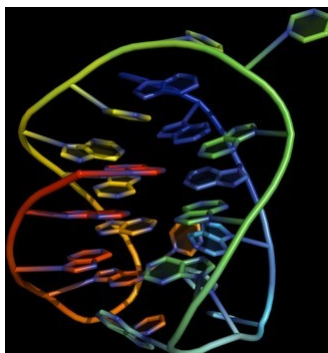


Figure 1: G-quadruplex structure.

A G-quadruplex is a single-stranded DNA secondary structure that consists of multiple vertically stacked guanine tetrads. It is characterized from Hoogsteen hydrogen bonds between the four guanines to form a planar G-tetrad<sup>35</sup>.

<sup>33</sup> N. W. Luedtke, *Chimia*, (2009), 63, 134-139.

<sup>34</sup> M. Gellert, M. N. Lipsett, D. R. Davies, *Proc. Natl. Acad. Sci USA*, (1962), 48, 2013-2018).

<sup>35</sup> Y. Qin, L. H. Hurley, *Biochimie*, (2008), 90, 1149-1171.

This DNA complex has different features, but common elements include:

- Four DNA strands formed from one or more DNA sequences;
- The presence of many overlays of  $\pi$ - $\pi$  stacked G-quartets, linked by phosphodiester backbone;
- The existence of non-G nucleotides as T and A can form non-helical loop regions;
- DNA complex can assume a parallel or anti-parallel structure or a mixture of both;
- For the stability of the complex is required the presence of cations like  $\text{Na}^+$  and  $\text{K}^+$ .

G-quadruplexes exhibit a remarkable dependency on alkali cations for their formation and stabilization. It has been reported that  $\text{Na}^+$  induces an anti-parallel strand; while  $\text{K}^+$  causes a completely different parallel structure<sup>36</sup>.

Finally the ions in the solution and the crowding in the environment influence the conformation of the complex.

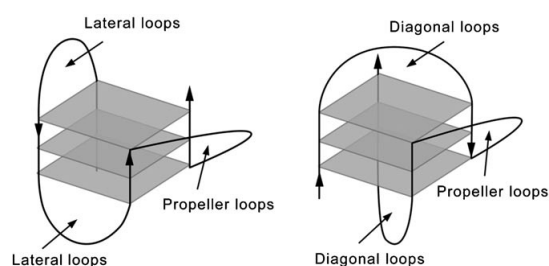


**Figure 2:** Loop region in G-quadruplex structures.

DNA complex can form intermolecular G-quadruplex structures as intermediates or precursors of recombination and/or viral integration, while intramolecular G-quadruplex has been implicated in the regulation of gene expression and chromosome stability<sup>39</sup>.

<sup>36</sup> J. Cuesta, M. A. Read, S. Neidle, *Mini Rev. Med. Chem.*, (2003), 3, 11-19.

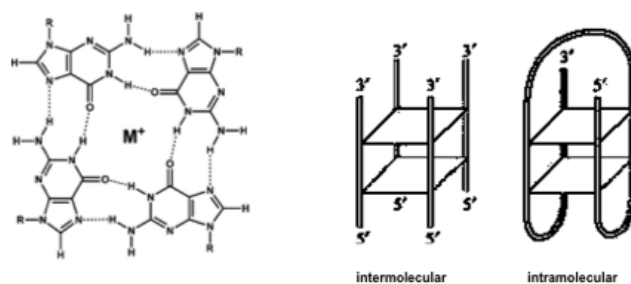


**Figure 3:** Structure of G-tetrad and an example of inter- and intramolecular G-quadruplex.

It is known that the variable polymorphism of DNA complex can adopt another structure called *i*-motif. The guanine tracts of a G-rich strand can form G-quadruplex structures, which are independent of pH and readily form at physiological pH; while cytosine tracts form the *i*-motif structures, that require hemiprotonated cytosine-cytosine pairs and they are dependant of pH. To provide an *i*-motif an acidic environment is often required<sup>37</sup>.

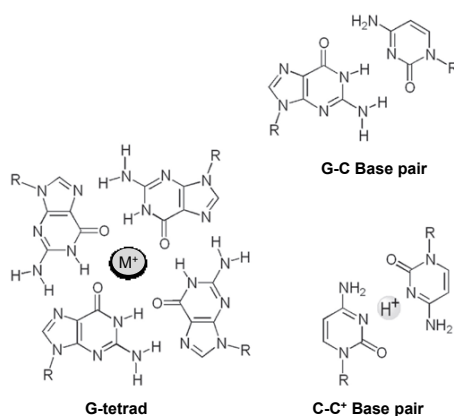


**Figure 4:** G-C base pair in G-quadruplex and C-C<sup>+</sup> base pairs in *i*-motif complex.

Approximately 30-40% human promoters contain a G-quadruplex motif and they are known to regulate many human genes (retinoblastoma susceptibility, insulin, muscle-specific, vascular endothelial growth factor, hypoxia inducible factor 1a, fragile X mental retardation genes), including oncogenes (c-myc, Bcl-2, c-kit, VEGF)<sup>38</sup>.

The important interest in this particular complex grew for its relevant biological role to “turn on” and “turn off” some physiological events<sup>39</sup>.

<sup>37</sup> S. Dhakal, J. Schonhoff, D. Koirala, Z. Yu, S. Basu, H. Mao, *J. Am. Chem. Soc.*, (2010), 132, 8991-8997.

<sup>38</sup> D. Monchaud, M.-P. Teulade-Fichou, *Org. Biomol. Chem.*, 6, (2008), 627-636.

<sup>39</sup> T.-M. Ou, Y.-J. Lu, J.-H. Tan, Z.-S. Huang, K.-Y. Wong, L.-Q. Gu, *ChemMedChem*, (2008), 3, 690-713).

## 1.2 Important G-quadruplexes in the human genome

A relevant number of important regions in the humane genome adopt G4 structures such as regulatory sequences, switch region, telomeric ends and oncogene promoters.

### Telomeres

Telomeres are non-coding DNAs consisting of tandem repeats of the sequence d(TTAGGG), located at the end of linear chromosomes and they are a safety system within each chromosome arm.

The control of telomere length is very important for cell cycle control, cellular immortalization and tumorigenesis. For this reasons the folding and the stabilization of a variety of G-quadruplexes in G-rich at the ends of telomeres sequences induce a normal regulation of their activities of in the cell cycle and other events<sup>45</sup>.

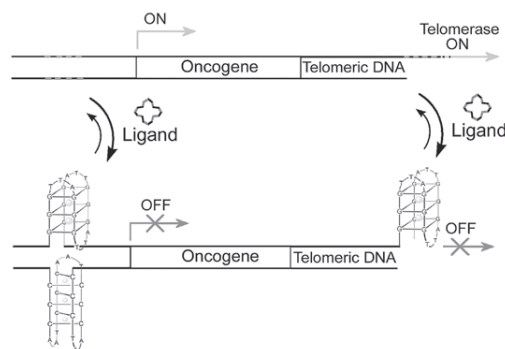


**Figure 5:** Scheme of the stabilization through a specific ligand of G4 and the switch off of telomerase activity.

### Bcl-2

The human Bcl-2 gene contains a G-rich tract upstream of the P1 promoter, which is critical for the regulation of Bcl-2 expression. It is a proto-oncogene and with other proteins it is involved in the control of programmed cell death. In different cancers it has been shown to be overexpressed.

The control of these G-rich sequences allows a crucial step in the regulation of Bcl-2 transcription<sup>45</sup>.

### VEGF

VEGF is human vascular endothelial growth factor with a G-rich sequence that controls its expression. It is a pluripotent cytochine and angiogenic growth factor, and it is involved in the stimulation of the proliferation, migration, survival and

permeability of endothelial cell. This factor, in many tumor processes, has a high activity, because during the cancer disease mechanism there is an elevated production of new blood vessels that require nutrients and oxygen. The regulation of this factor could be a fundamental point to slow this uncontrolled growth<sup>45</sup>.

### **c-kit**

c-kit is a proto-oncogene and belongs of the family of growth factor receptors. It contains G-rich tracts in the site essential for the promoter activity, which have high conservation in primates.

It has a crucial role in the regulation of the stimulus of proliferation, differentiation, migration and survival signal cell system<sup>45</sup>.

### **c-Myc**

c-Myc is an oncogene , which has a putative G-quadruplex-forming sequence in the promoter region of the gene<sup>40</sup>.

Simonsson *et al.* proposed the first intramolecular G-quadruplex structure within the c-Myc NHE III1 region, which was described as an antiparallel-stranded structure involving three G-tetrads formed from four G-tracts linked by two lateral loops and a central diagonal loop. c-Myc is linked to a wide range of human cancers, it modulates 10-15% of all cellular genes involved in cell cycle regulation, apoptosis, metabolism, cellular differentiation and cell adhesion. Its overexpression is linked with many malignant tumors, the stabilization of G4 in this region can suppress c-Myc transcriptional activation, down-regulate the expression of it, inhibit cell proliferation and induce apoptosis of cells<sup>45 41</sup>.

---

<sup>40</sup> H. T. Le, M. C. Miller, R. Buscaglia, W. L. Dean, P. A. Holt, J. B. Chaires, J. O. Trent, *Org. Biomol. Chem.*, (2012), 10, 9393-9404.

<sup>41</sup> V. Gonz'alez, L. H. Hurley, *Annu. Rev. Pharmacol. Toxicol.*, (2010), 50, 111-129.

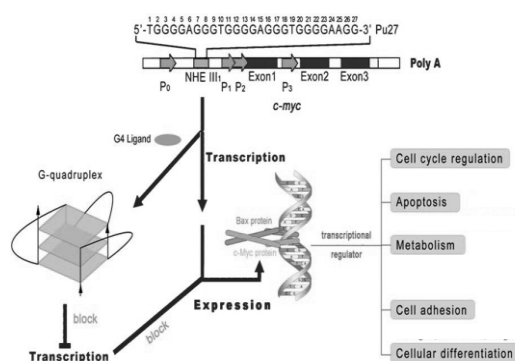


**Figure 6:** Scheme of the structure and biological role of c-Myc.

### ILPR: insulin linked polymorphic region

The insulin-linked polymorphic region is non coding minisatellite in the human insulin gene promoter. It is located 363 base pairs upstream of the insulin gene, known like a genetic loci involved in the genetic dysfunction associated with insulin-dependent diabetes mellitus<sup>42</sup>. It is composed of tandem repeats of the consensus sequence 5'-ACAG<sub>4</sub>T(G/C)(T/C)G<sub>4</sub>-3'<sup>43</sup>. The polymorphism of this region comes from a different repeat number of the oligonucleotides and as such the ILPRs are divided into three classes in relation to their length: class 1 (up to 700bp), class 2 (up to 1600bp) and class 3 (up to 2500bp)<sup>44</sup>. Variants of the ILPR sequence, that destabilize or preclude G-quadruplex formation, are also related with lower transcription rates, suggesting a possible role of G-quadruplex formation in the regulation of transcription the insulin gene. Supporting information was observed in the transcription factor Pur-1, which preferentially binds to ILPR tandem repeats that form inter- or intramolecular G-quadruplex structures. This has suggested the hypothesis that Pur-1 regulates insulin transcription through recognition of G-quadruplex structures in the ILPR; however, seems that regulation insulin gene transcription depending on an interplay of mutiple protein factors binding.

The G-quadruplex recognition did not in all cases correlate with transcriptional activity, suggesting that there may be different regulatory mechanisms that involve other protein interactions with the transcription mechanism or modifications of the ILPR complex<sup>48</sup>. The involvement of ILPR G-quadruplex in insulin gene expression suggests the possibility that a stabilization of this complex could restore the correct expression of the INS gene in diseases such as diabetes.

<sup>42</sup> A. C. Connor, K. A. Frederick, E. J. Morgan, L. B. McGown, *J. Am. Chem. Soc.*, (2006), 128, 4986-4991.

<sup>43</sup> M. C. U. Hammond-Kosack, K. Docherty, *FEBS Letters*, (1992), 301, 79-82.

<sup>44</sup> M. C. U. Hammond-Kosack, B. Dobrinski, R. Lurz, K. Docherty, M. W. Kilpatrick, *Nucleic Acids Research*, (1992), 20, 231-236.

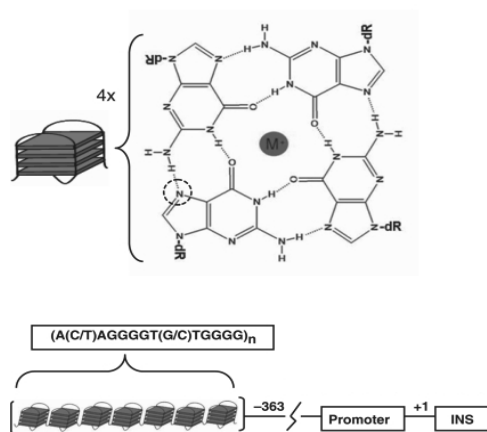


**Figure 7:** G-tetrad and schematic representation of ILPR upstream of insulin gene.

### 1.3 Small molecules binding to G-quadruplexes structures

The prevalence of these G-quadruplexes and their importance in biological processes has led to the study and development of small molecule ligands of the complex. The stabilization of the tetraplex can successfully restore some biological events involved in fundamental physiological mechanisms.

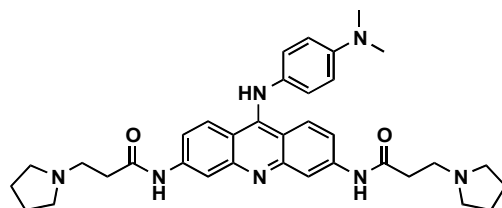
There are several ways to classify the different ligands<sup>44</sup>.

#### Protonated G-quadruplex ligands

Neidle, Hurley *et al.* suggest the development of compounds that are conceived with large flat aromatic systems prone to  $\pi$ -stacking with a G-tetrad platform, while retaining reasonable water solubility. The molecule has to show both hydrophobic and hydrophilic characteristics. An usual way to ensure this duality is to introduce protonable side arms like amine groups around an aromatic core; the potential ligand become watersoluble, with the charge far from the hydrophobic centre<sup>45</sup>.

The best compound produced was BRACO-19 able to interact simultaneously with three G-quadruplex grooves thanks to three side arms. Subsequently investigations have recently demonstrated the efficiency of BRACO-19, but it has been somewhat limited by pharmacological parameters (such as cellular uptake or membrane permeability<sup>44</sup>).

<sup>45</sup> D. Sun, B. Thompson, B. E. Cathers, M. Salazar, S. M. Kerwin, J. O. Trent, T. C. Jenkins, S. Neidle, L. H. Hurley, *J. Med. Chem.*, (1997), 40, 2113-2116.

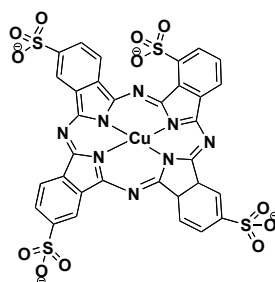


BRACO-19

### Anionic G-quadruplex ligands

Molecules belonging to this category are less known because the protonable side chains play a relevant role in the interaction with the complex.

A recent study of Sugimoto *et al.* suggests that the cationic molecules have high affinity but insufficient selectivity to G-quadruplexes compared with double-stranded DNA (dsDNA). Cu-APC (anionic copper phthalocyanine) is an anionic G-quadruplex-ligand and it should not engage in electrostatic interactions with G-quadruplex because of their negative charges; however, it should engage in  $\pi$ - $\pi$  stacking interactions with G-quadruplex. The binding affinity is apparently sacrificed for selectivity. Consequently, large  $\pi$ -planar compounds with anionic groups can be new scaffolds to develop G-quadruplex ligands<sup>46</sup>.



Cu-APC

### Metallo-organic G-quadruplex ligands

This class of molecules is highly interesting thanks to their easy synthetic access and their very promising G-quadruplex ligand properties. The central metal assumes the same position of the cation channel of G-quadruplex, enhancing the stacking interactions of the chelating agent inside<sup>47</sup>. Their cationic or highly polarized nature is also a clear advantage to improve the association with the negatively charged G-quadruplex-DNA.

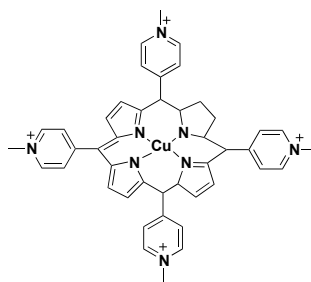
The metal centre is a parameter that plays an important role in the selectivity.

An example of metallo-organic ligand is Cu TMPyP4.

<sup>46</sup> H. Yaku, T. Murashima, D. Miyoshi, N. Sugimoto, *Chem. Commun.*, (2010), 46, 5740-5742.

<sup>47</sup> J. E. Reed, A. A. Arnal, S. Neidle, R. Vilar, *J. Am. Chem. Soc.*, (2006), 128, 5992-5993.

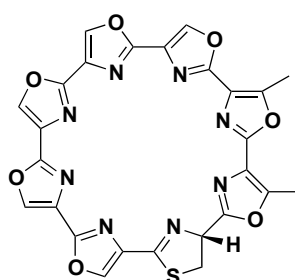




Cu TMPyP4

### Neutral macrocyclic G-quadruplex ligands

This class of ligands is small, with Telomestatin belonging to this category. Its one of lead compound used to recognize the G-quadruplex. The interest for Telomestatin is grown for its selectivity toward DNA single strand and for its neutral and cyclic shape. The peculiarity of this macrocyclic is that it works very well as a telomerase inhibitor, stabilize G-quadruplex without the presence of a cation salt, contain the proliferation of telomerase positive cells through the change of the length and conformation of telomeres, and finally induces the dissociation of telomere-related protein from telomeres. Other macrocyclic molecules were synthesized with the same core characterized from a tetra- or hexa-oxazole with different substitutions to mimic Telomestatin activity<sup>48 44</sup>.



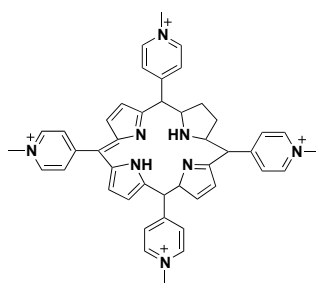
Telomestatin

### N-Methylated aromatic G-quadruplex ligands

<sup>48</sup> G. S. Minhas, D. S. Pilch, J. E. Kerrigan, E. J. LaVoie, J. E. Rice, *Bioorg. Med. Chem. Lett.*, (2006), 16, 3891–3895.

The design of the molecules of this category is based on the introduction of *N*-methylated aza-aromatic moieties.

This allows for a reduction of the electron density of the aromatic portion, an increasing of the  $\pi$ -stacking ability of the ligand and an improvement of the water solubility without the presence of cationic functionalities in side-chains. An example reported from Hurley *et al.*<sup>49</sup> explains that TMPyP4 belongs to this class and it has exclusive characteristics: good affinity for G-quadruplex, the ability to inhibit telomerase<sup>50</sup>, down-regulate the oncogenes expression and convert the antiparallel system in to a parallel structure of the G-complex. It works with an intercalation between adjacent G-tetrads and stacking of the porphyrin onto the external G-quartet without direct contact with the DNA-complex<sup>44 45</sup>.



**TMPyP4**

<sup>49</sup> K. Guo, A. Pourpak, K. Beetz-Rogers, V. Gokhale, D. Sun, L. H. Hurley, *J. Am. Chem. Soc.*, (2007), 129, 10220-10228.

<sup>50</sup> R. T. Wheelhouse, D. Sun, H. Han, F. X. Han, L. H. Hurley, *J. Am. Chem. Soc.*, (1998), 120, 3261-3262.

## 2. AIM OF THE PROJECT

The insulin-linked polymorphic region (ILPR) is a regulatory sequence located 363 base pairs (bp) upstream of the human insulin gene. It is characterized by multiple repeats of consensus sequence rich in guanine residues. The ILPR sequence is 5'-ACAG<sub>4</sub>T(G/C)(T/C)G<sub>4</sub>-3'. This kind of sequence assumes a particular structure defined as a G-quadruplex (G4) or tetraplex, characterized from only oligomers containing one or several runs of guanine residues.

These kind of structures are stabilized by Hoogsteen hydrogen bonding, involving the N-7 positions of the constitutive G-tracts<sup>49</sup>.

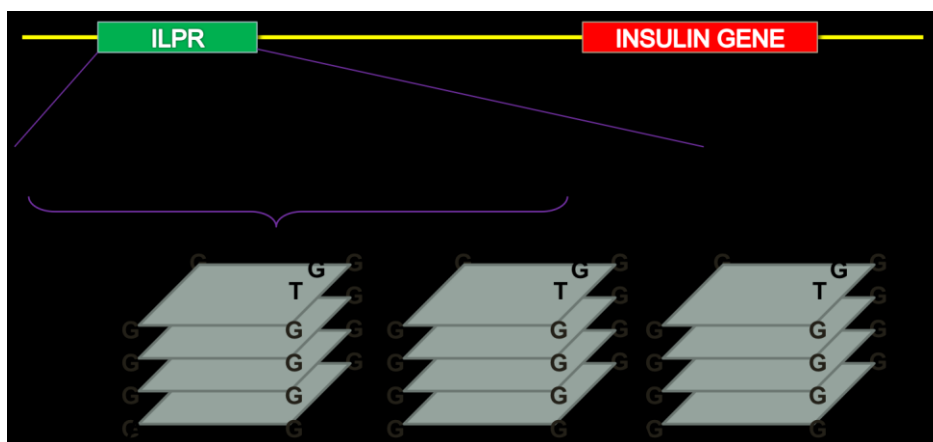


**Figure 8:** Schematic representation of ILPR upstream of the INS gene.

The ILPR is able to allow the activation and the expression of insulin gene, probably not directly inducing the expression of the gene, but through a relevant role in the midst of mechanisms of different binding proteins that participate in the activation of the gene itself<sup>48</sup>.

In the literature there is some evidence consistent with *in vivo* formation of G-quadruplexes, which have been proposed to increase the expression of insulin<sup>51</sup>.

Since insulin is directly related to the pathogenesis of diabetes, the potential regulatory role of the G quadruplex in the insulin expression has received close attention.

Some cations and small molecules stabilize this DNA complex. These types of molecules are able to intercalate in this structure and create different interactions<sup>45</sup>.

<sup>51</sup> G. Catignani Kennedy, M. S. German, W. J. Rutter, *Nature Genetics*, (1995), 9, 293-298.

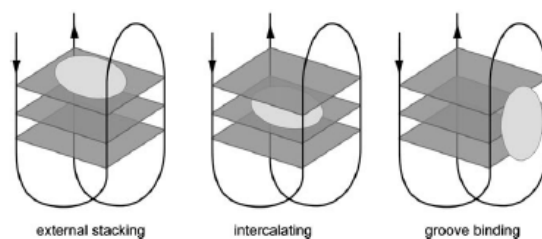


**Figure 9:** A representation of the possible interaction of a ligand with G4.

The main project aim is to alter the functionality of the ILPR, and subsequently alter INS gene expression using small molecules as ligands that will bind to and regulate the ILPR.

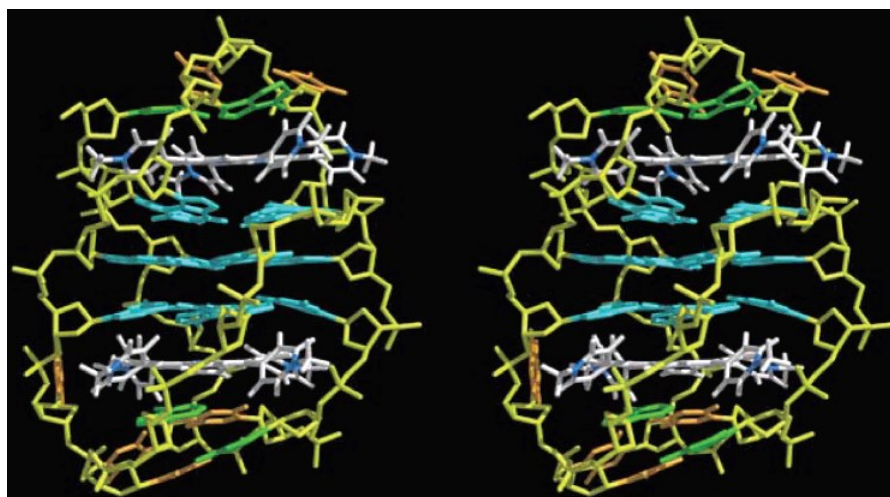


**Figure 10:** Structure of the docking model from a G4 and an interaction of a small molecule like TMPyP4.

This project was developed in some different steps.

*First step:* it was analyzed the concentration appropriate of oligonucleotides to proceed with the EMSA assay. It was used a library of oligonucleotides and then selected the best for these needs. (see table 1 experimental part).

*Second step:* initial focus on molecules known in literature to have a good ability to stabilize the tetraplex<sup>52</sup>. They are commercially available chemicals, such as porphyrins, in particular TMPyP4 (one of lead compound) and two molecules derived from this, Mesoporphyrin IX Dihydrochloride and Protoporphyrin IX<sup>42</sup>.

<sup>52</sup> D.-F. Shi, R. T. Wheelhouse, D. Sun, L. H. Hurley, *J. Med. Chem.*, (2001), 44, 4509-4523.

*Third step:* it is planned a synthesis of a new compound triazine derivate to enhance the binding and stabilize the G-quadruplex.

In order to show the changing of conformation of ILPR, it is examined other oligonucleotides such as c-Myc (Pu27) and Bcl-2 as sequences known capable of forming G-quadruplex.

### 3. DISCUSSION

#### 3.1 EMSA system approach and evaluation of different oligonucleotides

We tried to use different concentrations of oligonucleotides to know the best concentration to be analyzed by EMSA. Every oligos are involved in the gene expression.

<b>Tel.(1xG4)</b> [Btn]TTAGGGTTAAGGGTTAGGGTT AGGG	<b>Tel.(2xG4)</b> [Btn]TTAGGGTTAAGGGTTAGGGTTAGGGTTAGGGTTAAGGGTTAGG GTTAGGG
<b>ILPR-1(1xG4)</b> [Btn]ACAGGGGTGTGGGGACAGG GGTGTGGGG	<b>ILPR-1(2xG4)</b> [Btn]ACAGGGGTGTGGGGACAGGGGTGTGGGGACAGGGGTGTGGG GACAGGGGTGTGGGG
<b>Bcl-2</b> [Btn]GGGCGCGGGAGGAAGGGGG CGG	<b>c-Myc(Pu27)</b> [Btn]TGGGGAGGGTGGGGAGGGTGGGGAAGG
<b>VEGF</b> [Btn]GGGCGGGCCGGGGGCGGG	<b>c-Kit21</b> [Btn]GGGCGGGCGCGAGGGAGGG
<b>ILPR-2</b> [Btn]ACAGGGGTCTGGGGACAGGG GTCTGGGG	<b>ILPR-3</b> [Btn]AGAGGGGTCTGGGGAGAGGGGTCTGGGG
<b>ILPR-4</b> [Btn]ATAGGGGTGTGTGGATAGGG GTGTGTGG	

**Table 1:** The above table shows all oligos used in the gel-based assays, with sequences being shown in a 5' to 3' orientation. [Btn], biotin label covalently linked to 5' end of each oligo

Oligos use in this study (Table 1) undergo a process of denaturation by heating to 95°C for 5 minutes; followed by a gradual decrease (-1°C/minute) in temperature down to 4°C. As a control oligos were also heated to 95°C only with no slow cooling.

Preliminary experiments shown in figure a, b, c, d of each oligos lead to an oligo concentration of 10 nM being chosen for the experiments that follow.

Oligos were tested at different concentrations: 10 µM, 100 nM, 50 nM, 10 nM and 1 nM. In a preliminary screening of all oligos, conformational changes in the

presence or absence of KCl were tested. Previous studies by Simonsson *et al.* have demonstrated that under physiological conditions, the guanine-rich sequences can create a G-quadruplex structure and that is K<sup>+</sup>-dependent<sup>41</sup>.

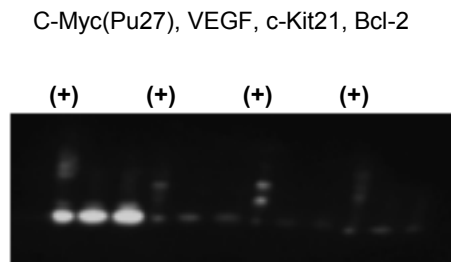


**Figure 11:** The EMSA intramolecular G-quadruplex structures of C-Myc(Pu27), VEGF, c-Kit21, Bcl-2 promoter in the presence (+) or absence of 100 mM KCl.

All oligos tested showed a large increase in the amount of secondary structure formation in the presence of K<sup>+</sup> (Figure 11). KCl concentrations of 100 mM are at physiological concentrations of K<sup>+</sup> found in most human cells.

### 3.2 Investigation of interaction between G-quadruplexes and small-molecules ligands

Four oligos were selected to be tested further:

ILPR-1(1xG4); ILPR-1(2xG4); c-Myc(Pu27) and Bcl-2. ILPR oligos are either one or two repeats of the ILPR G-quadruplex sequence with 1 or 2 repeats of 5'-ACAGGGGTGTGGGGACAGGGGTGT-3' DNA sequence. c-Myc(Pu27) and Bcl-2 oligos were used as controls because they are examples of well characterised and studied G-quadruplexes.

*TMPyP4* (5,10,15,20Tetrakis(1methylpyridinium4yl)porphyrinetetra(*p*-toluenesulfonate)) is a cationic porphyrin which is known to inhibit the telomerase in both a cell-free system and living cells and to downregulate the expression of oncogenes, such as c-Myc, and to convert anti-parallel topologies to parallel forms of quadruplexes<sup>44</sup>.

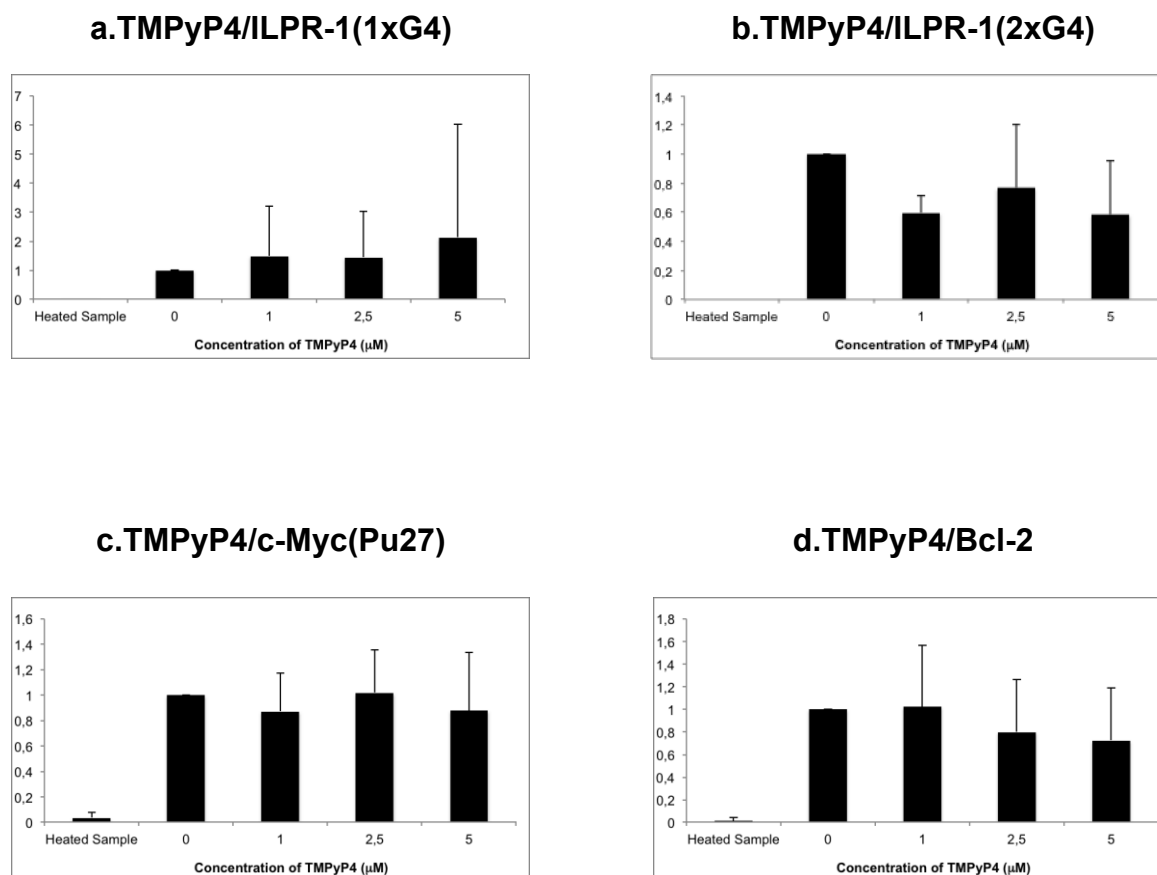


**Figure 12(a,b,c,d):** Bar graph showing the gel-based assay results of the effect of TMPyP4 on formation of secondary structure. Bars represent the average of five experiments quantified using Image J software. The samples were heated to 95°C then cooled slowly as explained on page 162. **Heated sample**, control; **0**, 100 mM KCl; **1**, 1  $\mu\text{M}$  TMPyP4; **2,5**, 2,5  $\mu\text{M}$  TMPyP4; **5**, 5  $\mu\text{M}$  TMPyP4.

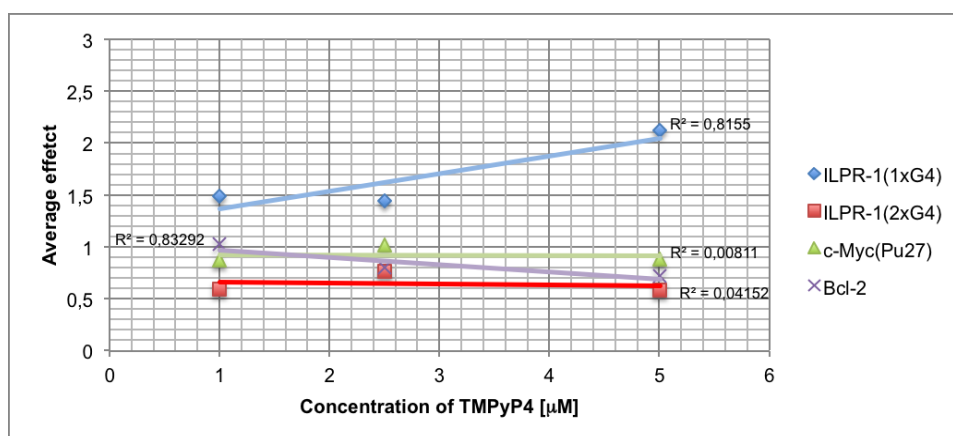


**Figure 13:** x y scattergraph that summarizes the data shown in the bar graphs in figures 12(a,b,c,d).

In literature, there are some evidence that the best concentrations of Porphyrins in the sample are in range between  $[1\mu\text{M}] \geq [5\mu\text{M}]$ <sup>53</sup>.

<sup>53</sup> M. A. Shammam, R. J. S. Reis, M. Akiyama, H. Koley, D. Chauhan, T. Hideshima, R.K. Goyal, L. H. Hurley, K. C. Anderson, N. C. Munshi, *Mol. Cancer. Ther.*, (2003), 2, 825-833.



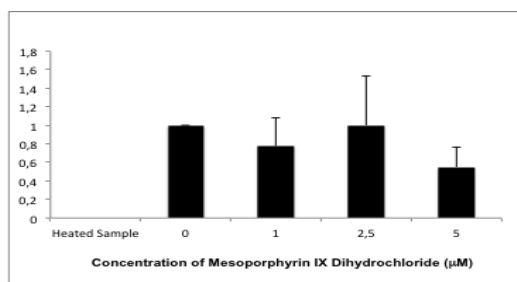
Indeed summarizing the data (Figure 12), it is clear TMPyP4 [5 $\mu$ M] can induce the formation of secondary structure with ILPR-1(1xG4), while ILPR-1(2xG4) produces less secondary structure in the presence of TMPyP4. One possible explanation of this effect could be the weight and the length of the ILPR-1(2xG4) structure that reduce the intra- and intermolecular interaction of the ligand. In x y scattergraph (Figure 13) the  $R^2$  is a value of the linear regression that puts in linear relationship a dependent variable (the average effect) with an independent value (substance concentration). In figure 13 ILPR-1(1xG4) ( $R^2 = 0.8155$ ) and Bcl-2 ( $R^2 = 0.8329$ ) demonstrate a good fit with the regression line; while ILPR-1 (2xG4) and c-Myc (Pu27) gave results that did not fit well to the linear regression line for these data.

The second ligand tested was *Mesoporphyrin IX Dihydrochloride*, a different kind of porphyrin for its different functionality in the external chains, the aromatic system is substituted with alifatic chains. Previous research has identified this compound as a potential quadruplex ligand<sup>54</sup>.

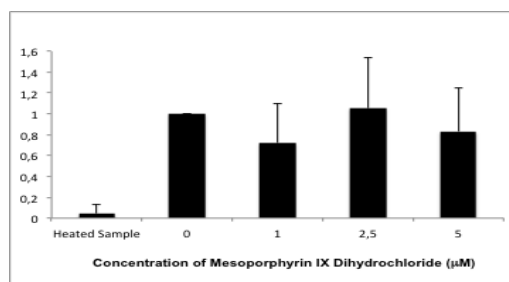
---

<sup>54</sup> J. M. Nicoludis, S. P. Barrett, J.-L. Mergny, L. A. Yatsunyk, *Nucleic Acids Research*, (2012), 40, 5432-5447.

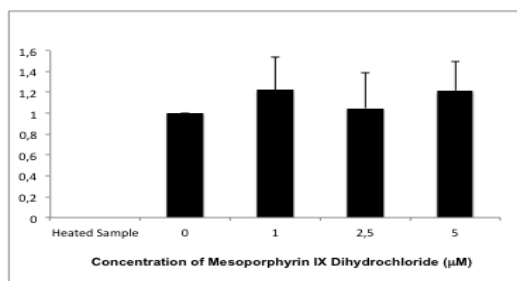
**a. Mesoporphyrin IX Dihydrochloride/ILPR-1(1xG4)**



**b. Mesoporphyrin IX Dihydrochloride/ILPR-1(2xG4)**



**c. Mesoporphyrin IX Dihydrochloride/c-Myc(Pu27)**



**d. Mesoporphyrin IX Dihydrochloride/Bcl-2**

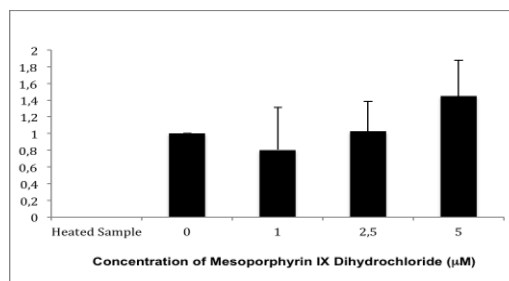


**Figure 14(a,b,c,d):** Bar graph showing the gel-based assay results of the effect of Mesoporphyrin IX Dihydrochloride on formation of secondary structure. Bars represent the average of five experiments quantified using Image J software. The samples were heated to 95°C then cooled slowly as explained on page 162. **Heated sample**, control; **0**, 100 mM KCl; **1**, 1μM Mesoporphyrin IX Dihydrochloride; **2,5**, 2,5μM Mesoporphyrin IX Dihydrochloride; **5**, 5μM Mesoporphyrin IX Dihydrochloride.

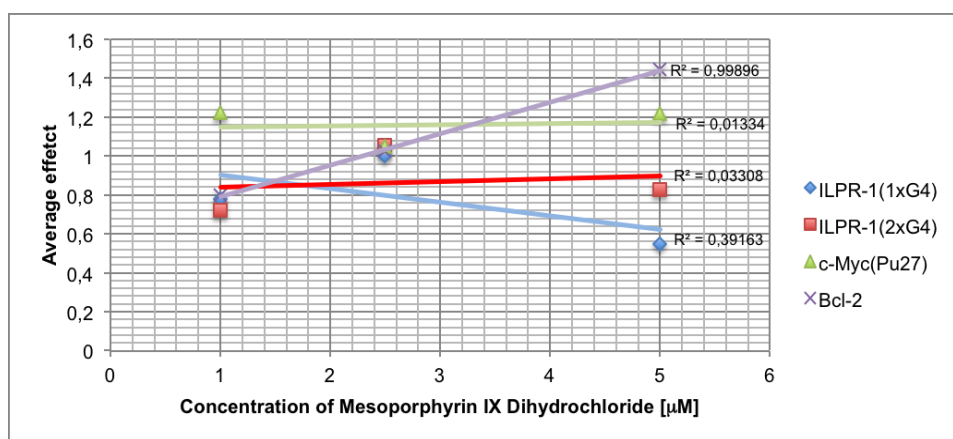


**Figure 15:** x y scattergraph that collects the data displayed in the bar graphs in figures 14(a,b,c,d).

Mesoporphyrin IX dihydrochloride was incubated with different oligos.

Each data set (Figure 14) showed Mesoporphyrin IX dihydrochloride had a good activity at [2.5μM], that is not significantly able to stabilize the G-quadruplex but it can change the quadruplex conformation. In the x y scattergraph  $R^2$  indicates that

only the Bcl-2 oligo shows a strong correlation with the linear regression line ( $R^2=0.99896$ ).

The third ligand analyzed was *Protoporphyrin IX*, which has similar lateral chains of Mesoporphyrin with more conjugations of alkene chains. In the literature it has been shown to interact with different DNA structures<sup>55</sup>.

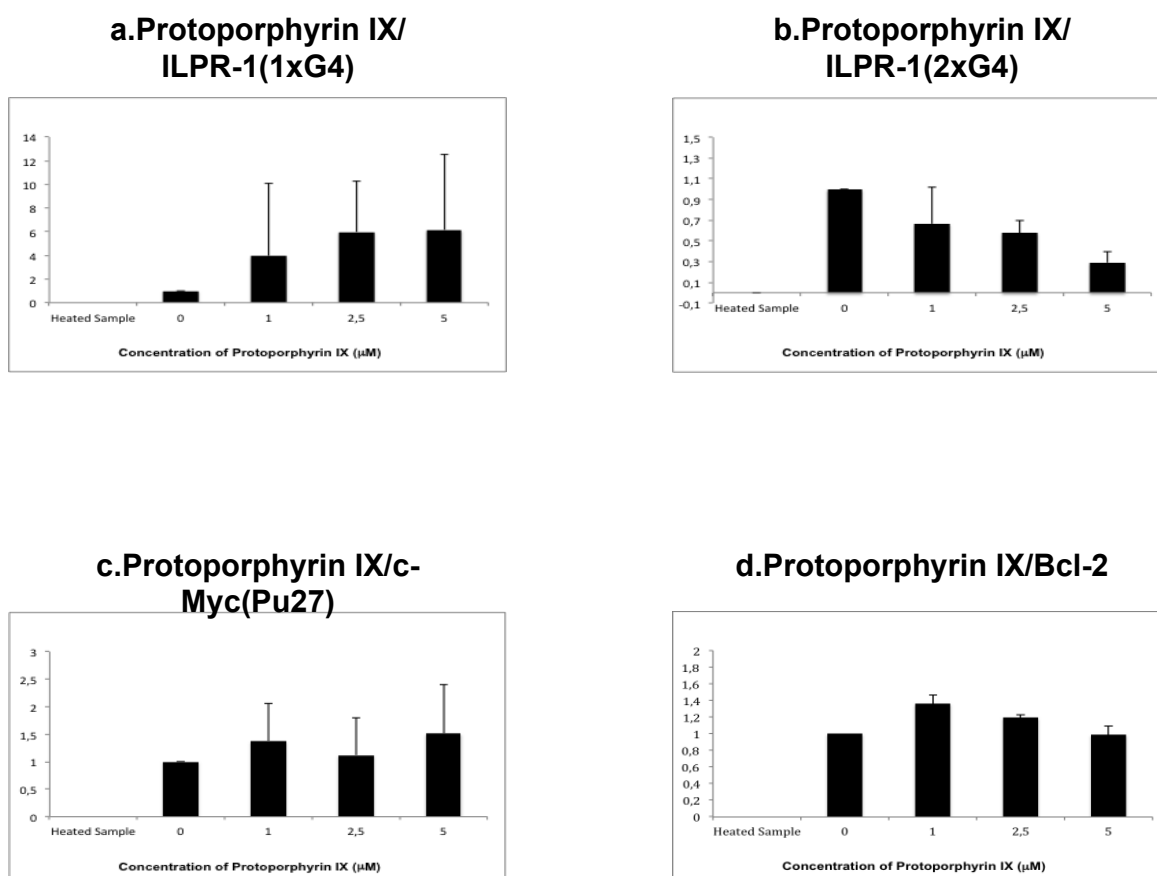


**Figure 16(a,b,c,d):** Bar graph showing the gel-based assay results of the effect of Protoporphyrin IX on formation of secondary structure. Bars represent the average of five experiments quantified using Image J software. The samples were heated to 95°C then cooled slowly as explained on page 162. **Heated sample**, control; **0**, 100 mM KCl; **1**, 1 $\mu\text{M}$  Protoporphyrin IX; **2,5**, 2,5 $\mu\text{M}$  Protoporphyrin IX; **5**, 5 $\mu\text{M}$  Protoporphyrin IX.

<sup>55</sup> T. Li, E. Wang, S. Dong, *Anal. Chem.*, (2010), 82, 7576-7580.

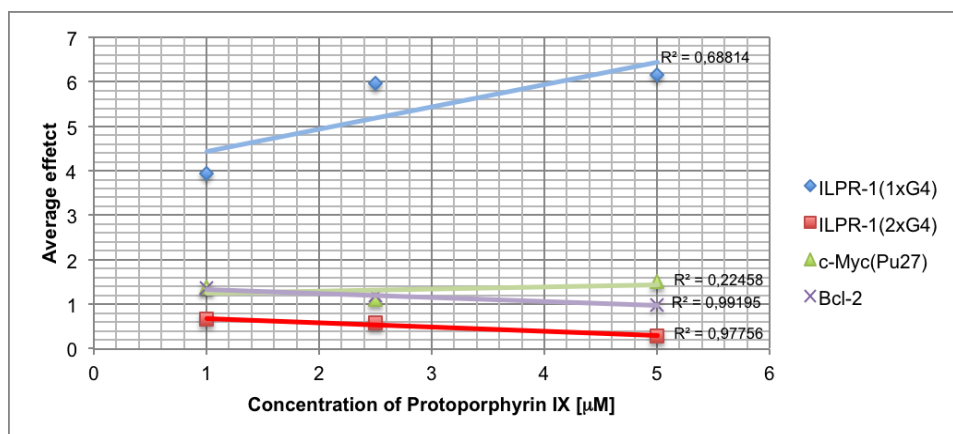


**Figure 17:** x y scattergraph that gathers the data seen above in the bar graphs in figures 16(a,b,c,d).

In the bar graph (Figure 16) we can observe that ILPR-1(1xG4) with Protoporphyrin has a large change of conformation, at [2.5 µM] and [5µM]. These data are not backed up by the x y scattergraph (Figure 17) because the  $R^2$  value is better for Bcl-2 ( $R^2 = 0,99195$ ) and ILPR-1(2xG4) ( $R^2 = 0,97756$ ).

Every oligonucleotide have a different behaviour in the presence of Protoporphyrin.

Taking a general comparison between the three porphyrins studied we can observe that TMPyP4 is able to induce change in DNA conformation, while Mesoporphyrin having an intermediate activity and Protoporphyrin is the least effective.

### 3.3 Rational synthesis of the new compound

The quadruplex-stabilization happens via  $\pi$ - $\pi$  stacking and electrostatic interactions due to the binding of the ligand (usually a flat aromatic molecule) on the G-quartet usually on the top and/or bottom of the external- face of the quadruplex<sup>42</sup>. Electrostatic interactions are required between charged ligands and the G-quadruplex DNA scaffold, they induce an important selectivity, but also pinpoint the role of protonated sidearms for strongly participation in the stabilization.

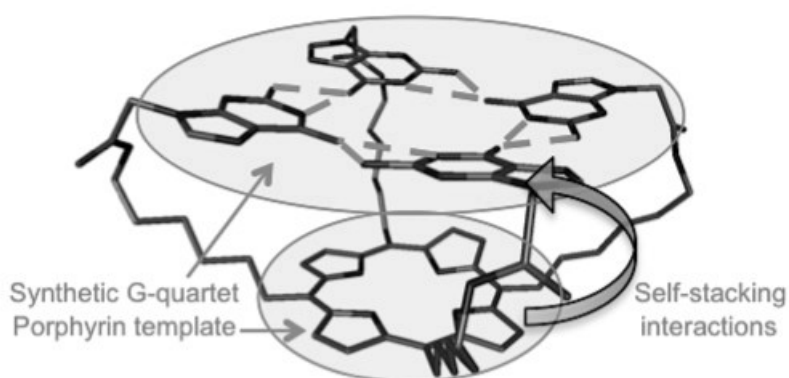
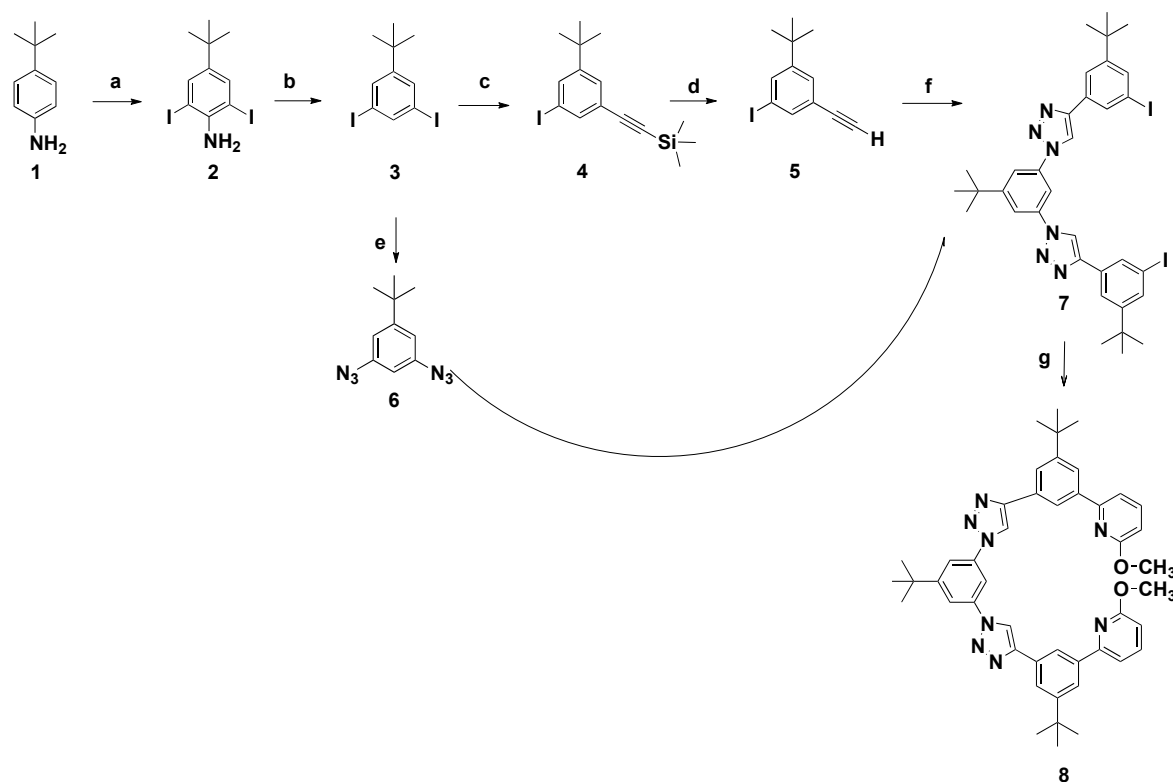


**Figure 18:** Interactions between G-quartet and ligand with protonated sidearms.

Synthesizing a compound with similar characteristics required to bind with DNA structures like the aromatic core, basic functionality like pyridine and an hydrophobic portion, was designed. In the literature there are different types of G-quadruplex ligand<sup>39 44</sup>.

The synthesis of the new compound has been designed with the idea of using a strategy of synthesis well known: the "Click chemistry", in particular exploiting the advantages of Cu(I)-catalyzed Huisgen cycloaddition reaction<sup>56</sup>.

<sup>56</sup> A. D. Moorhouse, A. M. Santos, M. Gunaratnam, M. Moore, S. Neidle, J. E. Moses, *J. Am. Chem. Soc.*, (2006), 128, 15972-15973.



a.  $\text{BnEt}_3\text{ICl} + \text{ICl} \Rightarrow (\text{BnEt}_3\text{N})\text{ICl}_2$ , DCM,  $\text{CaCO}_3$ , MeOH (Y=50%); b.  $^t\text{Bu}$ -nitrite, DMF,  $60^\circ\text{C}$  (Y=92%); c. ethynyltrimethylsilane,  $\text{PdCl}_2/(\text{PPh}_3)_2/\text{CuI}$ ,  $i\text{-Pr}_2\text{NH}/\text{THF}/\text{N}_2$  (Y=59%); d.  $\text{KF}/\text{MeOH}/\text{THF}$  (Y=34%); e.  $\text{NaN}_3/\text{CuI}/\text{DMEA}$ , Na ascorbate,  $\text{EtOH}:\text{H}_2\text{O}:\text{PhMe}$  (7:3:1), reflux (Y=71%); f.  $\text{CuSO}_4/\text{Na}$  ascorbate,  $\text{EtOH}:\text{H}_2\text{O}:\text{PhMe}$  (7:3:1) (Y=81%); g.  $\text{CsF}/\text{Pd}(\text{PPh}_3)_4$ , 2-Butylstannanyl-6-Methoxy-pyridine,  $\text{CH}_3\text{CN}$ ,  $90^\circ\text{C}$  (Y=31%9)

**Scheme 1:** Scheme of synthesis.

From  $^t\text{Bu}$ -aniline it was did a iodination (compound 2) and a deamination to obtain the compound 4-(*tert*-butyl)-2,6-diiodoaniline each in a quantitative yield (compound 3)<sup>57</sup>.

Then it is introduced an alkinic function through a Sonogashira reaction to achieve ((3-(*tert*-butyl)-5-iodophenyl)ethynyl)trimethylsilane (compound 4) in a middle yield. The release of the protecting group has allowed to yield the desired alkyne compound 5.

In the same time from the compound 3 it was synthetized its diazide (compound 6). Subsequently the reaction between the compound 1,3-diazido-5-(*tert*-butyl)benzene (compound 6) and 1-(*tert*-butyl)-3-ethynyl-5-iodobenzene

<sup>57</sup> PCT/US2005/001875.

(compound 5) has produced the 1,1'-(5-(tert-butyl)-1,3-phenylene)bis(4-(3-(tert-butyl)-5-iodophenyl)-1H-1,2,3-triazole) in a good yield (compound 7)<sup>58</sup>.

In order to get the compound ZAL026 (compound 8) it was used a Stille reaction, in which it was done a bi-substitution of the iodine with a 2-methoxy-6-(tributylstannyl)pyridine.

For observe the activity of this compound was tested with the selected oligos with the same procedure in the EMSA assay.

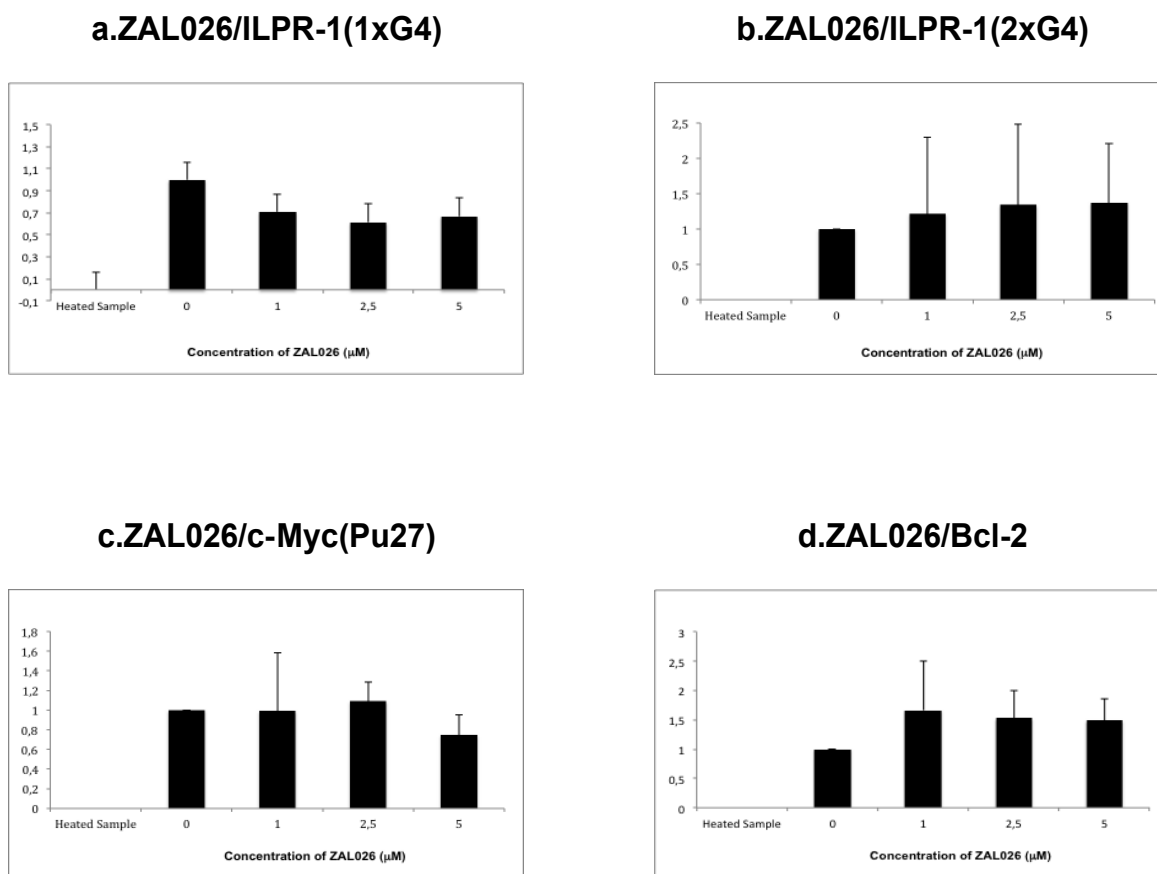


**Figure 19(a,b,c,d):** Bar graph showing the gel-based assay results of the effect of ZAL026 on formation of secondary structure. Bars represent the average of five experiments quantified using Image J software. The samples were heated to 95°C then cooled slowly as explained on page 162. **Heated sample**, control; **0**, 100 mM KCl; **1**, 1μM ZAL026; **2,5**, 2,5μM ZAL026; **5**, 5μM ZAL026.

<sup>58</sup> Y. Li, A. H. Flood, *Angew. Chem.*, (2008), 120, 2689-2692.

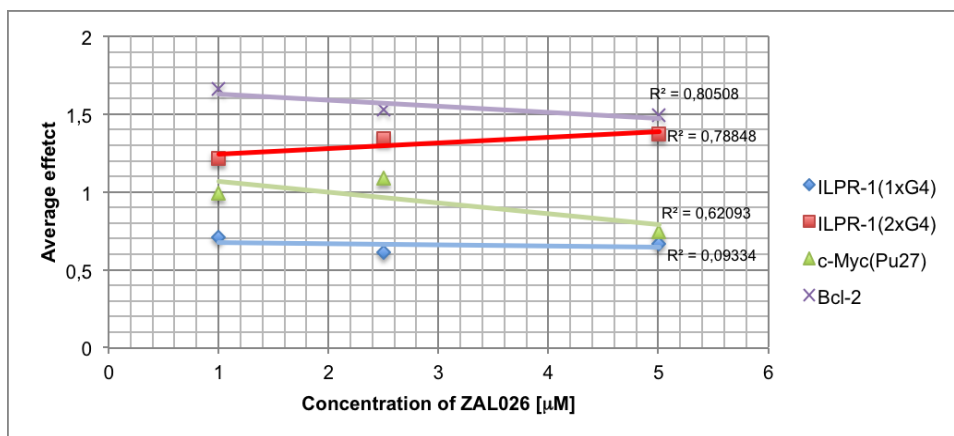


**Figure 20:** x y scattergraph that puts together the informations collected in the bar graphs in figure 19(a,b,c,d).

The compound ZAL026 shows a slight activity with the DNA complex, but the data obtained with x y scattergraph indicate that the  $R^2$  values are not indicative of a string correlation (e.g. ILPR-1(2xG4)  $R^2=0,78848$ ).

### 3.4 Circular dichroism analysis

Each sample was prepared with oligonucleotides of interest in TE buffer, plus or minus addition of KCl and in different thermal conditions.

#### ILPR-1(1xG4)

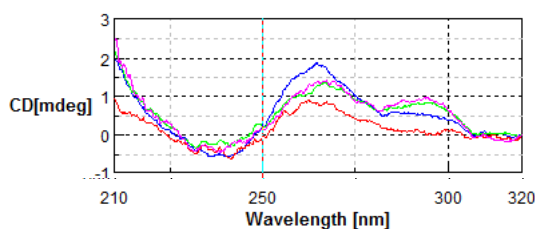


**Figure 21a:** CD spectra of ILPR-1(1xG4). **Blue spectra**, TE buffer +KCl; **Red spectra**, heated to 95°C; **Pink spectra**, post thermal cooling to 20°C; **Green spectra**, post thermal cooling to 5°C.

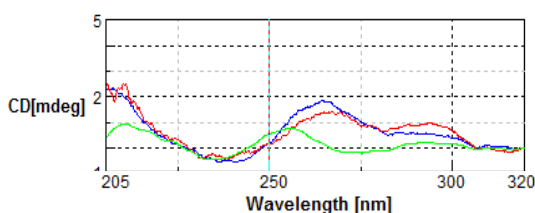


**Figure 21b:** CD spectra of ILPR-1(1xG4). **Blue spectra**, TE buffer +KCl; **Red spectra**, TE buffer post thermal incubation and cooling to 20 °C.



In figure 21a and 21b the spectra of ILPR-1(1xG4) without addition of chemical is shown. The pink and green line are similar, the blue and red line are slightly different. There are four identificative peaks: positive band at 210 nm, negative band close to 240 nm, positive band at 260 nm and 290 nm. In the figure 21b the green line is representative of oligo in the absence of KCl, which shows peaks are at the same wavelength but are lower and wider, which may be indicative of a mixture of different G-quadruplex structures, that are not stable. Following this observation the spectra is representative that ILPR-1(1xG4) forms apparently a propeller-type structure of G-quadruplex<sup>59</sup>.

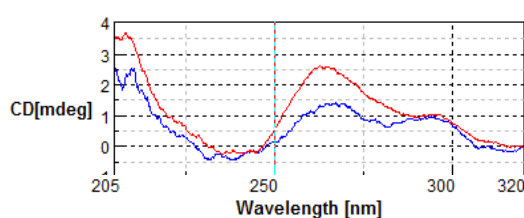


**Figure 22:** CD spectra of ILPR-1(1xG4). **Blue spectra**, TE buffer +KCl; **Red spectra**, TE buffer +KCl+TMPyP4 post thermal cooling to 20 °C.

In this case the addition of TMPyP4 highlights the peaks of the red line which are very similar to those of the blue line of the reference spectrum. TMPyP4 therefore appears to show an important role in the stabilization of propeller-type structure of ILPR-1(1xG4).

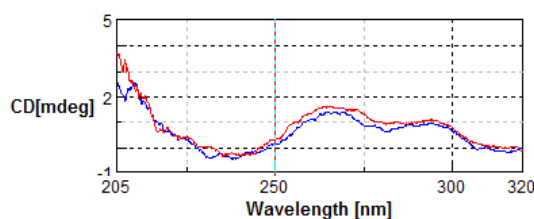


**Figure 23:** CD spectra of ILPR-1(1xG4). **Blue spectra**, TE buffer +KCl; **Red spectra**, TE buffer +KCl+Mesoporphyrin IX Dihydrochloride post thermal cooling to 20 °C.

The addition of Mesoporphyrin does not change clearly the spectra, the peaks are the same explained above but they are less marked (pink and green line in the figure 21a). This chemical does not therefore define the G-quadruplex complex.

<sup>59</sup> E. M. Rezler, J. Seenisamy, S. Bashyam, M.-Y. Kim, E. White, W. D. Wilson, L. H. Hurley, *J. Am. Chem. Soc.*, (2005), 127, 9439-9447.

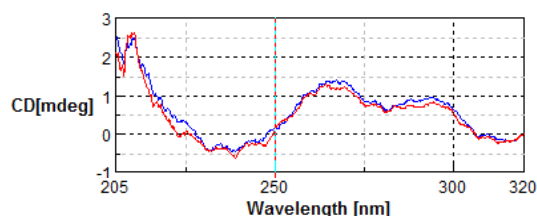


**Figure 24:** CD spectra of ILPR-1(1xG4). **Blue spectra**, TE buffer +KCl; **Red spectra**, TE buffer +KCl+ Protoporphyrin IX post thermal cooling to 20 °C.

Protoporphyrin seems more able than Mesoporphyrin, to produce quadruplex structures, but it does not work like TMPyP4. The peaks are the same and the ILPR-1(1xG4) has a propeller-type structure.

### ILPR-1(2xG4)

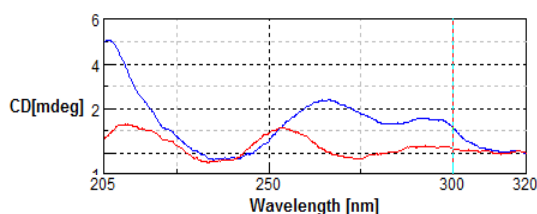


**Figure 25:** CD spectra of ILPR-1(2xG4). **Blue spectra**, TE buffer +KCl; **Red spectra**, TE buffer post thermal cooling to 20 °C.

ILPR-1(2xG4) is twice the length of ILPR-1(1xG4).

These data highlight the difference between the presence or absence of KCl.

The introduction of KCl presents a clearly peaks (line blue) at 210 nm, 260 nm and 290 nm positive bands while at 240 nm negative band. The CD spectrum exhibits a maxima-minima pattern similar to the propeller-type structure of ILPR-1(2xG4).

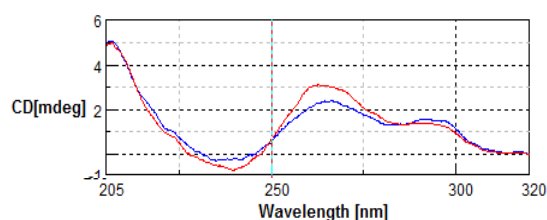


**Figure 26:** CD spectra of ILPR-1(2xG4). **Blue spectra**, TE buffer +KCl; **Red spectra**, TE buffer +KCl+ TMPyP4 post thermal cooling to 20 °C.

The spectrum of the sample with TMPyP4 has a much more pronounced feature near 260 nm in positive typical of the parallel structure of DNA quadruplex, the other band at 290 nm in positive confirms the stabilization of a propeller-type G-complex.

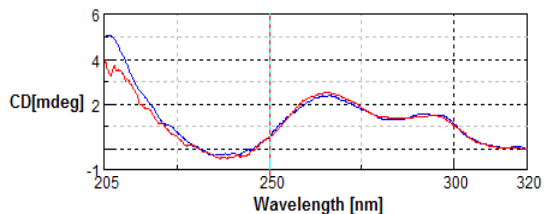


**Figure 27:** CD spectra of ILPR-1(2xG4). **Blue spectra**, TE buffer +KCl; **Red spectra**, TE buffer +KCl+ Mesoporphyrin IX Dihydrochloride post thermal cooling to 20 °C.

The CD spectra of DNA is very similar when no Mesoporphyrin is present in the solution. There is no difference between the spectra in the presence or absence of mesoporphyrin.

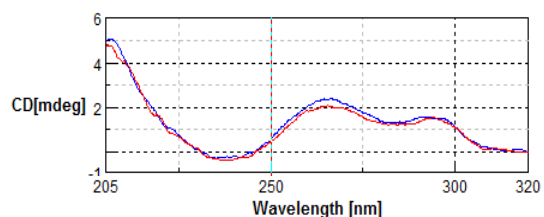


**Figure 28:** CD spectra of ILPR-1(2xG4). **Blue spectra**, TE buffer +KCl; **Red spectra**, TE buffer +KCl+ Protoporphyrin IX post thermal cooling to 20 °C.

The Porphyrin IX introduction demonstrates a lack of functionality as it cannot enhance quadruplex DNA formation.

Probably the binding is not enough to stabilize more the complex.

The data about ZAL026 are under study in Glasgow University.

#### 4. CONCLUSION

This preliminary study was used to test the capacity for different small molecules to alter the structure of the ILPR G-quadruplex structure. This was achieved through the use of electrophoretic mobility shift assays (EMSA) carried out on ILPR DNA oligo sequences, to show secondary structure formation. This was then further validated through the use of circular dichroism (CD).

Overall, the main aim was to alter the functionality of the ILPR, and ultimately alter INS gene expression using small molecules that will bind to and regulate the ILPR. Firstly, a series of oligos were tested for their ability to form secondary structure following a denaturation by heating to 95°C. Gradual cooling of the oligo samples then allowed secondary structure to form. As a control oligos were also heated to 95°C without gradual cooling. The oligos were shown to exhibit secondary structure formation only in the presence of K<sup>+</sup> cations, as is well documented in the literature.

For this project four oligos were selected: ILPR-1(1xG4); ILPR-1(2xG4); c-Myc(Pu27) and Bcl-2. The ILPR-1 oligos are based on the endogenous ILPR sequence found in the human genome, while the last two were chosen as well known G-quadruplex structures found in oncogene promoters.

Each of the above oligos were analyzed with different small molecules to understand if they were able to stabilize them in their secondary structure or G4. The molecules tested were TMPyP4, Mesoporphyrin IX Dihydrochloride and Protoporphirin IX.

The above small molecules were chosen as they have shown stabilization of G-quadruplexes in line with the data in literature. Based on previous experiments in the literature, they have exhibited the best activity with a concentration of 2.5 μM and 5 μM. Furthermore, CD analyses were carried out on these samples (oligos + chemical compound + cation + buffer) and the data obtained confirm that TMPyP4 is the best stabilizer of DNA complex. In every CD spectra obtained it was confirmed that the ILPR quadruplex assumes a propeller-type structure in the presence of TMPyP4.

Subsequently, a new molecule ligand was synthesised that was shown to interact and stabilise the quadruplex oligos (compound ZAL026). It was designed maintaining the main requirements, known in literature, to achieve a good interaction with the complex. This molecule was only tested with EMSA assay and

it has shown a slight ability to interact with the G-quadruplex. Unfortunately there is not CD analysis because this is currently under study.

This study was planned with the idea to build some knowledge of how these small molecules may interact and influence G-quadruplex structure. Future work will be based around the development of a cell culture system using luciferase and/or other reporter genes. This will provide a robust and physiologically relevant assay to test the ability of small molecules to alter gene expression.

*Chapter 3*  
*Experimental Section*

## **PART 1**

### **4.1 General Methods**

Aminoacids, protected amino acids, resins for solid phase peptide synthesis and chemicals were purchased from Bachem, Novabiochem, Iris Biotech GmbH or Fluka. All other reagents were from Sigma or Merck and were of the highest purity available.

Flash chromatography was performed on Silica gel Merck 60-200 mesh.

Analytical Thin Layer Chromatographies (TLC) were performed on Macherey-Nagel poligram SIL/UV 254 of 0,25 mm plate, using detection systems such as a UV lamp at 254 nm and  $\text{KMnO}_4$  in aqueous solution at 2%.

NMR data were recorded on VARIAN 200MHz and 400MHz. All chemical shifts ( $\delta$ ) are expressed in parts per million and coupling constant (J) are given in Hertz. Abbreviations used for peak multiplicity are: s, singlet; br s, broad singlet; d, doublet; t, triplet; q, quadruplet; quint, quintuplet; m, multiplet.

The molecular weights of the intermediates and final products were determined by a mass spectrometer electrospray ESI MICROMASS ZMD 2000.

The exact mass was found with a HPLC-CHIP Cube ESI-Q-TOF Agilent 6520.

## 4.2 Peptide synthesis

The peptides of Table 3, table 4 and [Cys<sup>18</sup>] N / OFQ were synthesized in SPPS using the chemical strategy Fmoc/<sup>t</sup>Bu<sup>60</sup>, using an automatic synthesizer Syro XP (Biotage Sweden).

This synthetic method involves the synthesis of the peptide from the C-terminal residue linked to a solid support, through subsequently reactions of deprotection of  $\alpha$ -amino acid group attached to the peptide chain, followed by acylation of the amino group with the carboxyl component of the next aminoacid, suitably activated. For the peptide analogues were used a rink amide MBHA resin (*p*-Methylbenzhydrylamine resin). It is characterized from a neutral aminoacid (valine) connected to a polystyrene support (copolymer of vinylbenzene linear bridges with 1% of divinylbenzene) and the linker (Fmoc-Rink amide). This type of linker allows the removal of the peptide from the resin by treatment with TFA in order to obtain the C-terminal end free.

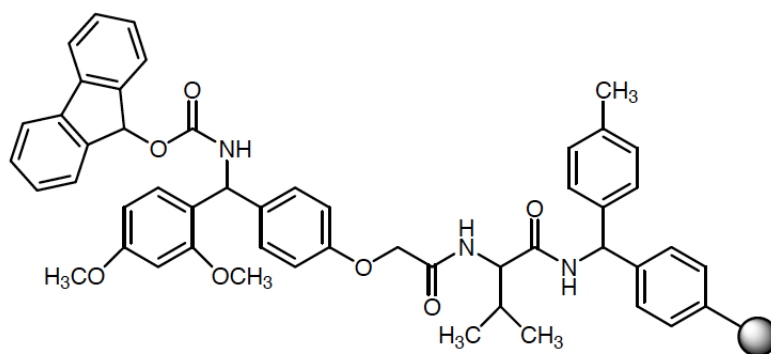


**Figure 34:** Chemical formula of the resin linker rink amide MBHA.

The starting point for each synthetic cycle begins with the removal of the Fmoc protecting group from the  $\alpha$ -amino function using a solution of 40% piperidine in DMF. The  $\alpha$ -carboxyl functionality of each single aminoacid was activated with DIPCIDI (N,N'-Diisopropylcarbodiimide) in the presence of HOBt (Hydroxybenzotriazole) using a molar excess of 4x respect to the amine component anchored to the resin. The side chains of the aminoacids were protected, when necessary, with acid labile protecting groups such as Boc for Lys; Pmc for Arg, <sup>t</sup>Bu for Tyr, Ser and Thr, Trt for Asn, Gln and Cys. At the end of the synthesis process, the peptide was removed from the resin and simultaneously deprived of the protecting groups in the side chain, through the treatment for 1.5 h

<sup>60</sup> N. L. Benoiton, *Chemistry of Peptide Synthesis*. Taylor & Francis, (2005), 125–154.



with a solution of TFA, H<sub>2</sub>O, Et<sub>3</sub>SiH (9:0.5:0.5); the exhausted resin was removed by filtration and then the mixture of residue solvent evaporated.

The crude peptide was crystallized in diethyl ether and the resulting solid purified by preparative HPLC. In figure 35 is reported the synthesis of peptide 20.

The other compounds were synthesized in a similar way.

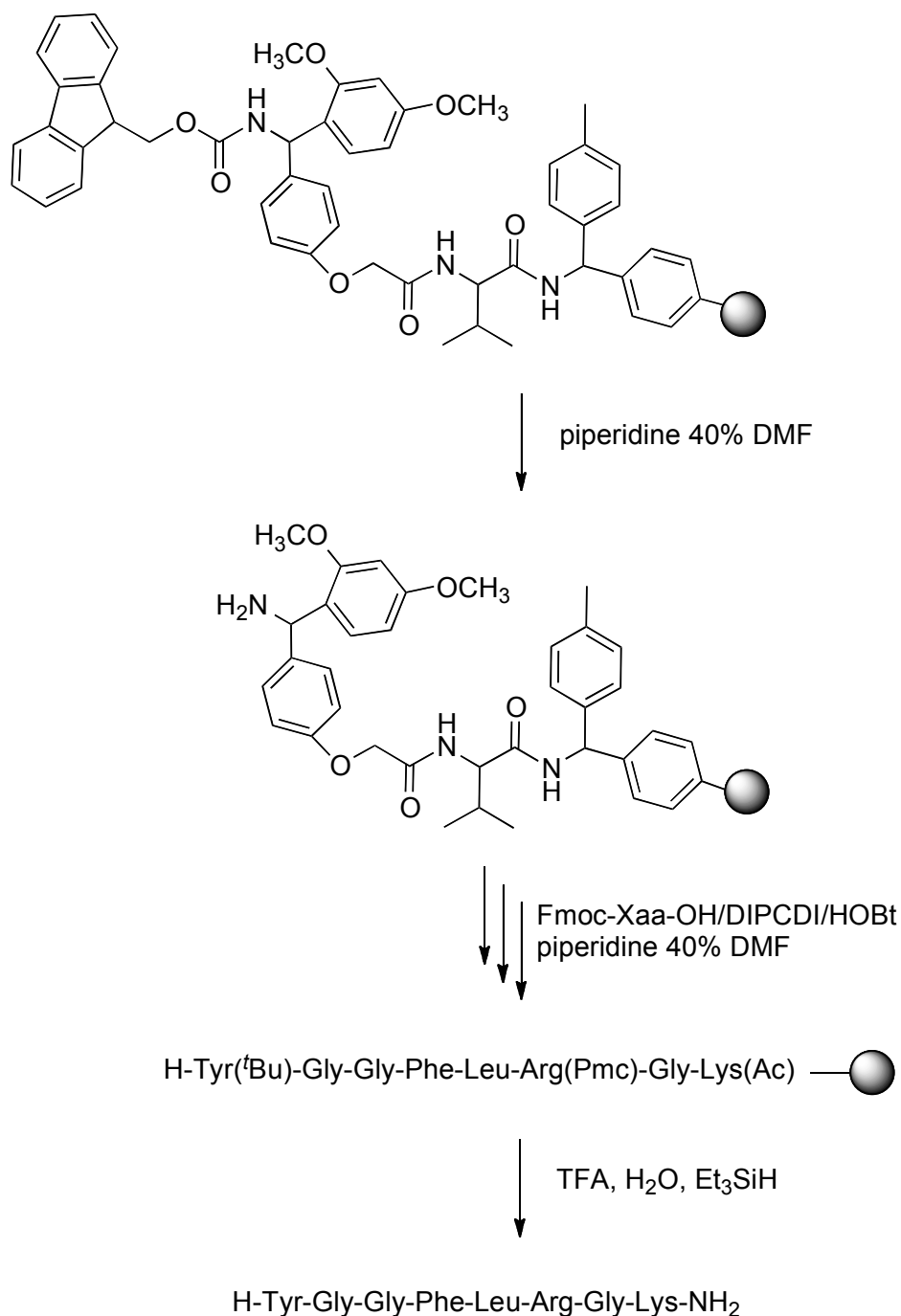


**Figure 35:** Scheme of synthesis of the compound 20.

The peptide 20 was resynthesized and in position 7 was inserted Lys (Dde) and in position 1 Boc-Tyr. This strategy has been used to avoid that the basic conditions, necessary for the reaction with hydrazine, could make a deprotection of the terminal amine and a secondary reaction with the maleimide derivative to give an unwanted product. The deprotection of the side aminoacid residue of Lys(Dde) was done with a solution of 2% hydrazine in DMF with a reaction time of three minutes. The resin was extracted with DMF and CH<sub>2</sub>Cl<sub>2</sub> and the process of deprotection was repeated for a second time<sup>61</sup>.

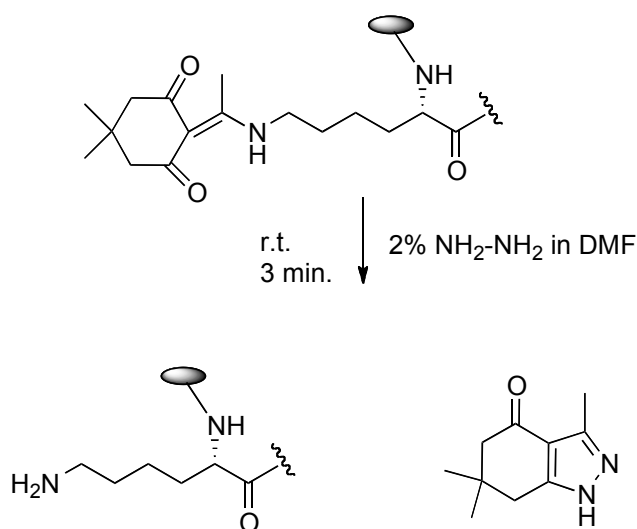


**Figure 36:** Removal reaction of Lys(Dde).

At this point, the NH<sub>2</sub> in position  $\gamma$  of Lys, is acylated with the 4 - (2,5-dioxo-2,5-dihydro-pyrrol-1-yl) butyric acid according to the following stoichiometry: the amine component (0.05 mmol corresponding to 200 mg of resin) was suspended in DMF (2mL) and it was reacted with a molar excess of 4x with the 4 - (2,5-dioxo-2,5-dihydro-pyrrol-1-yl) butyric acid (0.2 mmol, 40 mg), HOBt (0.2mmol, 31 mg), WSC (0.2 mmol, 40 mg).

After 2 h the resin was extracted with DMF and CH<sub>2</sub>Cl<sub>2</sub>, dried and treated with the mixture release like for every compounds of Table 3 and [Cys<sup>18</sup>] N/OFQ-NH<sub>2</sub> to give the compound 20bis (Figure 37).

<sup>61</sup> B. W. Bycroft, W. C. Chan, S. R. Chhabra, N. D. Hone, *J. Chem. Soc. Chem. Commun.*, (1993), 778-779.

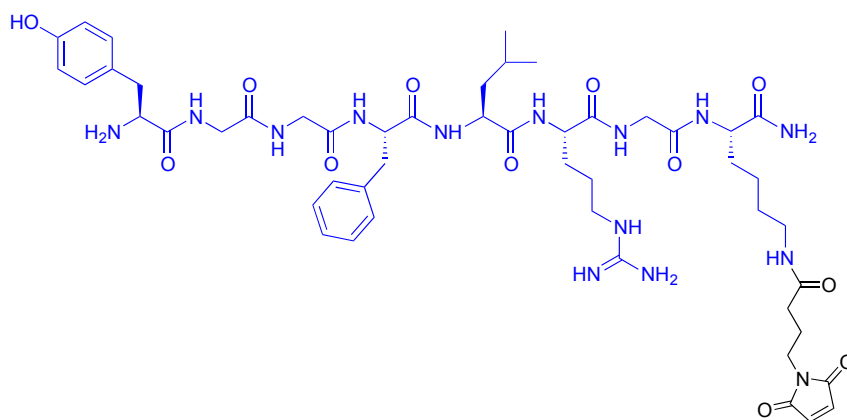


**Figure 37:** Compound 20bis.

The compound 20bis, after purification, was condensed with the [Cys<sup>18</sup>] N/OFQ-NH<sub>2</sub> using the thio-Michael reaction with following stoichiometry: the compound 20bis (0.0031 mmol, 4 mg) was reacted with a molar excess of 10% of [Cys<sup>18</sup>] N/OFQ-NH<sub>2</sub> (0.0034 mmol, 8.48 mg).

Each compound was separately dissolved in 1 ml of H<sub>2</sub>O and 1 ml of CH<sub>3</sub>CN. The two solutions were combined and it was added to 5% NaHCO<sub>3</sub> (0.05 mL) to speed the Thio-Michael reaction (figure 38). After 5 minutes the reaction mixture was purified by preparative HPLC giving the desired compound 25.

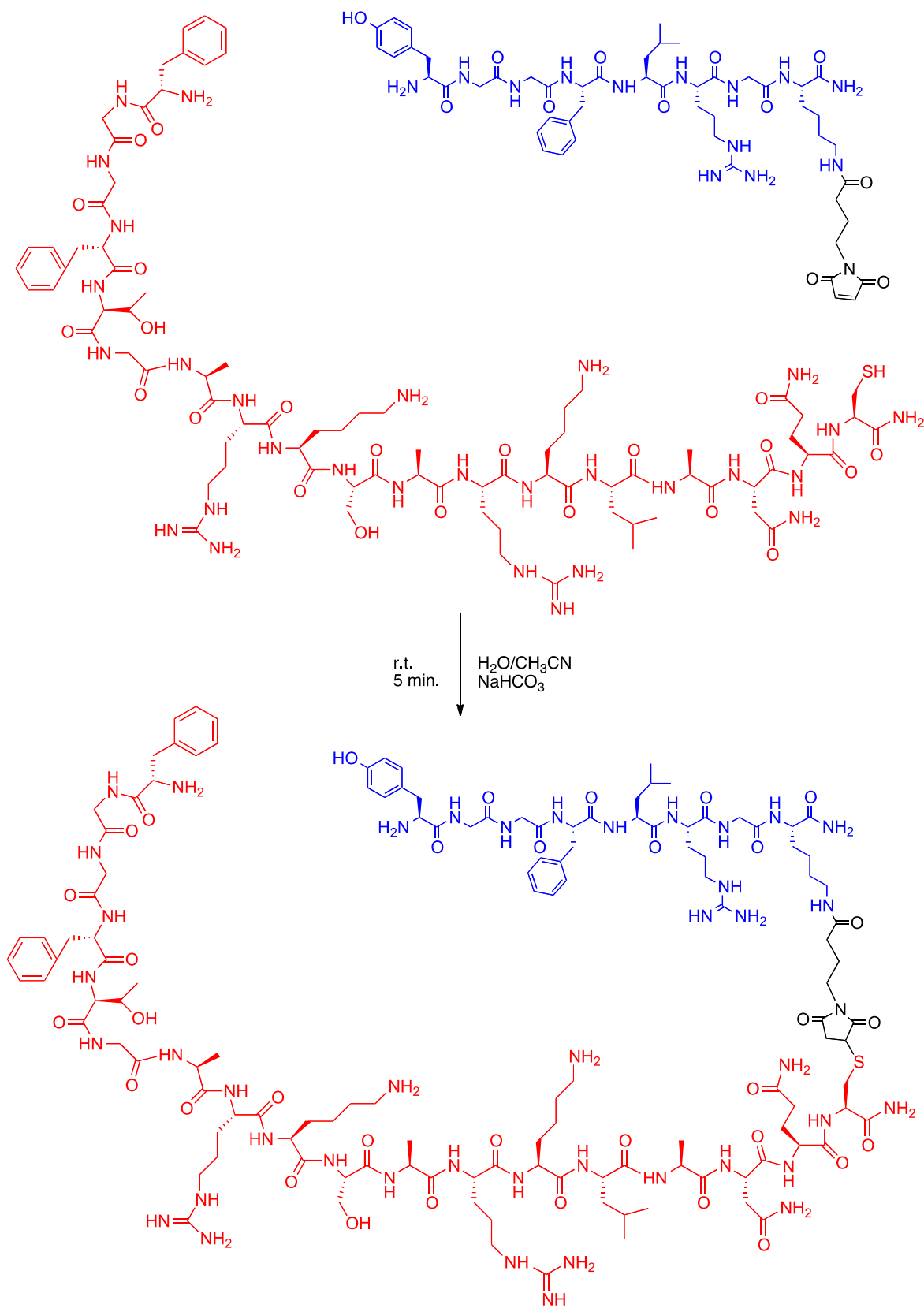


**Figure 38:** Scheme of Thio-Michael synthesis for the bivalent 25.

### 4.3 Purification and analytical control

The evaluation of the purity of the crude reaction products and final products was made with analytical control by HPLC using a Beckman System Gold 168 KNAUER C-18 column (250 mm x 4.6 mm) and a UV detector with variable wavelength fixed at 220 nm. The mobile phase consisted in a binary eluent made up H<sub>2</sub>O (solvent A) and CH<sub>3</sub>CN (solvent B) each containing 0.1% v / v TFA, at a flow rate of 1 ml / min. The gradient used is: 100% A from 0 (t<sub>0</sub>) to 25 minutes (t<sub>25</sub>) and then rebalance the initial gradient within 30 minutes (t<sub>30</sub>). The identification of each compound was based on a combination of retention time (t<sub>r</sub>) and spectral matching.

The crude peptides were purified by preparative HPLC Waters Delta Prep 3000 equipped with a Jupiter C18 column 15 μm eluted with the same mobile phase used for analytical HPLC and with a gradient programmed from time to time depending on the analytical profile of the crude product.

In the figures below are shown the crude, purified HPLC profile and mass spectrum of compound 25 and [Cys<sup>18</sup>] N/OFQ-NH<sub>2</sub>.

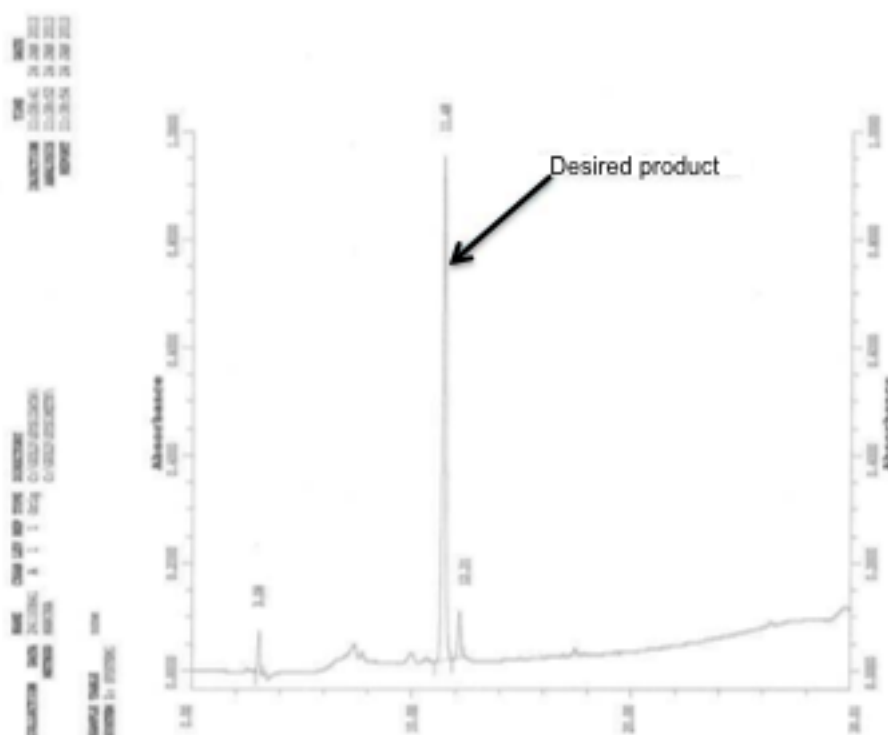


Figure 39: Crude profile HPLC of the compound 20.

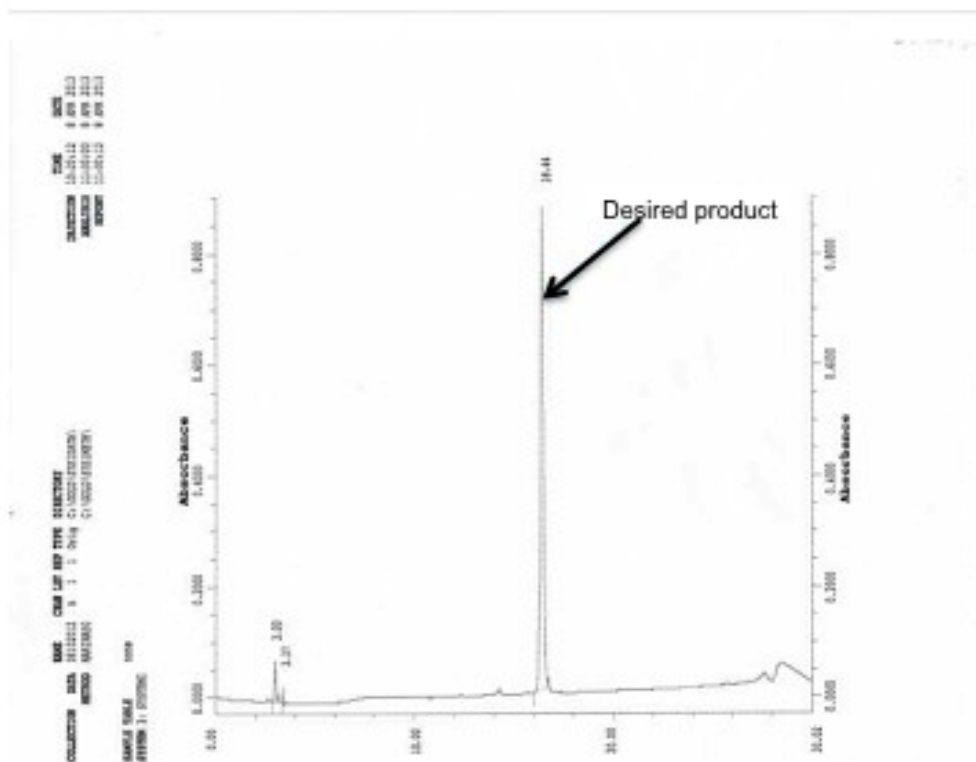


Figure 40: Purified profile HPLC Of the compound 20.

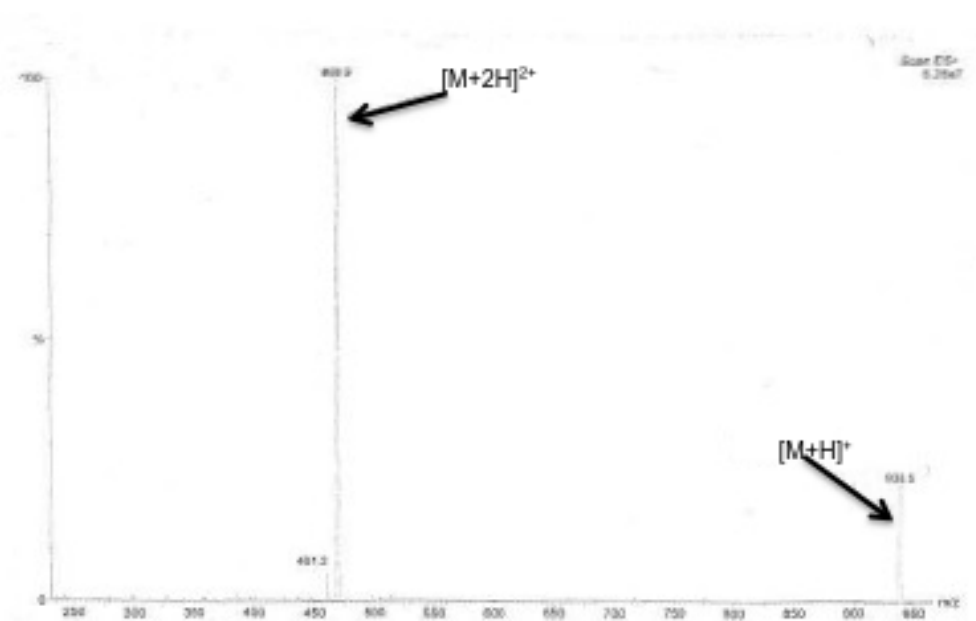


Figure 41: MS spectra of the purified compound 20.

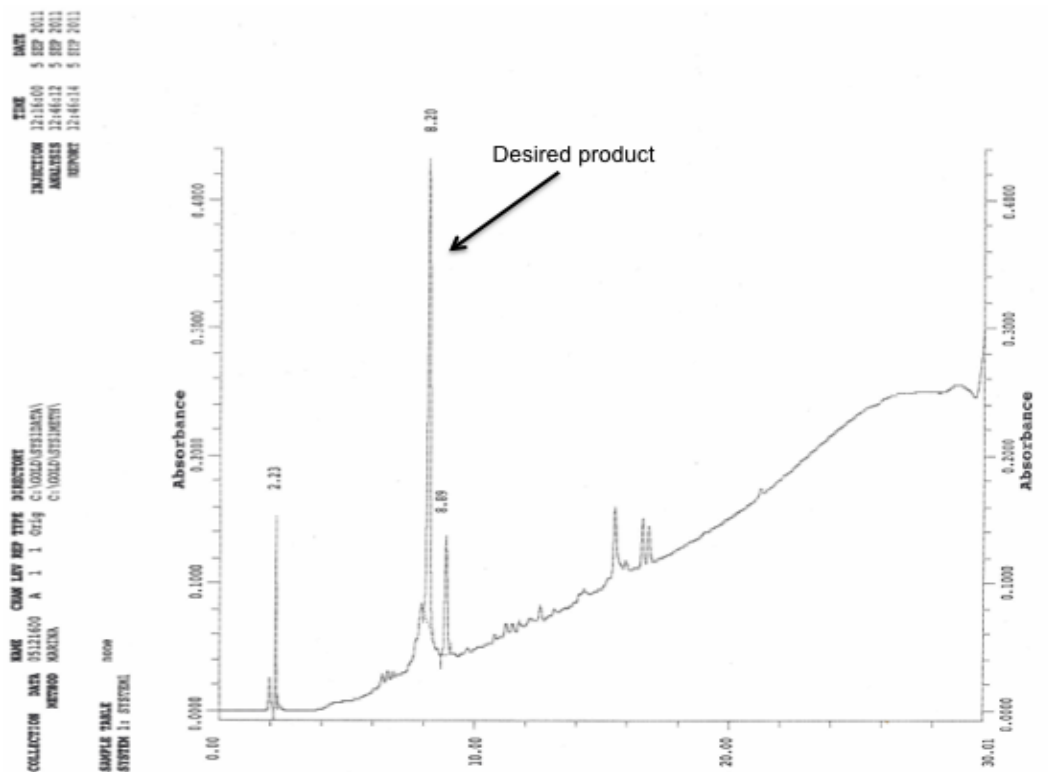


Figure 42: Crude profile of [Cys<sup>18</sup>] N/OFQ-NH<sub>2</sub>.

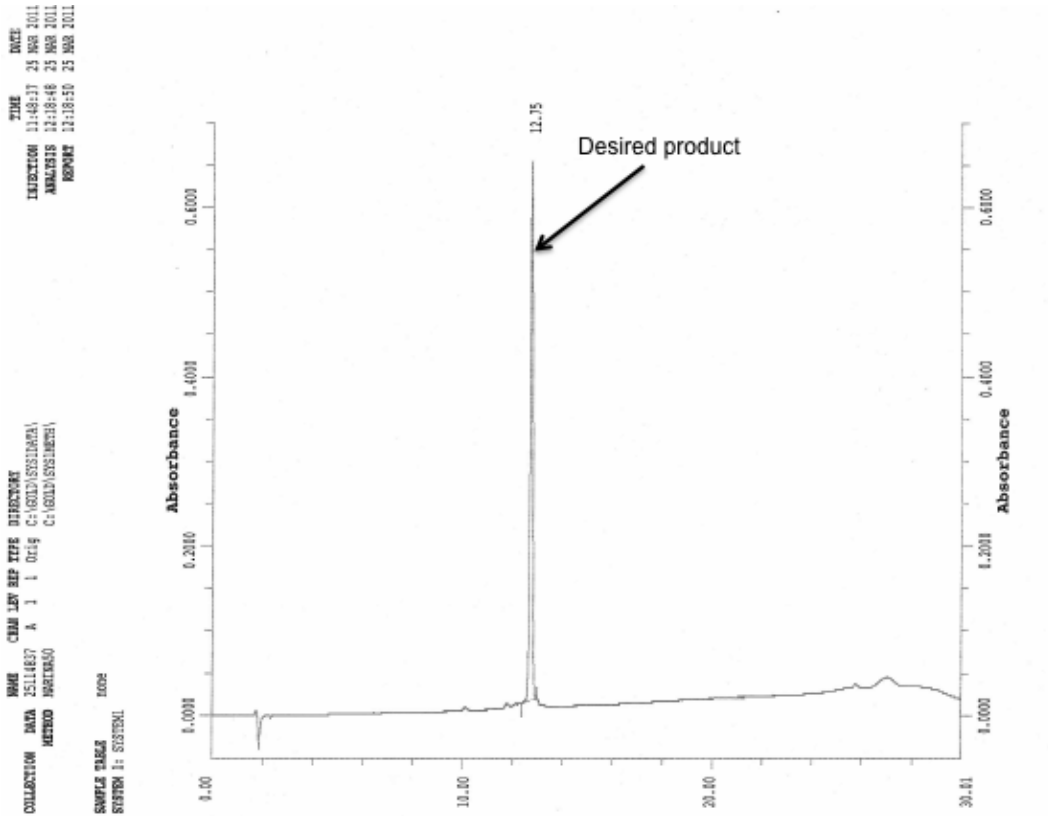


Figure 43: Purified profile of [Cys<sup>18</sup>] N/OFQ-NH<sub>2</sub>.

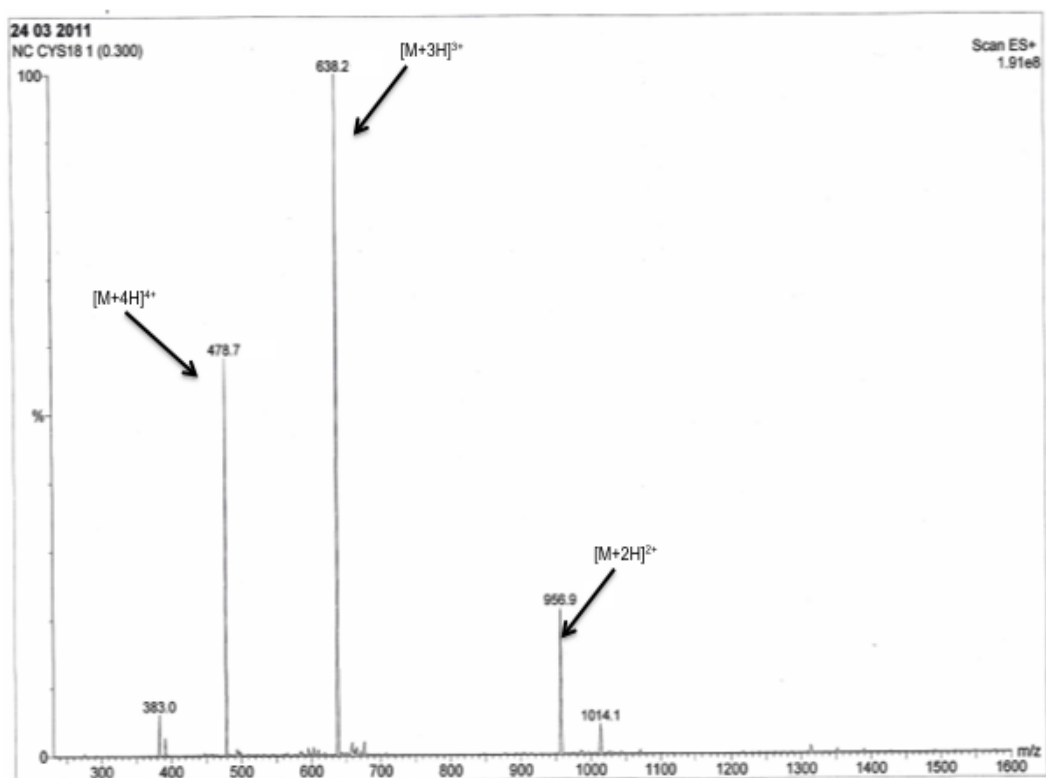


Figure 44: MS spectra of [Cys<sup>18</sup>] N/OFQ-NH<sub>2</sub>.



Peptide	Sequence	M <sub>w</sub> calculated	[M+H] <sup>+</sup> found	t <sub>r</sub> HPLC
<b>Dermorphin</b>	H-Tyr-DAla-Phe-Gly-Tyr-Pro-Ser-NH <sub>2</sub>	852.94	853.98	12.31min.
<b>Leu-enkephalin</b>	H-Tyr-Gly-Gly-Phe-Leu- NH <sub>2</sub>	554.64	555.31	16.30min.
<b>Endomorphin 1</b>	H-Tyr-Pro-Trp-Phe- NH <sub>2</sub>	610.27	611.17	17.20min.
<b>1</b>	H-Tyr-DAla-Phe-Gly-Tyr-Pro-Ser-Lys(Ac)- NH <sub>2</sub>	973,1	974,1	15.88min
<b>2</b>	H-Tyr-Pro-Trp-Phe-Lys(Ac)- NH <sub>2</sub>	780.80	781.40	15.93min.
<b>3</b>	H-Tyr-Pro-Trp-Phe-Gly-Gly-Lys(Ac)- NH <sub>2</sub>	894.99	895.80	12.73min.
<b>4</b>	H-Tyr-Pro-Trp-Phe-O <sub>2</sub> Oc-Lys(Ac)- NH <sub>2</sub>	925.54	926.74	17.60min.
<b>5</b>	H-Tyr-Pro-Trp-Phe-AVA-Lys(Ac)- NH <sub>2</sub>	881.82	882.82	13.26min.
<b>6</b>	H-Tyr-Gly-Gly-Phe- NH <sub>2</sub>	441.48	442.51	13.19min.
<b>7</b>	H-Tyr-Gly-Gly-Phe-Lys(Ac)- NH <sub>2</sub>	611.30	612.50	14.79min.
<b>8</b>	H-Tyr-Gly-Gly-Phe-Gly-Lys(Ac)- NH <sub>2</sub>	668.33	669.4	17.20min.
<b>9</b>	H-Tyr-Gly-Gly-Phe-Gly-Gly-Lys(Ac)- NH <sub>2</sub>	726.35	726.35	14.73min.
<b>10</b>	H-Tyr-Gly-Gly-Phe-O <sub>2</sub> Oc-Lys(Ac)- NH <sub>2</sub>	757.85	757.20	16.30min.
<b>11</b>	H-Tyr-Gly-Gly-Phe-AVA-Lys(Ac)- NH <sub>2</sub>	710.82	711.38	15.30min.
<b>12</b>	H-Tyr-Gly-Gly-Phe-Lys- NH <sub>2</sub>	569.66	570.73	11.82min.
<b>13</b>	H-Tyr-Gly-Gly-Phe-Lys-Lys(Ac)- NH <sub>2</sub>	739.40	740.30	14.05min.
<b>14</b>	H-Tyr-Gly-Gly-Phe-Lys-Gly-Lys(Ac)- NH <sub>2</sub>	796.42	797.42	15.83min.
<b>15</b>	H-Tyr-Gly-Gly-Phe-Lys-Gly-Gly-Lys(Ac)- NH <sub>2</sub>	854.45	854.45	13.26min.
<b>16</b>	H-Tyr-Gly-Gly-Phe-Lys-O <sub>2</sub> Oc-Lys(Ac)- NH <sub>2</sub>	886.03	885.4	15.08min.
<b>17</b>	H-Tyr-Gly-Gly-Phe-Lys-AVA-Lys(Ac)- NH <sub>2</sub>	838.99	839.47	14.13min.
<b>18</b>	H-Tyr-Gly-Gly-Phe-Leu-Arg- NH <sub>2</sub>	710.82	711.77	15.40min.
<b>19</b>	H-Tyr-Gly-Gly-Phe-Leu-Arg-Lys(Ac)- NH <sub>2</sub>	880.49	881.50	17.00min.
<b>20</b>	H-Tyr-Gly-Gly-Phe-Leu-Arg-Gly-Lys(Ac)- NH <sub>2</sub>	937.52	938.52	16.44min.
<b>21</b>	H-Tyr-Gly-Gly-Phe-Leu-Arg-Gly-Gly-Lys(Ac)- NH <sub>2</sub>	995.54	995.54	16.37min.
<b>22</b>	H-Tyr-Gly-Gly-Phe-Leu-Arg-O <sub>2</sub> Oc-Lys(Ac)- NH <sub>2</sub>	1027.20	1026.5	17.60min.
<b>23</b>	H-Tyr-Gly-Gly-Phe-Leu-Arg-AVA-Lys(Ac)- NH <sub>2</sub>	980.16	980.57	16.74min.

**Table 3:** List of peptides synthesized with relative MW calculated, MW found and retention times in analytical HPLC using a gradient that goes from a 100% H<sub>2</sub>O at t<sub>0</sub> to 100% CH<sub>3</sub>CN at time t<sub>25</sub>, to return to the initial conditions at t<sub>30</sub>.

#### 4.4 Test of intracellular calcium mobilization

*Cell cultures* - for biological assays have been used Chinese Hamster Ovary cells (CHO) stably transfected with the human receptor NOP (CHO<sub>NOP</sub>) and MOP (CHO<sub>MOP</sub>) and with a chimeric G protein. This allows the receptor normally coupled to G<sub>i</sub> protein to activate phospholipase C, producing inositol triphosphate (IP3) and diacylglycerol (DAG), obtaining in increased concentrations of intracellular calcium<sup>62</sup>. This protein was created by replacing 5 aminoacids of the C-terminal portion of the alpha subunit of G<sub>q</sub> protein with the respective aminoacids of G<sub>i</sub>, obtaining the protein G<sub>αqi5</sub>. The cells were cultured in

Falcon flasks sterile type with screw cap and kept in a suitable medium consisting DMEM (Dulbecco's Minimum Essential Medium) and Ham's F-12 (50/50) to which they were added hygromycin B and geneticin as selection factors. The cells were kept in an incubator at 37 ° C, in ideal conditions of temperature, humidity and in the presence of 5% CO<sub>2</sub>. The day before the experiment the cells were seeded in 96-well plates with black walls and transparent bottom like type Constar.

50,000 cells were plated per well in a volume of 100 µl.

After twenty-four hours, you get a confluence of 90-100% per well.

*FlexStation II* - For the study of intracellular calcium mobilization was used the equipment FlexStation II (Molecular Devices)(Figure 45).

The instrument is a bench top fluorometer that measures the change in fluorescence due to changes in intracellular levels of cytosolic calcium. The variation in the levels of intracellular calcium is expressed as a percentage change of the fluorescence values compared to the baseline value, which is determined experimentally before the beginning of each experiment.

The unit consists of:

-Light source equipped of a xenon lamp (Figure 46)

-Multichannel Pipettes automatic eight-channel

- Side trays:

- \* higher for disposable tips
- \* central plate for drug substances to be tested
- \* lower for 96-well plate containing the cells

The instrument has a system that allows to perform the experiments at defined temperature and a software for configuration and management of the instrument (SoftMax PRO v.4.8) (Figure 50).

---

<sup>62</sup> B.R. Conklin, Z. Farfel, K. D. Lustig, D. Julius, H.R. Bourne. *Nature*, (1993), 363, 274-276.

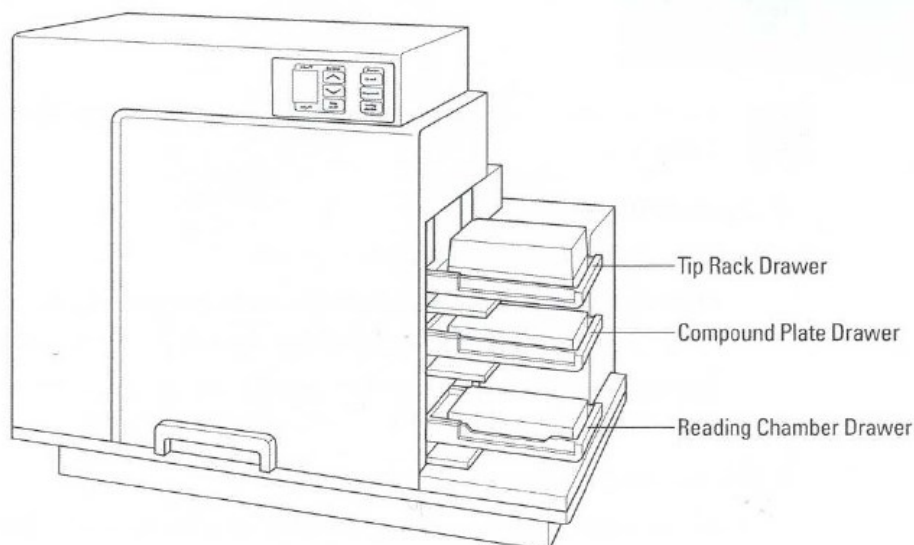


**Figure 45:** FlexStation®.

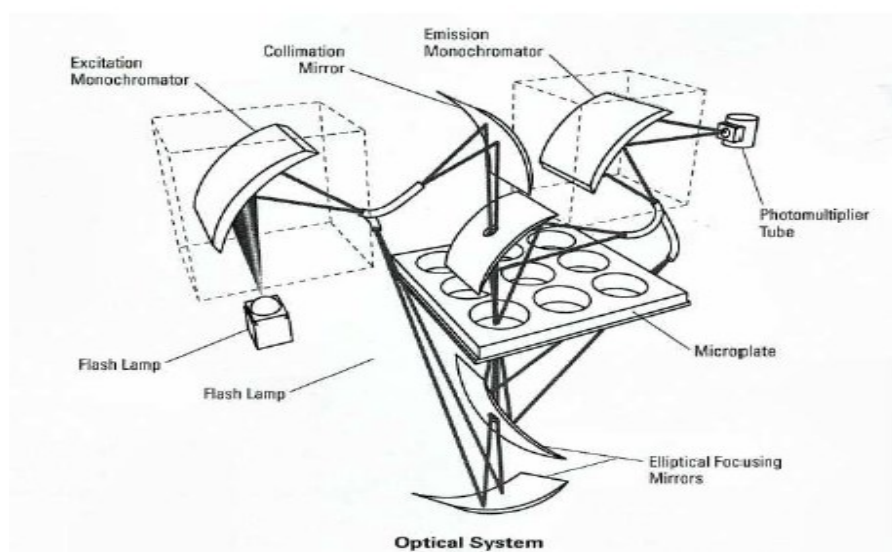


**Figure 46:** Scheme of the detection system of fluorescence in FlexStation II®.

The instrument is equipped with an optical system consisting of a double monochromator and a xenon lamp.

The xenon lamp, inside the instrument, emits a beam of light at desired wavelength ( $\lambda$ ) by the operator (488 nm). This light gets to the emission monochromator which reflects on the mirror of collimation and then on the wells of the plate reading. The cells inside the plate, previously incubated with calcium-dependent fluorophore, are affected by the light beam from the lamp, emitting radiation at a wavelength ( $\lambda$ ) of 525 nm.

*Samples preparation-* All compounds tested were dissolved in ddH<sub>2</sub>O at [1mM] and they were stored in aliquots of 20 μl at -20°C. The subsequent dilutions were done in HBSS characterized by HEPES [20mM] (pH 7.4) and albumin bovine serum (BSA) 0.02%. The solutions of the test substances are loaded into a 96-plate drugs wells (Figure 47) with a V-bottom. The dilutions useful for the experiments curve concentration-response are made directly in the micro plate.

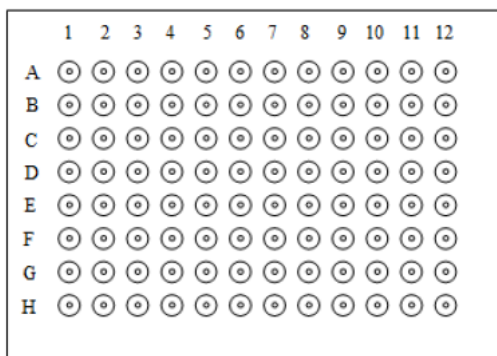


**Figure 47:** System of 96-wells where you add the samples to analyse.

*Experiment* - The day of the experiment the cells plated were incubated 30 minutes with medium containing the fluorescent dye FLUO-4.

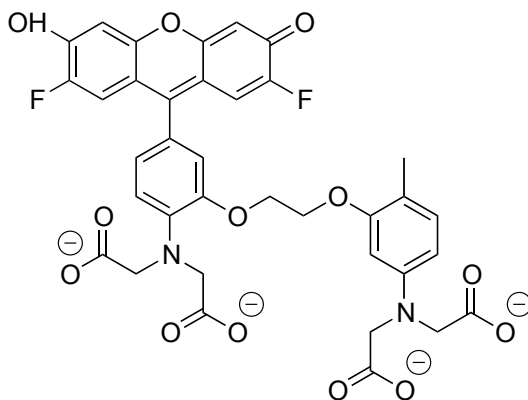


**Figure 48:** Chemical formula of the fluorescent dye FLUO-4.

The fluorescent dye FLUO-4-AM penetrates the cell by passive diffusion, due to its lipophilic nature; once inside it is degraded by esterases that hydrolyse the ester bonds thus freeing the carboxyl functions on capable to chelate the calcium mobilized. When the carboxyl functions are free, FLUO-4 is no longer able to passively cross the cell membrane, but is expelled through an anion carrier.

To prevent the expulsion of the fluorescent dye from the cell is added Probenecid, a blocker of anion carrier. The calcium complex, excited by the incident

electromagnetic radiation is capable of emitting a radiation; whose is proportional in intensity to the amount of complex formed. After 30 minutes of incubation the liquid loading is aspirated and the wells are filled with a wash solution containing the black dye Brilliant Black. This solution has the power of screening, thanks to its colour, the background due to fluorescence of the FLUO-4 who is not internalized by the cells (Figure 49).

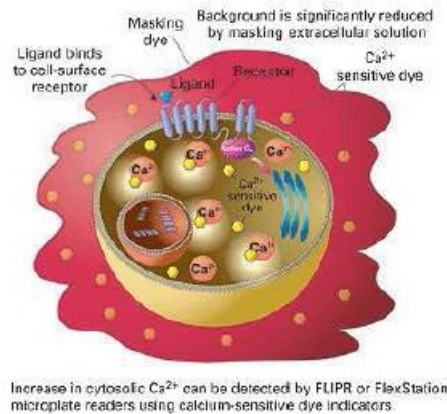


**Figure 49:** Experimental protocol of the assay of intracellular calcium mobilization.

The injection of the test substances on cells is automated and it occurs by subsequent columns according to a protocol established by the operator. The instrument reads the values of the fluorescence data from the mobilization of intracellular calcium and returns them as a percentage change from baseline with graphical representation of the evolution of fluorescence values (Figure X).

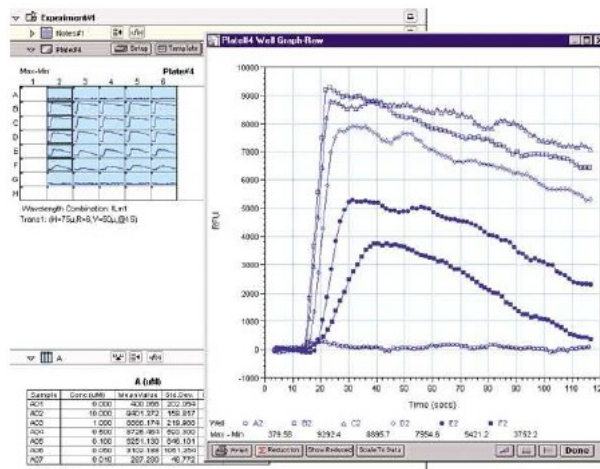


**Figure 50:** Software SoftMax 4.8 to management the instrument.

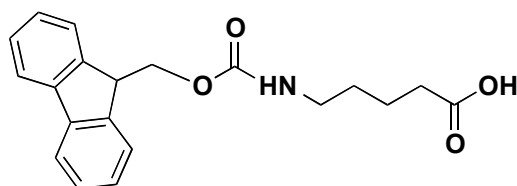
**Data Analysis** - The potency of agonists is expressed in terms of pEC<sub>50</sub>, which is the negative logarithm of the EC<sub>50</sub> value. It represents the concentration of agonist

where 50% of its maximal effect is observed in defined experimental conditions. For the potency values are reported the confidence limits of 95%.

$E_{\max}$  is the maximal response that an agonist can be produce in particular experimental conditions. For the construction of concentration-response curves and calculation of  $pEC_{50}$  and  $E_{\max}$  it has been used the software GraphPad Prism 5.0. All data are expressed like average  $\pm$  standard error of n experiments.

## 4.5 Synthesis and NMR spectra of the compounds

### Synthesis of Fmoc-AVA-OH (**61**)



C<sub>20</sub>H<sub>21</sub>NO<sub>4</sub>  
Mol.Wt.: 339,4

The 5-aminopentanoic acid (586 mg, 5 mmol) was dissolved in a flask in a solution H<sub>2</sub>O/Dioxane (1:1) (100ml). After it was added Na<sub>2</sub>CO<sub>3</sub> (1.5 g, 15 mmol), the reaction was brought to 0°C and then it is added dropwise Fmoc-Cl (1.17 g, 4.5 mmol) previously dissolved in dioxane. It was checked the pH with universal indicator. The reaction was left for 6 h at r.t.. Subsequently it was introduced HCl sat. (40ml) and the organic phase was extracted with AcOEt (100ml), neutralized with Brine, dried with Na<sub>2</sub>SO<sub>4</sub> and under vacuum to afford the crude product 1.49 g.

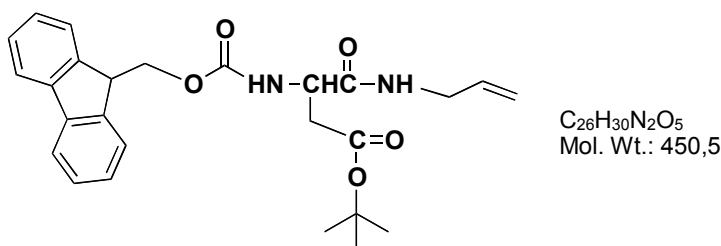
Flash chromatography (SiO<sub>2</sub>) 2:8:0.3 (AcOEt:EtPt:AcOH) to afford 1.85 g of compound X (Y=92%)<sup>63</sup>.

**MS (ESI):** [M+H]<sup>+</sup> = 340.1

**t<sub>r</sub>** = 14.87

**<sup>1</sup>H NMR (200 MHz, CDCl<sub>3</sub>):** δ 9.45 (s, 1H), 7.76 (d, J = 1.5 Hz, 1H), 7.74 (d, J = 1.5 Hz, 1H), 7.46 – 7.38 (m, 4H), 7.36 – 7.31 (m, 2H), 4.72 – 4.67 (d, 2H), 4.46 (s, 1H), 4.07 (s, 1H), 3.10 (d, J = 37.3 Hz, 2H), 2.30 – 2.23 (t, 2H), 1.69 – 1.58 (m, 4H).

<sup>63</sup> L. A. Carpino, G. Y. Han, *J. Org. Chem.*, (1972), 37, 3404-3409.

Synthesis of Fmoc-allyl-Asp(O<sup>t</sup>Bu) (**62**)

In a flask at 0°C it was added 2-(((9*H*-fluoren-9-yl)methoxy)carbonyl)amino)-4-(*tert*-butoxy)-4-oxobutanoic acid (2 g, 5 mmol) dissolved in DMF (10ml), WSC (1.1 g, 5.5 mmol) and Oxyma Pure (782 mg, 5.5 mmol). It was left to stir for 10 min. allylamine (314 mg, 5.5 mmol) was dissolved in DMF (3 ml) and then dripped in the flask through a syringe. The reaction was left o.n. at r.t.. The DMF was evaporated under vacuum. The reaction was dissolved in AcOEt, then extracted before with citric acid (10%), after with NaHCO<sub>3</sub> 5% and finally with Brine. The organic layer was dried under vacuum. Flash chromatography (SiO<sub>2</sub>) 5:5 (AcOEt:EtPt) to afford 2.1 g of product (Y= 100%).

**MS (ESI):** [M+H]<sup>+</sup> = 451.2

**t<sub>r</sub>** = 14.68

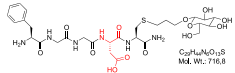
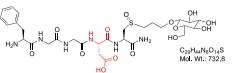
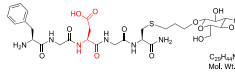
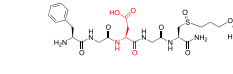
**<sup>1</sup>H NMR (200 MHz, CDCl<sub>3</sub>):** δ 7.63 (m, 4H), 7.41 – 7.33 (m, 4H), 6.11 (m, 1H), 5.18 (m, 2H), 5.00 (t, J = 7.5 Hz, 1H), 4.72 – 4.68 (m, 2H), , 4.04 (m, 2H), 3.11 (dd, J = 8.7, 3.4 Hz, 2H), 1.42 (s, 9H).



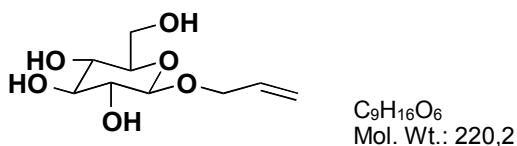
Peptide	Sequence	Mw	Mw	tr	Thiol-ene between
		calculated	found		
<b>26 AGGFC</b>	Ala-Gly-Gly- <b>Phe</b> -Cys-NH <sub>2</sub>	452.54	452.9	10.3	Thiol-ene with ally-glucose( <b>43-43bis</b> ) and with allyl-Asp(O <sup>t</sup> Bu)( <b>44-44bis</b> )
<b>27 AGFGC</b>	Ala-Gly- <b>Phe</b> -Gly-Cys-NH <sub>2</sub>	452.54	452.9	10.43	Incomplete, reaction under study
<b>28 AGGHC</b>	Ala-Gly-Gly- <b>His</b> -Cys-NH <sub>2</sub>	442.5	443.2	9.81	Thiol-ene with ally-glucose( <b>45-45bis</b> )
<b>29 AGHGC</b>	Ala-Gly- <b>His</b> -Gly-Cys-NH <sub>2</sub>	442.5	442.9	9.98	Thiol-ene with ally-glucose( <b>46-46bis</b> ) and with allyl-Asp(O <sup>t</sup> Bu)( <b>47-47bis</b> )
<b>30 AGGWC</b>	Ala-Gly-Gly- <b>Trp</b> -Cys-NH <sub>2</sub>	491.57	492.2	10.67	Thiol-ene with ally-glucose( <b>48-48bis</b> )
<b>31 AGWGC</b>	Ala-Gly- <b>Trp</b> -Gly-Cys-NH <sub>2</sub>	491.57	492.1	10.74	Incomplete, reaction under study
<b>32 AGGYC</b>	Ala-Gly-Gly- <b>Tyr</b> -Cys-NH <sub>2</sub>	468.53	468.8	10.89	Incomplete, reaction under study
<b>33 FGGTC</b>	Phe-Gly-Gly- <b>Thr</b> -Cys-NH <sub>2</sub>	482.56	483.4	9.60	Thiol-ene with ally-glucose( <b>49-49bis</b> )
<b>34 FGTGC</b>	Phe-Gly- <b>Thr</b> -Gly-Cys-NH <sub>2</sub>	482.56	483.43	9.34	Thiol-ene with ally-glucose( <b>50-50bis</b> )
<b>35 FGGNC</b>	Phe-Gly-Gly- <b>Asn</b> -Cys-NH <sub>2</sub>	495.56	495.58	8.48	Thiol-ene with ally-glucose( <b>51-51bis</b> )
<b>36 FGNGC</b>	Phe-Gly- <b>Asn</b> -Gly-Cys-NH <sub>2</sub>	495.56	496.7	8.50	Thiol-ene with ally-glucose( <b>52-52bis</b> ) and Dodecene(commmercially available)( <b>53-53bis</b> )
<b>37 FGGQC</b>	Phe-Gly-Gly- <b>Gln</b> -Cys-NH <sub>2</sub>	509.59	510.65	8.86	Thiol-ene with ally-glucose( <b>54-54bis</b> )
<b>38 FGQGC</b>	Phe-Gly- <b>Gln</b> -Gly-Cys-NH <sub>2</sub>	509.59	510.38	8.83	Thiol-ene with ally-glucose( <b>55-55bis</b> )
<b>39 FGGEC</b>	Phe-Gly-Gly- <b>Glu</b> -Cys-NH <sub>2</sub>	510.57	511.66	9.11	Thiol-ene with ally-glucose( <b>56-56bis</b> )
<b>40 FGE GC</b>	Phe-Gly- <b>Glu</b> -Gly-Cys-NH <sub>2</sub>	510.57	511.66	9.13	Thiol-ene with ally-glucose( <b>57-57bis</b> )
<b>41 FGGDC</b>	Phe-Gly-Gly- <b>Asp</b> -Cys-NH <sub>2</sub>	496.55	497.77	8.64	Thiol-ene with ally-glucose( <b>58-58bis</b> )
<b>42 FGDGC</b>	Phe-Gly- <b>Asp</b> -Gly-Cys-NH <sub>2</sub>	496.55	497.64	8.96	Thiol-ene with ally-glucose(X)

**Table 4:** List of peptides synthesized with relative MW calculated, MW found and retention times in analytical HPLC using a gradient that goes from a 100% H<sub>2</sub>O at t<sub>0</sub> to 100% CH<sub>3</sub>CN at time t<sub>25</sub>, to return to the initial conditions at t<sub>30</sub>.

Peptide	Mw Thiol-ene products
26 AGGFC	<div style="display: flex; justify-content: space-around; align-items: flex-end;"> <div style="text-align: center;">   <b>43</b>  <small>C<sub>22</sub>H<sub>32</sub>N<sub>2</sub>O<sub>10</sub>S Mol. Wt: 672.7</small> </div> <div style="text-align: center;">   <b>43bis</b>  <small>C<sub>22</sub>H<sub>32</sub>N<sub>2</sub>O<sub>10</sub>S Mol. Wt: 688.7</small> </div> <div style="text-align: center;">   <b>44</b>  <small>C<sub>27</sub>H<sub>36</sub>N<sub>2</sub>O<sub>10</sub>S Mol. Wt: 702.1</small> </div> <div style="text-align: center;">   <b>44bis</b>  <small>C<sub>27</sub>H<sub>36</sub>N<sub>2</sub>O<sub>10</sub>S Mol. Wt: 718.1</small> </div> </div>
28 AGGHC	<div style="display: flex; justify-content: space-around; align-items: flex-end;"> <div style="text-align: center;">   <b>45</b>  <small>C<sub>22</sub>H<sub>32</sub>N<sub>2</sub>O<sub>10</sub>S Mol. Wt: 692.7</small> </div> <div style="text-align: center;">   <b>45bis</b>  <small>C<sub>22</sub>H<sub>32</sub>N<sub>2</sub>O<sub>10</sub>S Mol. Wt: 692.7</small> </div> </div>
29 AGHGC	<div style="display: flex; justify-content: space-around; align-items: flex-end;"> <div style="text-align: center;">   <b>46</b>  <small>C<sub>22</sub>H<sub>32</sub>N<sub>2</sub>O<sub>10</sub>S Mol. Wt: 692.7</small> </div> <div style="text-align: center;">   <b>46bis</b>  <small>C<sub>22</sub>H<sub>32</sub>N<sub>2</sub>O<sub>10</sub>S Mol. Wt: 692.7</small> </div> <div style="text-align: center;">   <b>47</b>  <small>C<sub>27</sub>H<sub>36</sub>N<sub>2</sub>O<sub>10</sub>S Mol. Wt: 688.9</small> </div> <div style="text-align: center;">   <b>47bis</b>  <small>C<sub>27</sub>H<sub>36</sub>N<sub>2</sub>O<sub>10</sub>S Mol. Wt: 693.9</small> </div> </div>
30 AGGWC	<div style="display: flex; justify-content: space-around; align-items: flex-end;"> <div style="text-align: center;">   <b>48</b>  <small>C<sub>22</sub>H<sub>32</sub>N<sub>2</sub>O<sub>10</sub>S Mol. Wt: 713.8</small> </div> <div style="text-align: center;">   <b>48bis</b>  <small>C<sub>22</sub>H<sub>32</sub>N<sub>2</sub>O<sub>10</sub>S Mol. Wt: 727.8</small> </div> </div>
33 FGGTC	<div style="display: flex; justify-content: space-around; align-items: flex-end;"> <div style="text-align: center;">   <b>49</b>  <small>C<sub>22</sub>H<sub>32</sub>N<sub>2</sub>O<sub>10</sub>S Mol. Wt: 722.8</small> </div> <div style="text-align: center;">   <b>49bis</b>  <small>C<sub>22</sub>H<sub>32</sub>N<sub>2</sub>O<sub>10</sub>S Mol. Wt: 718.8</small> </div> </div>
34 FGTGC	<div style="display: flex; justify-content: space-around; align-items: flex-end;"> <div style="text-align: center;">   <b>50</b>  <small>C<sub>22</sub>H<sub>32</sub>N<sub>2</sub>O<sub>10</sub>S Mol. Wt: 702.8</small> </div> <div style="text-align: center;">   <b>50bis</b>  <small>C<sub>22</sub>H<sub>32</sub>N<sub>2</sub>O<sub>10</sub>S Mol. Wt: 718.8</small> </div> </div>
35 FGGNC	<div style="display: flex; justify-content: space-around; align-items: flex-end;"> <div style="text-align: center;">   <b>51</b>  <small>C<sub>22</sub>H<sub>32</sub>N<sub>2</sub>O<sub>10</sub>S Mol. Wt: 718.8</small> </div> <div style="text-align: center;">   <b>51bis</b>  <small>C<sub>22</sub>H<sub>32</sub>N<sub>2</sub>O<sub>10</sub>S Mol. Wt: 731.8</small> </div> </div>
36 FGNGC	<div style="display: flex; justify-content: space-around; align-items: flex-end;"> <div style="text-align: center;">   <b>52</b>  <small>C<sub>22</sub>H<sub>32</sub>N<sub>2</sub>O<sub>10</sub>S Mol. Wt: 715.8</small> </div> <div style="text-align: center;">   <b>52bis</b>  <small>C<sub>22</sub>H<sub>32</sub>N<sub>2</sub>O<sub>10</sub>S Mol. Wt: 731.8</small> </div> <div style="text-align: center;">   <b>53</b>  <small>C<sub>27</sub>H<sub>36</sub>N<sub>2</sub>O<sub>10</sub>S Mol. Wt: 693.9</small> </div> <div style="text-align: center;">   <b>53bis</b>  <small>C<sub>27</sub>H<sub>36</sub>N<sub>2</sub>O<sub>10</sub>S Mol. Wt: 679.9</small> </div> </div>
37 FGGQC	<div style="display: flex; justify-content: space-around; align-items: flex-end;"> <div style="text-align: center;">   <b>54</b>  <small>C<sub>22</sub>H<sub>32</sub>N<sub>2</sub>O<sub>10</sub>S Mol. Wt: 728.8</small> </div> <div style="text-align: center;">   <b>54bis</b>  <small>C<sub>22</sub>H<sub>32</sub>N<sub>2</sub>O<sub>10</sub>S Mol. Wt: 745.8</small> </div> </div>
38 FGQGC	<div style="display: flex; justify-content: space-around; align-items: flex-end;"> <div style="text-align: center;">   <b>55</b>  <small>C<sub>22</sub>H<sub>32</sub>N<sub>2</sub>O<sub>10</sub>S Mol. Wt: 728.8</small> </div> <div style="text-align: center;">   <b>55bis</b>  <small>C<sub>22</sub>H<sub>32</sub>N<sub>2</sub>O<sub>10</sub>S Mol. Wt: 745.8</small> </div> </div>
39 FGGEC	<div style="display: flex; justify-content: space-around; align-items: flex-end;"> <div style="text-align: center;">   <b>56</b>  <small>C<sub>22</sub>H<sub>32</sub>N<sub>2</sub>O<sub>10</sub>S Mol. Wt: 730.8</small> </div> <div style="text-align: center;">   <b>56bis</b>  <small>C<sub>22</sub>H<sub>32</sub>N<sub>2</sub>O<sub>10</sub>S Mol. Wt: 748.8</small> </div> </div>
40 FGECC	<div style="display: flex; justify-content: space-around; align-items: flex-end;"> <div style="text-align: center;">   <b>57</b>  <small>C<sub>22</sub>H<sub>32</sub>N<sub>2</sub>O<sub>10</sub>S Mol. Wt: 730.8</small> </div> <div style="text-align: center;">   <b>57bis</b>  <small>C<sub>22</sub>H<sub>32</sub>N<sub>2</sub>O<sub>10</sub>S Mol. Wt: 748.8</small> </div> </div>

<b>41 FGGDC</b>	 <b>58</b>	 <b>58bis</b>
<b>42 FGDGC</b>	 <b>59</b>	 <b>59bis</b>

**Table 5:** Summary of compounds obtained through the Thiol-ene reaction.

Synthesis of allyl-glucose (**63**)

To a suspension of D-glucose (2 g, 11.10 mmol) in anhydrous ethanol (40 ml) was added BF<sub>3</sub> etherate (233 mg, 1.64 mmol). After it was introduced Ac<sub>2</sub>O (20 ml) and pyridine (50 ml) and it was left to stir o.n. at r.t.<sup>64</sup>.

The solution was concentrated and then extracted with AcOEt/ NaOH(2N) (basic wash) and AcOEt/ HCl(1M) (acid wash). The organic phase was concentrated under vacuum to obtain the crude product.

Flash chromatography (SiO<sub>2</sub>) 5:5 (Et<sub>2</sub>O/EtPt) to afford 134.2 mg (Y=21%).

In order to have (2*R*,3*R*,4*S*,5*S*,6*R*)-2-(allyloxy)-6-(hydroxymethyl)tetrahydro-2*H*-pyran-3,4,5-triol it was prepared a solution with Na<sup>o</sup> dissolved in MeOH and it was added few ml at a time with the sugar.

The reaction was checked by TLC 5:5 (Et<sub>2</sub>O/EtPt).

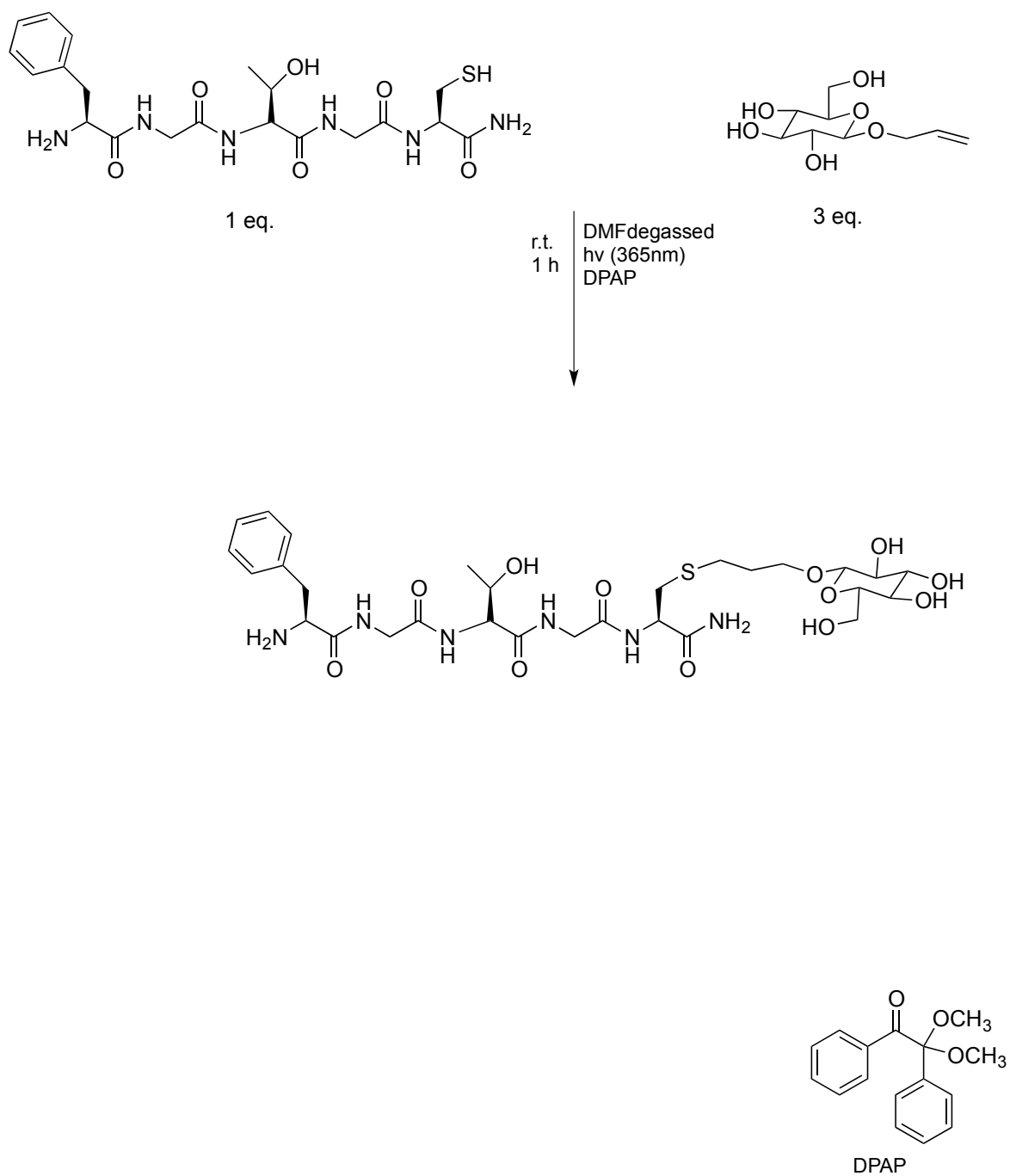
Finally the reaction was quenched with Amberlite until the pH=7. The mixture obtained was filtered through a gooch funnel, dried under vacuum to afford 76.1 mg of compound X (Y= 54%).

**<sup>1</sup>H NMR (400 MHz, D<sub>2</sub>O)** δ 5.95 (dddd, J = 16.9, 10.4, 6.4, 5.6 Hz, 1H), 5.35 (dq, J = 17.2, 1.6 Hz, 1H), 5.26 (ddd, J = 10.4, 1.9, 0.9 Hz, 1H), 4.47 (d, J = 8.0 Hz, 1H), 4.36 (ddt, J = 12.7, 5.6, 1.4 Hz, 1H), 4.25 -4.13 (m, 1H), 3.89 (dd, J = 12.3, 2.2 Hz, 1H), 3.68 (dd, J = 12.3, 5.9 Hz, 1H), 3.45 (t, J = 9.1 Hz, 1H), 3.42 - 3.38 (m, 1H), 3.35 (dd, J = 9.8, 8.9 Hz, 1H), 3.25 (dd, J = 9.3, 8.0 Hz, 1H).

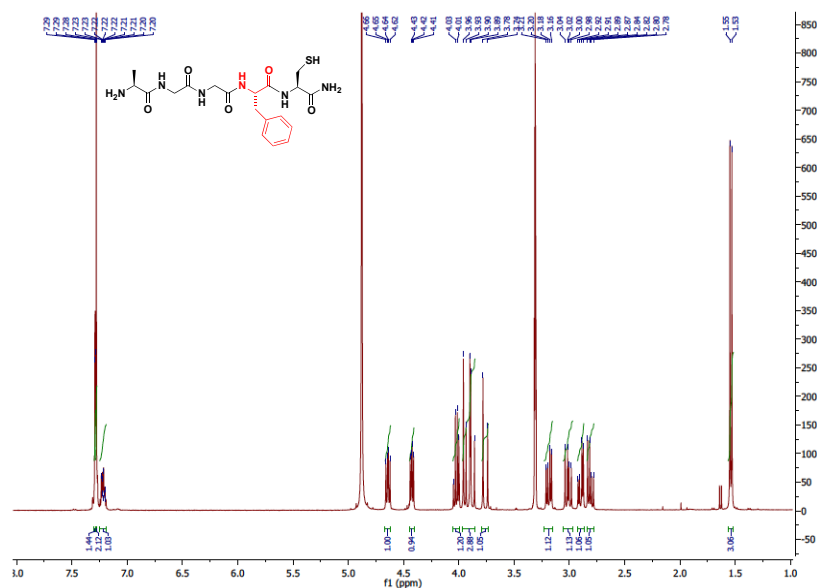
**<sup>13</sup>C NMR (100 MHz, D<sub>2</sub>O)** δ 133.19, 118.66, 101.08, 75.82, 75.70, 73.02, 70.53, 69.57, 60.66.

<sup>64</sup> J. M. J. Tronchet, M. Zsély, M. Geoffroy, *Carbohydrate Research*, 275, (1995), 245-258.

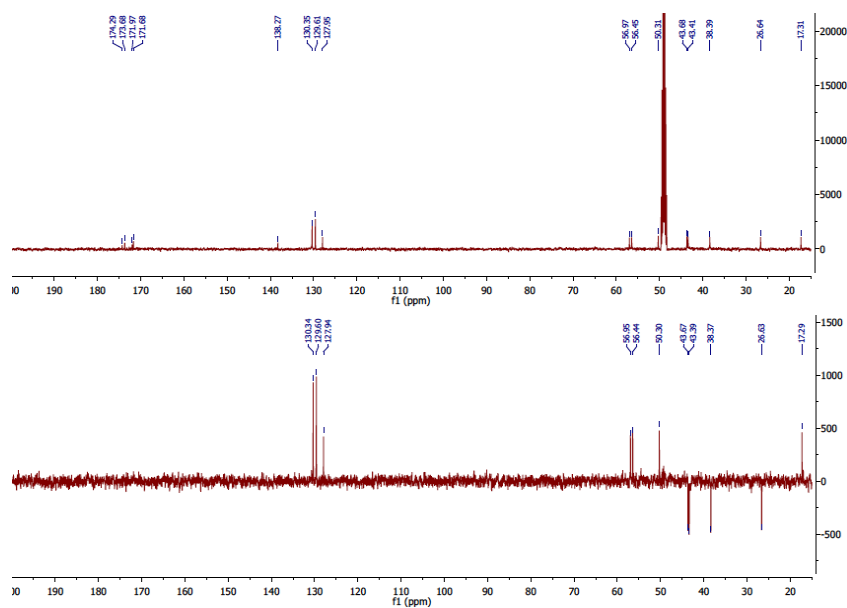
## General procedure of synthesis for Thiol-ene reaction



## NMR study first series of pentapeptide

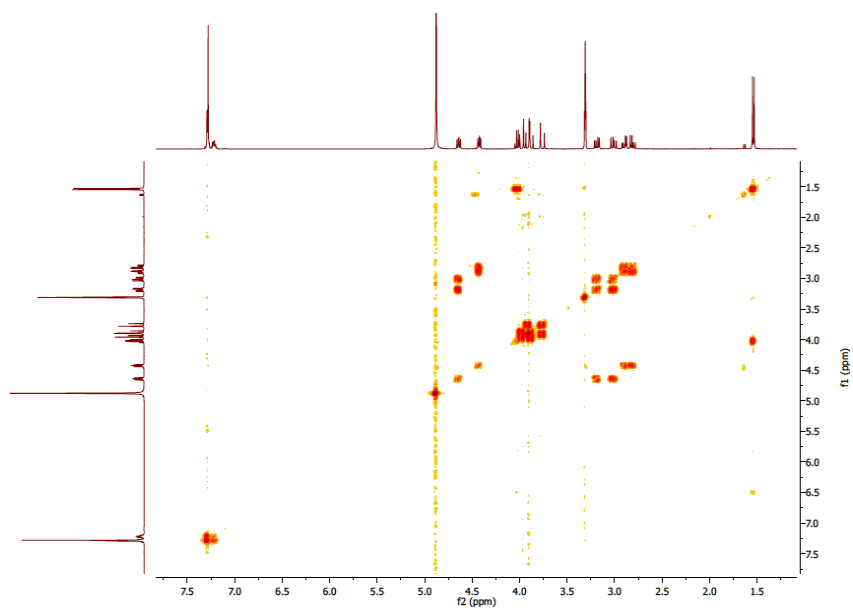
<sup>1</sup>H AGGFC (26)

**<sup>1</sup>H NMR (400 MHz, Methanol-d<sub>4</sub>)**  $\delta$  7.29 (d,  $J$  = 1.3 Hz, 2H), 7.28 (s, 2H), 7.25 - 7.18 (m, 1H), 4.64 (dd,  $J$  = 8.9, 6.0 Hz, 1H), 4.43 (dd,  $J$  = 7.5, 5.1 Hz, 1H), 4.06 - 3.99 (m, 1H), 3.97 - 3.85 (m, 3H), 3.76 (d,  $J$  = 16.7 Hz, 1H), 3.19 (dd,  $J$  = 13.9, 6.1 Hz, 1H), 3.01 (dd,  $J$  = 13.8, 8.9 Hz, 1H), 2.90 (dd,  $J$  = 13.9, 5.1 Hz, 1H), 2.81 (dd,  $J$  = 13.9, 7.6 Hz, 1H), 1.54 (d,  $J$  = 7.1 Hz, 3H).

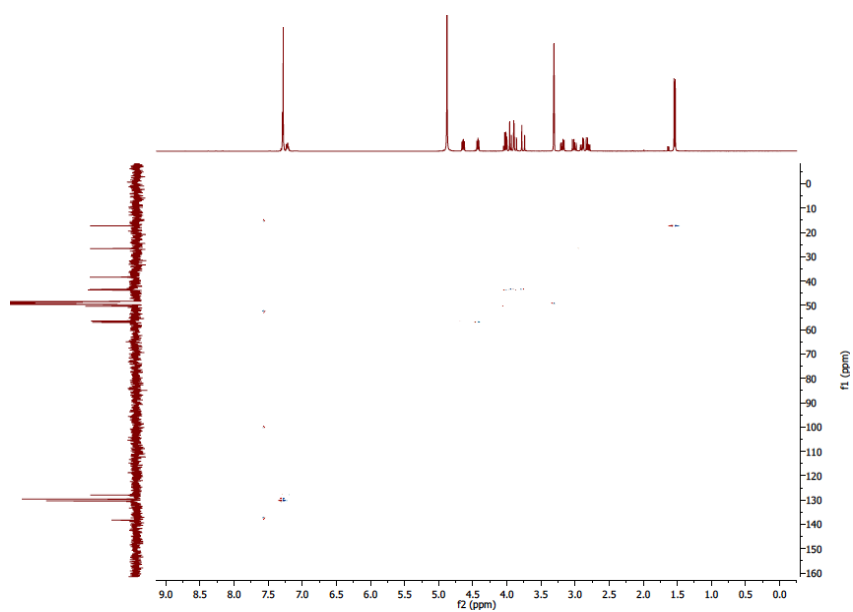
<sup>13</sup>C-DEPT AGGFC (26)

**<sup>13</sup>C NMR (100 MHz, Methanol-d<sub>4</sub>)**  $\delta$  174.29, 173.68, 171.97, 171.68, 138.27, 130.35, 129.61, 127.95, 56.97, 56.45, 50.31, 43.68, 43.41, 38.39, 26.64, 17.31.

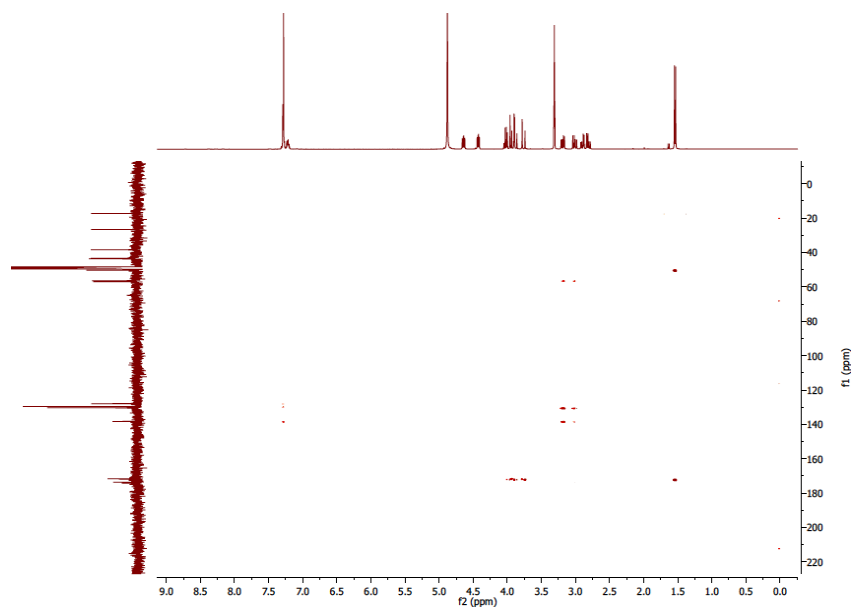
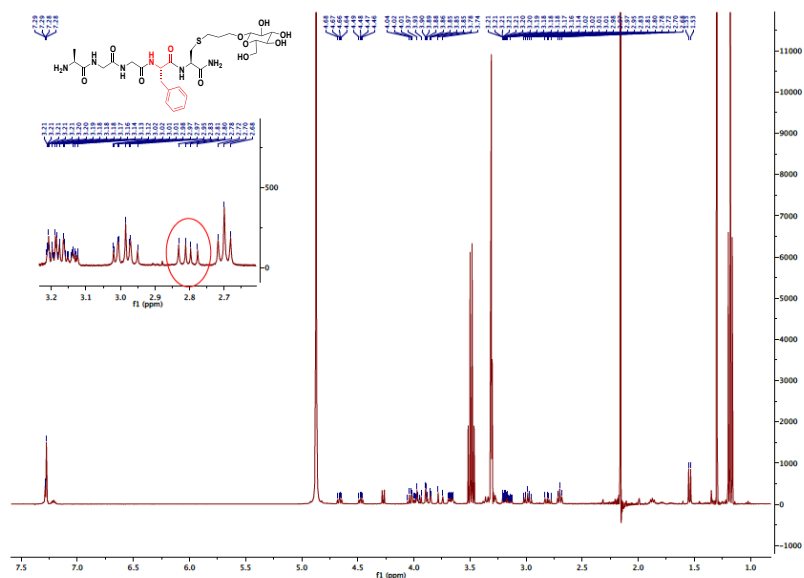
**COSY AGGFC (26)**



**HMBC AGGFC (26)**



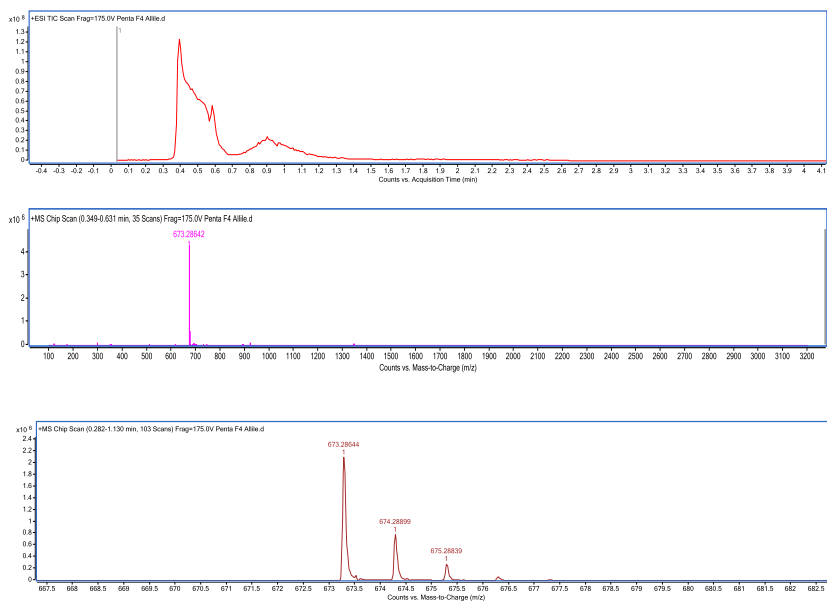
## HMQC AGGFC (26)

<sup>1</sup>H Thiol-ene I product (43)

**<sup>1</sup>H NMR (400 MHz, Methanol-*d*<sub>4</sub>)**  $\delta$  7.29 - 7.28 (m, 1H), 7.28 (s, 2H), 4.66 (dd,  $J$  = 9.1, 5.7 Hz, 1H), 4.47 (dd,  $J$  = 8.0, 5.9 Hz, 1H), 4.07 - 3.92 (m, 2H), 3.91 - 3.83 (m, 2H), 3.76 (d,  $J$  = 16.7 Hz, 1H), 3.71 - 3.62 (m, 1H), 3.22 - 3.10 (m, 2H), 3.03 - 2.93 (m, 1H), 2.80 (dd,  $J$  = 13.9, 8.0 Hz, 1H), 2.70 (t,  $J$  = 7.2 Hz, 2H).

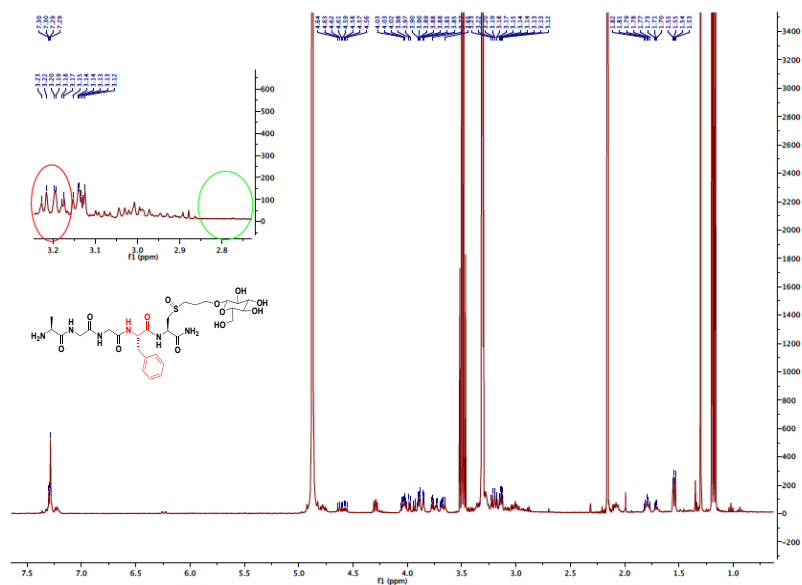
**MS (ESI):**  $[M+H]^+$  = 672.7



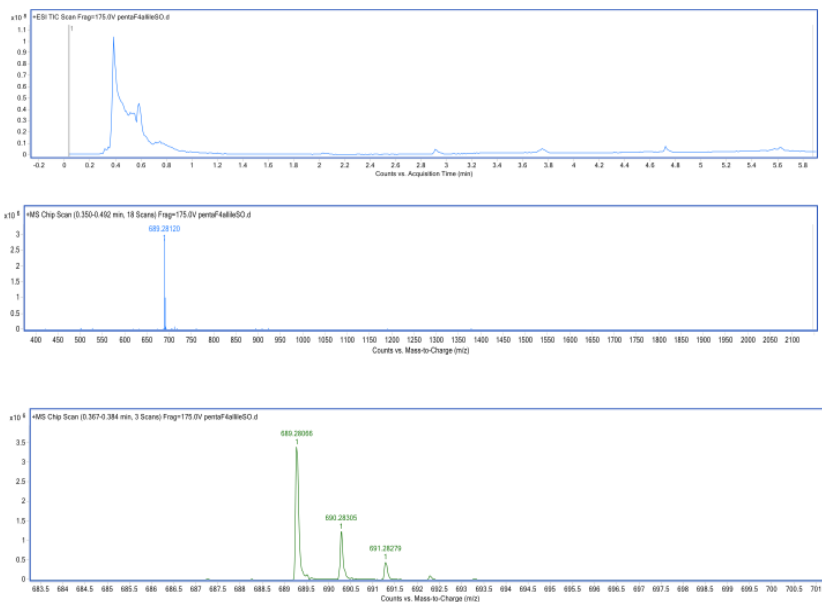


HRMS spectra of Thiol-ene primary product.

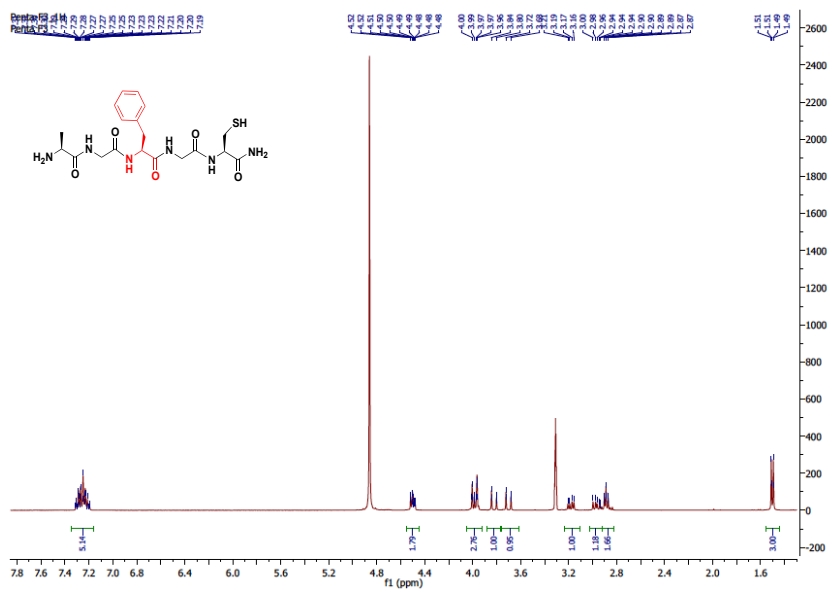
### $^1\text{H}$ Thiol-ene II product (43bis)



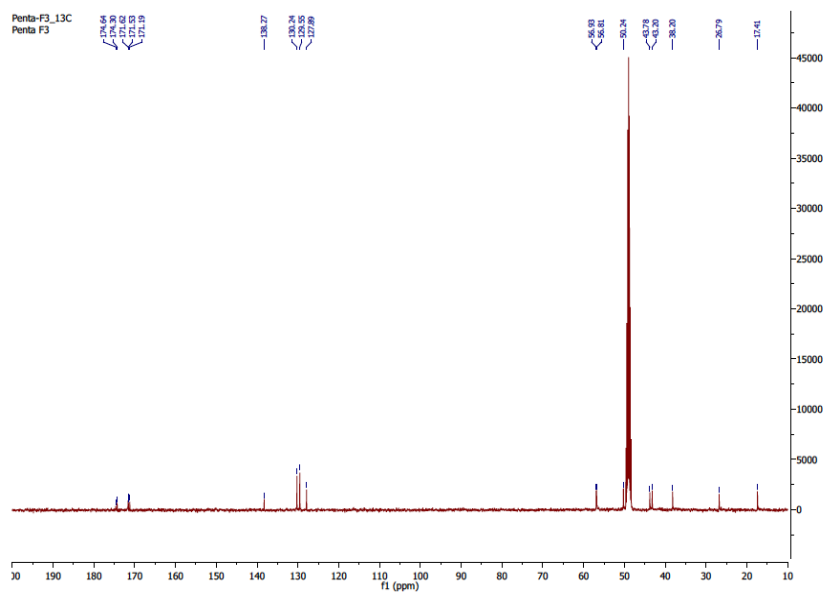
MS (ESI):  $[\text{M}+\text{H}]^+ = 688.7$



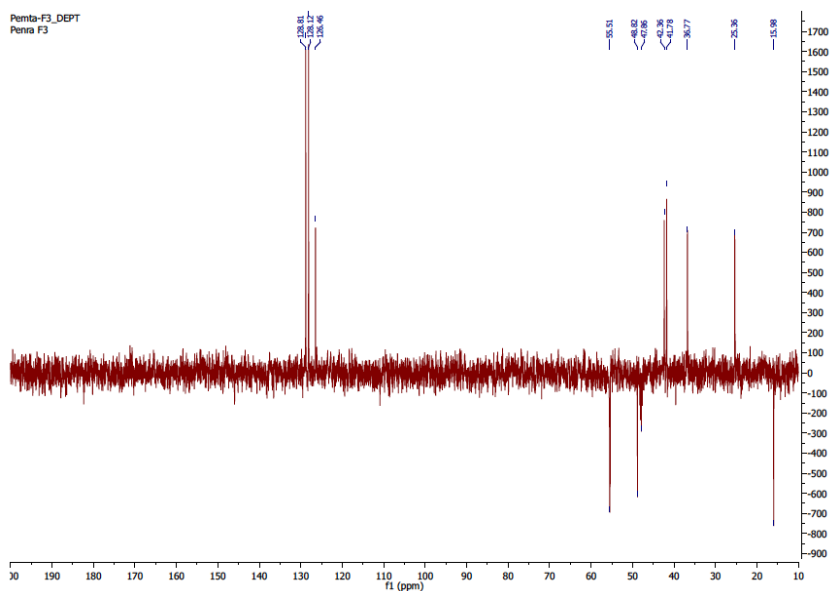
HRMS spectra of Thiol-ene secondary product.

**<sup>1</sup>H AGFGC (27)**

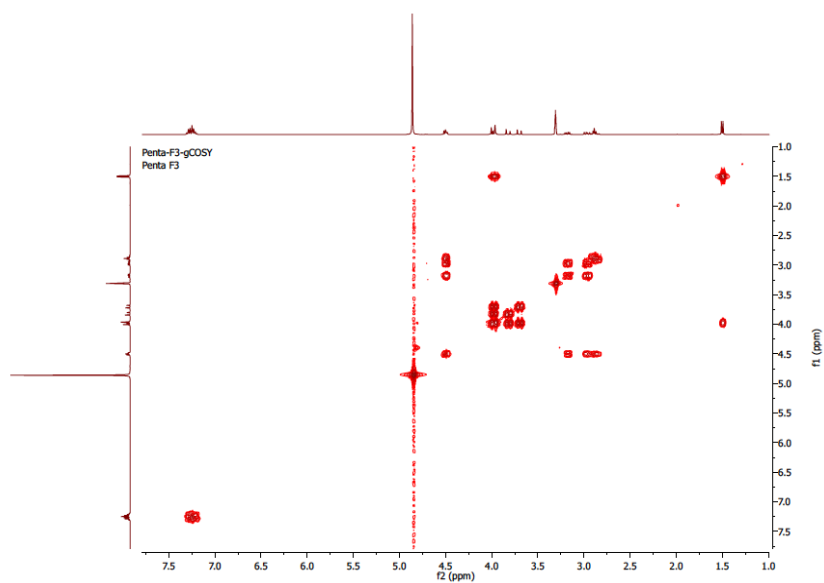
**<sup>1</sup>H NMR (400 MHz, Methanol-d<sub>4</sub>)** δ 7.34 - 7.17 (m, 5H), 4.50 (ddd, *J* = 8.3, 5.9, 1.9 Hz, 2H), 4.04 - 3.93 (m, 3H), 3.82 (dd, *J* = 16.6, 1.2 Hz, 1H), 3.70 (dd, *J* = 16.7, 1.2 Hz, 1H), 3.18 (dd, *J* = 13.8, 6.2 Hz, 1H), 3.03 - 2.92 (m, 1H), 2.92 - 2.85 (m, 2H), 1.50 (dd, *J* = 7.1, 1.3 Hz, 3H).

**$^{13}\text{C}$  AGFGC (27)**

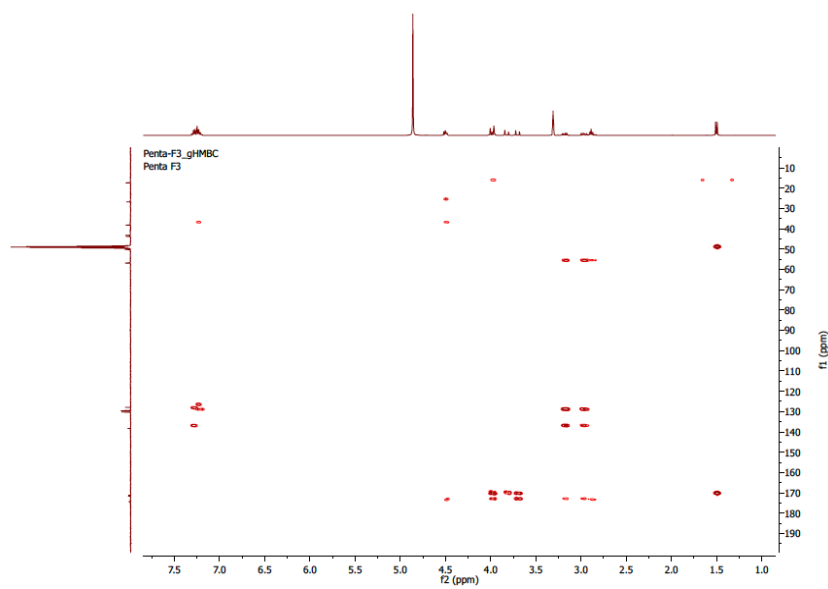
**$^{13}\text{C}$  NMR (100 MHz, Methanol- $d_4$ )**  $\delta$  174.64, 174.30, 171.62, 171.53, 171.19, 138.27, 130.24, 129.55, 127.89, 56.93, 56.81, 50.24, 43.78, 43.20, 38.20, 26.79, 17.41.

**DEPT AGFGC (27)**

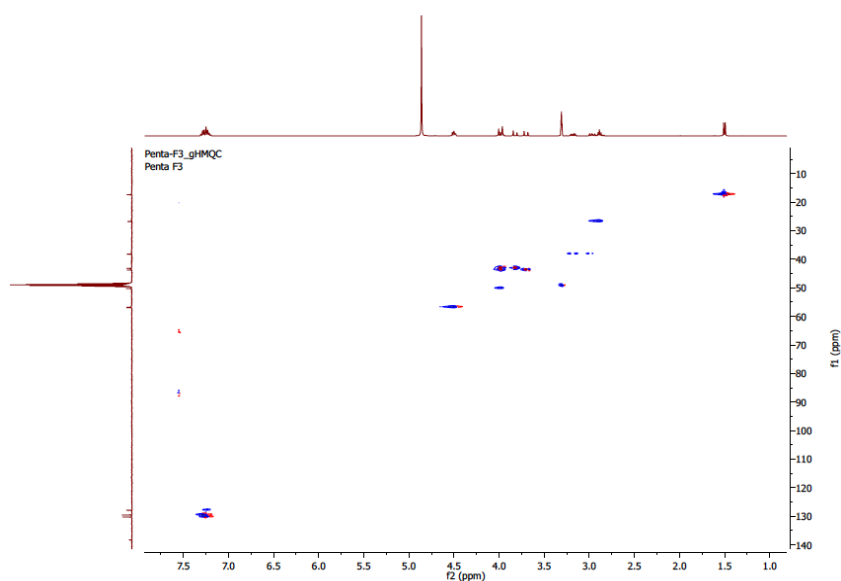
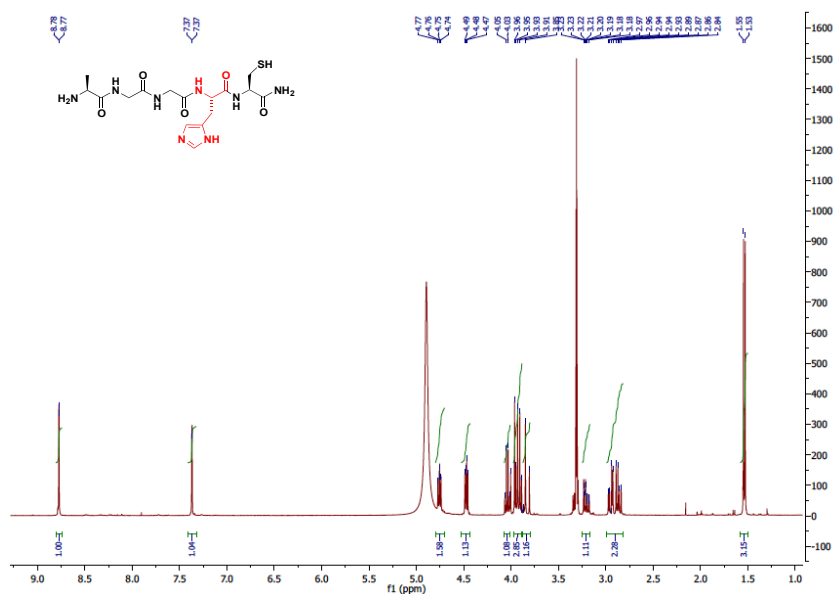
**COSY AGFGC (27)**



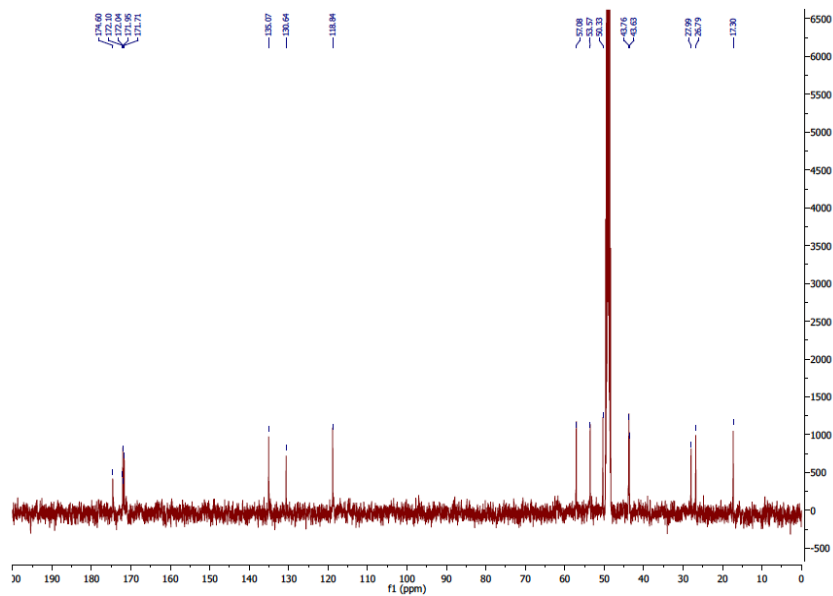
**HMBC AGFGC (27)**



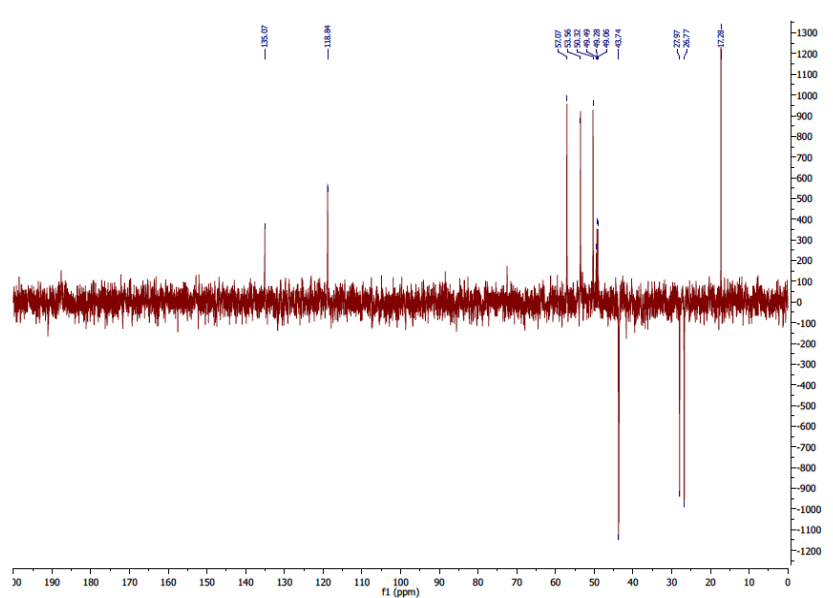
## HMQC AGFGC (27)

 $^1\text{H}$  AGGHC (28)

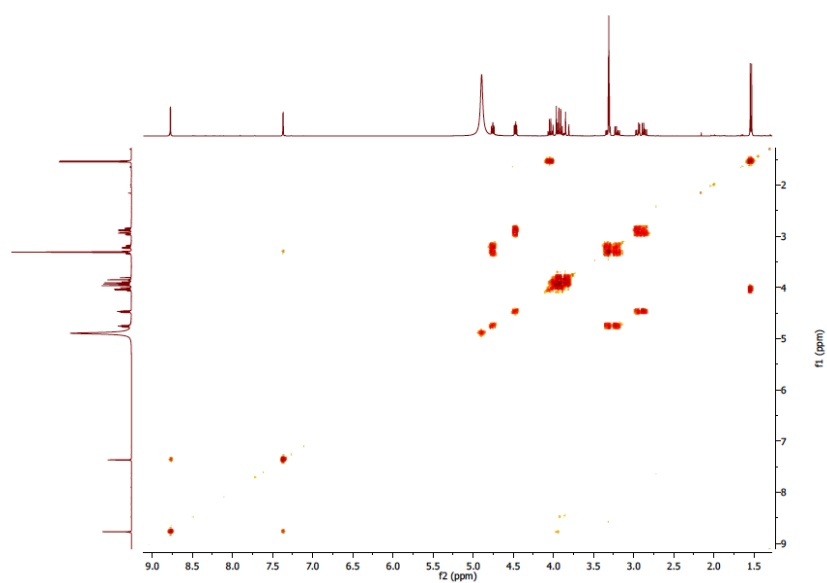
$^1\text{H}$  NMR (400 MHz, Methanol- $d_4$ )  $\delta$  8.77 (d,  $J$  = 1.4 Hz, 1H), 7.37 (d,  $J$  = 1.4 Hz, 1H), 4.76 (dd,  $J$  = 7.6, 5.8 Hz, 2H), 4.47 (dd,  $J$  = 7.7, 4.9 Hz, 1H), 4.04 (q,  $J$  = 7.1 Hz, 1H), 3.97 - 3.88 (m, 3H), 3.83 (d,  $J$  = 16.7 Hz, 1H), 3.20 (ddd,  $J$  = 15.3, 7.6, 0.8 Hz, 1H), 3.02 - 2.74 (m, 2H), 1.54 (d,  $J$  = 7.1 Hz, 3H).

**$^{13}\text{C}$  AGGHC (28)**

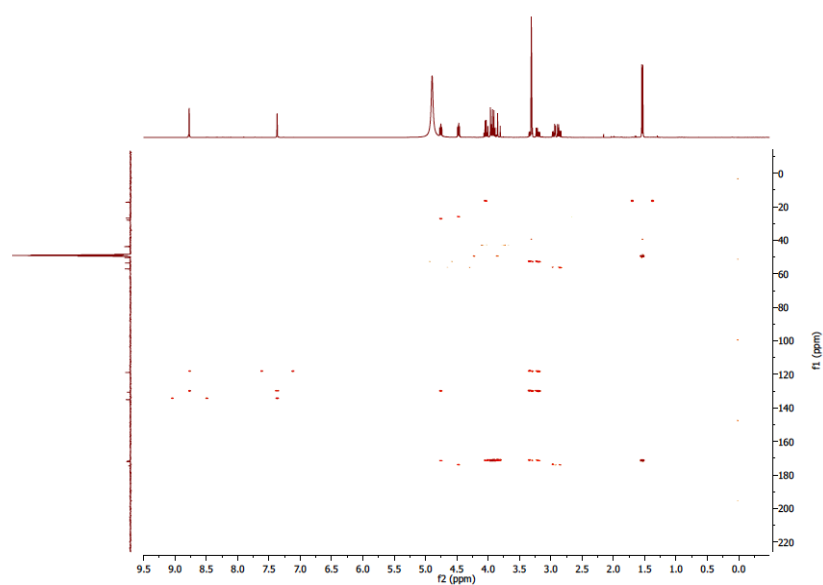
**$^{13}\text{C}$  NMR (100 MHz, Methanol- $d_4$ )  $\delta$  174.60, 172.10, 172.04, 171.95, 171.71, 135.07, 130.64, 118.84, 57.08, 53.57, 50.33, 43.76, 43.63, 27.99, 26.79, 17.30.**

**DEPT AGGHC (28)**

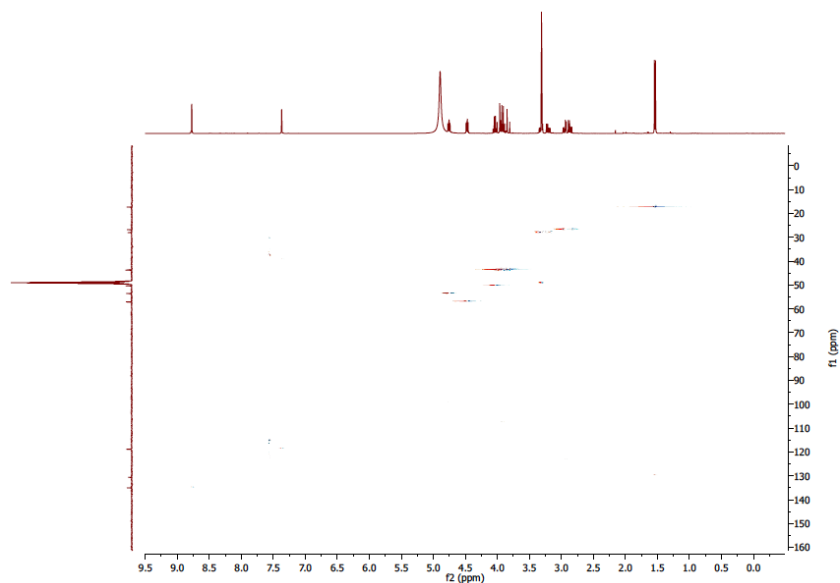
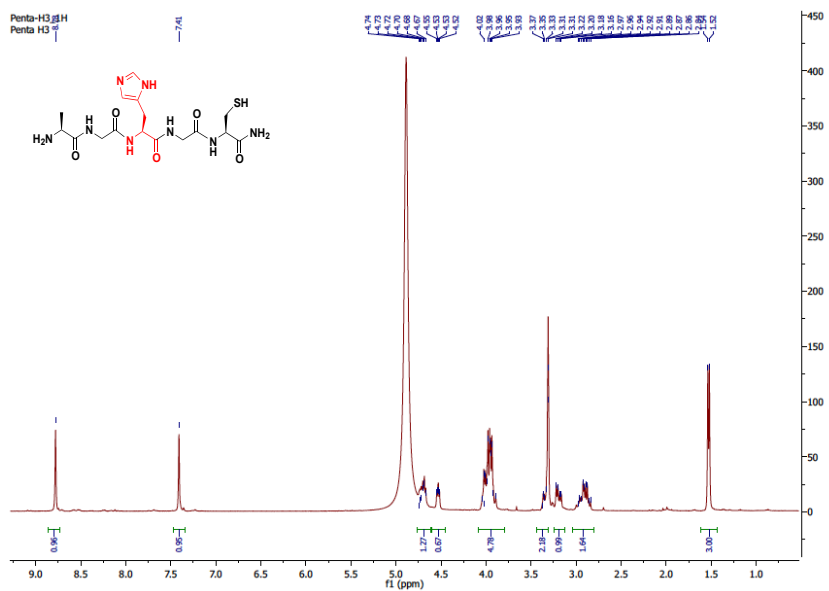
**COSY AGGHC (28)**



**HMBC AGGHC (28)**

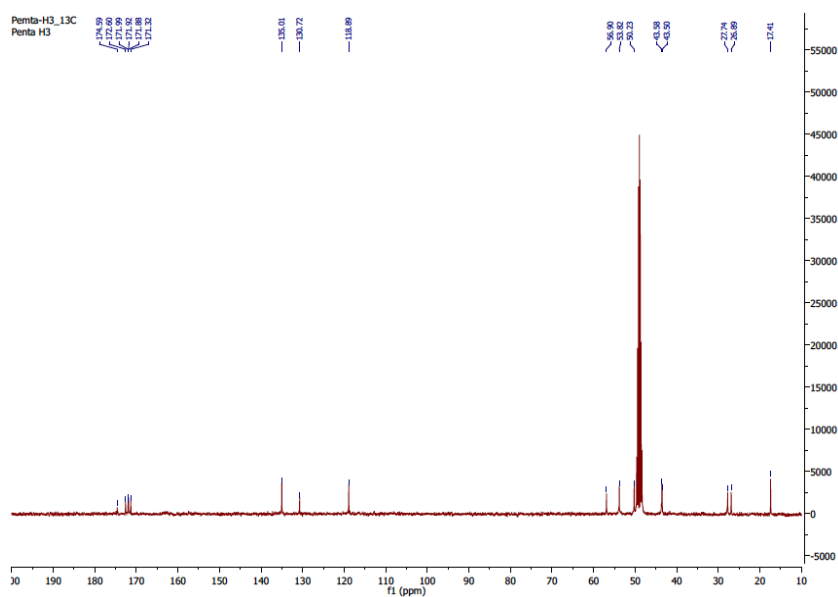


## HMQC AGGHC (28)

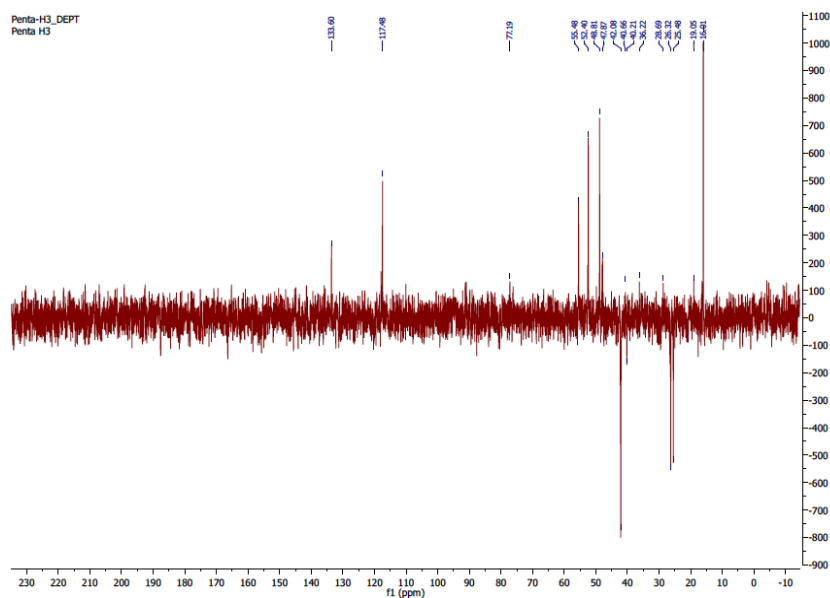
<sup>1</sup>H AGHGC (29)

**<sup>1</sup>H NMR (400 MHz, Methanol-d<sub>4</sub>)**  $\delta$  8.78 (s, 1H), 7.41 (s, 1H), 4.70 (dt,  $J = 13.1, 6.1$  Hz, 1H), 4.53 (dd,  $J = 7.4, 5.0$  Hz, 1H), 3.96 (qt,  $J = 16.0, 8.6$  Hz, 5H), 3.40 - 3.32 (m, 1H), 3.19 (dd,  $J = 15.4, 7.2$  Hz, 1H), 2.90 (qd,  $J = 14.1, 6.5$  Hz, 2H), 1.53 (d,  $J = 7.0$  Hz, 3H).

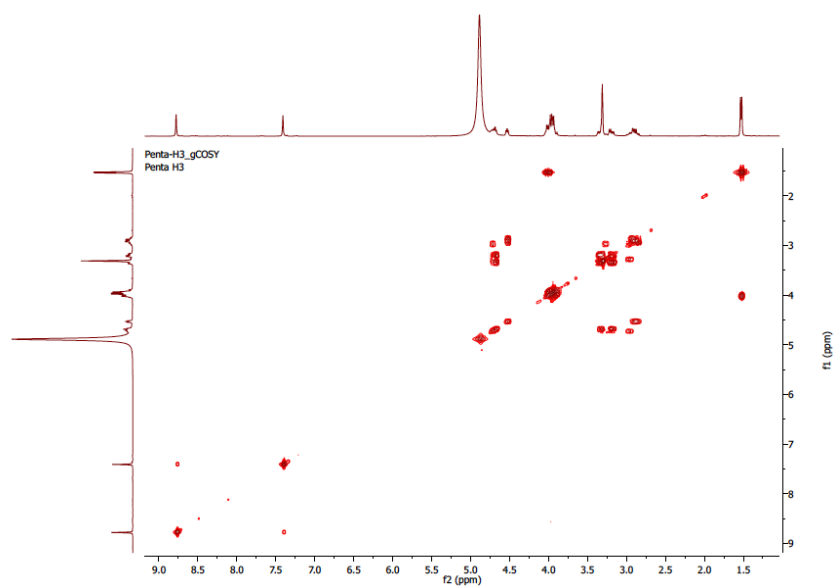


**$^{13}\text{C}$  AGHGC (29)**

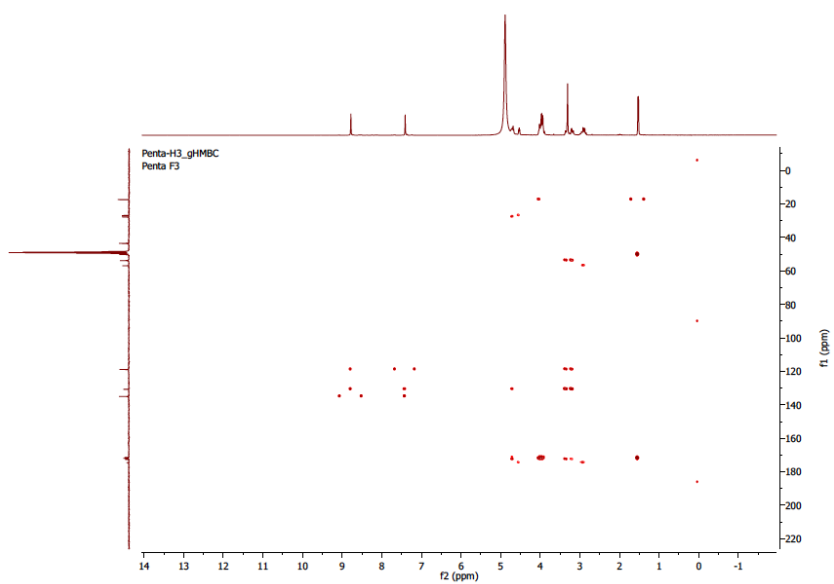
$^{13}\text{C}$  NMR (100 MHz, Methanol- $d_4$ )  $\delta$  174.59, 172.60, 171.99, 171.92, 171.88, 171.32, 135.01, 130.72, 118.89, 56.90, 53.82, 50.23, 43.58, 43.50, 27.74, 26.89, 17.41.

**DEPT AGHGC (29)**

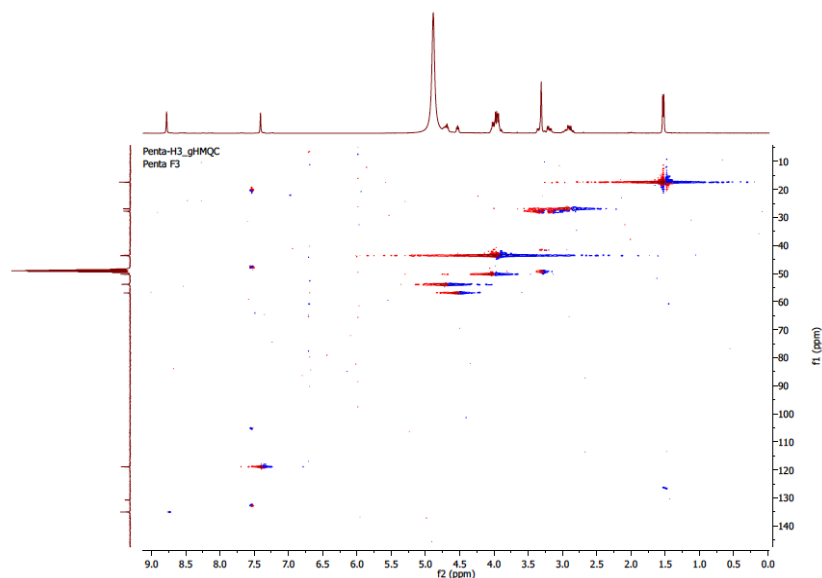
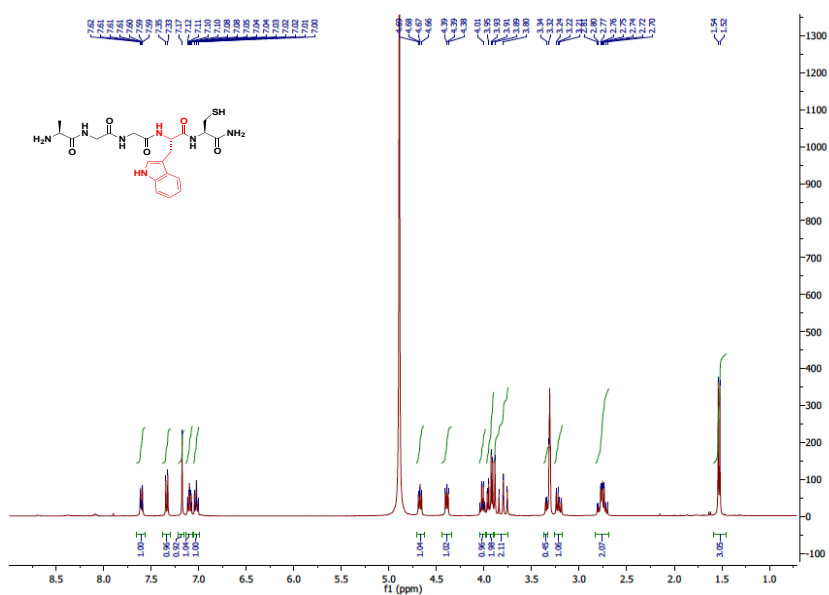
**COSY AGHGC (29)**



**HMBC AGHGC (29)**

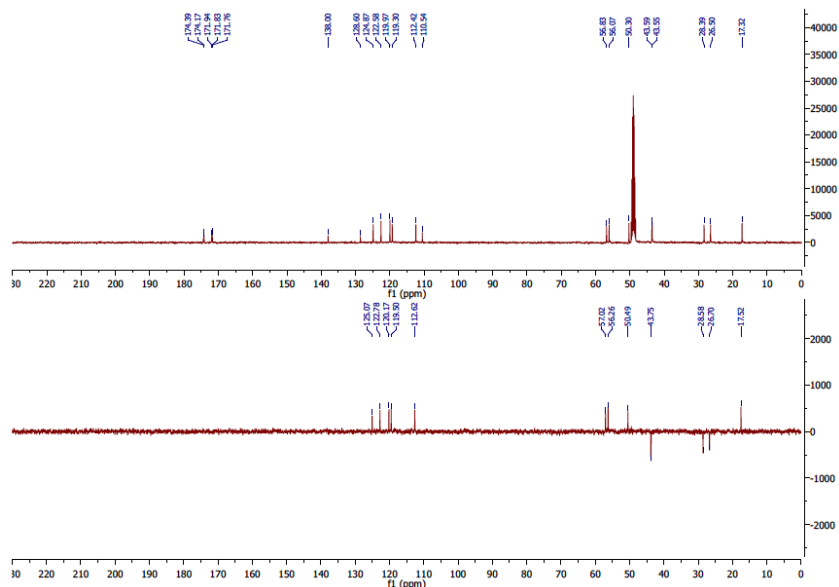


## HMQC AGHGC (29)

<sup>1</sup>H AGGWC (30)

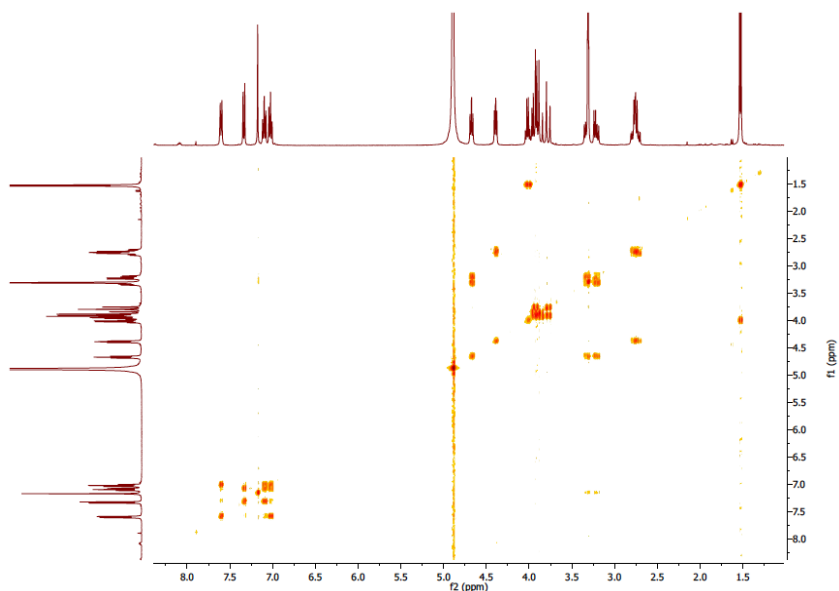
**<sup>1</sup>H NMR (400 MHz, Methanol-d<sub>4</sub>)**  $\delta$  7.69 -7.53 (m, 1H), 7.34 (d,  $J$  = 8.0 Hz, 1H), 7.17 (s, 1H), 7.13 - 7.07 (m, 1H), 7.02 (ddd,  $J$  = 8.0, 6.9, 1.1 Hz, 1H), 4.67 (dd,  $J$  = 7.7, 6.3 Hz, 1H), 4.39 (dd,  $J$  = 7.2, 5.2 Hz, 1H), 4.02 (q,  $J$  = 7.1 Hz, 1H), 3.94 (dd,  $J$  = 16.6, 6.6 Hz, 2H), 3.89 - 3.74 (m, 2H), 3.35 (d,  $J$  = 6.4 Hz, 1H), 3.21 (dd,  $J$  = 14.6, 7.7 Hz, 1H), 2.85 - 2.66 (m, 2H), 1.53 (d,  $J$  = 7.0 Hz, 3H).

**<sup>13</sup>C-DEPT AGGWC (30)**

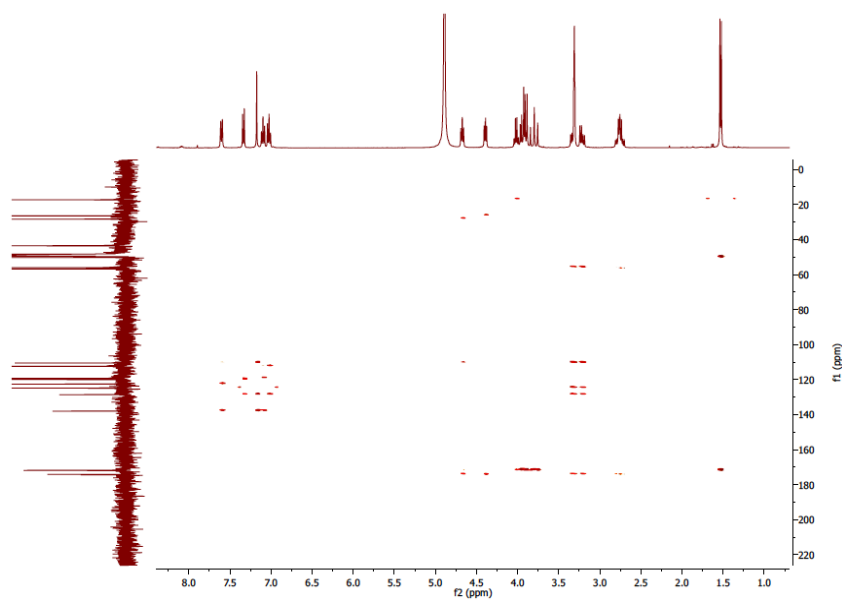


**<sup>13</sup>C NMR (100 MHz, Methanol-d<sub>4</sub>)**  $\delta$  174.39, 174.17, 171.94, 171.83, 171.76, 138.00, 128.60, 124.87, 122.58, 119.97, 119.30, 112.42, 110.54, 56.83, 56.07, 50.30, 43.59, 43.55, 28.39, 26.50, 17.32.

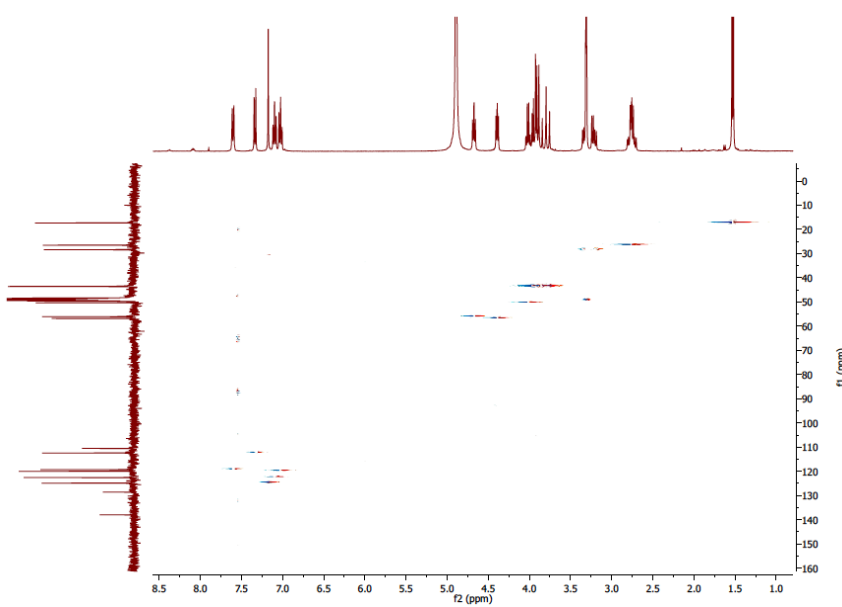
**COSY AGGWC (30)**

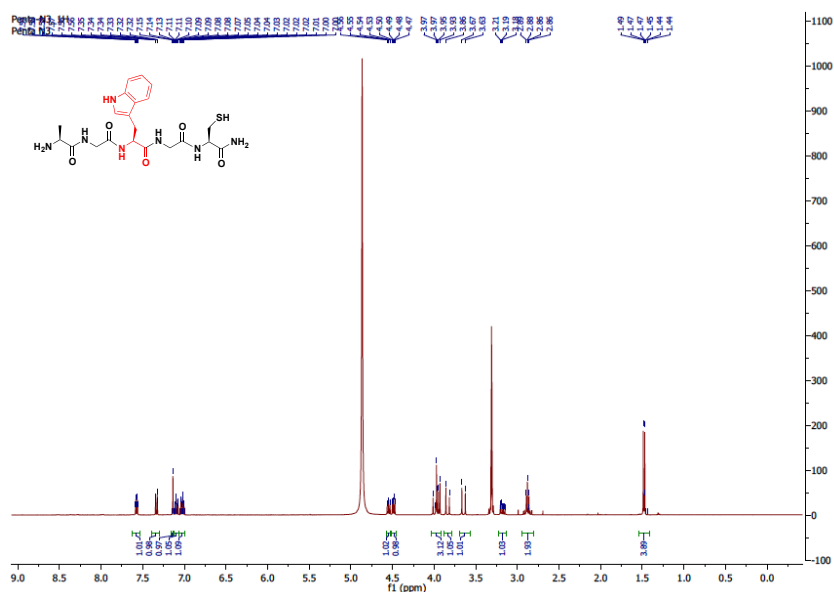


**HMBC AGGWC (30)**

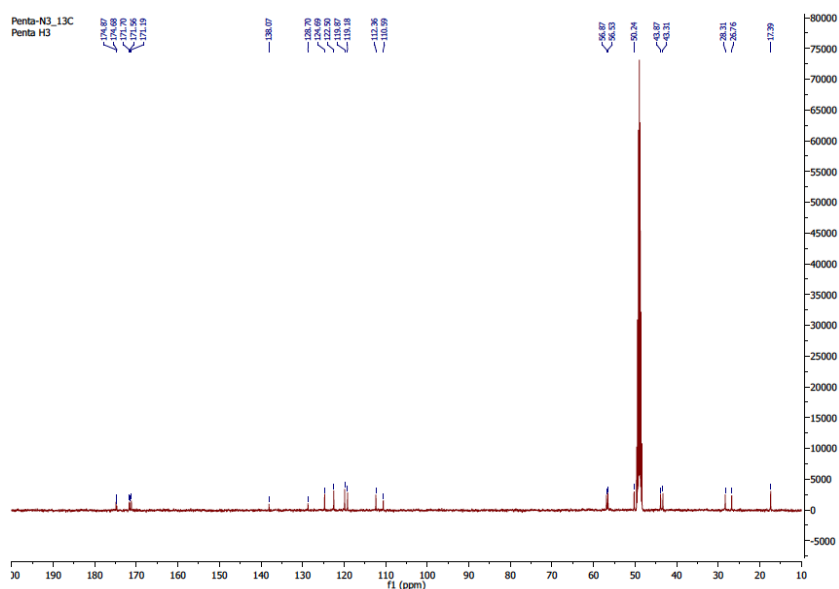


**HMQC AGGWC (30)**



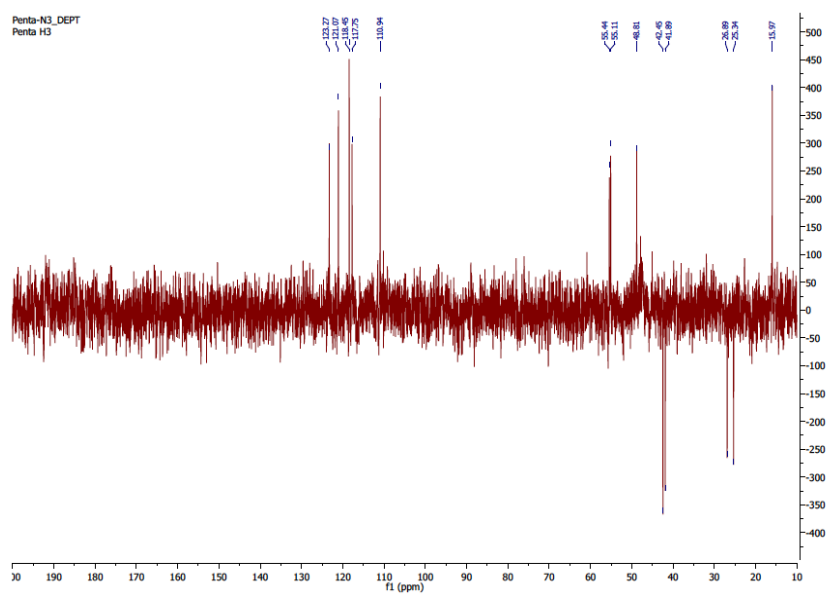
**<sup>1</sup>H AGWGC (31)**

**<sup>1</sup>H NMR (400 MHz, Methanol-d<sub>4</sub>)**  $\delta$  7.63 - 7.53 (m, 1H), 7.39 - 7.28 (m, 1H), 7.14 (s, 1H), 7.09 (ddd, J = 8.2, 7.0, 1.2 Hz, 1H), 7.02 (ddd, J = 8.0, 7.0, 1.1 Hz, 1H), 4.55 (dd, J = 7.6, 6.7 Hz, 1H), 4.49 (dd, J = 7.3, 5.3 Hz, 1H), 4.03 - 3.91 (m, 3H), 3.84 (d, J = 16.6 Hz, 1H), 3.65 (d, J = 16.7 Hz, 1H), 3.18 (ddd, J = 14.5, 7.6, 0.7 Hz, 1H), 2.92 - 2.81 (m, 2H), 1.48 (d, J = 7.1 Hz, 4H).

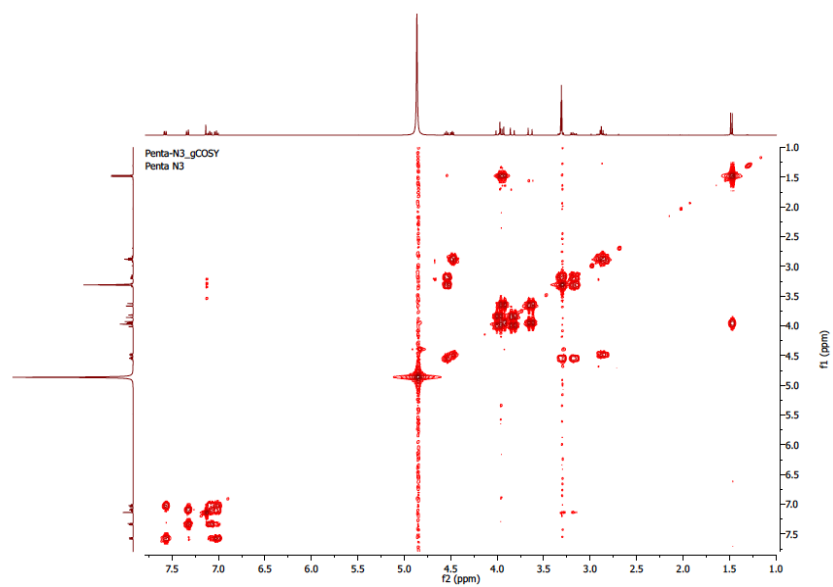
**<sup>13</sup>C AGWGC (31)**

**<sup>13</sup>C NMR (100 MHz, , Methanol-d<sub>4</sub>)**  $\delta$  174.87, 174.68, 171.70, 171.56, 171.19, 138.07, 128.70, 124.69, 122.50, 119.87, 119.18, 112.36, 110.59, 56.87, 56.53, 50.24, 43.87, 43.31, 28.31, 26.76, 17.39.

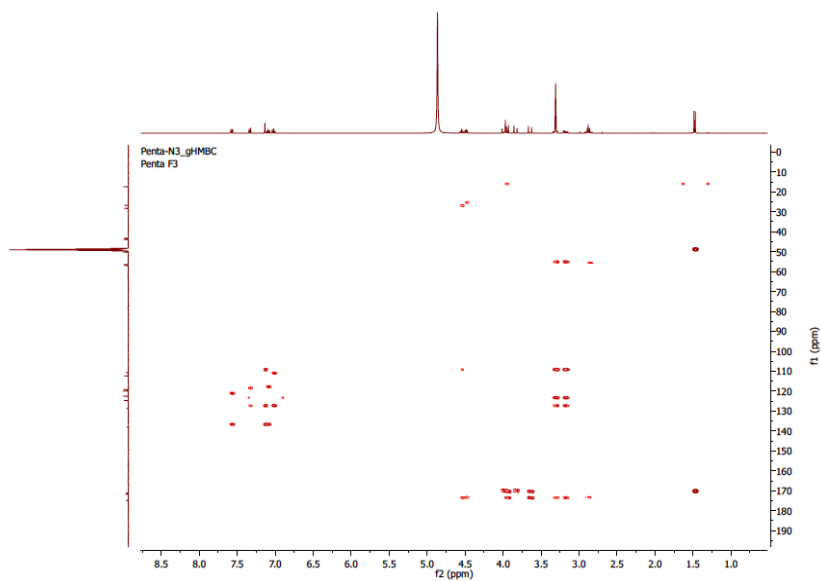
### DEPT AGWGC (31)



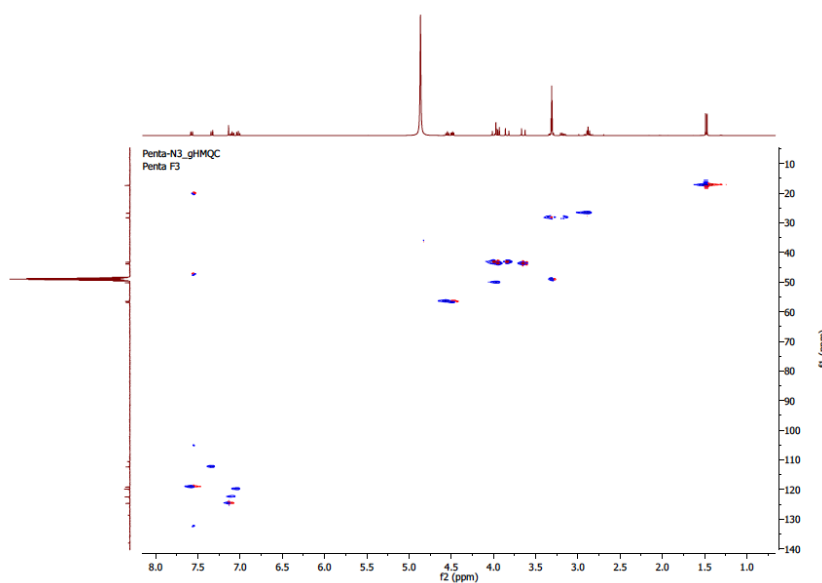
### COSY AGWG (31)



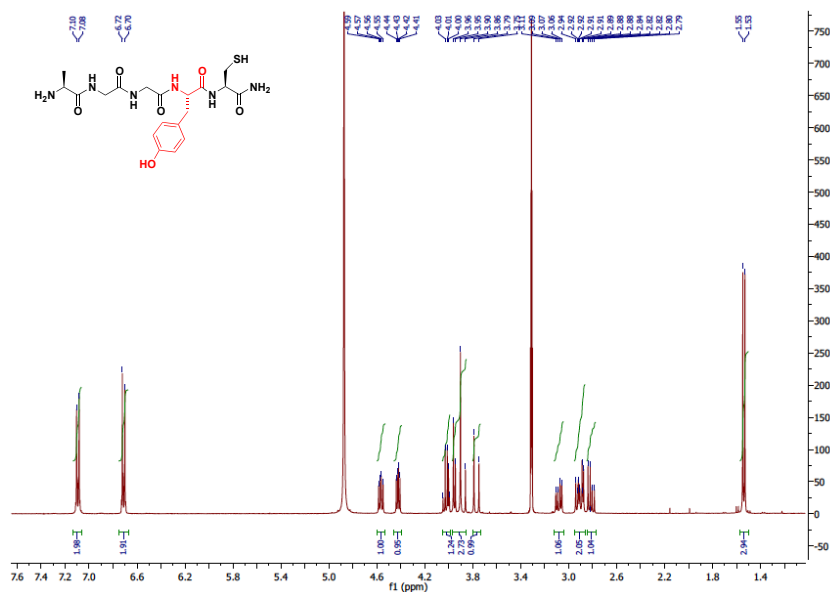
**HMBC AGWGC (31)**



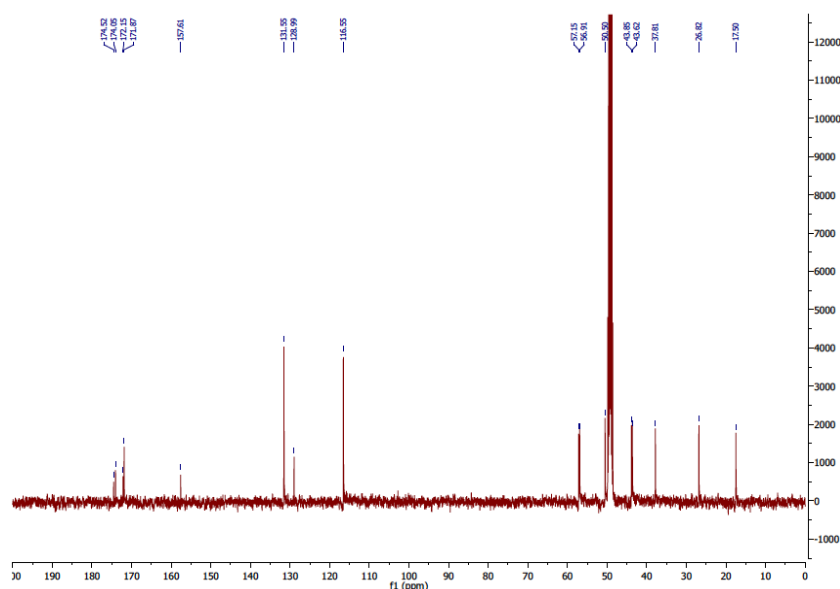
**HMQC AGWGC (31)**





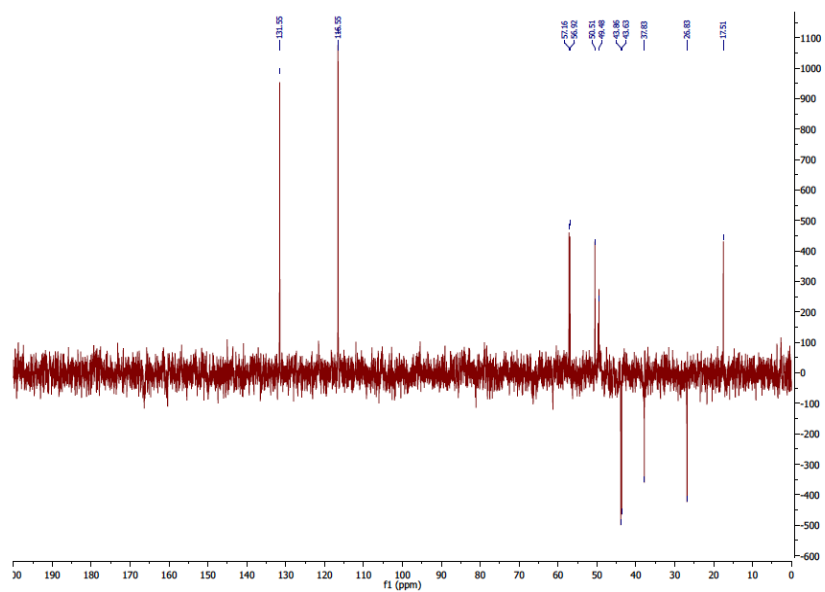
**<sup>1</sup>H AGGYC (32)**

**<sup>1</sup>H NMR (400 MHz, Methanol-d<sub>4</sub>)**  $\delta$  7.09 (d, J = 8.5 Hz, 2H), 6.71 (d, J = 8.5 Hz, 2H), 4.57 (dd, J = 8.7, 6.1 Hz, 1H), 4.42 (dd, J = 7.5, 5.1 Hz, 1H), 4.07 - 3.98 (m, 1H), 3.99 - 3.85 (m, 3H), 3.77 (d, J = 16.7 Hz, 1H), 3.08 (dd, J = 13.9, 6.1 Hz, 1H), 2.98 - 2.86 (m, 2H), 2.81 (dd, J = 13.9, 7.5 Hz, 1H), 1.54 (d, J = 7.1 Hz, 3H).

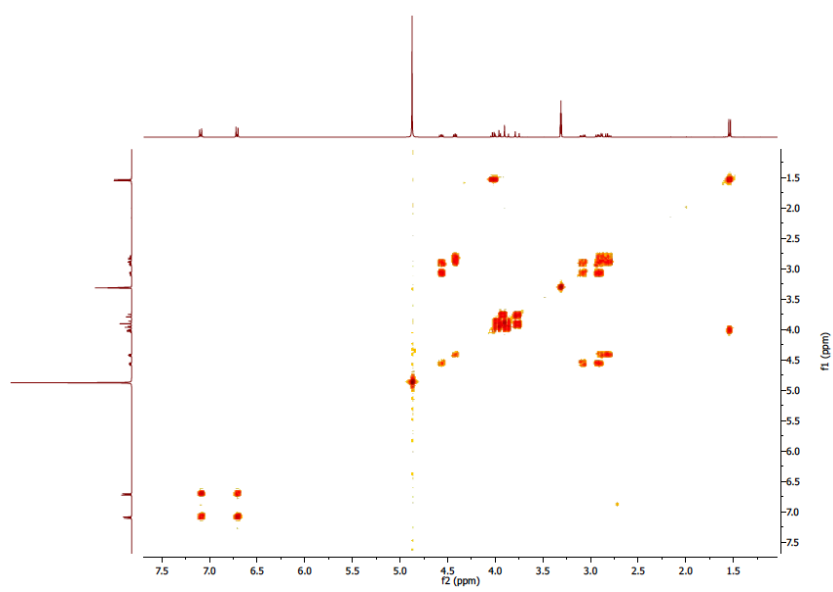
**<sup>13</sup>C AGGYC (32)**

**<sup>13</sup>C NMR (100 MHz, Methanol-d<sub>4</sub>)**  $\delta$  174.52, 174.05, 172.15, 171.87, 157.61, 131.55, 128.99, 116.55, 57.15, 56.91, 50.50, 43.85, 43.62, 37.81, 26.82, 17.50.

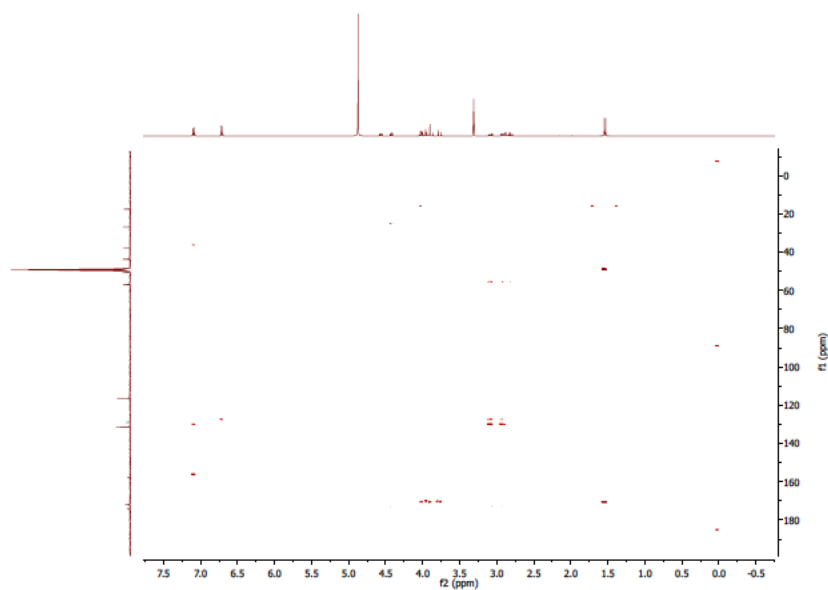
**DEPT AGGYC (32)**



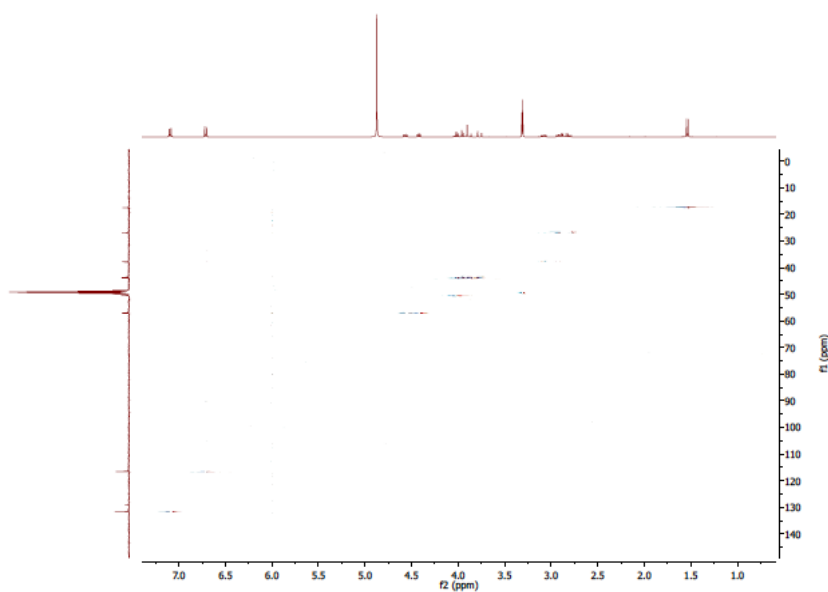
**COSY AGGYC (32)**



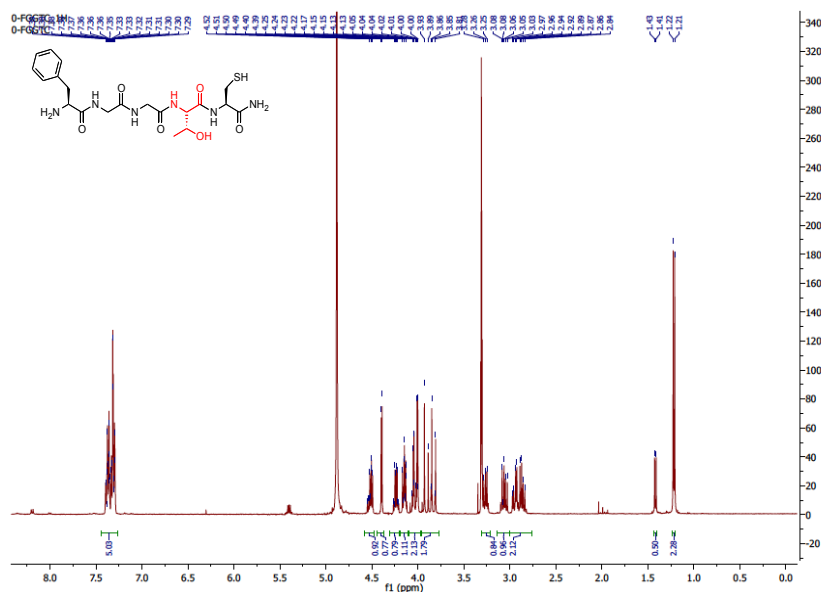
### HMBC AGGYC (32)



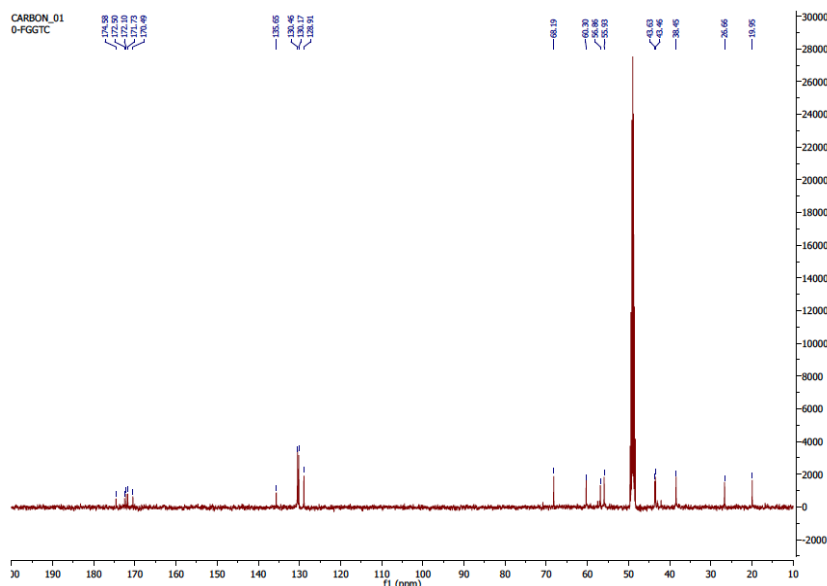
### HMQC AGGYC (32)



## NMR study second series of pentapeptide

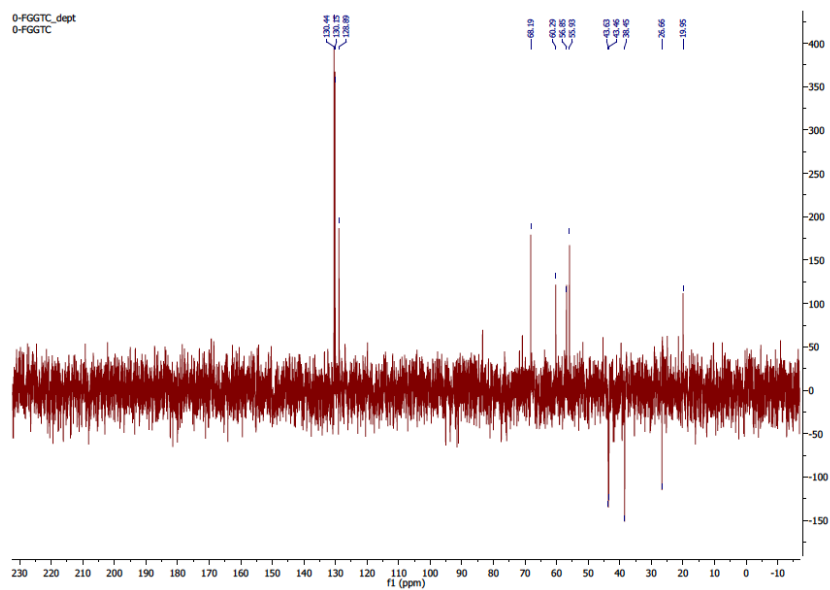
 $^1\text{H}$  FGGTC (33)

$^1\text{H}$  NMR (400 MHz, Methanol- $d_4$ )  $\delta$  7.44 -7.11 (m, 5H), 4.51 (dt,  $J$  = 7.4, 5.1 Hz, 1H), 4.39 (d,  $J$  = 4.0 Hz, 1H), 4.24 (qd,  $J$  = 6.4, 4.1 Hz, 1H), 4.19 - 4.11 (m, 2H), 4.09 - 3.70 (m, 2H), 3.29 - 3.22 (m, 1H), 3.06 (dd,  $J$  = 14.1, 8.3 Hz, 1H), 2.99 - 2.78 (m, 2H), 1.42 (d,  $J$  = 6.6 Hz, 1H), 1.22 (d,  $J$  = 6.4 Hz, 3H).

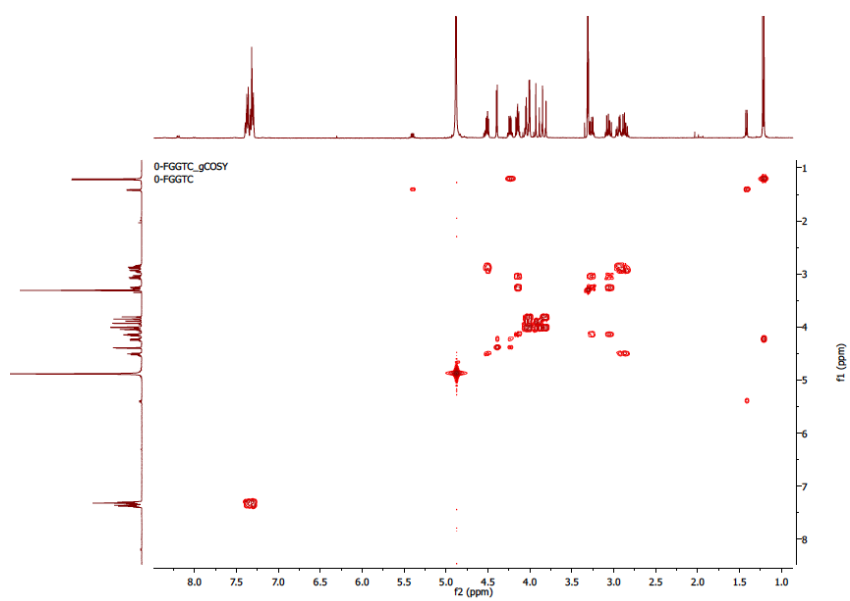
 $^{13}\text{C}$  FGGTC (33)

$^{13}\text{C}$  NMR (100 MHz, Methanol- $d_4$ )  $\delta$  174.58, 172.50, 172.10, 171.73, 170.49, 135.65, 130.46, 130.17, 128.91, 68.19, 60.30, 56.86, 55.93, 43.63, 43.46, 38.45, 26.66, 19.95.

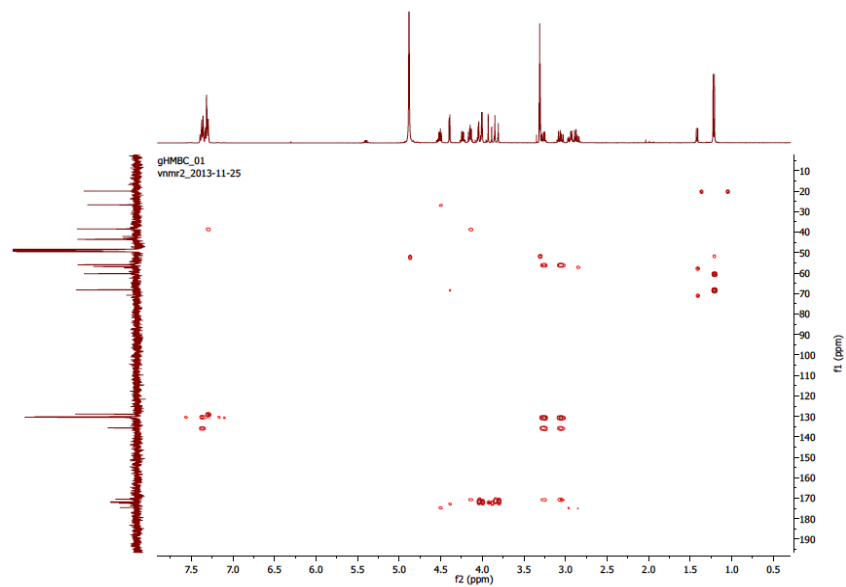
### DEPT FGGTC (33)



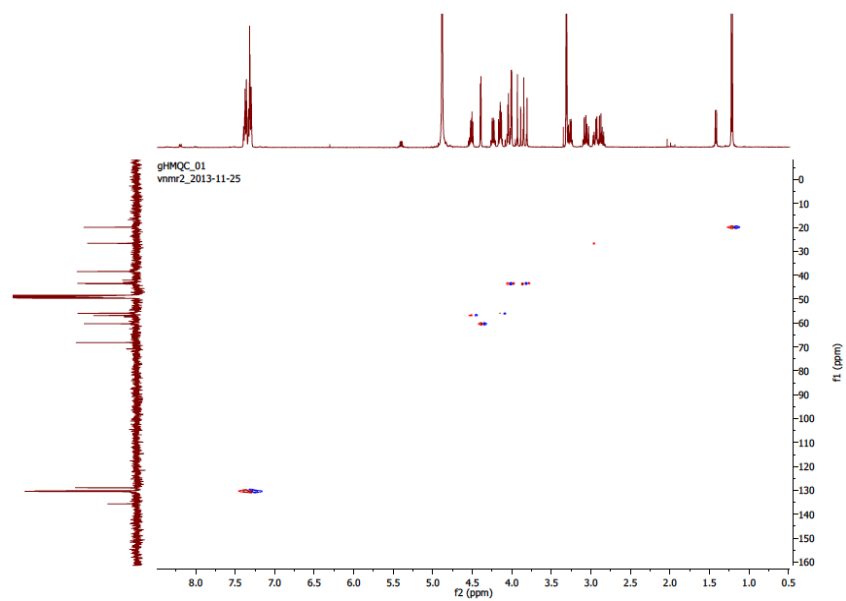
### COSY FGGTC (33)



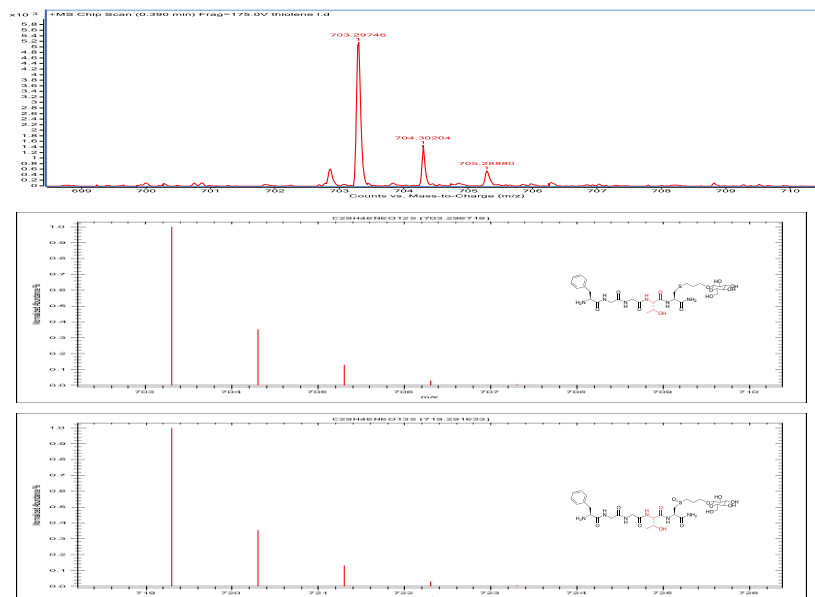
**HMBC FGGTC (33)**



**HMQC FGGTC (33)**

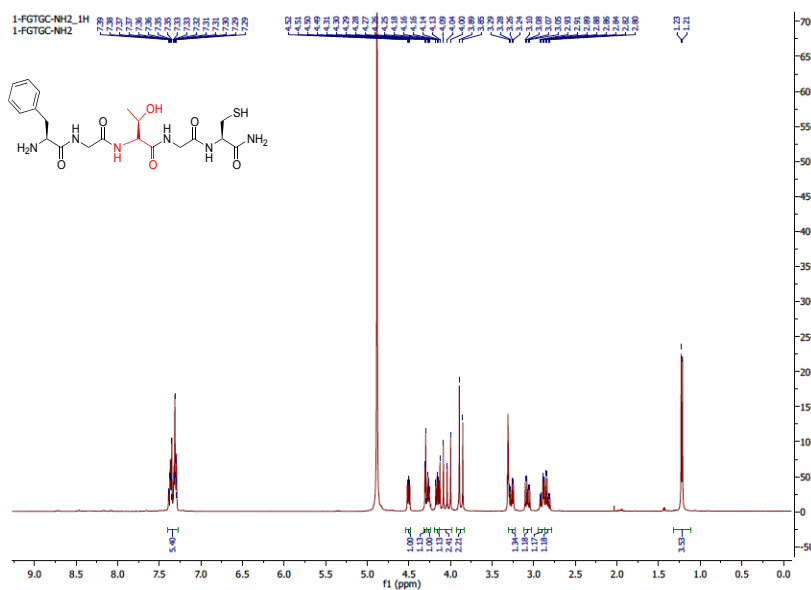


## THIOL-ENE COMPOUND (49)



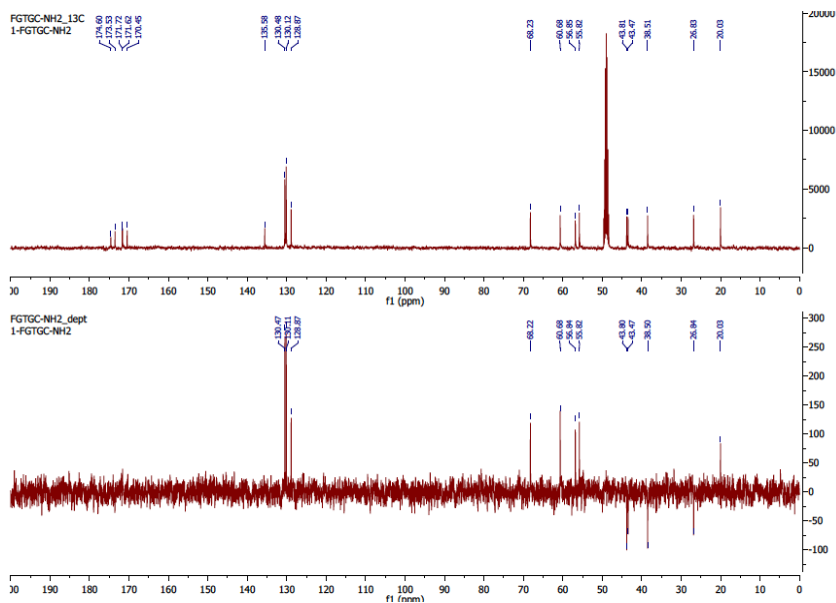
HRMS spectra of Thiol-ene product (49-49bis).

## <sup>1</sup>H FGTGC (34)



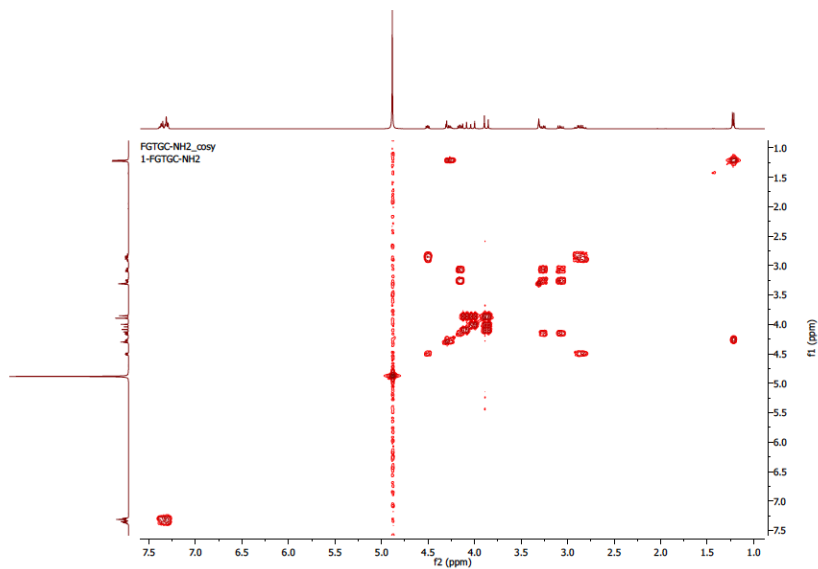
**<sup>1</sup>H NMR (400 MHz, Methanol-d<sub>4</sub>)**  $\delta$  7.42 -7.25 (m, 5H), 4.50 (dd, J = 7.5, 5.1 Hz, 1H), 4.32 - 4.23 (m, 2H), 4.16 (dd, J = 8.2, 6.3 Hz, 1H), 4.06 (dd, J = 34.7, 16.6 Hz, 2H), 3.87 (d, J = 16.6 Hz, 2H), 3.27 (dd, J = 14.1, 6.3 Hz, 1H), 3.07 (dd, J = 14.1, 8.2 Hz, 1H), 2.87 (qd, J = 13.9, 6.4 Hz, 1H), 1.22 (d, J = 6.3 Hz, 4H).

**<sup>13</sup>C-DEPT FGTGC (34)**



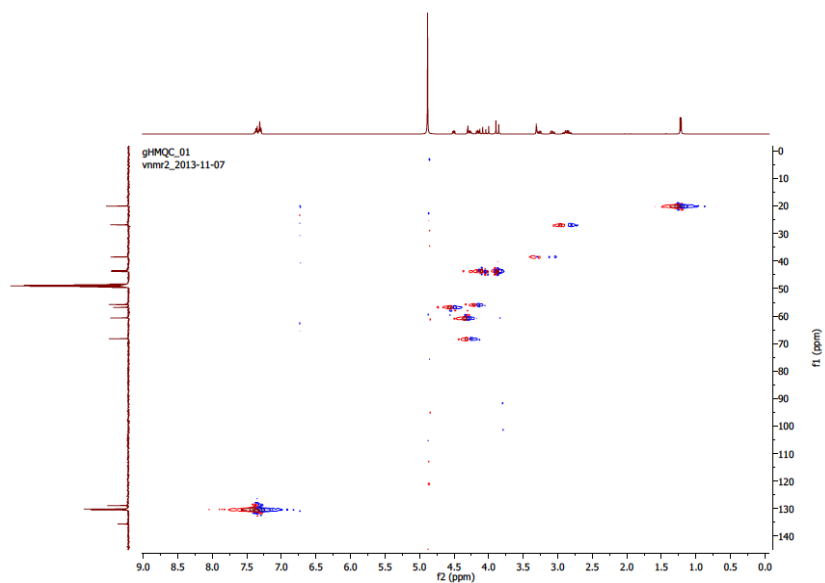
**<sup>13</sup>C NMR (100 MHz, Methanol-d<sub>4</sub>)**  $\delta$  174.60, 173.53, 171.72, 171.62, 170.45, 135.58, 130.48, 130.12, 128.87, 68.23, 60.68, 56.85, 55.82, 43.81, 43.47, 38.51, 26.83, 20.03.

**COSY FGTGC (34)**

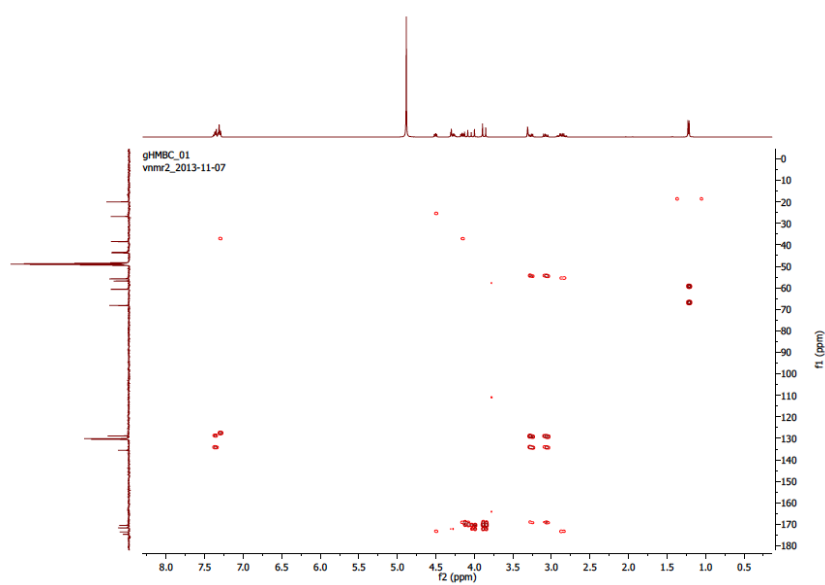




**HMBC FGTGC (34)**



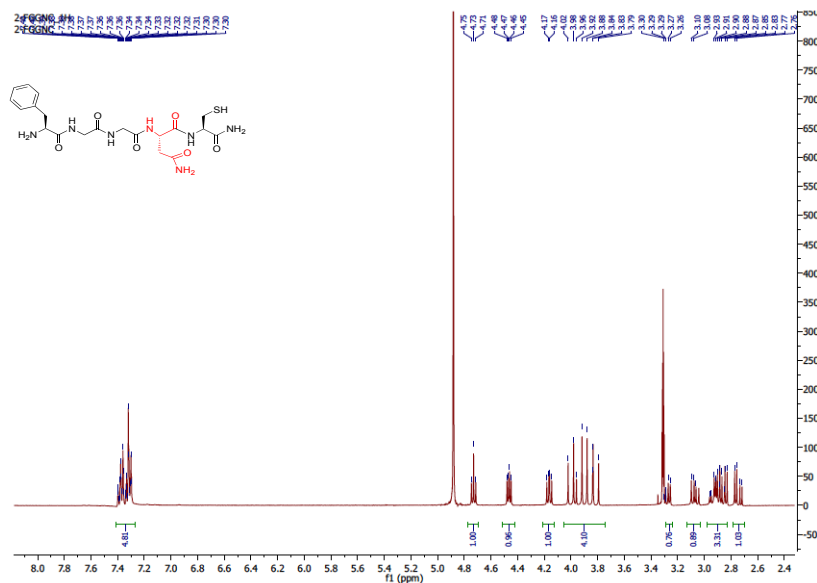
**HMQC FGTGC (34)**



## THIOL-ENE COMPOUND (50)

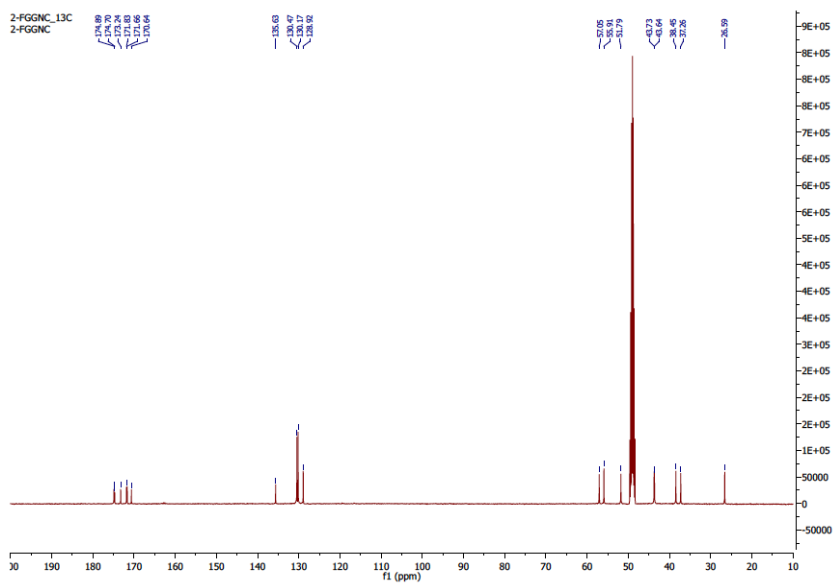


HRMS spectra of Thiol-ene product (50-50bis).

<sup>1</sup>H FGGNC (35)

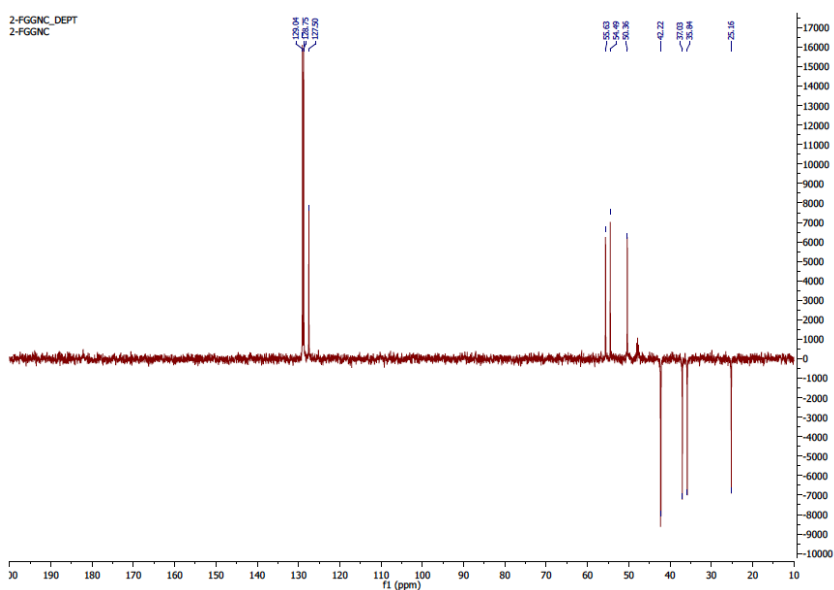
**<sup>1</sup>H NMR (400 MHz, Methanol-d<sub>4</sub>)** δ 7.49 -7.13 (m, 5H), 4.73 (t, J = 6.5 Hz, 1H), 4.46 (dd, J = 7.6, 4.8 Hz, 1H), 4.16 (dd, J = 8.4, 6.3 Hz, 1H), 4.05 - 3.77 (m, 4H), 3.30 - 3.24 (m, 1H), 3.13 - 3.02 (m, 1H), 2.98 - 2.80 (m, 3H), 2.75 (dd, J = 15.7, 6.4 Hz, 1H).

**<sup>13</sup>C FGGNC (35)**

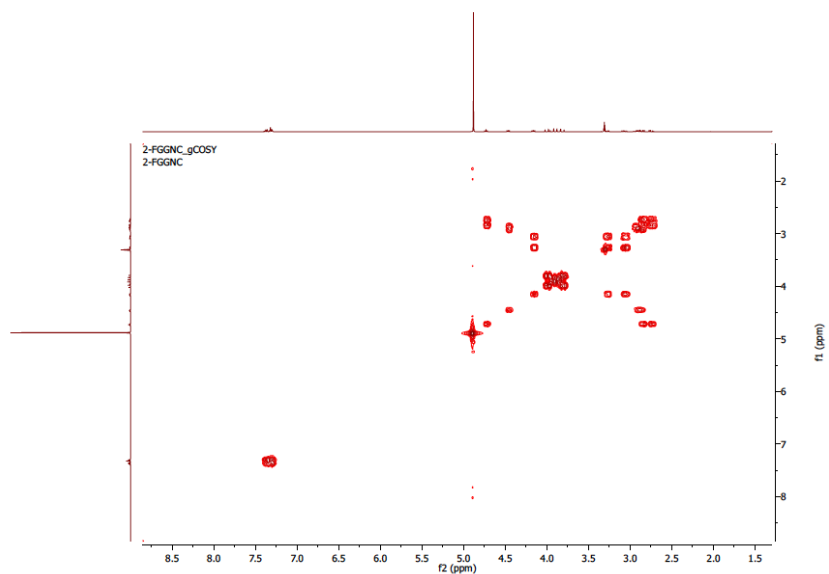


**<sup>13</sup>C NMR (100 MHz, Methanol-d<sub>4</sub>)** δ 174.89, 174.70, 173.24, 171.83, 171.66, 170.64, 135.63, 130.47, 130.17, 128.92, 57.05, 55.91, 51.79, 43.73, 43.64, 38.45, 37.26, 26.59.

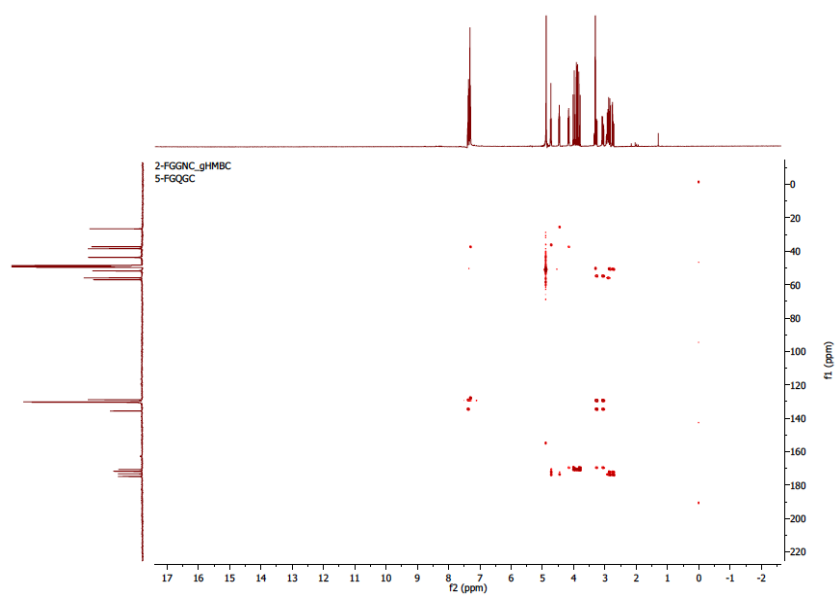
**DEPT FGGNC (35)**



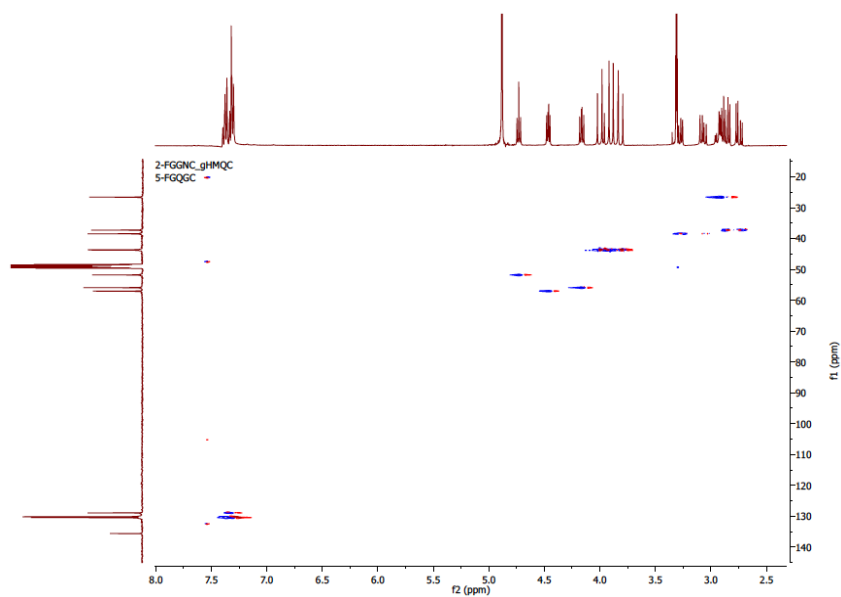
**COSY FGGNC (35)**



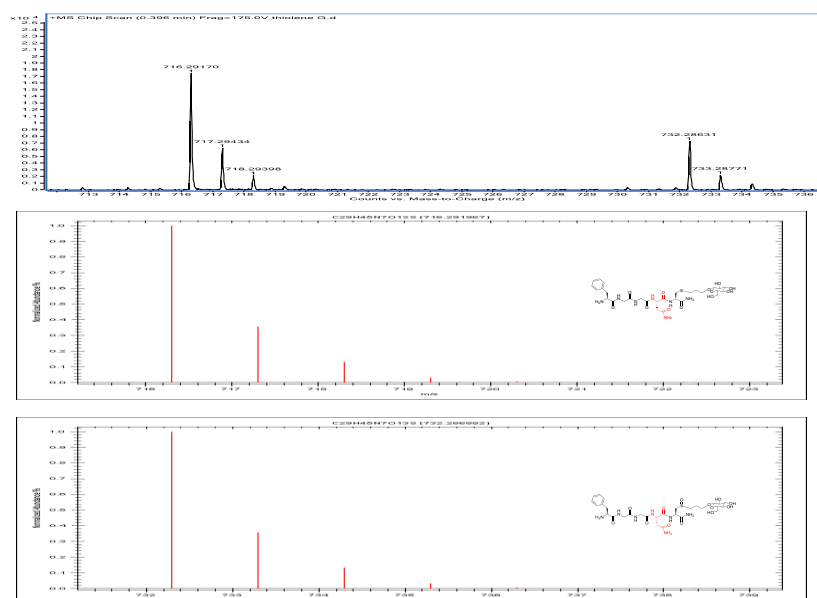
**HMBC FGGNC (35)**



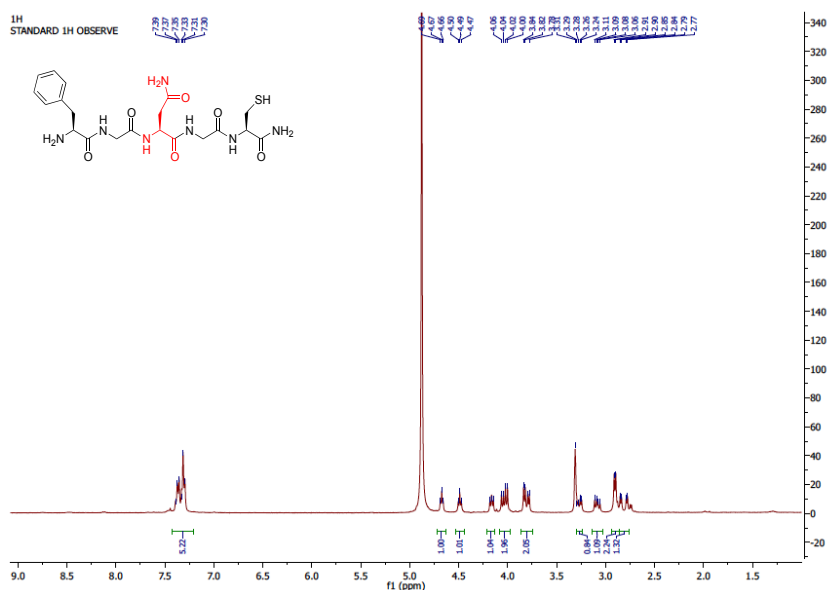
### HMQC FGGNC (35)



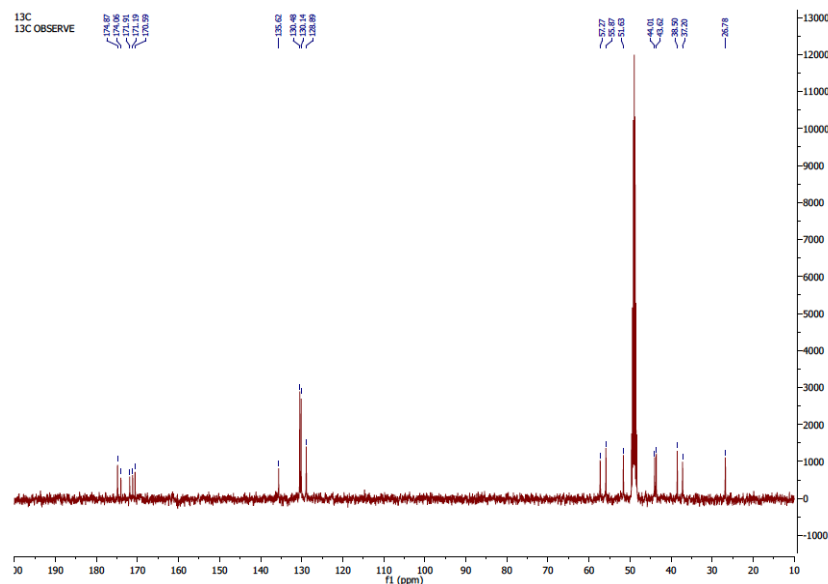
### THIOL-ENE COMPOUND (51)



HRMS spectra of Thiol-ene product (51-51bis).

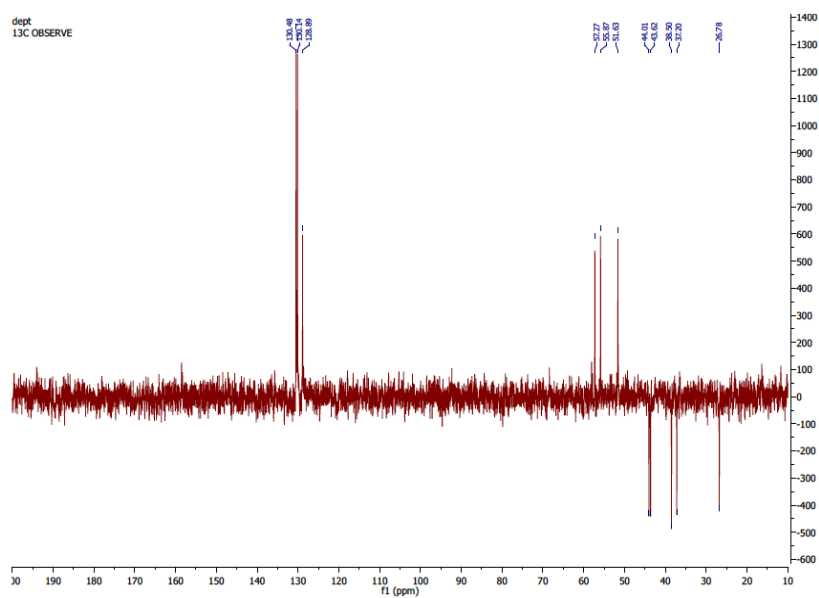
**<sup>1</sup>H FGNGC (36)**

**<sup>1</sup>H NMR (400 MHz, Methanol-d<sub>4</sub>)**  $\delta$  7.34 (dt,  $J = 23.5, 7.4$  Hz, 5H), 4.67 (t,  $J = 5.8$  Hz, 1H), 4.49 (t,  $J = 6.6$  Hz, 1H), 4.16 (dd,  $J = 8.2, 6.2$  Hz, 1H), 4.03 (dd,  $J = 16.7, 8.5$  Hz, 2H), 3.81 (dd,  $J = 16.7, 6.7$  Hz, 2H), 3.29 - 3.23 (m, 1H), 3.08 (dd,  $J = 14.1, 8.3$  Hz, 1H), 2.90 (d,  $J = 6.8$  Hz, 3H), 2.81 (dd,  $J = 25.0, 5.8$  Hz, 1H).

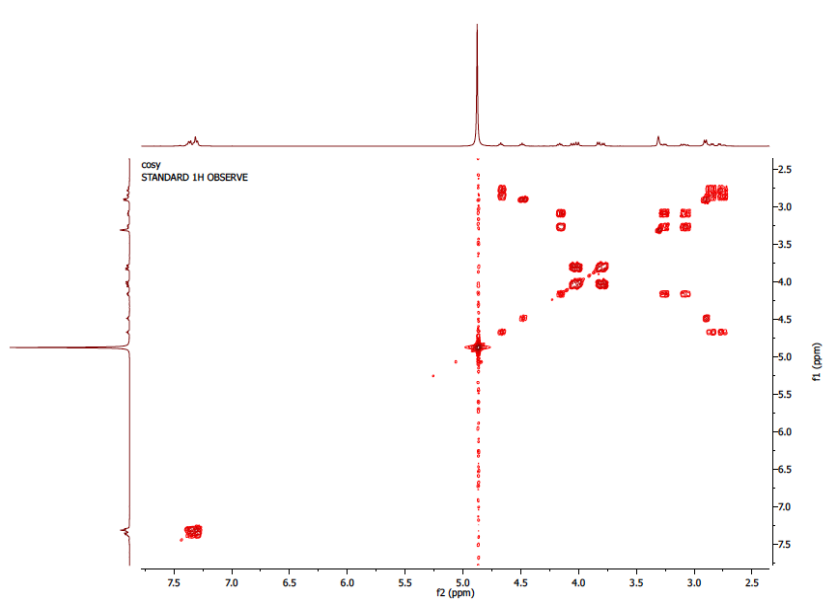
**<sup>13</sup>C FGNGC (36)**

**<sup>13</sup>C NMR (100 MHz, Methanol-d<sub>4</sub>)**  $\delta$  174.87, 174.06, 171.91, 171.19, 170.59, 135.62, 130.48, 130.14, 128.89, 57.27, 55.87, 51.63, 44.01, 43.62, 38.50, 37.20, 26.78.

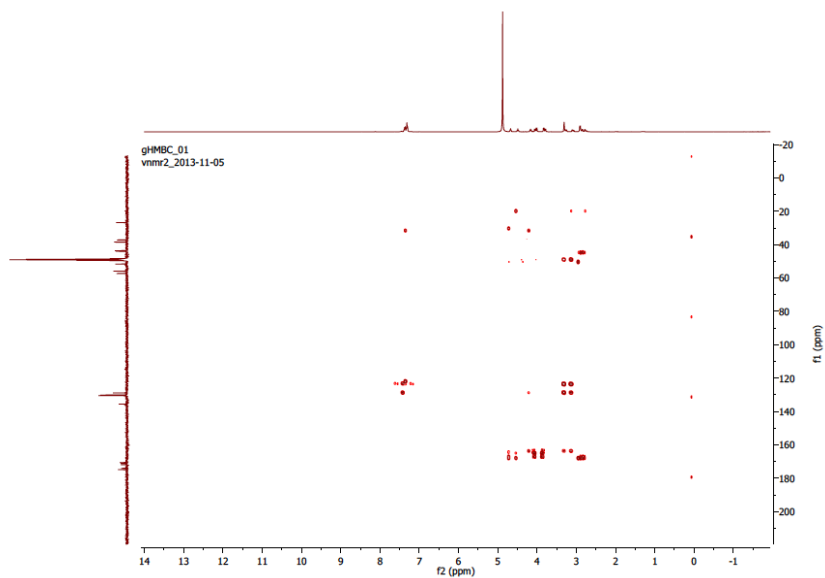
**DEPT FGNGC (36)**



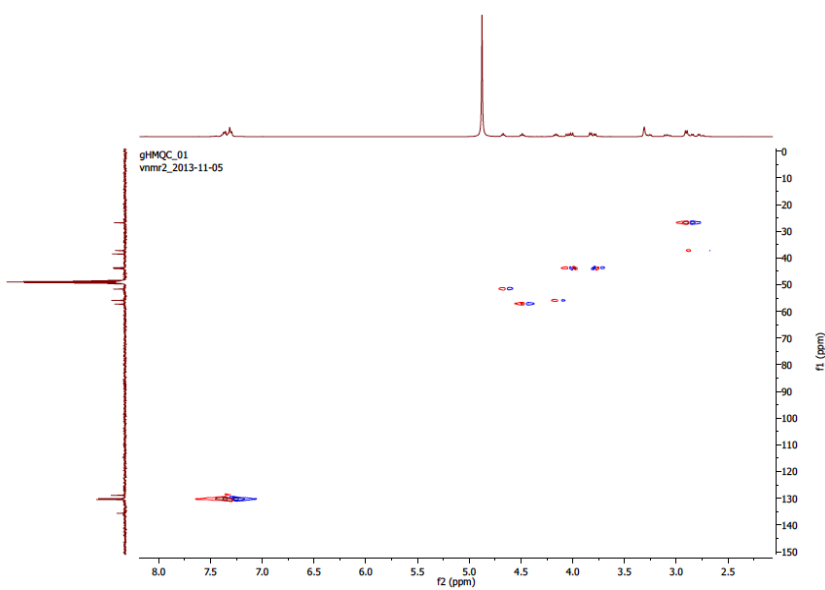
**COSY FGNGC (36)**



**HMBC FGNGC (36)**

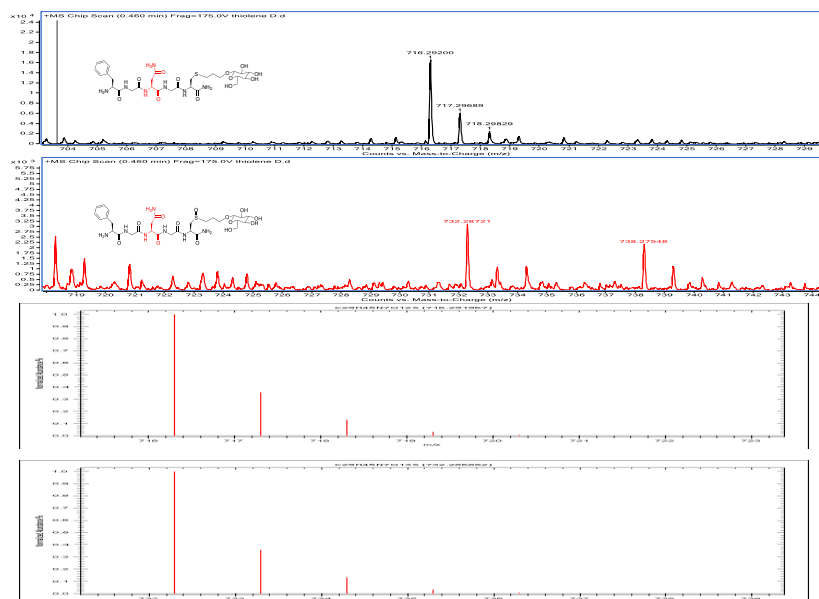


**HMQC FGNGC (36)**

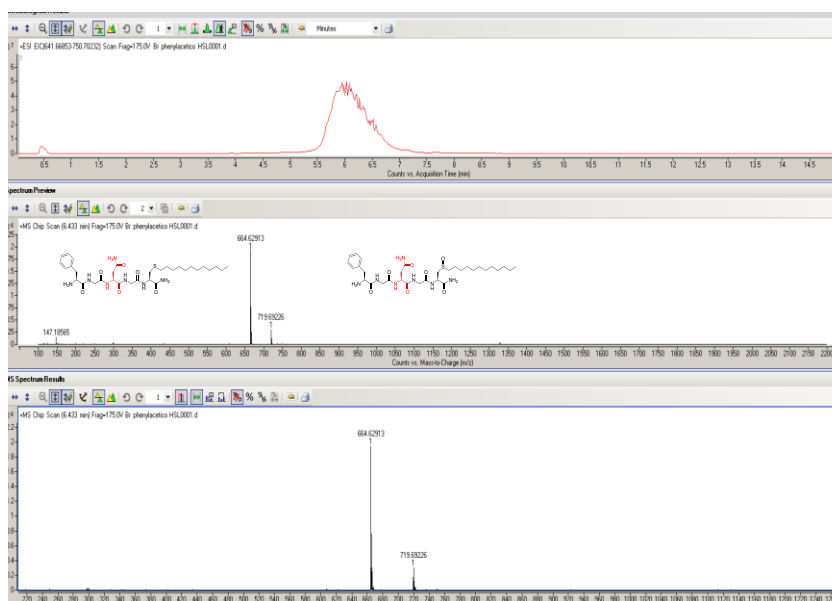


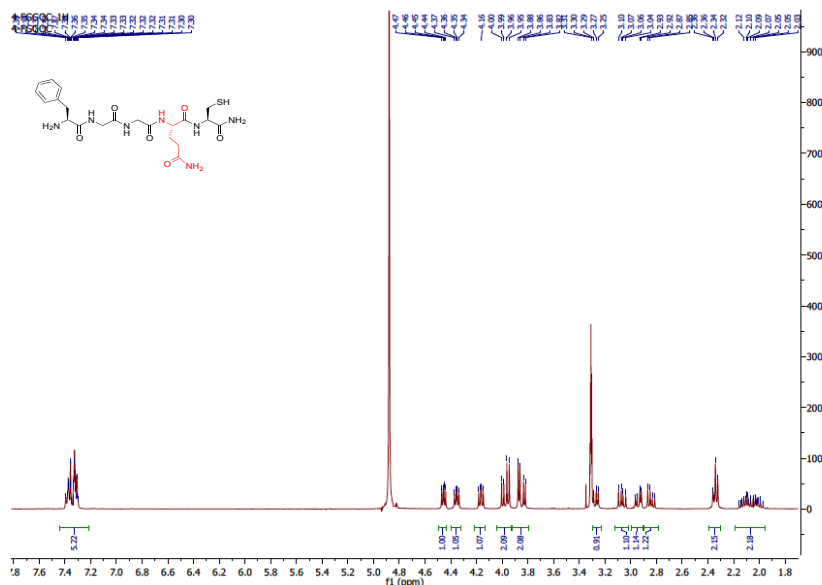


### THIOL-ENE COMPOUND (52)

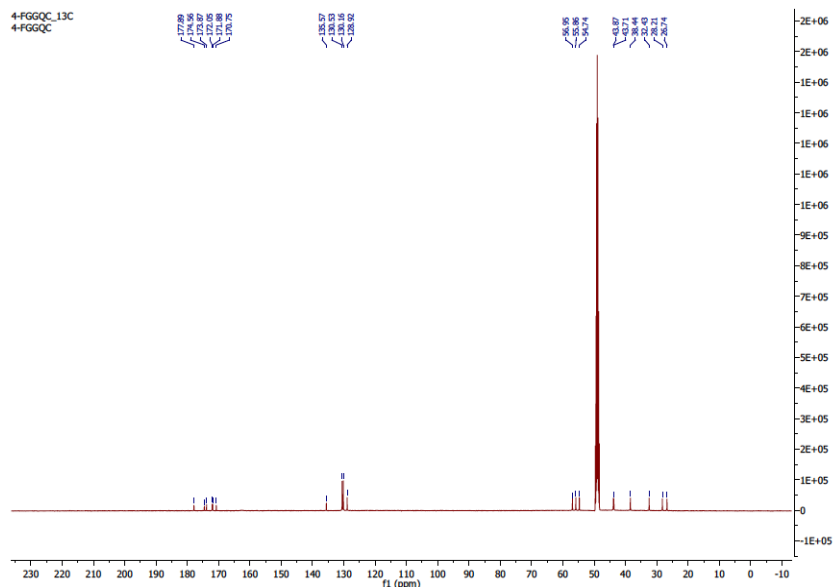


### THIOL-ENE COMPOUND (53)



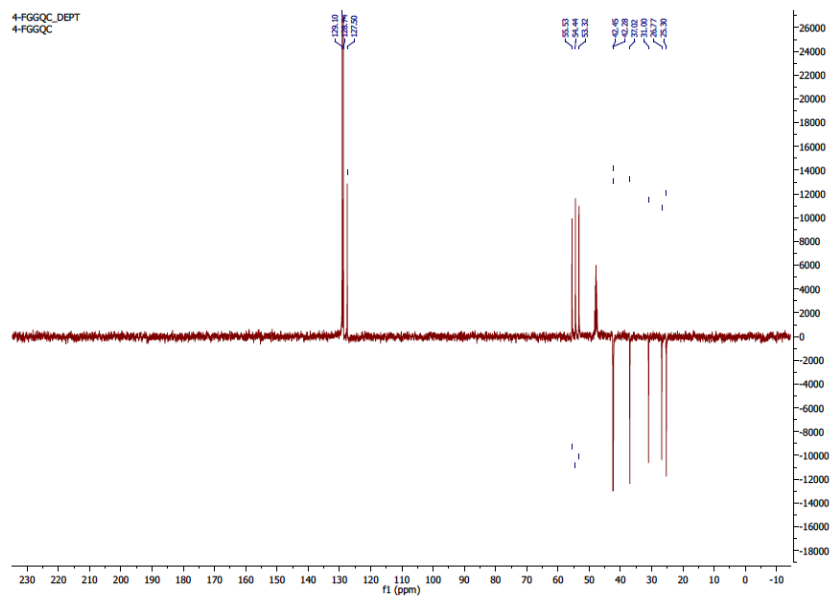
**<sup>1</sup>H FGGQC (37)**

**<sup>1</sup>H NMR (400 MHz, Methanol-d<sub>4</sub>)**  $\delta$  7.44 -7.26 (m, 5H), 4.46 (dd, J = 7.8, 5.0 Hz, 1H), 4.35 (dd, J = 8.6, 5.5 Hz, 1H), 4.16 (dd, J = 8.3, 6.1 Hz, 1H), 3.98 (dd, J = 16.6, 7.2 Hz, 2H), 3.85 (dd, J = 16.6, 5.7 Hz, 2H), 3.31 - 3.24 (m, 1H), 3.07 (dd, J = 14.2, 8.4 Hz, 1H), 2.94 (dd, J = 13.9, 5.0 Hz, 1H), 2.84 (dd, J = 13.9, 7.8 Hz, 1H), 2.34 (t, J = 7.7 Hz, 2H), 2.19 - 1.94 (m, 2H).

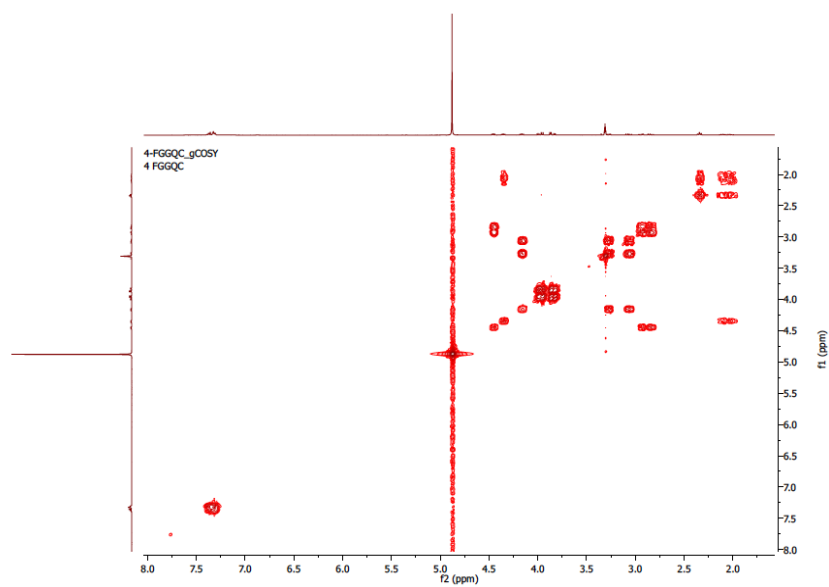
**<sup>13</sup>C FGGQC (37)**

**<sup>13</sup>C NMR (100 MHz Methanol-d<sub>4</sub>)**  $\delta$  177.89, 174.56, 173.87, 172.05, 171.88, 170.75, 135.57, 130.53, 130.16, 128.92, 56.95, 55.86, 54.74, 43.87, 43.71, 38.44, 32.43, 28.21, 26.74.

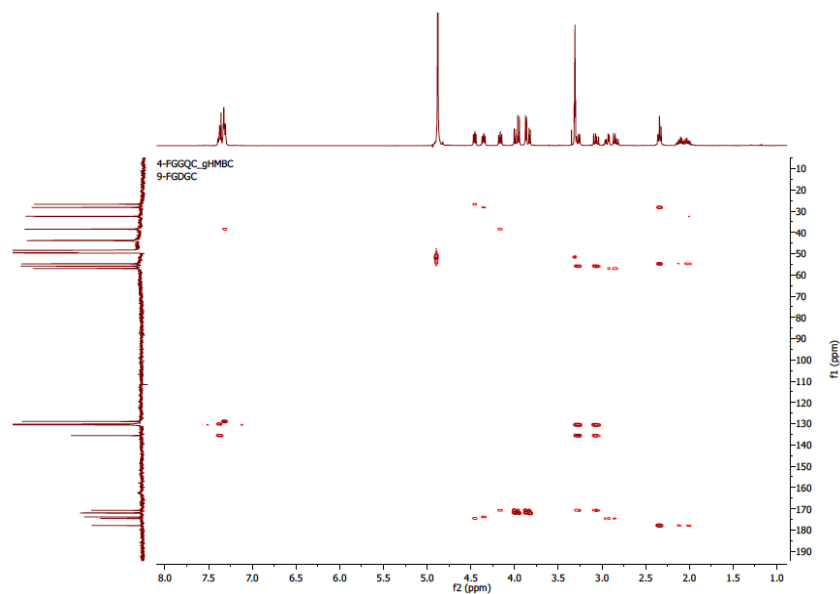
### DEPT FGGQC (37)



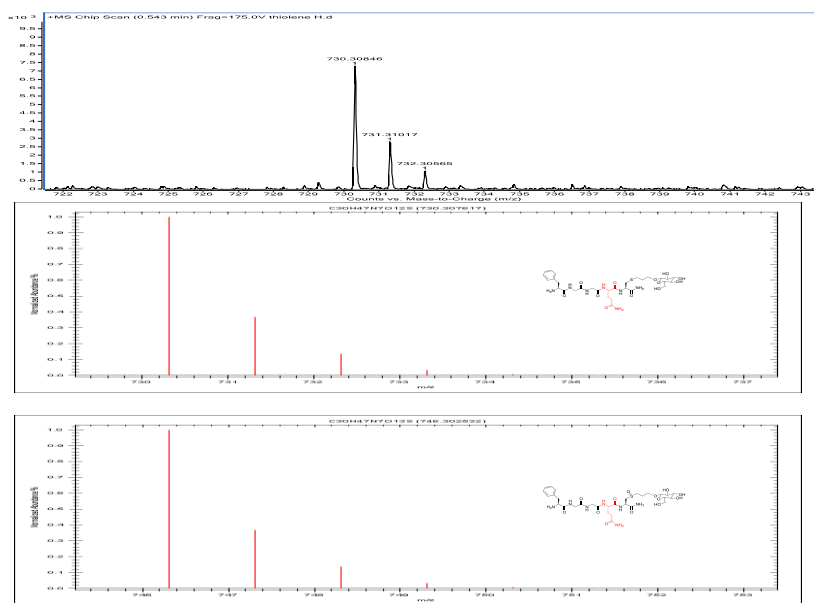
### COSY FGGQC (37)



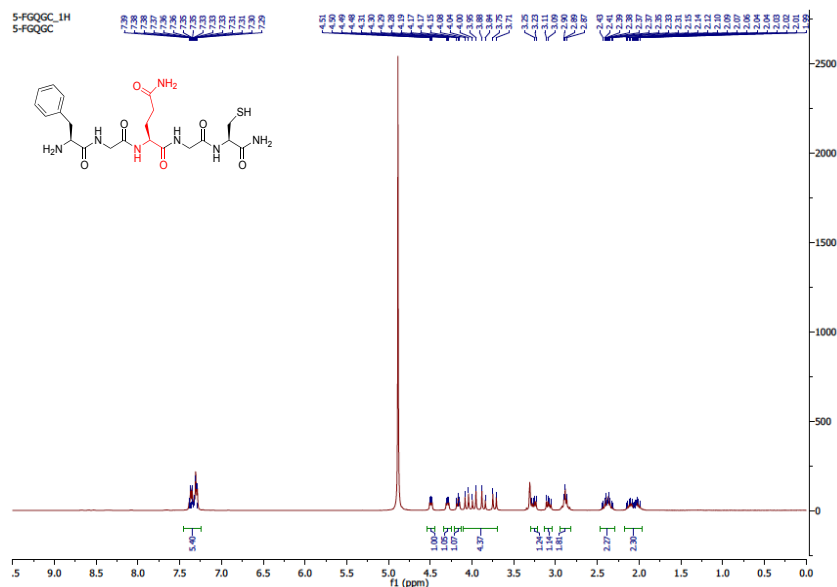
**HMBC FGGQC (37)**



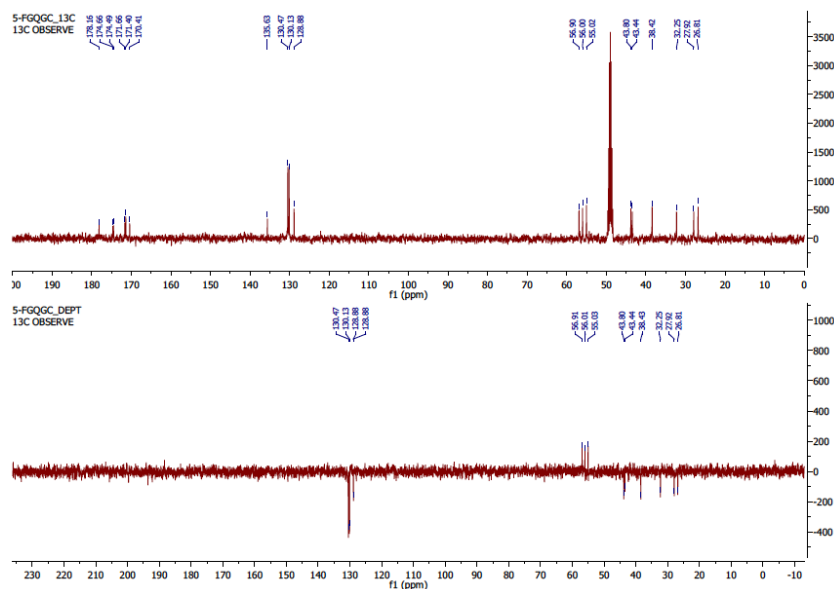
**THIOL-ENE COMPOUND (54)**



HRMS spectra of Thiol-ene product (54-54bis).

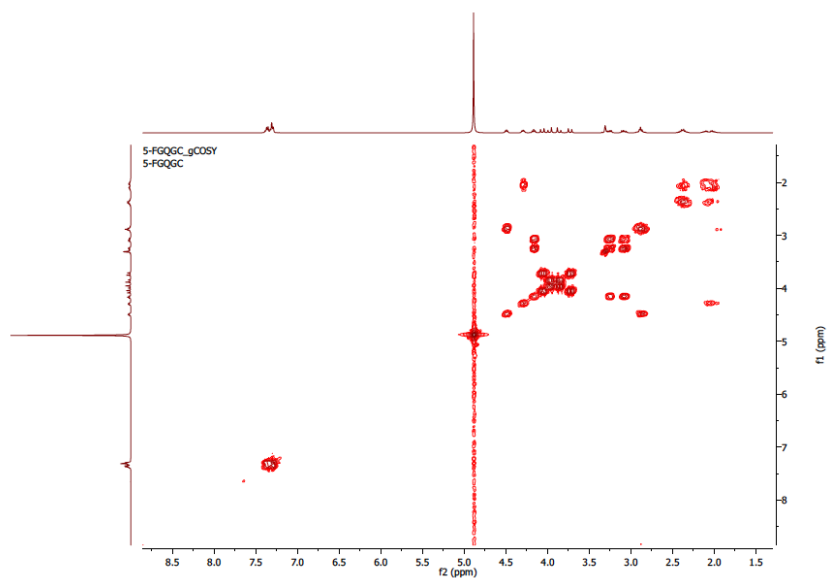
**<sup>1</sup>H FGQGC (38)**

**<sup>1</sup>H NMR (400 MHz, Methanol-d<sub>4</sub>)**  $\delta$  7.43 -7.21 (m, 5H), 4.49 (dd,  $J = 7.3, 5.0$  Hz, 1H), 4.29 (dd,  $J = 7.9, 5.2$  Hz, 1H), 4.17 (t,  $J = 7.3$  Hz, 1H), 4.11 - 3.68 (m, 4H), 3.26 (dd,  $J = 14.0, 6.7$  Hz, 1H), 3.08 (dd,  $J = 13.9, 8.0$  Hz, 1H), 2.88 (t,  $J = 6.7$  Hz, 2H), 2.49 - 2.26 (m, 2H), 2.20 - 1.92 (m, 2H).

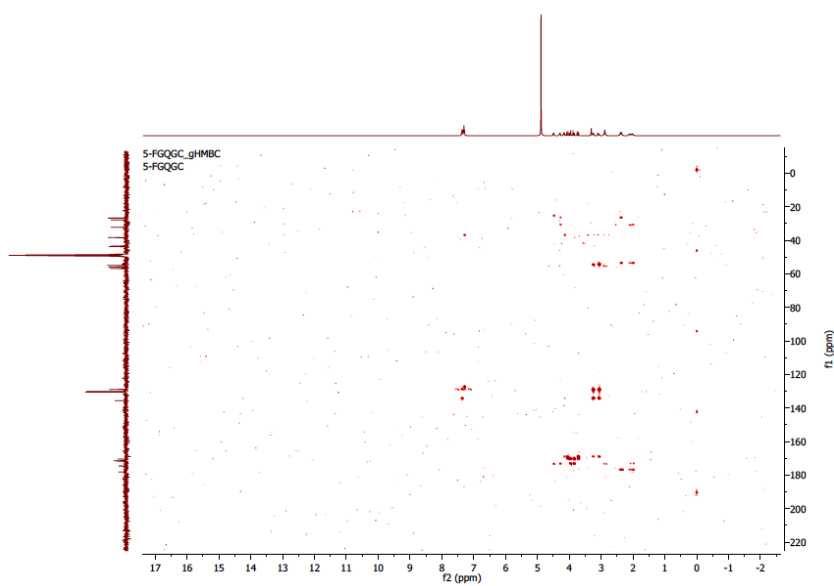
**<sup>13</sup>C-DEPT FGQGC (38)**

**<sup>13</sup>C NMR (100 MHz, Methanol-d<sub>4</sub>)**  $\delta$  178.16, 174.66, 174.49, 171.66, 171.40, 170.41, 135.63, 130.47, 130.13, 128.88, 56.90, 56.00, 55.02, 43.80, 43.44, 38.42, 32.25, 27.92, 26.81.

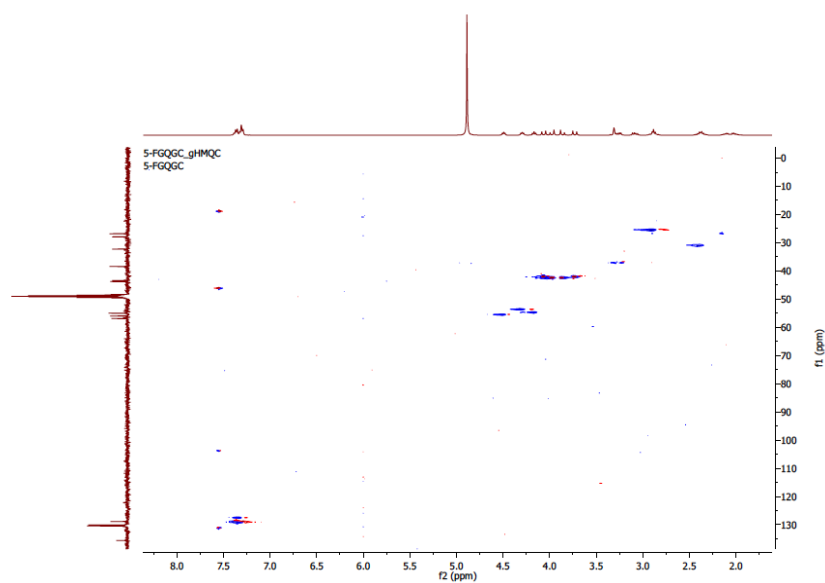
### COSY FGQGC (38)



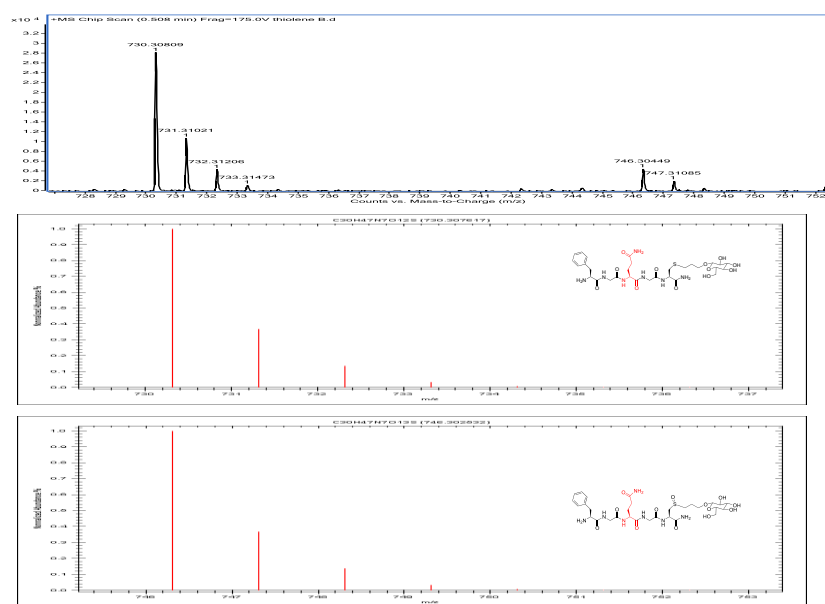
### HMBC FGQGC (38)



**HMQC FGQGC (38)**

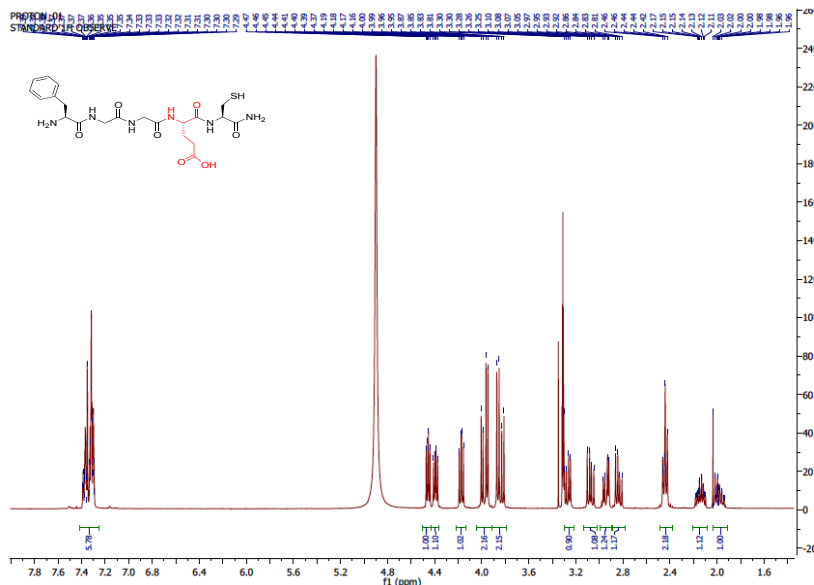


**THIOL-ENE COMPOUND (55)**



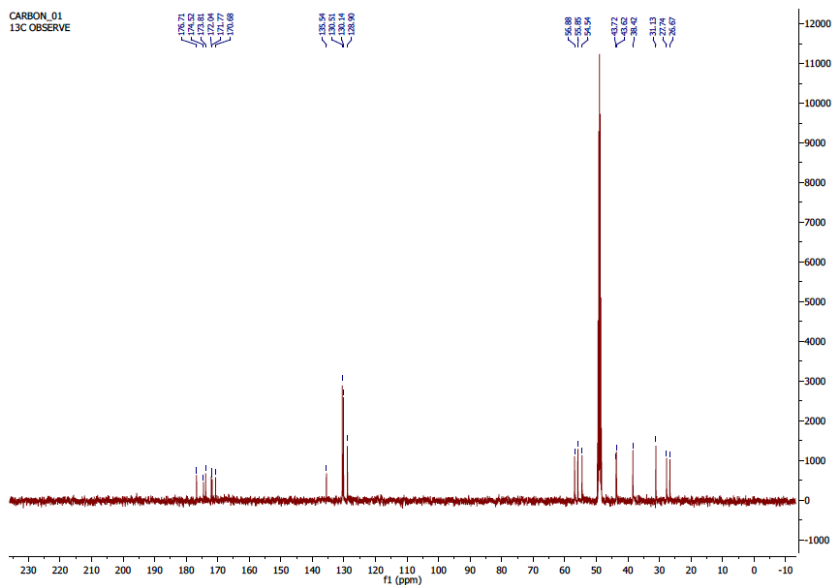
HRMS spectra of Thiol-ene product (55-55bis).

**<sup>1</sup>H FGGE (39)**



**<sup>1</sup>H NMR (400 MHz, Methanol-d<sub>4</sub>)**  $\delta$  7.45 - 7.25 (m, 5H), 4.46 (dd, J = 7.7, 5.1 Hz, 1H), 4.39 (dd, J = 8.7, 5.5 Hz, 1H), 4.17 (dd, J = 8.2, 6.3 Hz, 1H), 3.98 (dd, J = 16.6, 6.4 Hz, 2H), 3.84 (dd, J = 16.6, 7.8 Hz, 2H), 3.27 (dd, J = 14.1, 6.3 Hz, 1H), 3.08 (dd, J = 14.1, 8.2 Hz, 1H), 2.94 (dd, J = 13.9, 5.1 Hz, 1H), 2.84 (dd, J = 13.9, 7.7 Hz, 1H), 2.48 - 2.40 (m, 2H), 2.14 (dddd, J = 13.7, 8.2, 7.1, 5.5 Hz, 1H), 2.03 - 1.93 (m, 1H).

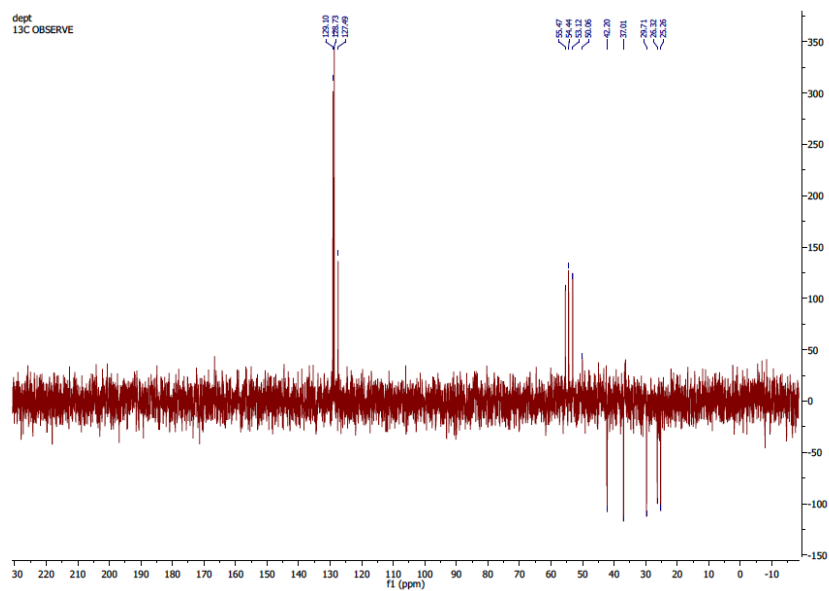
**<sup>13</sup>C FGGE (39)**



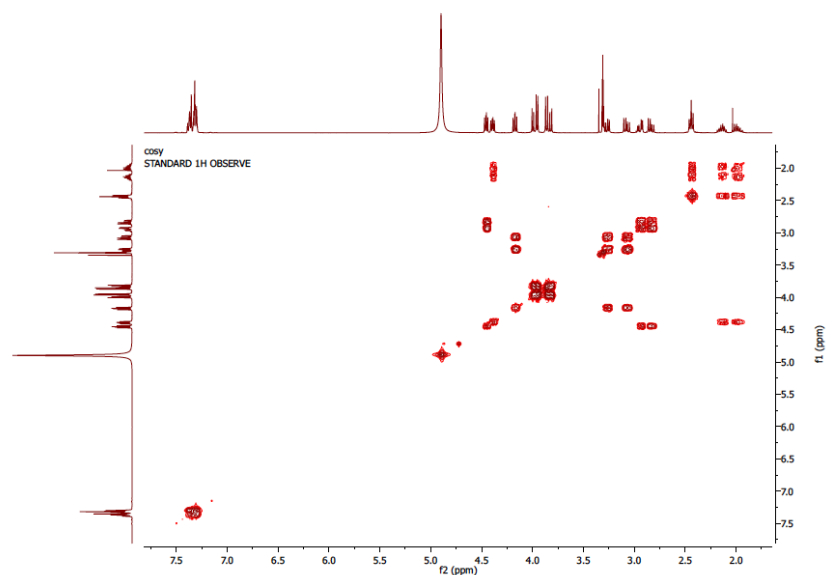


**$^{13}\text{C}$  NMR (100 MHz, Methanol- $d_4$ )  $\delta$  176.71, 174.52, 173.81, 172.04, 171.77, 170.68, 135.54, 130.51, 130.14, 128.90, 56.88, 55.85, 54.54, 43.72, 43.62, 38.42, 31.13, 27.74, 26.67.**

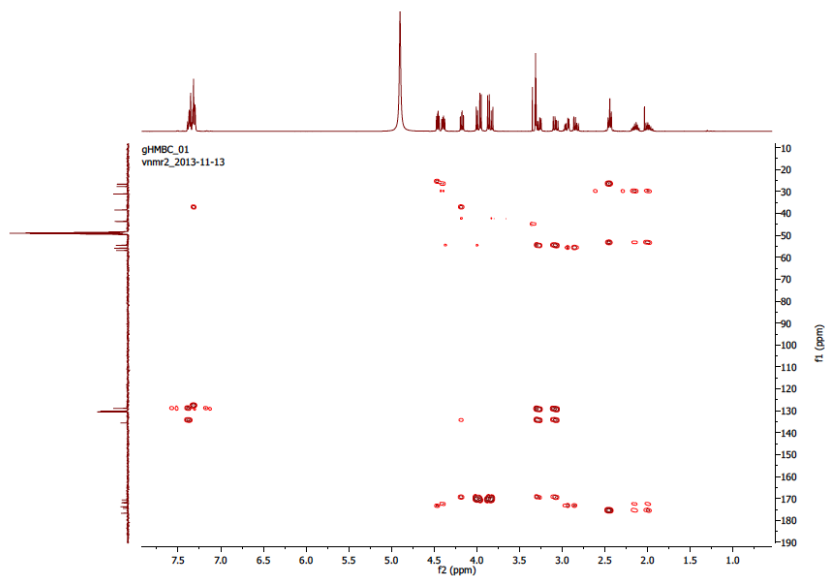
**DEPT FGGE (39)**



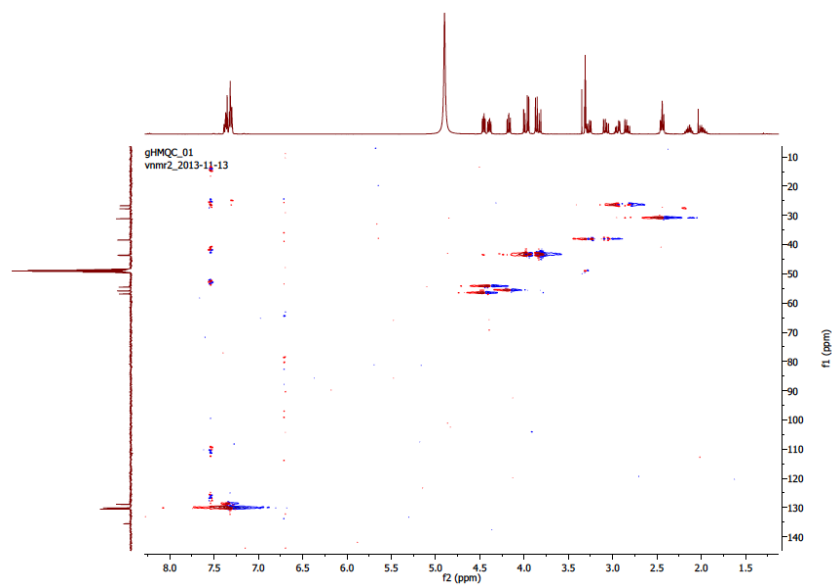
**COSY FGGE (39)**



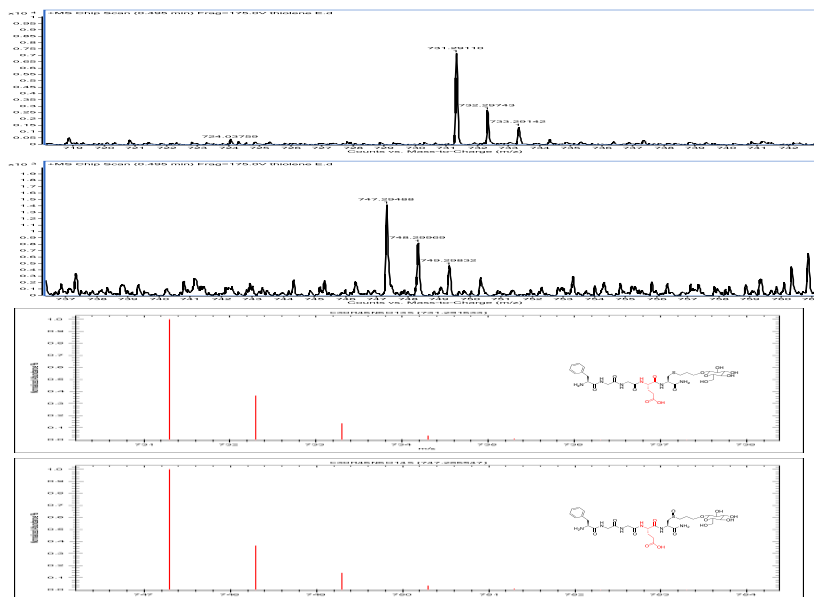
### HMBC FGGE (39)



### HMQC FGGE (39)

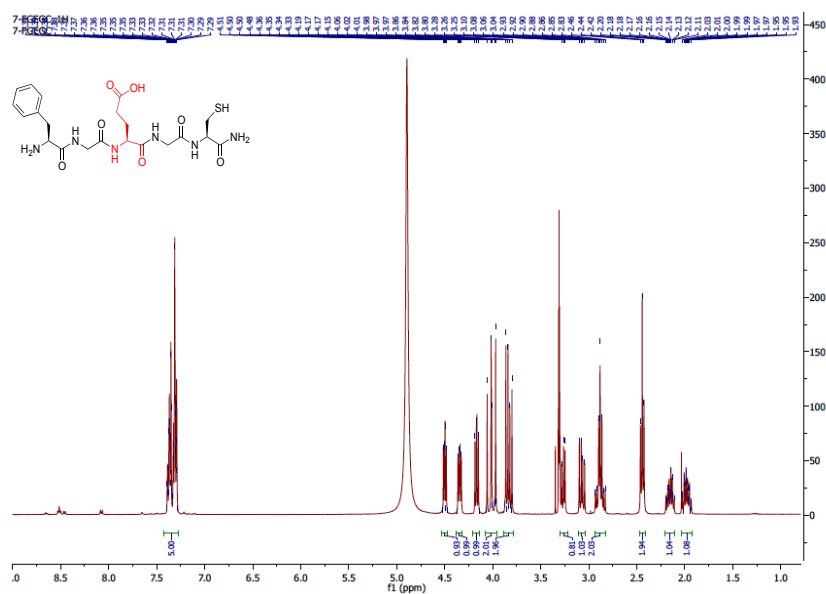


## THIOL-ENE COMPOUND (56)



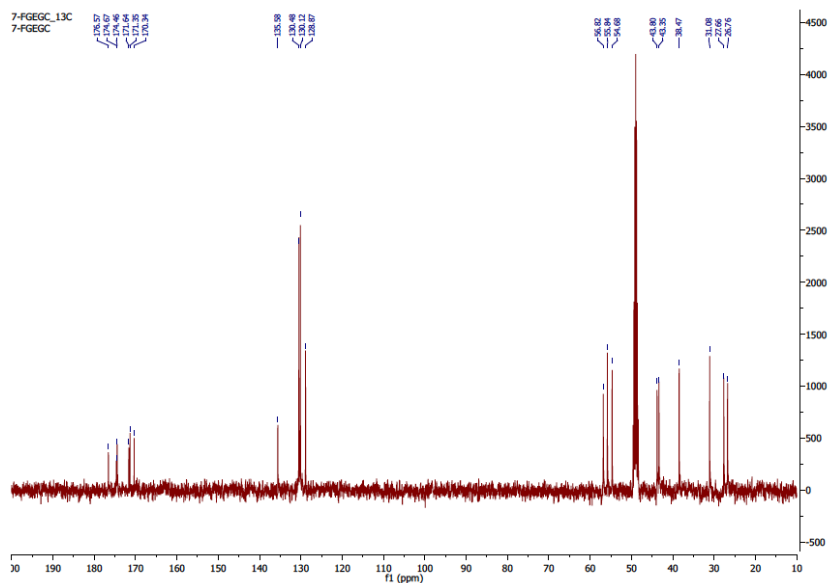
HRMS spectra of Thiol-ene product (56-56bis).

## <sup>1</sup>H FGEGC (40)



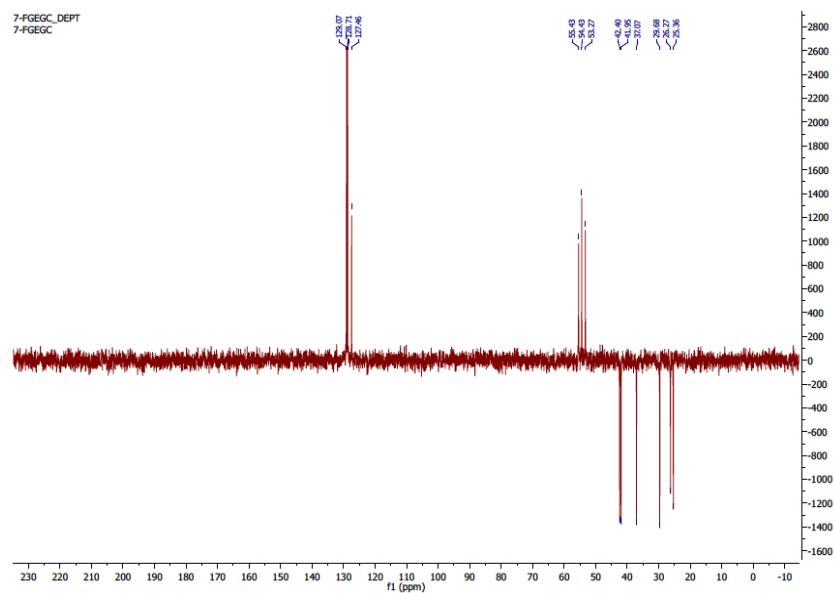
**<sup>1</sup>H NMR (400 MHz, Methanol-d<sub>4</sub>)**  $\delta$  7.43 -7.25 (m, 5H), 4.50 (dd, J = 7.3, 5.2 Hz, 1H), 4.34 (dd, J = 8.6, 5.4 Hz, 1H), 4.17 (dd, J = 8.2, 6.2 Hz, 1H), 4.01 (dd, J = 18.6, 16.6 Hz, 2H), 3.83 (dd, J = 16.6, 8.9 Hz, 2H), 3.32 - 3.22 (m, 1H), 3.07 (dd, J = 14.1, 8.2 Hz, 1H), 2.96 - 2.81 (m, 2H), 2.44 (t, J = 7.4 Hz, 2H), 2.21 - 2.10 (m, 1H), 1.98 (ddt, J = 14.2, 8.8, 7.3 Hz, 1H).

**<sup>13</sup>C FGEGC (40)**

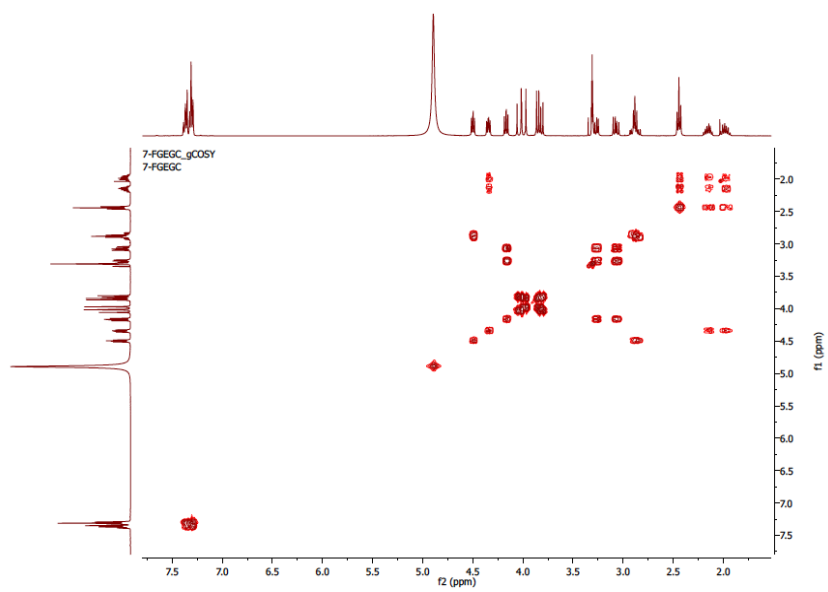


**<sup>13</sup>C NMR (100 MHz, Methanol-d<sub>4</sub>)**  $\delta$  176.57, 174.67, 174.46, 171.64, 171.35, 170.34, 135.58, 130.48, 130.12, 128.87, 56.82, 55.84, 54.68, 43.80, 43.35, 38.47, 31.08, 27.66, 26.76.

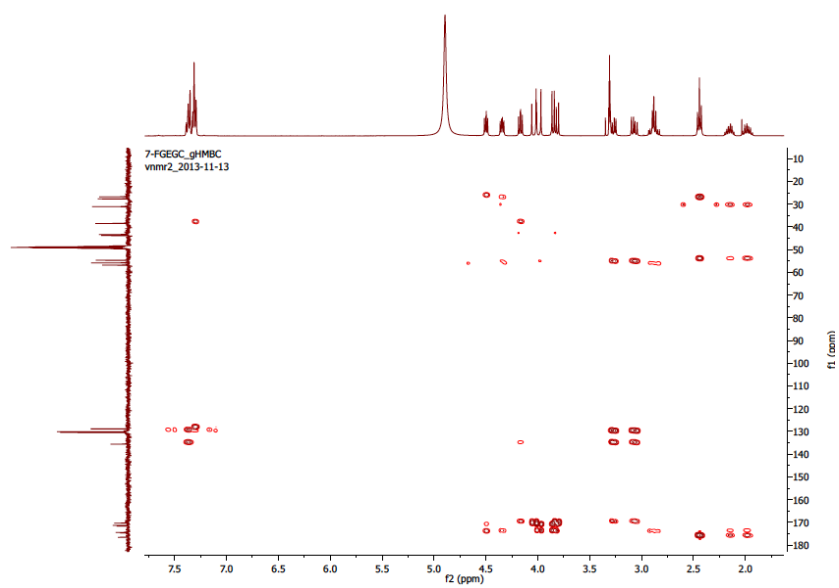
**DEPT FGEGC (40)**



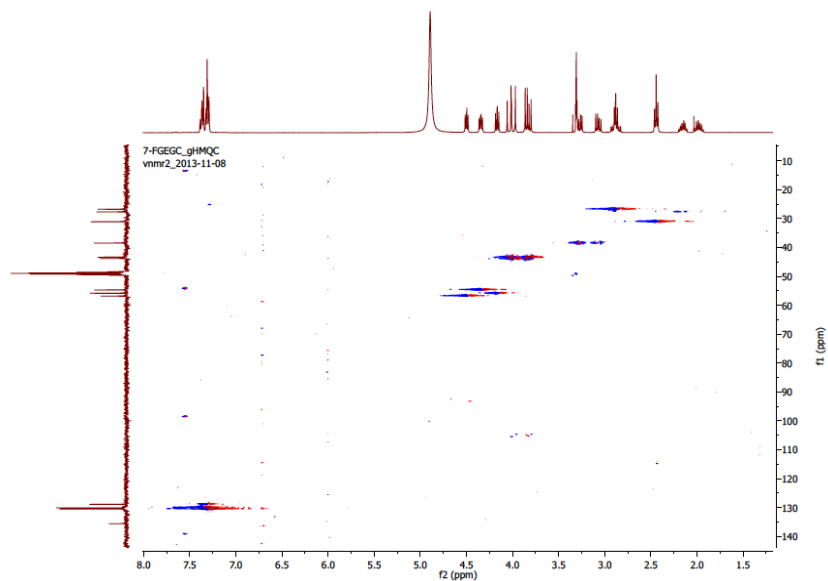
**COSY FGEGC (40)**



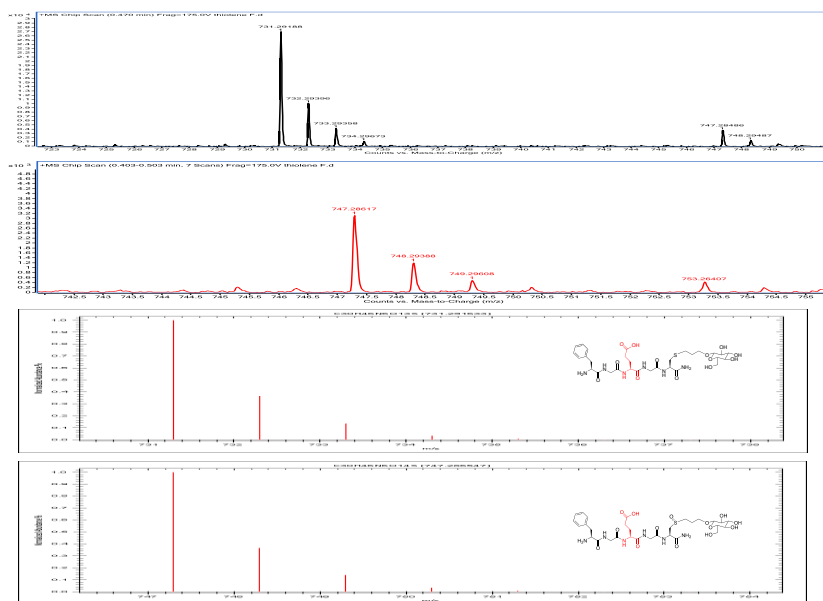
**HMBC FGEGC (40)**



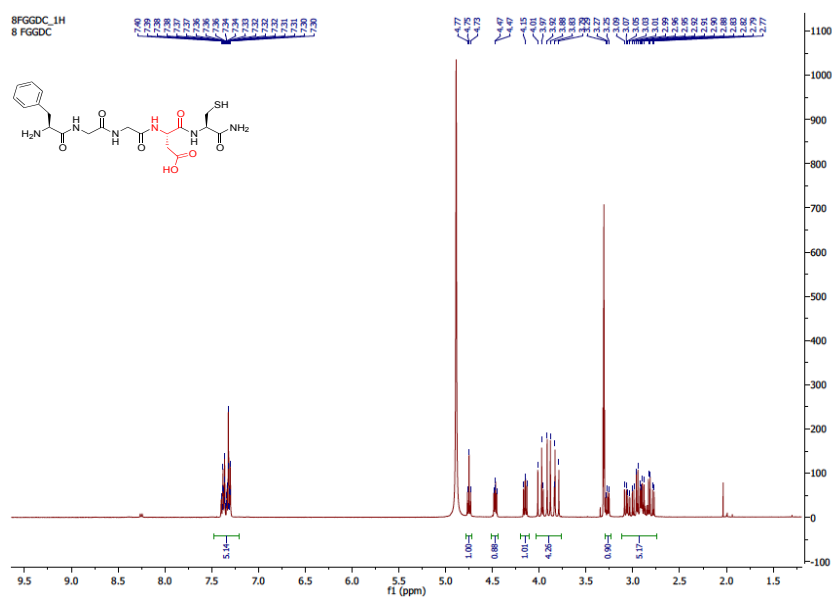
**HMQC FGEGC (40)**



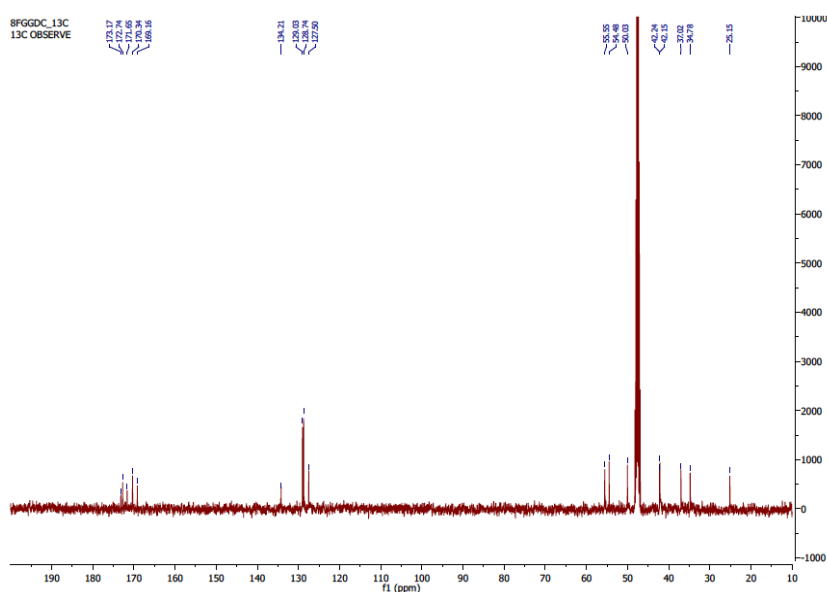
**THIOL-ENE COMPOUND (57)**



HRMS spectra of Thiol-ene product (57-57bis).

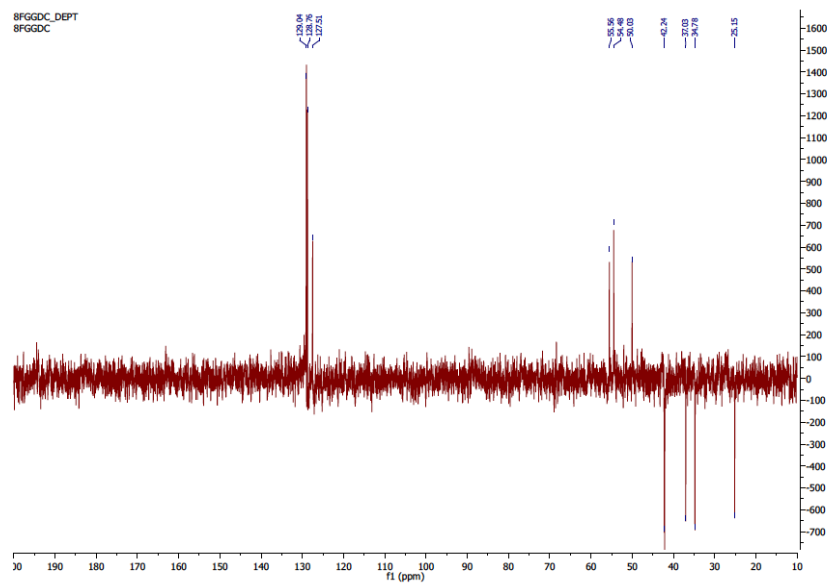
**<sup>1</sup>H FGGDC (41)**

**<sup>1</sup>H NMR (400 MHz, Methanol-*d*<sub>4</sub>)**  $\delta$  7.47 - 7.22 (m, 5H), 4.75 (t, *J* = 6.7 Hz, 1H), 4.47 (dd, *J* = 7.5, 4.9 Hz, 1H), 4.15 (dd, *J* = 8.4, 6.2 Hz, 1H), 4.04 - 3.75 (m, 4H), 3.29 - 3.23 (m, 1H), 3.10 - 2.76 (m, 5H).

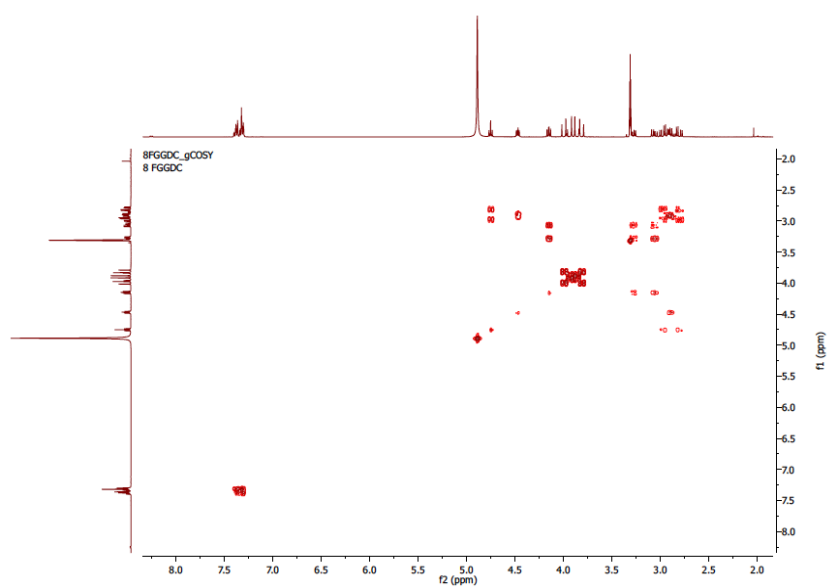
**<sup>13</sup>C FGGDC (41)**

**<sup>13</sup>C NMR (100 MHz, Methanol-*d*<sub>4</sub>)**  $\delta$  173.17, 172.74, 171.65, 170.34, 169.16, 134.21, 129.03, 128.74, 127.50, 55.55, 54.48, 50.03, 42.24, 42.15, 37.02, 34.78, 25.15.

**DEPT FGGDC (41)**

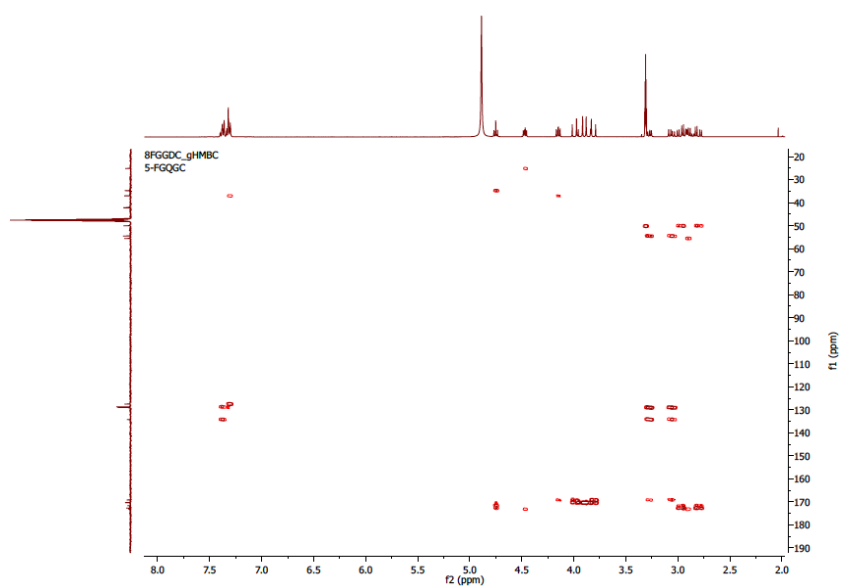


**COSY FGGDC (41)**

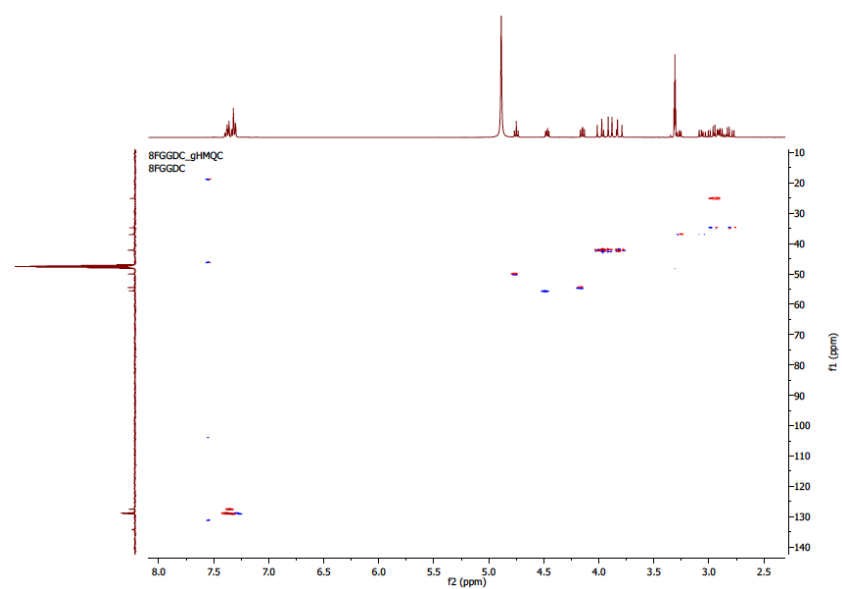




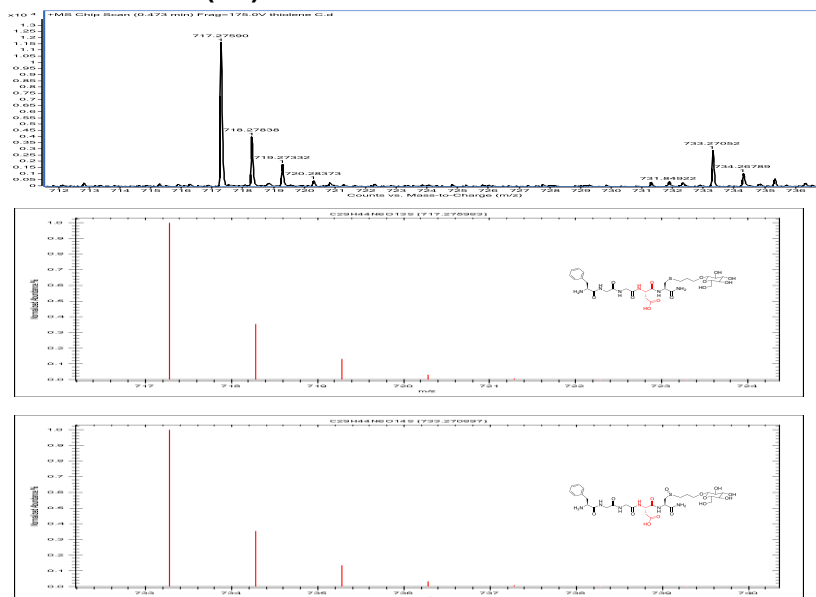
**HMBC FGGDC (41)**



**HMQC FGGDC (41)**

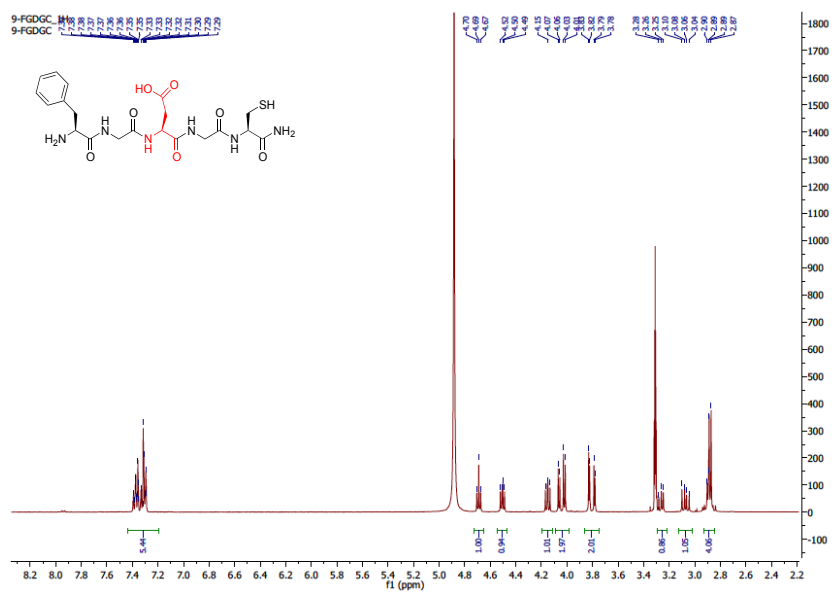


## THIOL-ENE COMPOUND (58)

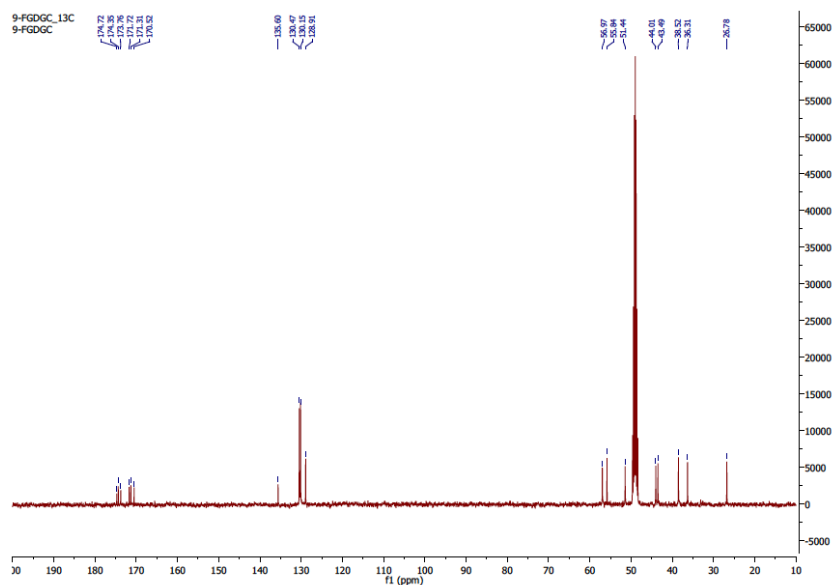


HRMS spectra of Thiol-ene product (58-58bis).

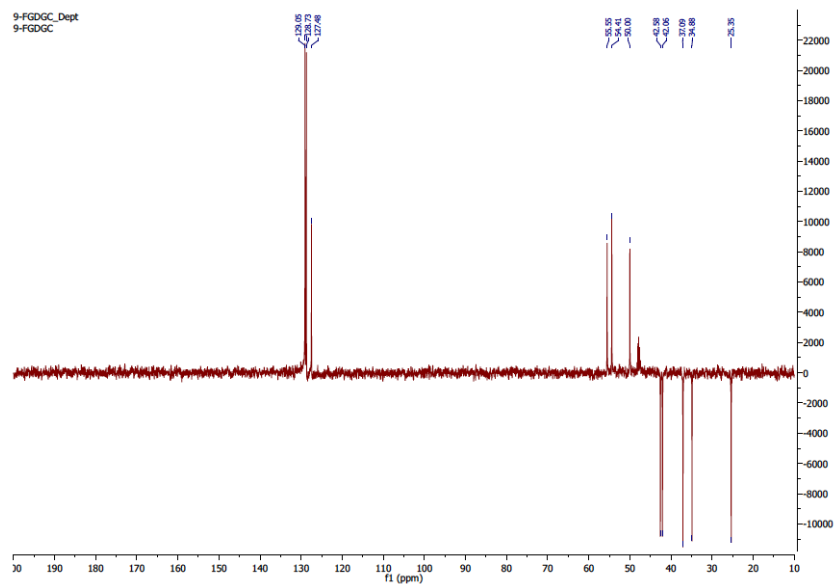
## $^1\text{H}$ FGDGC (42)



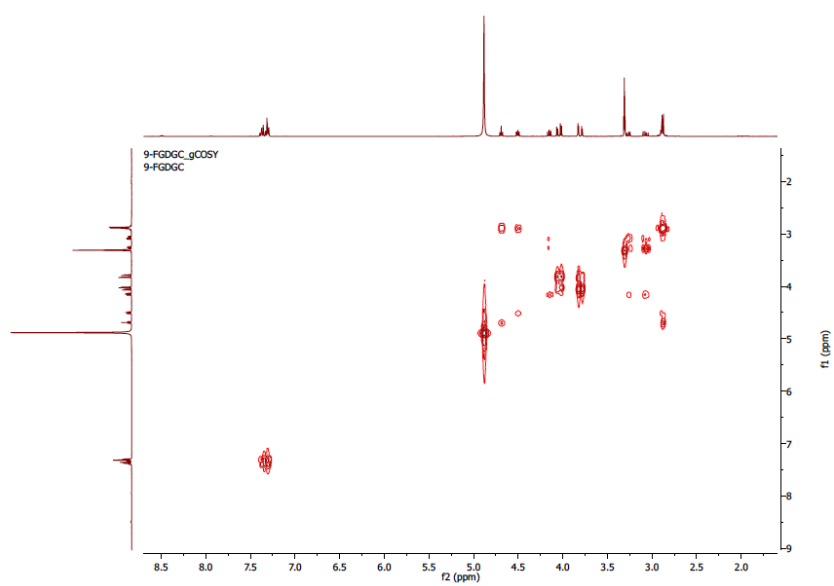
$^1\text{H}$  NMR (400 MHz, Methanol- $\text{d}_4$ )  $\delta$  7.42 - 7.26 (m, 5H), 4.75 - 4.64 (m, 1H), 4.50 (dd,  $J = 7.7, 5.4$  Hz, 1H), 4.15 (dd,  $J = 8.3, 6.2$  Hz, 1H), 4.04 (dd,  $J = 16.6, 5.3$  Hz, 2H), 3.81 (dd,  $J = 16.6, 3.3$  Hz, 2H), 3.29 - 3.22 (m, 1H), 3.07 (dd,  $J = 14.1, 8.3$  Hz, 1H), 2.89 (dd,  $J = 7.0, 5.3$  Hz, 4H).

**$^{13}\text{C}$  FGDGC (42)**

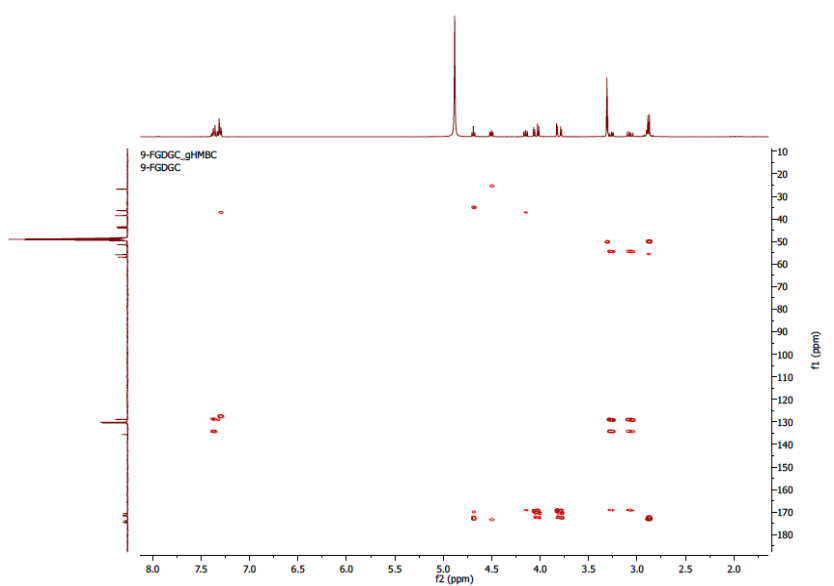
**$^{13}\text{C}$  NMR (100 MHz, Methanol- $d_4$ )  $\delta$  174.72, 174.35, 173.76, 171.72, 171.31, 170.52, 135.60, 130.47, 130.15, 128.91, 56.97, 55.84, 51.44, 44.01, 43.49, 38.52, 36.31, 26.78.**

**DEPT FGDGC (42)**

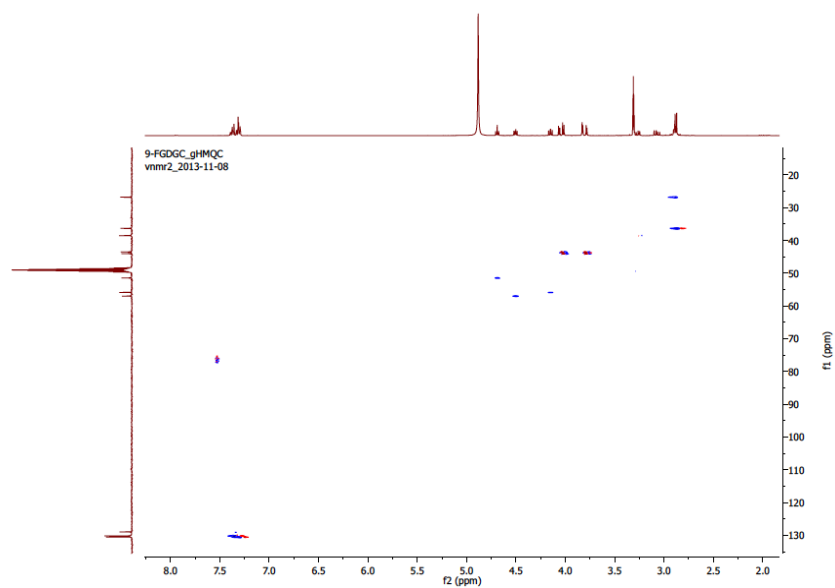
### COSY FGDGC (42)



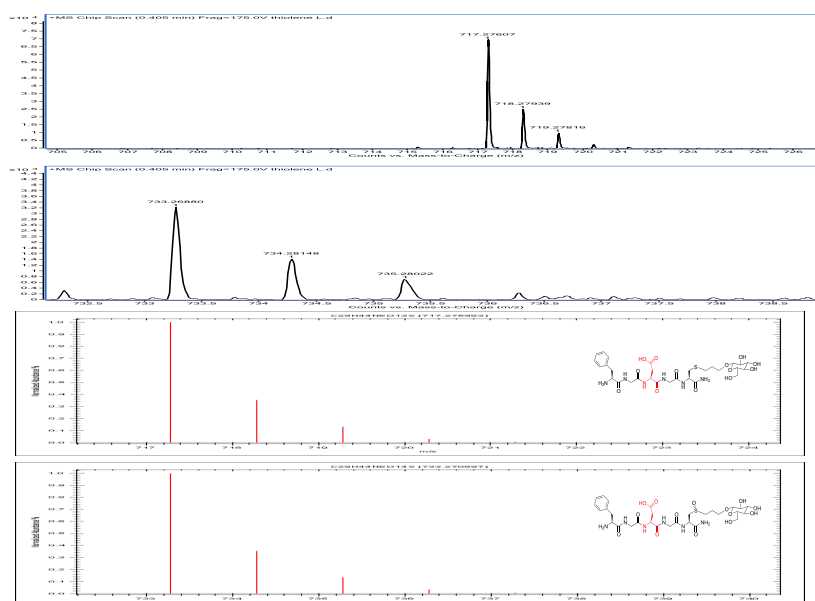
### HMBC FGDGC (42)



### HMQC FGDGC (42)



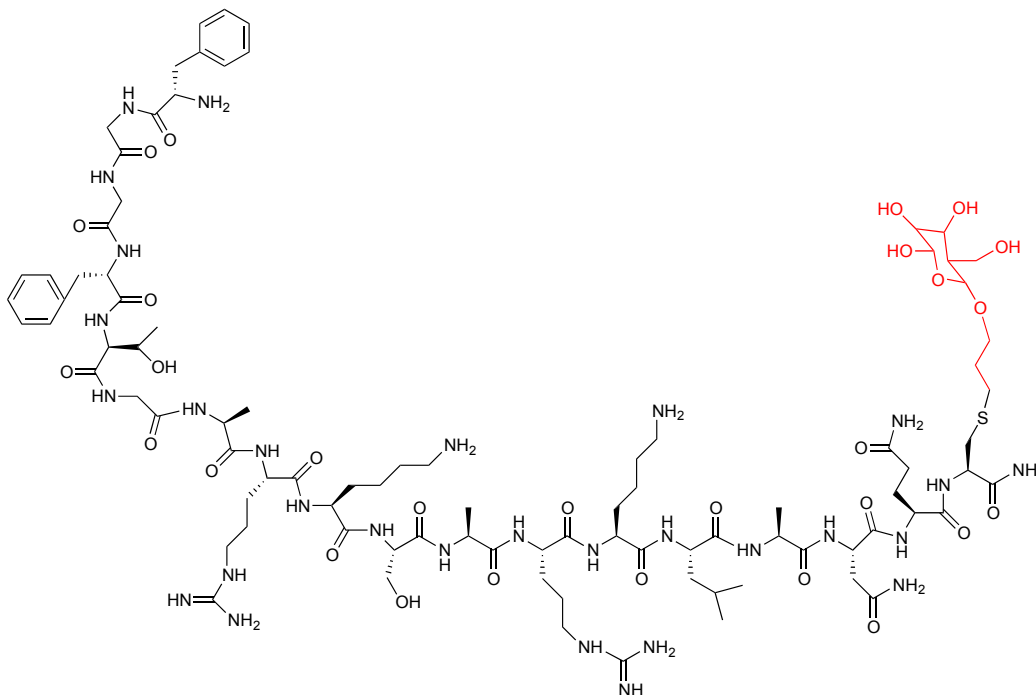
### THIOL-ENE COMPOUND (59)



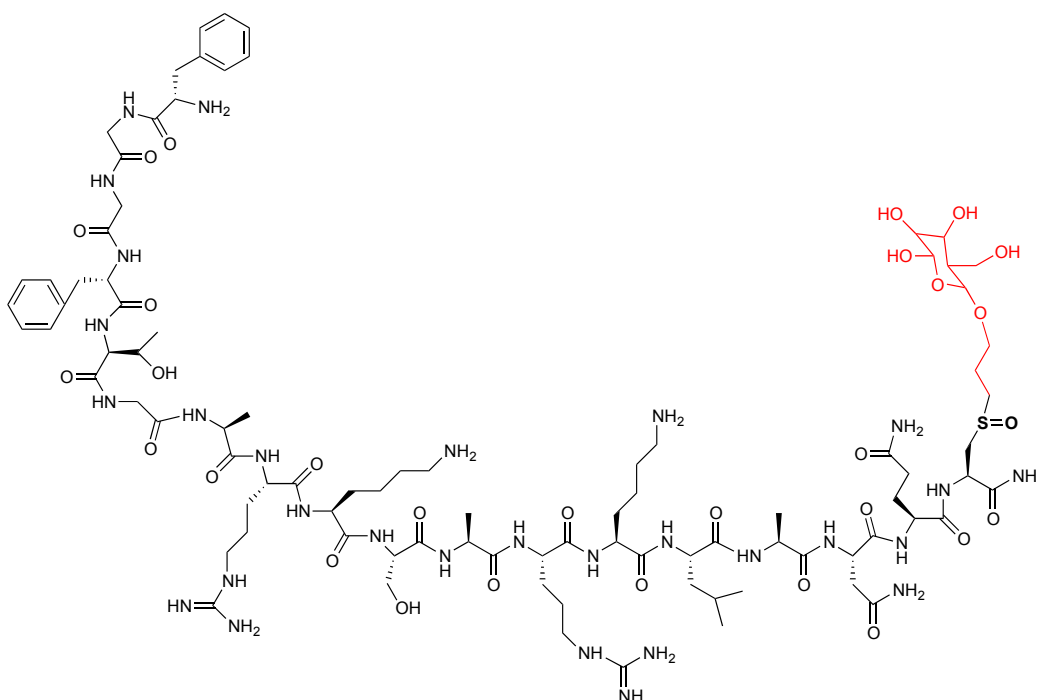
HRMS spectra of Thiol-ene product (59-59bis).

**Thiol-ene with a NOP ligand and allyl-glucose**

The reaction gave the expected result.

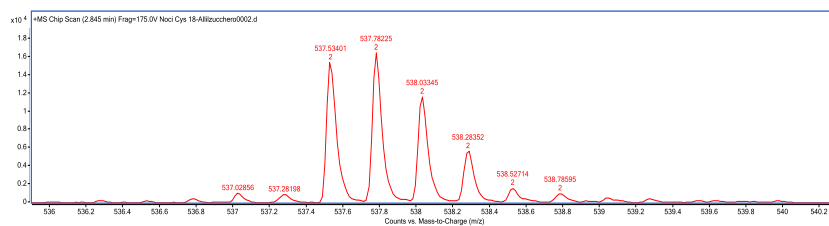
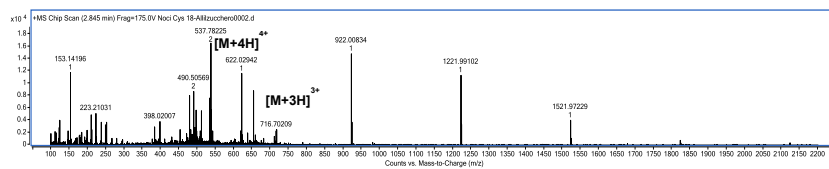
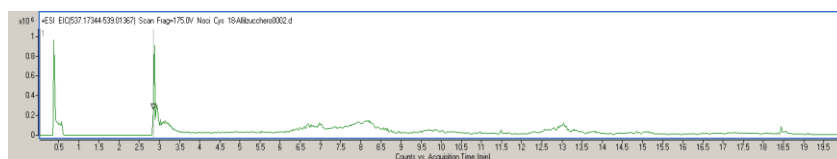
**COMPOUND (60)**

$C_{91}H_{151}N_{29}O_{28}S$   
Mw: 2131,4

**COMPOUND (60bis)**

$C_{91}H_{151}N_{29}O_{29}S$   
Mw: 2147,4

## THIOL-ENE COMPOUND (60-60bis)



HRMS spectra of Thiol-ene product (60-60bis).

## **PART 2**

### **4.1 General Methods**

Commercially available reagents were purchased from Alfa Aesar, Fisher, Sigma-Aldrich, Tocris bioscience and VWR. All of these chemicals were the highest grade and used without further purification.

Flash chromatography was performed on Silica gel Si 60 (40-63  $\mu\text{m}$ ).

Analytical Thin Layer Chromatographies (TLC) were performed Merck silica gel glass plate (60 A, particle size 40-63  $\mu\text{m}$ ).

NMR data were recorded on Bruker ADVANCE III (University of Aberdeen) for  $^1\text{H}$  at 400 MHz, for  $^{13}\text{C}$  at 100 MHz. All chemical shifts ( $\delta$ ) are expressed in parts per million and coupling constant (J) are given in Hertz. Abbreviations used for peak multiplicity are: s, singlet; br s, broad singlet; d, doublet; t, triplet; q, quadruplet; quint, quintuplet; m, multiplet.

LC-MS experiments were performed on an Agilent Technologies 1200 Series HPLC system equipped with a DAD and a 6120 MS detector composed by a ESI ionization source and a single quadrupole mass selective detector using a Analytical C18 RP column (Phenomenex Luna, C18(2) 250 mm  $\times$  4.60 mm, 5  $\mu\text{m}$ , 100  $\text{\AA}$ ).

FUSION-SL Advance 4.2 MP for Fluorescence and Chemiluminescence 4.2/10 megapixel CCD camera with fixed focal length lens, linked to FUSION-CAPT-Software.

JASCO J-600 spectropolarimeter using a quartz cell with 1-mm path length, under PC control with an additional (near IR) photomultiplier which allows data to be gathered over the wavelength range from 180 nm to 1000 nm, a cryostat accessory allows spectra to be recorded at temperatures down to -196 (or 15  $^\circ\text{C}$  for CD analyses) from University of Glasgow (Scotland).

#### **Image J Software**

Image J software is a full-featured, multifunction computer program to analyze and edit digital images of electrophoresis gels and blots that were acquired using gel documentation imagers or scanners.

The software comprises a complete set of easy-to-use research tools for the quantitative digital analysis of image data from electrophoresis gels and Western blots. The software uses a powerful algorithm to automatically select and identify lanes and band-boundaries for calculation of migration distances or densitometry.



It can provide molecular weight determination, relative and absolute quantity, and purity calculation.

#### **4.2 EMSA (electrophoretic mobility shift-assay)**

Electrophoresis is a simple, rapid, and sensitive analytical tool for separating proteins and nucleic acids based on their physical characteristics (as mass, isoelectric point). Most biological molecules carry a net charge at any pH other than their isoelectric point and migrate at a rate proportional to their charge density in an electrical field. The mobility of a biological molecule through an electric field depends on the following factors:

Field strength, net charge on the molecule, size and shape of the molecule, ionic strength and properties of the medium through which the molecules migrate (e.g., viscosity, pore size).

**Support Matrix.** Polyacrylamide and agarose are two types of support matrices used in electrophoresis. The support matrix is a porous media that acts as a molecular sieve. The sieving function depends on the pore size and concentration of the matrix. Agarose has a large pore size and is ideal for separating macromolecules such as nucleic acids and protein complexes. Polyacrylamide has a smaller pore size and is ideal for separating proteins and smaller nucleic acids.

**Polyacrylamide Gel Electrophoresis.** Polyacrylamide gels are formed by the polymerization of acrylamide monomers into long chains, crosslinked by bifunctional compounds such as N,N-methylene-bisacrylamide (bis) that react with the free functional groups at the chain termini. The pore size of the gel is governed by the concentration of acrylamide and bisacrylamide with a higher acrylamide concentration creating smaller pore sizes, allowing resolution of low molecular weight molecules.

**Buffer Systems.** Electrophoresis is performed using continuous or discontinuous buffer systems. In this case continuous buffer systems were utilized as a single buffer for the gel and the running buffer was used.

#### **Electrophoresis Sample Conditions.**

**Non-Denaturing (Native):** Electrophoresis is performed under non-denaturing (native) conditions using buffer systems that maintain the native protein conformation, cohesion of subunits, and biological activity. During native electrophoresis, proteins are separated based on their charge to mass ratios.

**Novex Gel Specifications.** The Novex Pre-Cast Gel cassette is 10 cm × 10 cm in size, and designed for use with the XCell SureLock™ Mini-Cell.

### 4.3 Nucleic Acid Separation Applications

**Gel shift assays.** The Novex® 6% DNA Retardation Gels are used to perform gel shift assays using polyacrylamide TBE Gels, which provide high-resolution analysis of restriction digests and PCR products. The TBE Gels give sharp, intense bands and provide separations of double-strand DNA fragments.

#### Preparation of oligonucleotide

The oligonucleotides purchased are diluted to achieve a concentration of 100 μM with ddH<sub>2</sub>O or DMSO (Sigma Aldrich), depending on the solubility of the compound. Aliquots are stored at -20°C.

#### Preparation of TE Buffer

Solution of 10 mM of Tris-HCl (pH 8) and 1 mM of EDTA. Finally the solution is sterilized by autoclaving.

#### PCR Block Program for Quadruplex Folding

*Stage 1 (1 cycle):*

- Temperature 95 °C
- Time 5 minutes

*Stage 2 (90 cycles):*

- Temperature 95°C
- Time 1 minutes

*Stage 3 (1 cycle):*

- Hold at 4 °C

#### 4.3.1 Protocol for Novex DNA Retardation gel

- **Prepare and Pre-Run Gel**

1. A native gel 0.5X TBE (solution stock is 5X TBE: 100 ml of TBE 5X is brought in 900 ml of ddH<sub>2</sub>O) is prepared.

- The gel was placed in the electrophoresis unit and it was clamped to obtain a seal. The inner chamber was filled with 0.5X TBE (to just above the bottom of the wells), which reduces heat during electrophoresis. Flush wells and pre-electrophoresis of the gel for 60 minutes. 100V is applied.

- **Prepare the sample for electrophoresis**

1. 2 μl of Hi-density TBE buffer is added.
2. 10 μl are put in the wells of electrophoresis.

- **Electrophoresis of sample**

1. Current to electrophoresis gel is switched for 63 minutes and 100V is applied.

- **Electrophoresis Transfer of Binding Reactions to Nylon Membran**

1. 0.5X TBE buffer was prepared and cooled at  $-10^{\circ}\text{C}$  with ice or a circulating water bath.
2. Nylon membrane is soaked in 0.5X TBE for at least 10 minutes.

- **Transferring on gel**

- At the end of electrophoresis each of the three bonded sides are separated from the cassette by inserting the Gel Knife into the gap between the two plastic plates until they will be divided.

- **DNA transfer**

1. All the components must be wet with 0.5X TBE cooled and they are put in this order in the block:

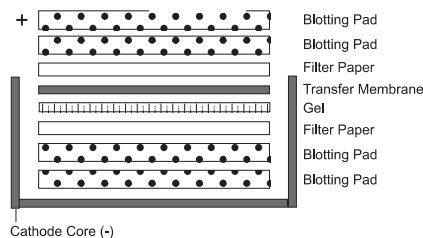


**Figure 29:** The block is positioned within the system as displayed above.

2. The inner chamber is filled with 0.5X TBE cooled to a height several millimetres above the top of the wells in the gel. Outside of the tank is filled with 600 ml  $\text{d}_2\text{H}_2\text{O}$  (to just above the bottom of the wells), which reduces heat during electrophoresis.
3. Transfer of DNA on to the membrane is carried out for 60 minutes at 380A.
4. When the transfer is complete, the membrane is placed with the bromophenol blue side up on a dry paper towel.. Buffer on the membrane surface is allowed to absorb into the membrane.

- **Crosslink Transferred DNA to Membrane**

1. The membrane face down is crosslinked for 10 minutes on a UV transilluminator equipped with 312 nm bulbs.

- **Detect Biotin-labelled DNA**

The recommended volumes are for an 8×10 cm membrane. All blocking and detection incubations are performed in clean trays or in plastic weigh boats on an orbital shaker.

1. The Blocking Buffer and the 4X Wash Buffer are gently warmed to 37-50°C in a water bath until all particulate is dissolved. These buffers may be used between room temperature and 50°C as long as all particulate remains in solution. The Substrate Equilibration Buffer may be used between 4°C and room temperature.
2. The membrane is added to 20 ml of Blocking Buffer and it is incubated for 15 minutes with gentle shaking.
3. Conjugate/blocking buffer solution is prepared by adding 67 µl Stabilized Streptavidin-Horseradish Peroxidase Conjugate to 20 ml Blocking Buffer (1:300 dilution)
4. Blocking Buffer is decanted from the membrane and it is replaced with the conjugate/blocking solution. The membrane is incubated in the conjugate/blocking buffer solution for 15 minutes with gentle shaking.
5. 1X wash solution is done by adding 40 ml of 4X Wash Buffer to 120 ml of  $\text{ddH}_2\text{O}$ .
6. The membrane is transferred to a new container and it is rinsed briefly with 20 ml of 1X wash solution (by hand).
7. The membrane is washed four times for 5 minutes each in 20 ml of 1X wash solution with gentle shaking.
8. The membrane is moved to a new container and it is introduced 30 ml of Substrate Equilibration Buffer. The membrane is incubated for 5 minutes with gentle shaking.
9. Substrate Working Solution is done by adding 6 ml Luminol/Enhancer Solution to 6 ml Stable Peroxide Solution.
10. The membrane is removed from the Substrate Equilibration Buffer, carefully blotting an edge of the membrane on a paper towel to take away the excess buffer. The membrane is placed in a clean container or into a clean sheet of plastic wrap on a flat surface.
11. The Substrate Working Solution is put onto the membrane so that it is completely covers both surfaces. Alternatively, the membrane is left in the substrate solution for 5 minutes without shaking.

12. The membrane is removed from the Working Solution and it is blotted an edge of the membrane on a paper towel for 2-5 seconds to delete excess buffer.
13. The moist membrane is wrapped in plastic wrap, avoiding bubbles and wrinkles.
14. The membrane is exposed to an appropriately equipped CCD camera, or place the membrane in a film cassette and expose to X-ray film for 2-5 minutes. The film is developed according to manufacturer's instructions. Exposure time may be adjusted to obtain the desired signal.

#### 4.4 Biochemistry: EMSA

Series of oligonucleotides analyzed to find the best concentration to work with EMSA.

<b>Tel.(1xG4)</b> [Btn]TTAGGGTTAAGGGTTAGGGTTAGGG	<b>Tel.(2xG4)</b> [Btn]TTAGGGTTAAGGGTTAGGGTTAGGGTTAGGGTTAAGGGTTAGGGTTAGGG
<b>ILPR-1(1xG4)</b> [Btn]ACAGGGGTGTGGGGACAGGGGTGTGGGG	<b>ILPR-1(2xG4)</b> [Btn]ACAGGGGTGTGGGGACAGGGGTGTGGGGACAGGGGTGTGGGGACAGGGGTGTGGGG
<b>Bcl-2</b> [Btn]GGGCGCGGGAGGAAGGGGGCGG	<b>c-Myc(Pu27)</b> [Btn]TGGGGAGGGTGGGGAGGGTGGGGAAAGG
<b>VEGF</b> [Btn]GGGCGGGCCGGGGGCGGG	<b>c-Kit21</b> [Btn]GGGCGGGCGCGAGGGAGGG
<b>ILPR-2</b> [Btn]ACAGGGGTCTGGGGACAGGGGTCTGGGG	<b>ILPR-3</b> [Btn]AGAGGGGTCTGGGGAGAGGGGTCTGGGG
<b>ILPR-4</b> [Btn]ATAGGGGTGTGTGGATAGGGGTGTGTGG	

**Table 1:** The above table shows all oligos adopted in the gel-based assays, with sequences being shown in a 5' to 3' orientation. [Btn], biotin label covalently linked to 5' end of each oligo.

Initially preliminary tests were made to assess the ability of oligonucleotides to modify its conformation.

## Tel.(2xG4), Tel.(1xG4), ILPR-1(2xG4), ILPR-1(1xG4)

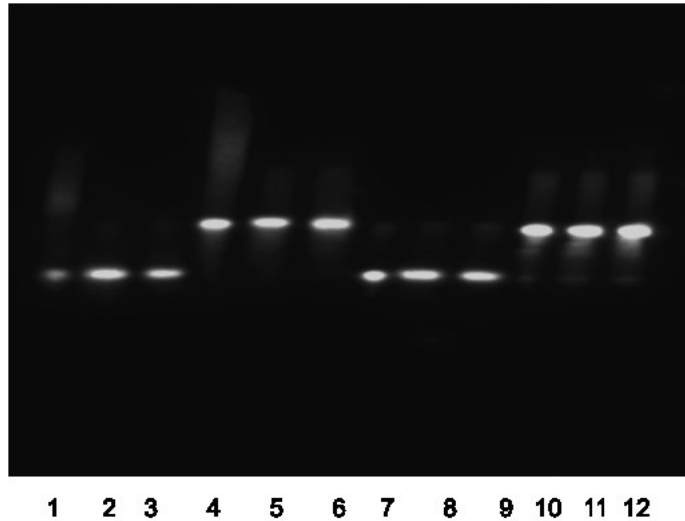


**Figure 30:** The EMSA intramolecular G-quadruplex structures of TEL.(2xG4), TEL.(1xG4), ILPR-1(2xG4), ILPR-1(1xG4). 1: 1µl [10nM] ILPR-1(1xG4) + 8µl TE + 1µl KCl; 2: 1µl [10nM] ILPR-1(1xG4) + 9µl TE; 3: 1µl [10nM] ILPR-1(1xG4) + 9µl TE\*; 4: 1µl [10nM] ILPR-1(2xG4) + 8µl TE + 1µl KCl; 5: 1µl [10nM] ILPR-1(2xG4) + 9µl TE; 6: 1µl [10nM] ILPR-1(2xG4) + 9µl TE\*; 7: 1µl [10nM] TEL.(1xG4) + 8µl TE + 1µl KCl; 8: 1µl [10nM] TEL.(1xG4) + 9µl TE; 9: 1µl [10nM] TEL.(1xG4) + 9µl TE\*; 10: 1µl [10nM] TEL.(2xG4) + 8µl TE + 1µl KCl; 11: 1µl [10nM] TEL.(2xG4) + 9µl TE; 12: 1µl [10nM] TEL.(2xG4) + 9µl TE  
\*: only heated at 95 degree for 5 minutes

## c-Myc(Pu27), VEGF, c-kit21, Bcl-2

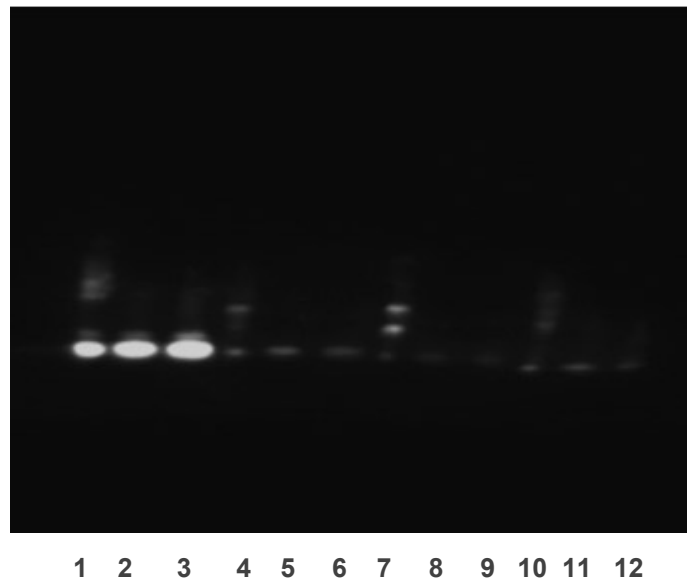


**Figure 31:** The EMSA intramolecular G-quadruplex structures of C-Myc(Pu27), VEGF, c-Kit21, Bcl-2. 1: 1µl [10nM] c-MYC(Pu27)+ 8µl TE + 1µl KCl; 2: 1µl [10nM] c-MYC(Pu27)+ 9µl TE; 3: 1µl [10nM] c-MYC(Pu27) + 9µl TE\*; 4: 1µl [10nM] VEGF + 8µl TE + 1µl KCl; 5: 1µl [10nM] VEGF + 9µl TE; 6: 1µl [10nM] VEGF + 9µl TE\*; 7: 1µl [10nM] c-Kit21+ 8µl TE + 1µl KCl; 8: 1µl [10nM] c-Kit21 + 9µl TE; 9: 1µl [10nM] c-Kit21 + 9µl TE\*; 10: 1µl [10nM] Bcl-2 + 8µl TE + 1µl KCl; 11: 1µl [10nM] Bcl-2 + 9µl TE; 12: 1µl [10nM] Bcl-2 + 9µl TE\*  
\*: only heated at 95 degree for 5 minutes

## ILPR-2, ILPR-3, ILPR-4, ILPR-1(2xG4)

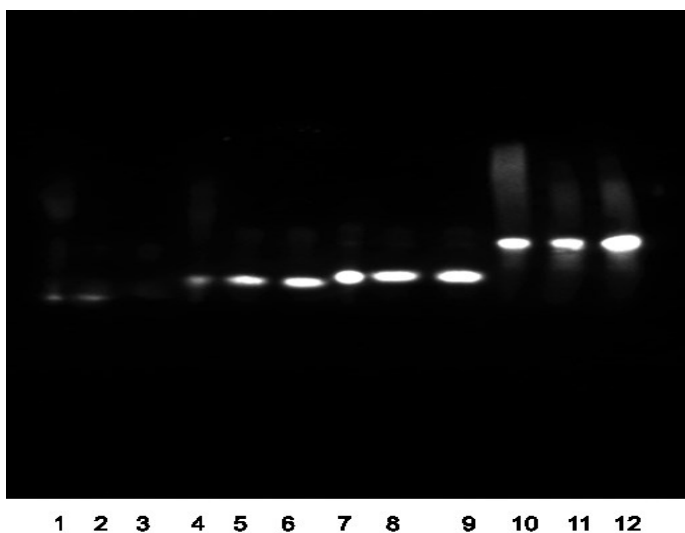
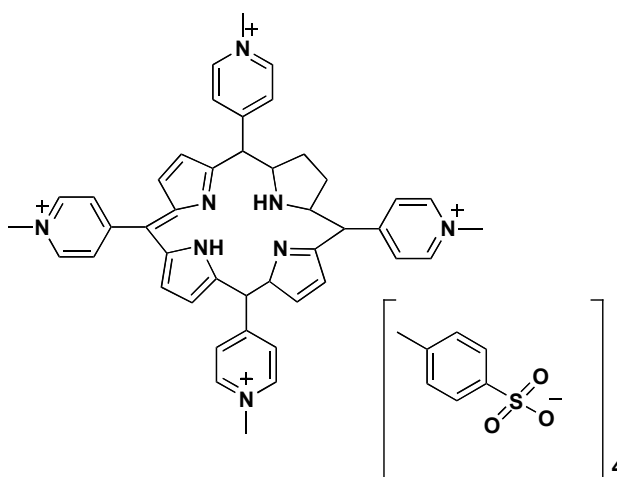


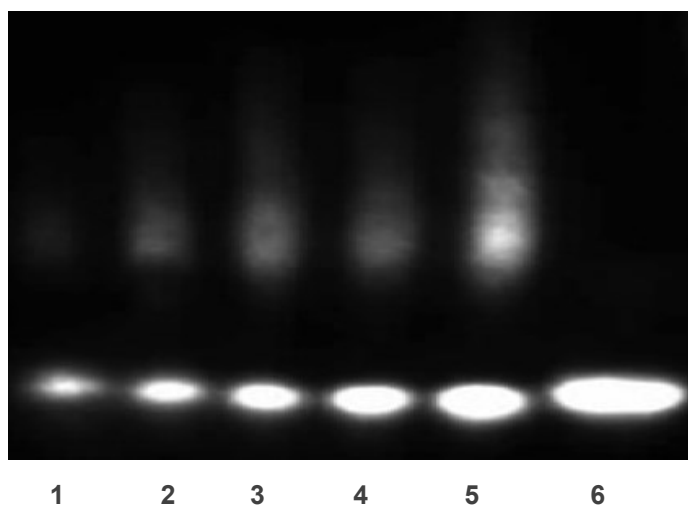
**Figure 32:** The EMSA intramolecular G-quadruplex structures of ILPR-2, ILPR-3, ILPR-4, ILPR-1(2xG4). 1: 1  $\mu$ l [10  $\eta$ M] ILPR-2 + 8  $\mu$ l TE + 1  $\mu$ l KCl; 2: 1  $\mu$ l [10  $\eta$ M] ILPR-2 + 9  $\mu$ l TE; 3: 1  $\mu$ l [10  $\eta$ M] ILPR-2 + 9  $\mu$ l TE\*; 4: 1  $\mu$ l [10  $\eta$ M] ILPR-3 + 8  $\mu$ l TE + 1  $\mu$ l KCl; 5: 1  $\mu$ l [10  $\eta$ M] ILPR-3 + 9  $\mu$ l TE; 6: 1  $\mu$ l [10  $\eta$ M] ILPR-3 + 9  $\mu$ l TE\*; 7: 1  $\mu$ l [10  $\eta$ M] ILPR-4 + 8  $\mu$ l TE + 1  $\mu$ l KCl; 8: 1  $\mu$ l [10  $\eta$ M] ILPR-4 + 9  $\mu$ l TE; 9: 1  $\mu$ l [10  $\eta$ M] ILPR-4 + 9  $\mu$ l TE\*; 10: 1  $\mu$ l [10  $\eta$ M] ILPR-1(2xG4) + 8  $\mu$ l TE + 1  $\mu$ l KCl; 11: 1  $\mu$ l [10  $\eta$ M] ILPR-1(2xG4) + 9  $\mu$ l TE; 12: 1  $\mu$ l [10  $\eta$ M] ILPR-1(2xG4) + 9  $\mu$ l TE\*  
\*: only heated at 95 degree for 5 minutes

Subsequently, the oligonucleotides of most interest were evaluated with the addition of a chemical compounds commercially available and known in the literature as stabilizers of the G-quadruplex.

**TMPyP4 tosylate** 5,10,15,20-Tetrakis(1-methylpyridinium-4-yl)porphyrin tetra(*p*-toluensulfonate)

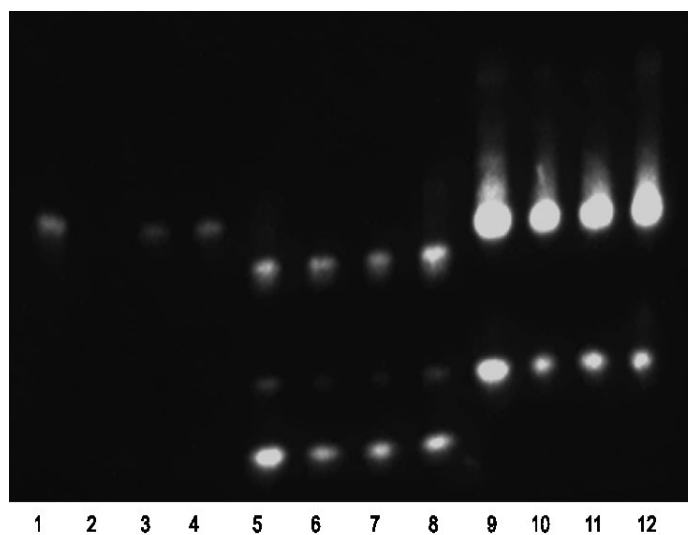


### ILPR-1(1xG4) with different concentration of TMPyP4 tosylate



**Figure 33:** The EMSA intramolecular G-quadruplex structures of ILPR-1(1xG4) with different concentration of TMPyP4 tosylate. **1:** 1  $\mu$ l  $ddH_2O$  + 1  $\mu$ l [10  $\eta$ M] ILPR-1(1xG4) + 8  $\mu$ l TE\*; **2:** 1  $\mu$ l  $ddH_2O$  + 1  $\mu$ l [10  $\eta$ M] ILPR-1(1xG4) + 7  $\mu$ l TE + 1  $\mu$ l KCl; **3:** 1  $\mu$ l [0.5  $\mu$ M] TMPyP4 + 1  $\mu$ l [10  $\eta$ M] ILPR-1(1xG4) + 7  $\mu$ l TE + 1  $\mu$ l KCl; **4:** 1  $\mu$ l [1  $\mu$ M] TMPyP4 + 1  $\mu$ l [10  $\eta$ M] ILPR-1(1xG4) + 7  $\mu$ l TE + 1  $\mu$ l KCl; **5:** 1  $\mu$ l [2.5  $\mu$ M] TMPyP4 + 1  $\mu$ l [10  $\eta$ M] ILPR-1(1xG4) + 7  $\mu$ l TE + 1  $\mu$ l KCl; **6:** 1  $\mu$ l [5  $\mu$ M] TMPyP4 + 1  $\mu$ l [10  $\eta$ M] ILPR-1(1xG4) + 7  $\mu$ l TE + 1  $\mu$ l KCl  
\*: only heated at 95 degree for 5 minutes

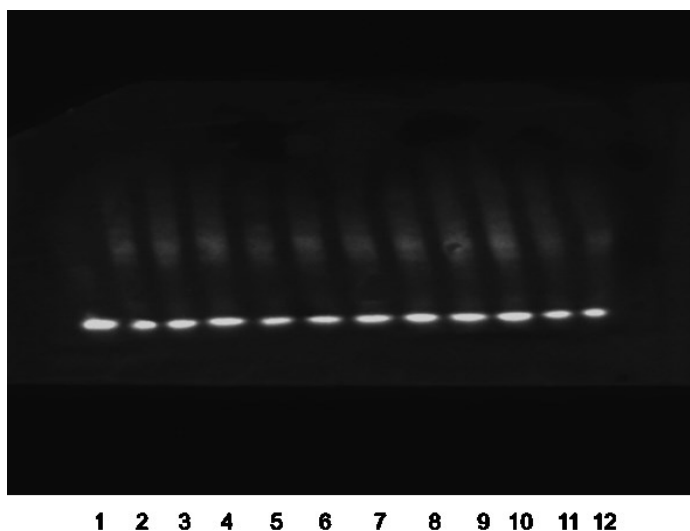
### ILPR-1(2xG4), Bcl-2, c-Myc(Pu27) with TMPyP4 tosylate



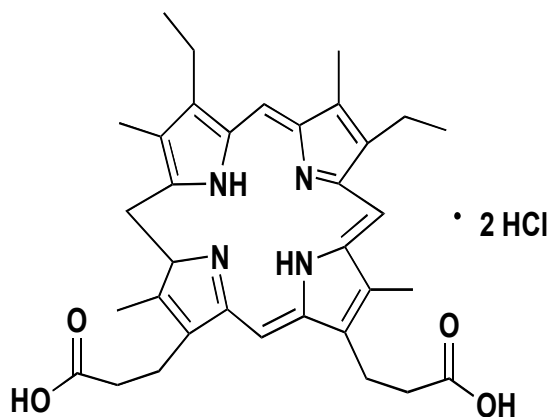
**Figure 34:** The EMSA intramolecular G-quadruplex structures of ILPR-1(2xG4); Bcl-2;c-Myc(Pu27) with TMPyP4 tosylate. **1:** 1  $\mu$ l  $ddH_2O$  + 1  $\mu$ l [10  $\eta$ M] ILPR-1(2xG4) + 7  $\mu$ l TE + 1  $\mu$ l KCl; **2:** 1  $\mu$ l [1  $\mu$ M] TMPyP4 + 1  $\mu$ l [10  $\eta$ M] ILPR-1(2xG4) + 7  $\mu$ l TE + 1  $\mu$ l KCl; **3:** 1  $\mu$ l [2.5  $\mu$ M] TMPyP4 + 1  $\mu$ l [10  $\eta$ M] ILPR-1(2xG4) + 7  $\mu$ l TE + 1  $\mu$ l KCl; **4:** 1  $\mu$ l [5  $\mu$ M] TMPyP4 + 1  $\mu$ l [10  $\eta$ M] ILPR-1(2xG4) + 7  $\mu$ l TE + 1  $\mu$ l KCl; **5:** 1  $\mu$ l  $ddH_2O$  + 1  $\mu$ l [10  $\eta$ M] Bcl-2 + 7  $\mu$ l TE + 1  $\mu$ l KCl; **6:** 1  $\mu$ l [1  $\mu$ M] TMPyP4 + 1  $\mu$ l [10  $\eta$ M] Bcl-2 + 7  $\mu$ l TE + 1  $\mu$ l KCl; **7:** 1  $\mu$ l [2.5  $\mu$ M] TMPyP4 + 1  $\mu$ l [10  $\eta$ M] Bcl-2 + 7  $\mu$ l TE + 1  $\mu$ l KCl; **8:** 1  $\mu$ l [5  $\mu$ M] TMPyP4 + 1  $\mu$ l [10  $\eta$ M] Bcl-2 + 7  $\mu$ l TE + 1  $\mu$ l KCl; **9:** 1  $\mu$ l  $ddH_2O$  + 1  $\mu$ l [10  $\eta$ M] c-Myc(Pu27) + 7  $\mu$ l TE + 1  $\mu$ l KCl; **10:** 1  $\mu$ l [1  $\mu$ M] TMPyP4 + 1  $\mu$ l [10  $\eta$ M] c-Myc(Pu27) + 7  $\mu$ l TE + 1  $\mu$ l KCl; **11:** 1  $\mu$ l [2.5  $\mu$ M] TMPyP4 + 1  $\mu$ l [10  $\eta$ M] c-Myc(Pu27) + 7  $\mu$ l TE + 1  $\mu$ l KCl; **12:** 1  $\mu$ l [5  $\mu$ M] TMPyP4 + 1  $\mu$ l [10  $\eta$ M] c-Myc(Pu27) + 7  $\mu$ l TE + 1  $\mu$ l KCl



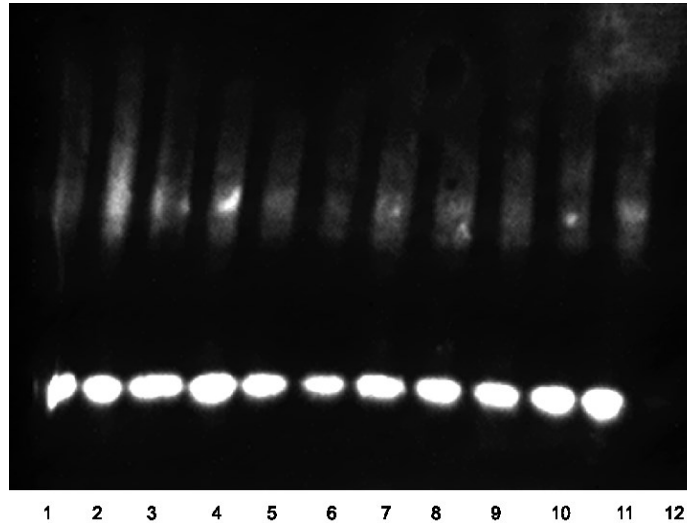
## ILPR-1(1xG4) with different concentration of TMPyP4 tosylate



**Figure 35:** The EMSA intramolecular G-quadruplex structures of ILPR-1(1xG4) with different concentration of chemical TMPyP4 tosylate. 1: 1  $\mu$ l  $d_0$ H<sub>2</sub>O + 1  $\mu$ l [10  $\eta$ M] ILPR-1(1xG4) + 8  $\mu$ l TE\*; 2: 1  $\mu$ l v + 1  $\mu$ l [10  $\eta$ M] ILPR-1(1xG4) + 7  $\mu$ l TE + 1  $\mu$ l KCl; 3: 1  $\mu$ l [0.001  $\mu$ M] TMPyP4 + 1  $\mu$ l [10  $\eta$ M] ILPR-1(1xG4) + 7  $\mu$ l TE + 1  $\mu$ l KCl; 4: 1  $\mu$ l [0.005  $\mu$ M] TMPyP4 + 1  $\mu$ l [10  $\eta$ M] ILPR-1(1xG4) + 7  $\mu$ l TE + 1  $\mu$ l KCl; 5: 1  $\mu$ l [0.01  $\mu$ M] TMPyP4 + 1  $\mu$ l [10  $\eta$ M] ILPR-1(1xG4) + 7  $\mu$ l TE + 1  $\mu$ l KCl; 6: 1  $\mu$ l [0.05  $\mu$ M] TMPyP4 + 1  $\mu$ l [10  $\eta$ M] ILPR-1(1xG4) + 7  $\mu$ l TE + 1  $\mu$ l KCl; 7: 1  $\mu$ l [0.1  $\mu$ M] TMPyP4 + 1  $\mu$ l [10  $\eta$ M] ILPR-1(1xG4) + 7  $\mu$ l TE + 1  $\mu$ l KCl; 8: 1  $\mu$ l [0.25  $\mu$ M] TMPyP4 + 1  $\mu$ l [10  $\eta$ M] ILPR-1(1xG4) + 7  $\mu$ l TE + 1  $\mu$ l KCl; 9: 1  $\mu$ l [0.5  $\mu$ M] TMPyP4 + 1  $\mu$ l [10  $\eta$ M] ILPR-1(1xG4) + 7  $\mu$ l TE + 1  $\mu$ l KCl; 10: 1  $\mu$ l [1  $\mu$ M] TMPyP4 + 1  $\mu$ l [10  $\eta$ M] ILPR-1(1xG4) + 7  $\mu$ l TE + 1  $\mu$ l KCl; 11: 1  $\mu$ l [2.5  $\mu$ M] TMPyP4 + 1  $\mu$ l [10  $\eta$ M] ILPR-1(1xG4) + 7  $\mu$ l TE + 1  $\mu$ l KCl; 12: 1  $\mu$ l [5  $\mu$ M] TMPyP4 + 1  $\mu$ l [10  $\eta$ M] ILPR-1(1xG4) + 7  $\mu$ l TE + 1  $\mu$ l KCl  
\*: only heated at 95 degree for 5 minutes

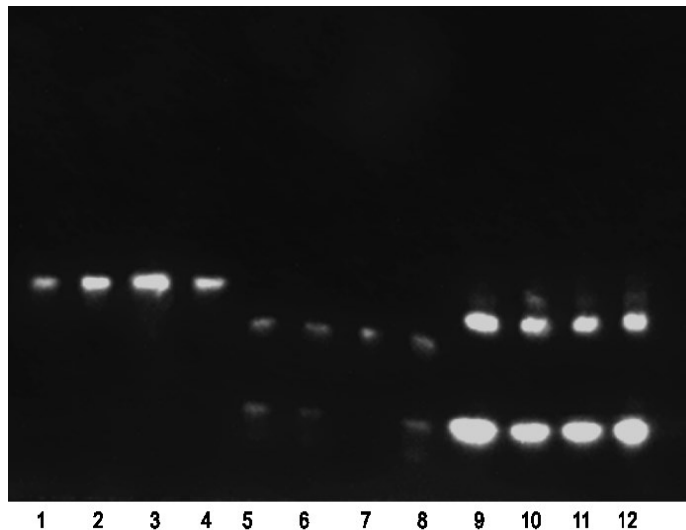
**Mesoporphyrin IX dihydrochloride**

### ILPR-1(1xG4) with different concentration of Mesoporphyrin IX Dihydrochloride

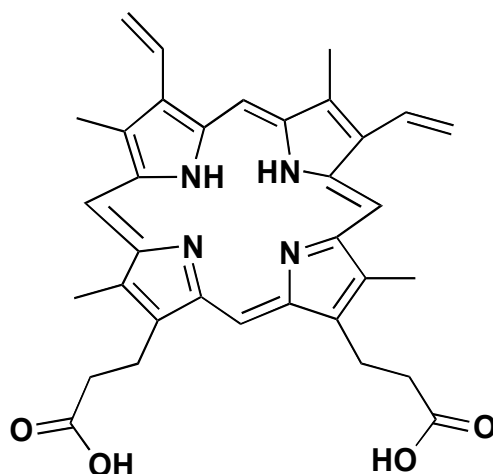


**Figure 36:** The EMSA intramolecular G-quadruplex structures of ILPR-1(1xG4) with different concentration of chemical Mesoporphyrin IX dihydrochloride. **1:** 1  $\mu\text{l}$   $\text{ddH}_2\text{O}$  + 1  $\mu\text{l}$  [10  $\eta\text{M}$ ] ILPR-1(1xG4) + 8  $\mu\text{l}$  TE\*; **2:** 1  $\mu\text{l}$   $\text{ddH}_2\text{O}$  + 1  $\mu\text{l}$  [10  $\eta\text{M}$ ] ILPR-1(1xG4) + 7  $\mu\text{l}$  TE + 1  $\mu\text{l}$  KCl; **3:** 1  $\mu\text{l}$  [0.001  $\mu\text{M}$ ] Mesoporphyrin + 1  $\mu\text{l}$  [10  $\eta\text{M}$ ] ILPR-1(1xG4) + 7  $\mu\text{l}$  TE + 1  $\mu\text{l}$  KCl; **4:** 1  $\mu\text{l}$  [0.005  $\mu\text{M}$ ] Mesoporphyrin + 1  $\mu\text{l}$  [10  $\eta\text{M}$ ] ILPR-1(1xG4) + 7  $\mu\text{l}$  TE + 1  $\mu\text{l}$  KCl; **5:** 1  $\mu\text{l}$  [0.01  $\mu\text{M}$ ] Mesoporphyrin + 1  $\mu\text{l}$  [10  $\eta\text{M}$ ] ILPR-1(1xG4) + 7  $\mu\text{l}$  TE + 1  $\mu\text{l}$  KCl; **6:** 1  $\mu\text{l}$  [0.05  $\mu\text{M}$ ] Mesoporphyrin + 1  $\mu\text{l}$  [10  $\eta\text{M}$ ] ILPR-1(1xG4) + 7  $\mu\text{l}$  TE + 1  $\mu\text{l}$  KCl; **7:** 1  $\mu\text{l}$  [0.1  $\mu\text{M}$ ] Mesoporphyrin + 1  $\mu\text{l}$  [10  $\eta\text{M}$ ] ILPR-1(1xG4) + 7  $\mu\text{l}$  TE + 1  $\mu\text{l}$  KCl; **8:** 1  $\mu\text{l}$  [0.25  $\mu\text{M}$ ] Mesoporphyrin + 1  $\mu\text{l}$  [10  $\eta\text{M}$ ] ILPR-1(1xG4) + 7  $\mu\text{l}$  TE + 1  $\mu\text{l}$  KCl; **9:** 1  $\mu\text{l}$  [0.5  $\mu\text{M}$ ] Mesoporphyrin + 1  $\mu\text{l}$  [10  $\eta\text{M}$ ] ILPR-1(1xG4) + 7  $\mu\text{l}$  TE + 1  $\mu\text{l}$  KCl; **10:** 1  $\mu\text{l}$  [1  $\mu\text{M}$ ] Mesoporphyrin + 1  $\mu\text{l}$  [10  $\eta\text{M}$ ] ILPR-1(1xG4) + 7  $\mu\text{l}$  TE + 1  $\mu\text{l}$  KCl; **11:** 1  $\mu\text{l}$  [2.5  $\mu\text{M}$ ] Mesoporphyrin + 1  $\mu\text{l}$  [10  $\eta\text{M}$ ] ILPR-1(1xG4) + 7  $\mu\text{l}$  TE + 1  $\mu\text{l}$  KCl; **12:** 1  $\mu\text{l}$  [5  $\mu\text{M}$ ] Mesoporphyrin + 1  $\mu\text{l}$  [10  $\eta\text{M}$ ] ILPR-1(1xG4) + 7  $\mu\text{l}$  TE + 1  $\mu\text{l}$  KCl  
\*: only heated at 95 degree for 5 minutes

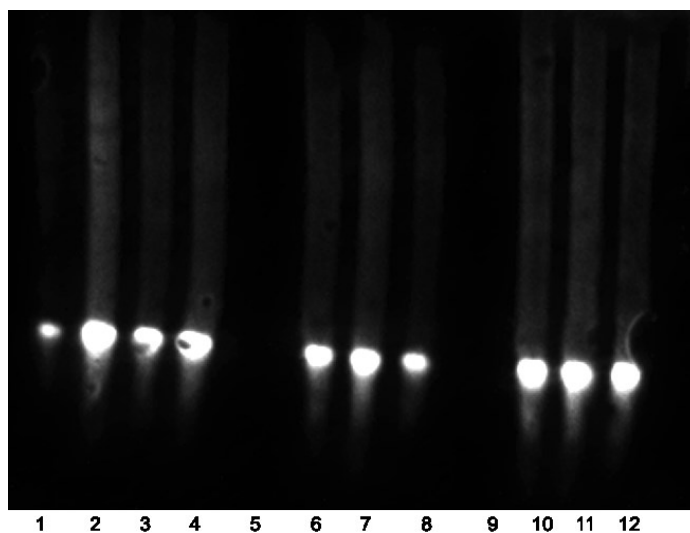
### ILPR-1(2xG4), Bcl-2, c-Myc(Pu27) with Mesoporphyrin IX Dihydrochloride



**Figure 37:** The EMSA intramolecular G-quadruplex structures of ILPR-1(2xG4); Bcl-2;c-Myc(Pu27) with different concentration of chemical Mesoporphyrin IX dihydrochloride. **1:** 1  $\mu\text{l}$   $\text{ddH}_2\text{O}$  + 1  $\mu\text{l}$  [10  $\eta\text{M}$ ] ILPR-1(2xG4) + 7  $\mu\text{l}$  TE + 1  $\mu\text{l}$  KCl; **2:** 1  $\mu\text{l}$  [1  $\mu\text{M}$ ] Mesoporphyrin + 1  $\mu\text{l}$  [10  $\eta\text{M}$ ] ILPR-1(2xG4) + 7  $\mu\text{l}$  TE + 1  $\mu\text{l}$  KCl; **3:** 1  $\mu\text{l}$  [2.5  $\mu\text{M}$ ] Mesoporphyrin + 1  $\mu\text{l}$  [10  $\eta\text{M}$ ] ILPR-1(2xG4) + 7  $\mu\text{l}$  TE + 1  $\mu\text{l}$  KCl; **4:** 1  $\mu\text{l}$  [5  $\mu\text{M}$ ] Mesoporphyrin + 1  $\mu\text{l}$  [10  $\eta\text{M}$ ] ILPR-1(2xG4) + 7  $\mu\text{l}$  TE + 1  $\mu\text{l}$  KCl; **5:** 1  $\mu\text{l}$   $\text{ddH}_2\text{O}$  + 1  $\mu\text{l}$  [10  $\eta\text{M}$ ] Bcl-2 + 7  $\mu\text{l}$  TE + 1  $\mu\text{l}$  KCl; **6:** 1  $\mu\text{l}$  [1  $\mu\text{M}$ ] Mesoporphyrin + 1  $\mu\text{l}$  [10  $\eta\text{M}$ ] Bcl-2 + 7  $\mu\text{l}$  TE + 1  $\mu\text{l}$  KCl; **7:** 1  $\mu\text{l}$  [2.5  $\mu\text{M}$ ] Mesoporphyrin + 1  $\mu\text{l}$  [10  $\eta\text{M}$ ] Bcl-2 + 7  $\mu\text{l}$  TE + 1  $\mu\text{l}$  KCl; **8:** 1  $\mu\text{l}$  [5  $\mu\text{M}$ ] Mesoporphyrin + 1  $\mu\text{l}$  [10  $\eta\text{M}$ ] Bcl-2 + 7  $\mu\text{l}$  TE + 1  $\mu\text{l}$  KCl; **9:** 1  $\mu\text{l}$   $\text{ddH}_2\text{O}$  + 1  $\mu\text{l}$  [10  $\eta\text{M}$ ] c-Myc(Pu27) + 7  $\mu\text{l}$  TE + 1  $\mu\text{l}$  KCl; **10:** 1  $\mu\text{l}$  [1  $\mu\text{M}$ ] Mesoporphyrin + 1  $\mu\text{l}$  [10  $\eta\text{M}$ ] c-Myc(Pu27) + 7  $\mu\text{l}$  TE + 1  $\mu\text{l}$  KCl; **11:** 1  $\mu\text{l}$  [2.5  $\mu\text{M}$ ] Mesoporphyrin + 1  $\mu\text{l}$  [10  $\eta\text{M}$ ] c-Myc(Pu27) + 7  $\mu\text{l}$  TE + 1  $\mu\text{l}$  KCl; **12:** 1  $\mu\text{l}$  [5  $\mu\text{M}$ ] Mesoporphyrin + 1  $\mu\text{l}$  [10  $\eta\text{M}$ ] c-Myc(Pu27) + 7  $\mu\text{l}$  TE + 1  $\mu\text{l}$  KCl

**Protoporphyrin IX**

Evaluation the best concentrations of porphyrin.

**3 times of ILPR-1(2xG4) with Protoporphyrin IX**

**Figure 38:** The EMSA intramolecular G-quadruplex structures of three series of ILPR-1(2xG4) with different concentration of chemical Protoporphyrin IX. **1:** 1 $\mu$ l  $_{\text{ad}}$ H<sub>2</sub>O + 1 $\mu$ l [10 $\eta$ M] ILPR-1(2xG4) + 7 $\mu$ l TE + 1 $\mu$ l KCl; **2:** 1 $\mu$ l [1 $\mu$ M] Protoporphyrin + 1 $\mu$ l [10 $\eta$ M] ILPR-1(2xG4) + 7 $\mu$ l TE + 1 $\mu$ l KCl; **3:** 1 $\mu$ l [2.5 $\mu$ M] Protoporphyrin + 1 $\mu$ l [10 $\eta$ M] ILPR-1(2xG4) + 7 $\mu$ l TE + 1 $\mu$ l KCl; **4:** 1 $\mu$ l [5 $\mu$ M] Protoporphyrin + 1 $\mu$ l [10 $\eta$ M] ILPR-1(2xG4) + 7 $\mu$ l TE + 1 $\mu$ l KCl; **6:** 1 $\mu$ l [1 $\mu$ M] Protoporphyrin + 1 $\mu$ l [10 $\eta$ M] ILPR-1(2xG4) + 7 $\mu$ l TE + 1 $\mu$ l KCl; **7:** 1 $\mu$ l [2.5 $\mu$ M] Protoporphyrin + 1 $\mu$ l [10 $\eta$ M] ILPR-1(2xG4) + 7 $\mu$ l TE + 1 $\mu$ l KCl; **8:** 1 $\mu$ l [5 $\mu$ M] Protoporphyrin + 1 $\mu$ l [10 $\eta$ M] ILPR-1(2xG4) + 7 $\mu$ l TE + 1 $\mu$ l KCl; **10:** 1 $\mu$ l [1 $\mu$ M] Protoporphyrin + 1 $\mu$ l [10 $\eta$ M] ILPR-1(2xG4) + 7 $\mu$ l TE + 1 $\mu$ l KCl; **11:** 1 $\mu$ l [2.5 $\mu$ M] Protoporphyrin + 1 $\mu$ l [10 $\eta$ M] ILPR-1(2xG4) + 7 $\mu$ l TE + 1 $\mu$ l KCl; **12:** 1 $\mu$ l [5 $\mu$ M] Protoporphyrin + 1 $\mu$ l [10 $\eta$ M] ILPR-1(2xG4) + 7 $\mu$ l TE + 1 $\mu$ l KCl  
**5, 9** are gap.

## ILPR-1(1xG4), Bcl-2, c-Myc(Pu27) with Protoporphyrin IX

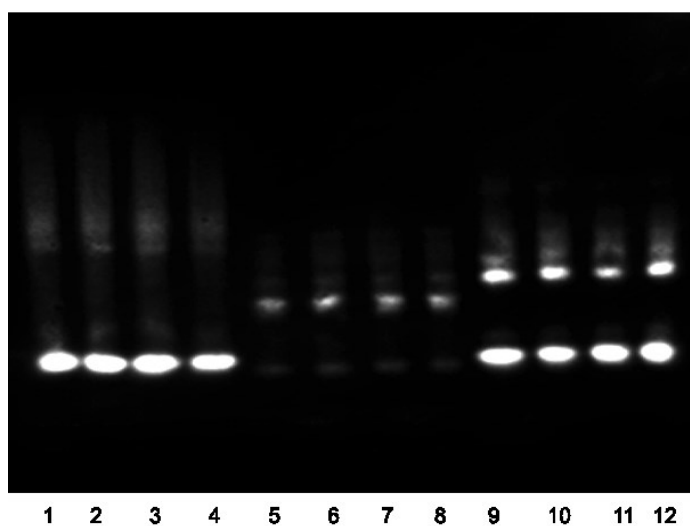
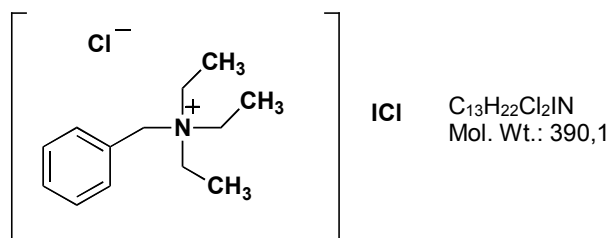


**Figure 39:** The EMSA intramolecular G-quadruplex structures of ILPR-1(1xG4); Bcl-2;c-Myc(Pu27). **1:** 1 $\mu$ l  $d_2$ H<sub>2</sub>O + 1 $\mu$ l [10 $\eta$ M] ILPR-1(1xG4) + 7 $\mu$ l TE + 1 $\mu$ l KCl; **2:** 1 $\mu$ l [1 $\mu$ M] Protoporphyrin + 1 $\mu$ l [10 $\eta$ M] ILPR-1(1xG4) + 7 $\mu$ l TE + 1 $\mu$ l KCl; **3:** 1 $\mu$ l [2.5 $\mu$ M] Protoporphyrin + 1 $\mu$ l [10 $\eta$ M] ILPR-1(1xG4) + 7 $\mu$ l TE + 1 $\mu$ l KCl; **4:** 1 $\mu$ l [5 $\mu$ M] Protoporphyrin + 1 $\mu$ l [10 $\eta$ M] ILPR-1(1xG4) + 7 $\mu$ l TE + 1 $\mu$ l KCl; **5:** 1 $\mu$ l  $d_2$ H<sub>2</sub>O + 1 $\mu$ l [10 $\eta$ M] Bcl-2 + 7 $\mu$ l TE + 1 $\mu$ l KCl; **6:** 1 $\mu$ l [1 $\mu$ M] Protoporphyrin + 1 $\mu$ l [10 $\eta$ M] Bcl-2 + 7 $\mu$ l TE + 1 $\mu$ l KCl; **7:** 1 $\mu$ l [2.5 $\mu$ M] Protoporphyrin + 1 $\mu$ l [10 $\eta$ M] Bcl-2 + 7 $\mu$ l TE + 1 $\mu$ l KCl; **8:** 1 $\mu$ l [5 $\mu$ M] Protoporphyrin + 1 $\mu$ l [10 $\eta$ M] Bcl-2 + 7 $\mu$ l TE + 1 $\mu$ l KCl; **9:** 1 $\mu$ l  $d_2$ H<sub>2</sub>O + 1 $\mu$ l [10 $\eta$ M] c-Myc(Pu27) + 7 $\mu$ l TE + 1 $\mu$ l KCl; **10:** 1 $\mu$ l [1 $\mu$ M] Protoporphyrin + 1 $\mu$ l [10 $\eta$ M] c-Myc(Pu27) + 7 $\mu$ l TE + 1 $\mu$ l KCl; **11:** 1 $\mu$ l [2.5 $\mu$ M] Protoporphyrin + 1 $\mu$ l [10 $\eta$ M] c-Myc(Pu27) + 7 $\mu$ l TE + 1 $\mu$ l KCl; **12:** 1 $\mu$ l [5 $\mu$ M] Protoporphyrin + 1 $\mu$ l [10 $\eta$ M] c-Myc(Pu27) + 7 $\mu$ l TE + 1 $\mu$ l KCl

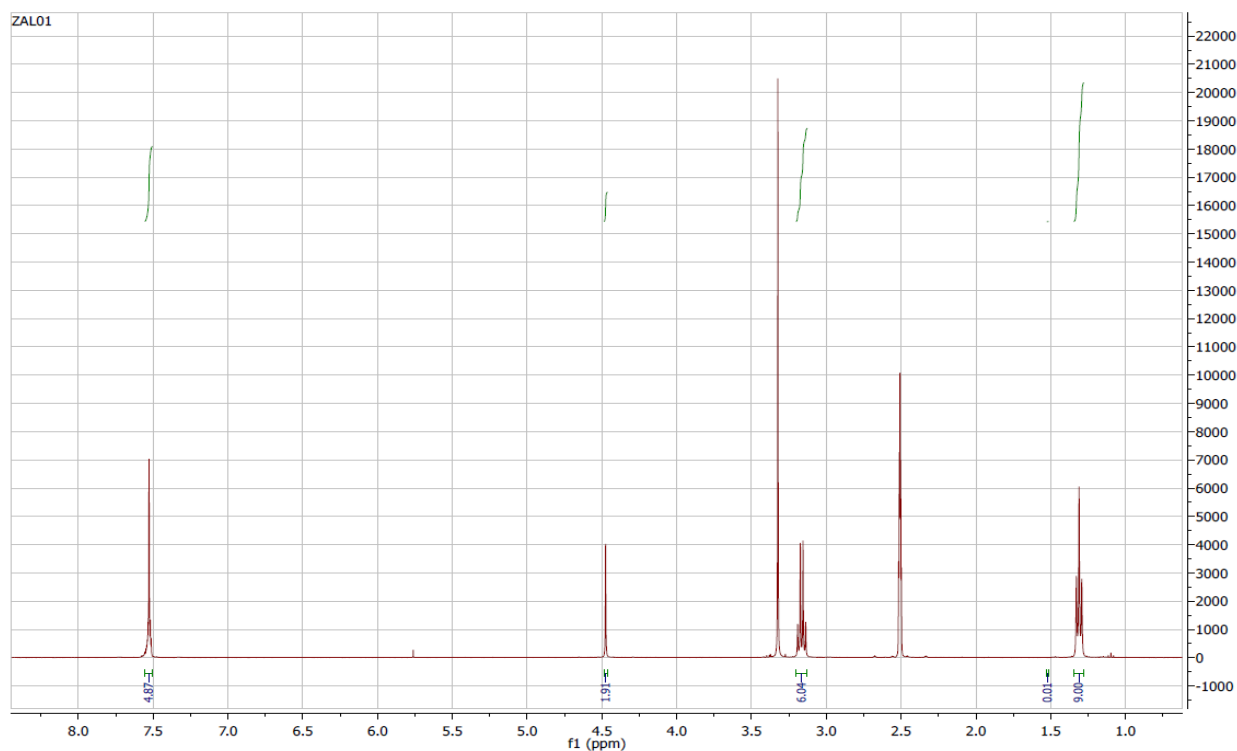
#### 4.5 Synthesis of a new compound triazole derivate

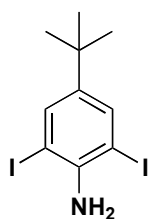
##### Synthesis of Benzyltriethylammonium dichloroiodate (9)



To a stirred solution of ICI (1.5 g, 9.2 mmol) in 20 ml of DCM was added BnEt<sub>3</sub>NCl (2.1 g, 9.2 mmol) in 10 ml of water via an addition funnel over 15 minutes. After stirring for 30/40 minutes the layers were separated, and the organic layer was dried (MgSO<sub>4</sub>), filtered and concentrated under reduced pressure. The residue was crystallized by taking it up in minimal DCM and back adding Et<sub>2</sub>O to 3:1 (DCM:Et<sub>2</sub>O) ratio. It was left overnight (o.n.). After the material was filtered and washed many times with Et<sub>2</sub>O and dried under vacuum to afford 2.9 g (Y=91%) of yellow crystals.

**<sup>1</sup>H NMR (400 MHz, d<sub>6</sub>-DMSO):** δ 7.57 - 7.50 (m, 5H), 4.48 (s, 2H), 3.16 (q, J = 7.2 Hz, 6H), 1.31 (t, J = 7.2Hz,9H).

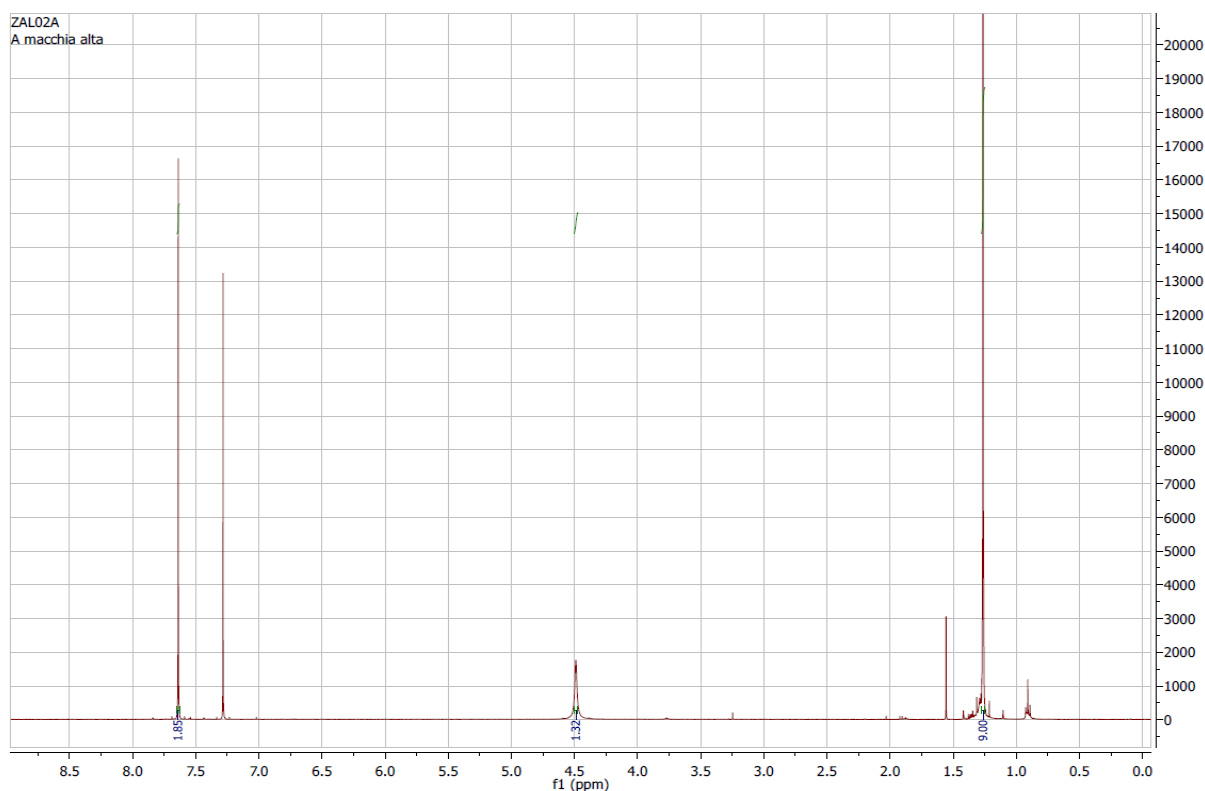


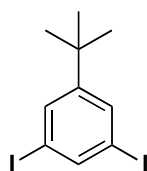
Synthesis of 4- Tert- butyl-2,6-diiodo-phenylamine (**2**)

C<sub>10</sub>H<sub>13</sub>I<sub>2</sub>N  
Mol. Wt.: 401,0

To a stirred solution of t-butyl aniline (306 mg, 2.04 mmol) in DCM (27.2 ml) and MeOH (13.6 ml) BnEt<sub>3</sub>NiCl<sub>2</sub> (1.5 g, 4.3 mmol) and CaCO<sub>3</sub> (817 mg, 8.2 mmol) were added. The reaction was stirred at 40°C on. After the reaction was monitored via TLC 9.5:0.5 (Hexane:AcOEt). It was filtered through a bed of celite and concentrated to 1/3 the volume. The organic phase was washed with 5% NaHSO<sub>3</sub>, sat NaHCO<sub>3</sub>, water and brine. The organic layer was dried (MgSO<sub>4</sub>), filtered and concentrated to give a red oil. The material was purified using flash chromatography (SiO<sub>2</sub>) 9.8:0.2 (Hexane:AcOEt) to afford 408 mg (Y=50%) of a dark brown oil.

**<sup>1</sup>H NMR (400 MHz, CDCl<sub>3</sub>):** δ 7.64 (s, 2H), 4.49 (s, 2H), 1.26 (s, 9H).

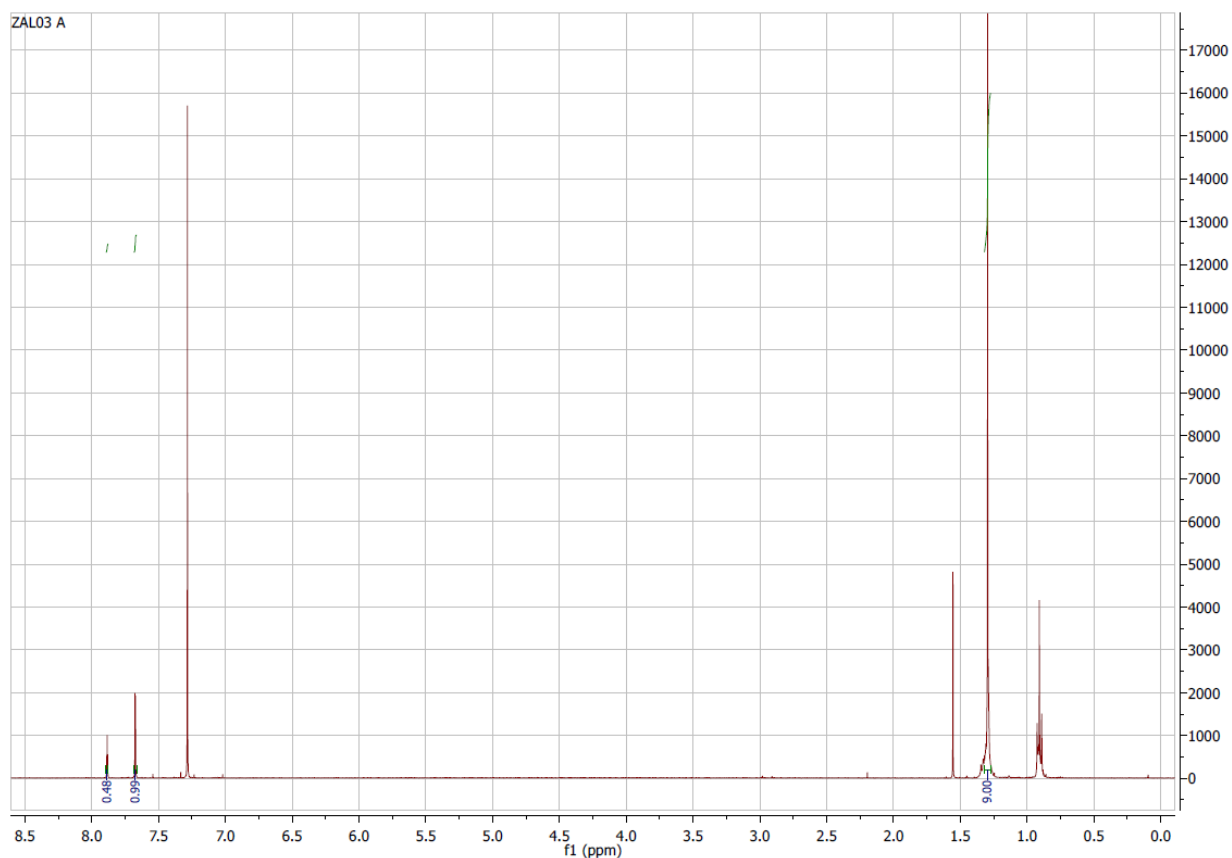


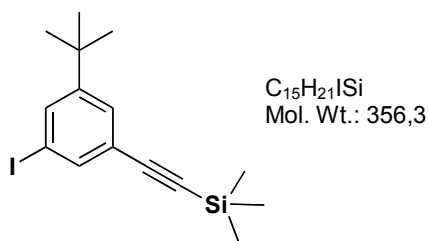
Synthesis of 1-Tert-butyl-3,5-diiodo-benzene (**3**)

C<sub>10</sub>H<sub>12</sub>I<sub>2</sub>  
Mol. Wt.: 386,0

To a stirred solution of DMF (1.2 ml) at 60°C was added *t*-butylnitrite (210 mg, 2.03 mmol) followed by 4-*tert*-Butyl-2,6-diiodo-phenylamine (408 mg, 1.02 mmol) in 581  $\mu$ l of DMF dropwise (\*Note to resume the product in the flask it was used about 1 ml of DMF). After stirring for 10 minutes, the reaction was allowed to cool, diluted with AcOEt (48 ml) and water (48 ml). The organic layer was washed with brine, dried over MgSO<sub>4</sub>, filtered and concentrated. TLC Hexane. The material was purified using flash chromatography (SiO<sub>2</sub>) 100% (Hexane) to afford 364 mg (Y=92%) of a solid pink clear<sup>63</sup>.

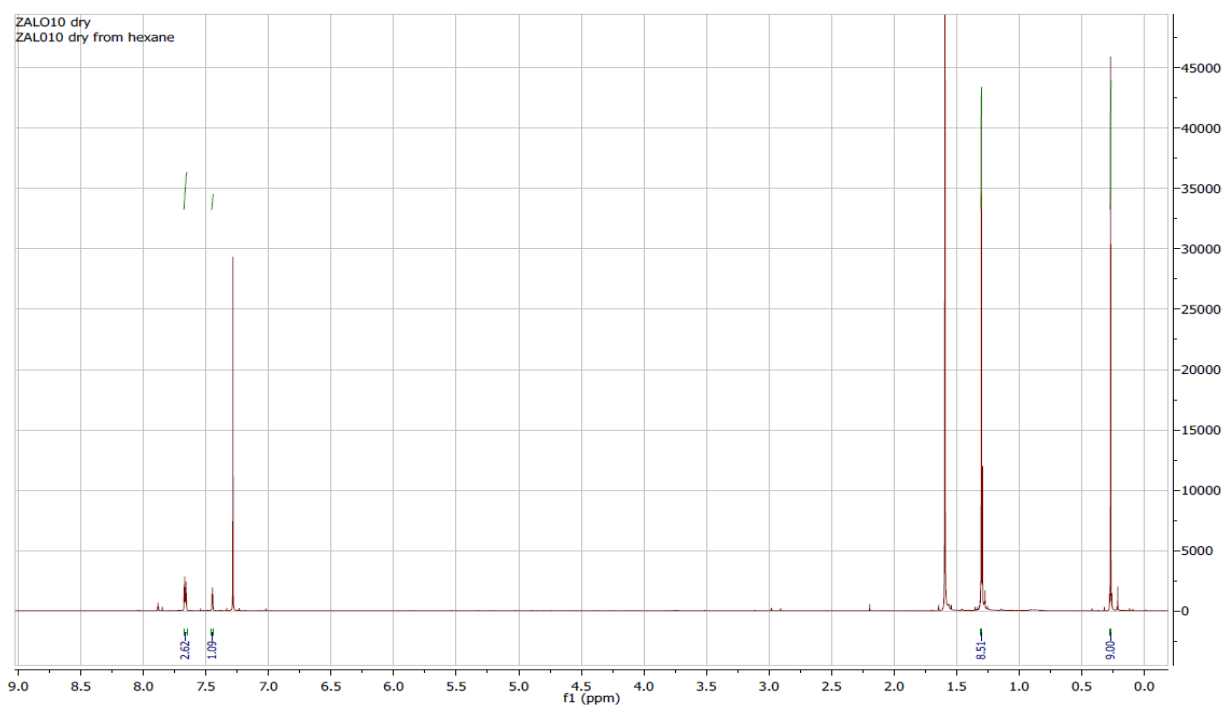
**<sup>1</sup>H NMR (400 MHz, CDCl<sub>3</sub>):**  $\delta$  7.89 (t, J = 1.5 Hz, 1H), 7.67 (d, J = 1.5 Hz, 2H), 1.32 – 1.27 (m, 9H).



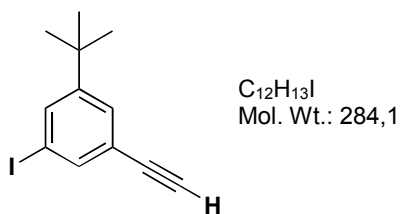
Synthesis of 3-iodo-1-tert-butyl-5-(trimethylsilylethynyl)benzene (**4**)

3,5-Diiodo-1-tert-butyl-benzene (155 mg, 0.4 mmol), CuI (1.5 mg, 0.008 mmol) and Pd(PPh<sub>3</sub>)Cl<sub>2</sub> (5.6 mg, 0.008 mmol) were placed in a two neck flask, which was degassed under high vacuum and back-filled with Nitrogen three times. Degassed THF (5 ml) and LDA (1 ml) were added followed by the dropwise addition of Ethynyltrimethylsilane (TMS) (19.6 mg, 0.2 mmol). The reaction mixture was stirred o.n. at r.t.. The reaction was checked by TLC 100% (Hexane). The volatiles were removed in vacuum and the yellow solid obtained was washed with water and extracted with CH<sub>2</sub>Cl<sub>2</sub> (three times), dried with MgSO<sub>4</sub> and concentrated under reduced pressure. Flash chromatography (SiO<sub>2</sub>) 100% (Hexane) to afford 83.4 mg of compound **4** (Y= 59%).

**<sup>1</sup>H NMR (400 MHz, CDCl<sub>3</sub>):** δ 7.66 (dt, J = 4.2, 1.7 Hz, 2H), 7.46 – 7.43 (m, 1H), 1.30 (s, 9H), 0.28 – 0.26 (m, 9H).

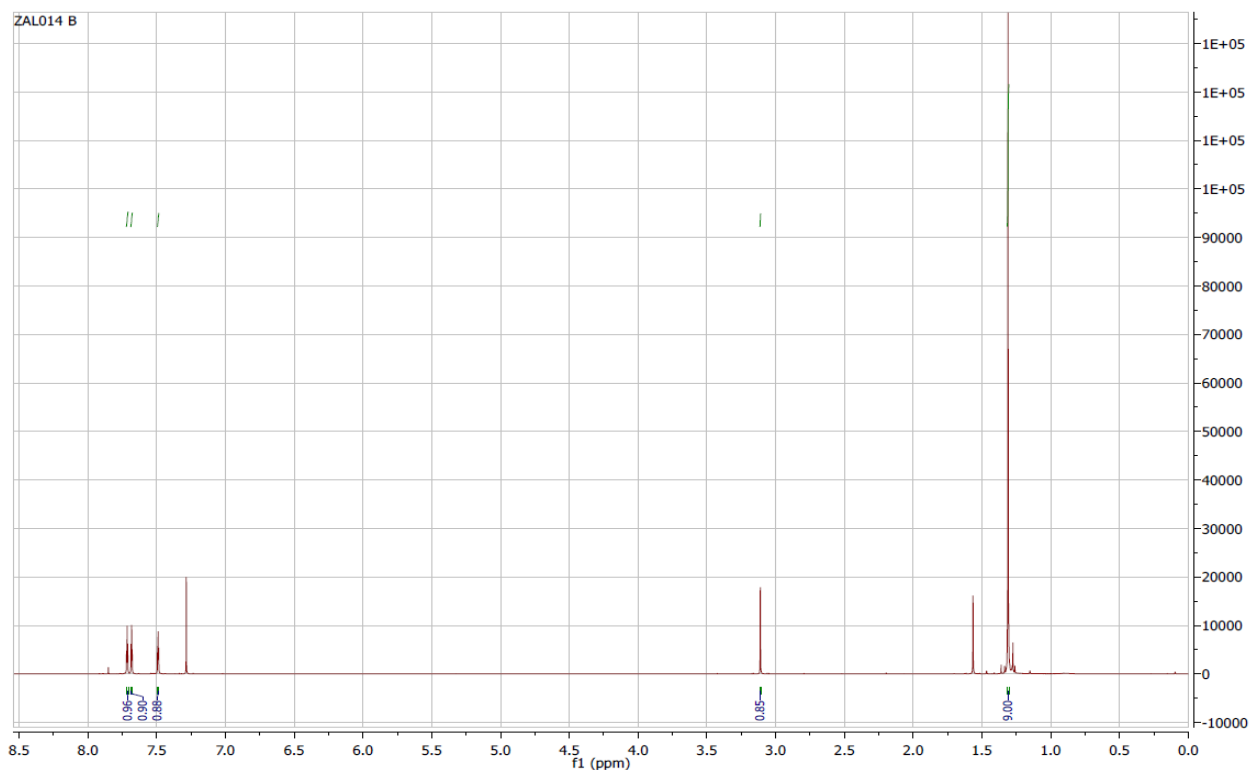


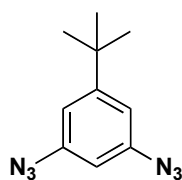


Synthesis of 3-iodo-5-ethynyl-1-tert-butylbenzene (**5**)

A 50 ml flask was charged with 3-iodo-1-tert-butyl-5-(trimethylsilylethynyl)benzene (163.2 mg, 0.458 mmol), KF (133 mg, 2.29 mmol), THF (1.64 ml) and methanol (1.64 ml) and stirred at r.t. for 8 h. The volatiles were removed in vacuo and the solid obtained was extracted with  $CH_2Cl_2$  and water (the last wash with brine), dried with  $MgSO_4$  and concentrated under pressure. Purification by preparative TLC 9.8:0.1 ( $CH_2Cl_2$ :Hexane) to afford 130 mg of compound **5** (Y= 34%).

$^1H$  NMR (400 MHz,  $CDCl_3$ ):  $\delta$  7.71 (t,  $J=1.7$  Hz, 1H), 7.68 (t,  $J=1.5$  Hz, 1H), 7.49 (t,  $J=1.6$  Hz, 1H), 3.11 (s, 1H), 1.31 (d,  $J=1.9$  Hz, 9H).



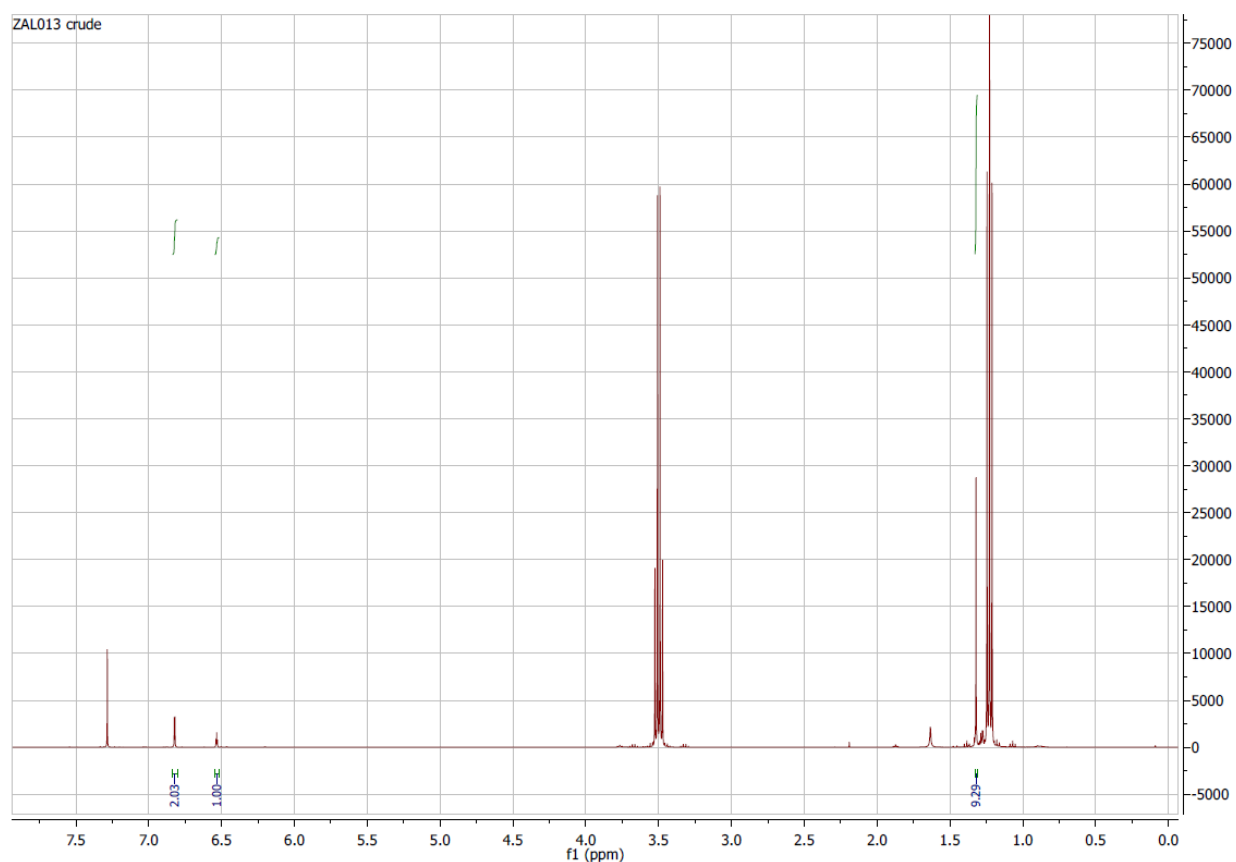
Synthesis of 3,5-diazido-1-tert-butylbenzene (**6**)

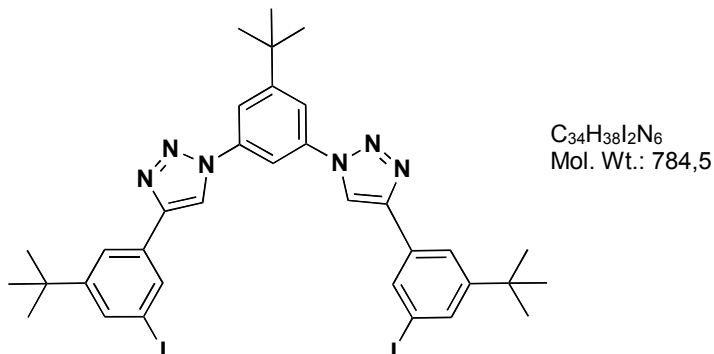
C<sub>10</sub>H<sub>12</sub>N<sub>6</sub>  
Mol. Wt.: 216,2

3,5-Diiodo-1-tert-butylbenzene (220 mg, 0.57 mmol), NaN<sub>3</sub> (111 mg, 1.71 mmol), sodium ascorbate (11.3 mg, 0.057 mmol), DMEA (15 mg, 0.171 mmol) were added to degassed solvent mixture EtOH:H<sub>2</sub>O:toluene (7:3:1, 3 ml). The reaction was followed by TLC.

When the 3,5-Diiodo-1-tert-butylbenzene was completely consumed (about 1h), the reaction mixture was allowed to cool down to r.t.. The reaction goes to completeness and it was formed only azide to afford 88 mg (Y= 71%).

**<sup>1</sup>H NMR (400 MHz, CDCl<sub>3</sub>):** δ 6.82 (d, J = 2.0 Hz, 2H), 6.53 (t, J = 2.0 Hz, 1H), 1.32 (s, 9H).

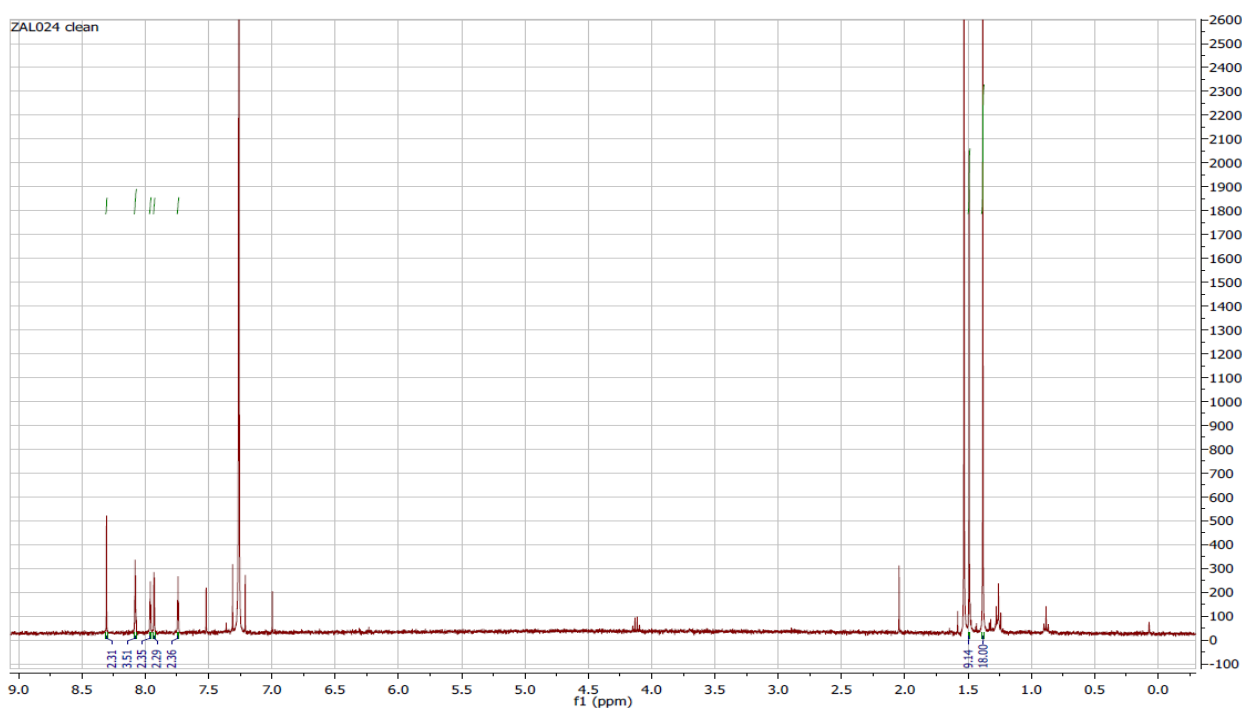


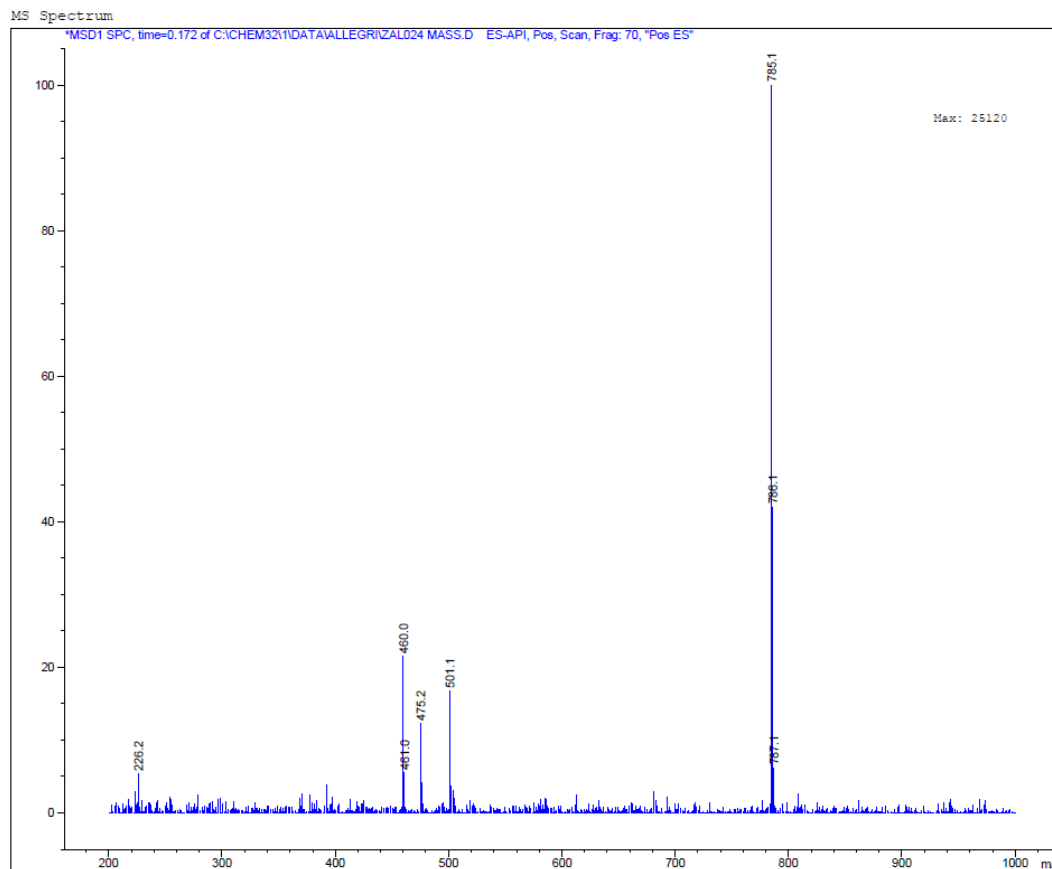
Synthesis of 1,1'-(5-(tert-butyl)-1,3-phenylene)bis(4-(3-(tert-butyl)-5-iodophenyl)-1H-1,2,3-triazole) (**7**)

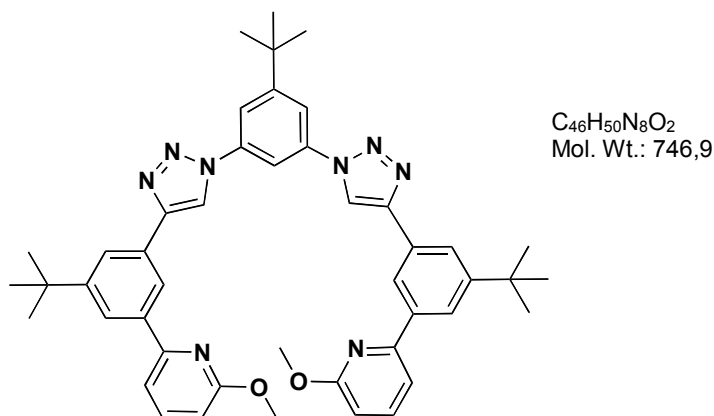
A solution of the diazide (15.32 mg, 0.0709 mmol), and monoacetylene (44.3 mg, 0.156 mmol), sodium ascorbate (1.4 mg, 0.00709 mmol) and  $CuSO_4$  (0.11mg; 0.000709 mmol) in 7:3:1 mixture of EtOH:H<sub>2</sub>O:Toluene (993  $\mu$ l) was stirred at r.t. for 24h with N<sub>2</sub>. Flash chromatography (SiO<sub>2</sub>) 9:1 (Hexane:AcOEt) to afford 44.8 mg of compound **7**<sup>64</sup> (Y= 81%).

**<sup>1</sup>H NMR (400 MHz, CDCl<sub>3</sub>):**  $\delta$  8.31 (s, 2H), 8.08 (m, J=1.6 Hz, 3H), 7.96 (t, J= 1.6 Hz, 2H), 7.93 (t, J=1.6 Hz, 2H), 7.93 (d, J=2 Hz, 2H), 7.74 (t, J=1.7 Hz, 2H), 1.49 (s, 9H), 1.38 (s, 18H).

**MS (ESI):** [M+H]<sup>+</sup>= 784.12





**ZAL026** Synthesis of 6,6'-((1,1'-(5-(tert-butyl)-1,3-phenylene)bis(1H-1,2,3-triazole-4,1-diyl))bis(3-(tert-butyl)-5,1-phenylene))bis(2-methoxypyridine) (**8**)

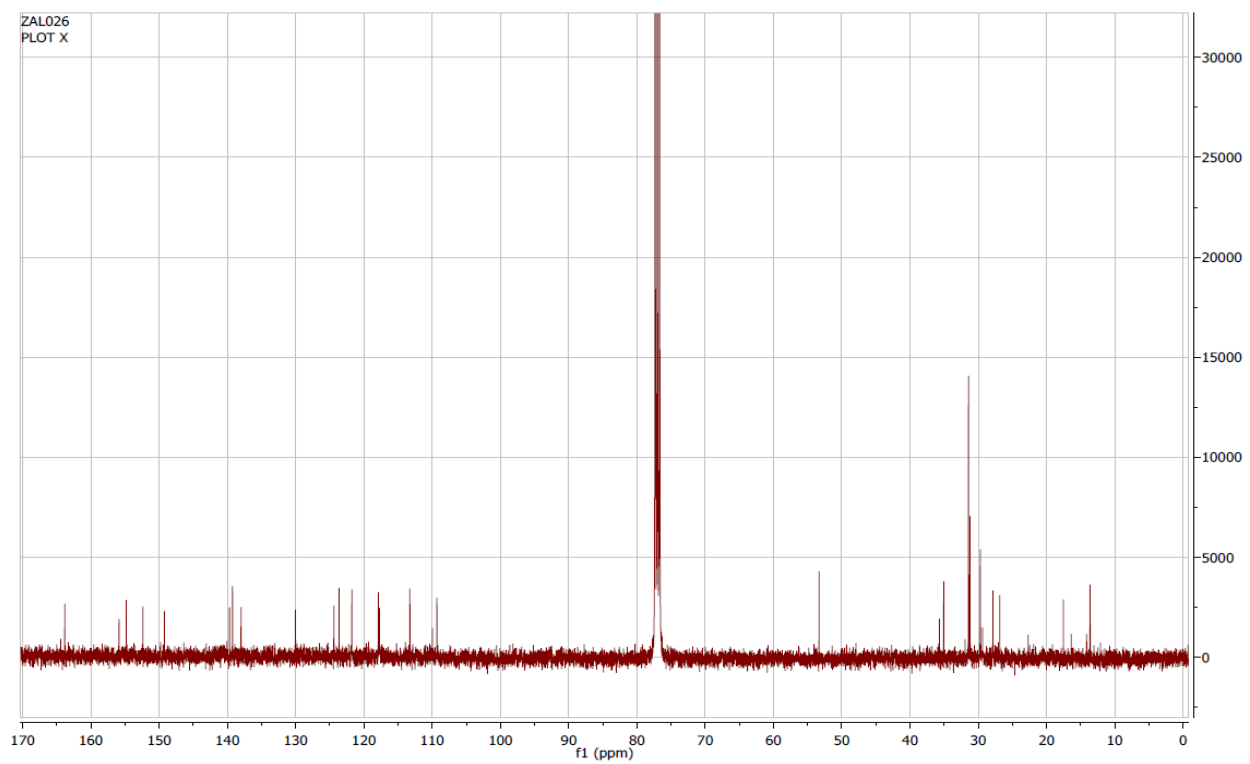
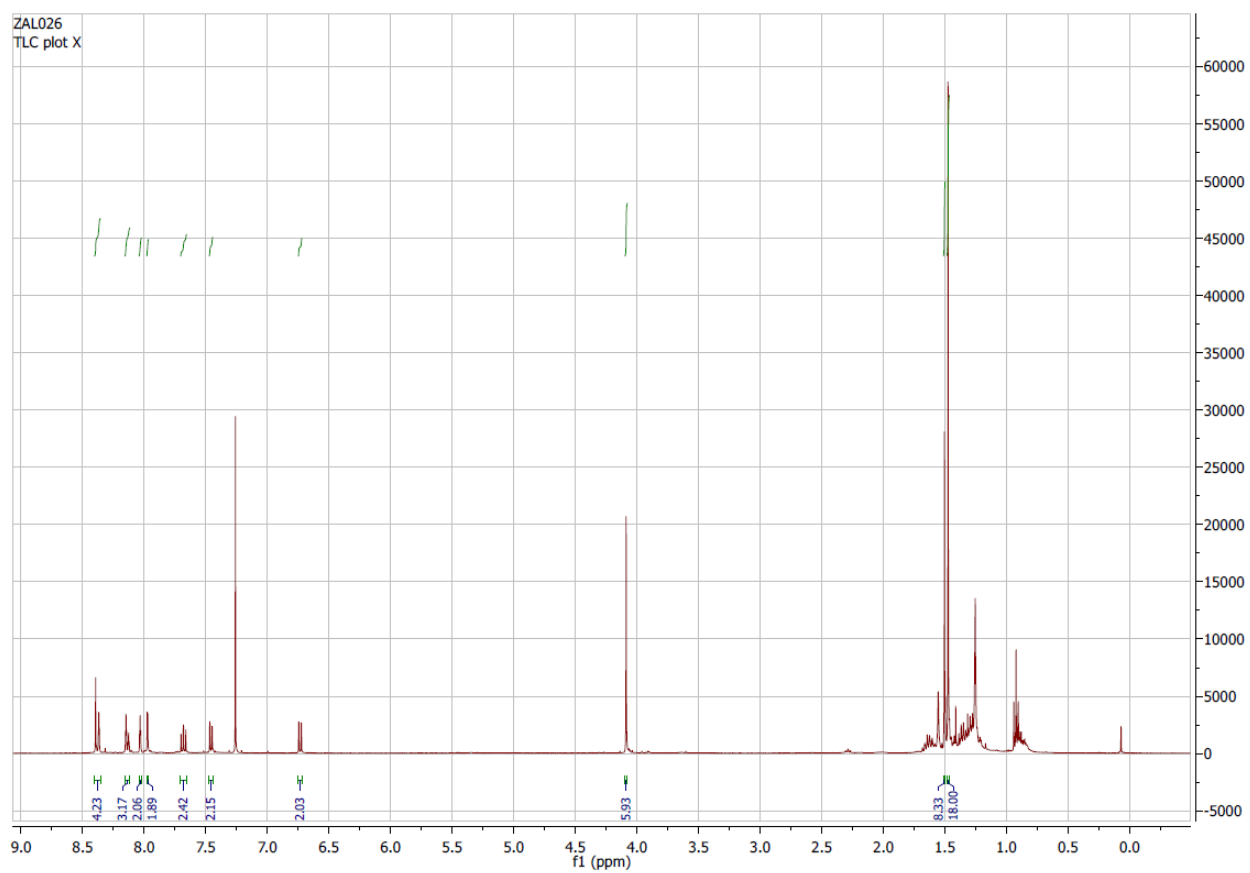
In a very small flask was degassed under high vacuum and back-filled with N<sub>2</sub> three times.

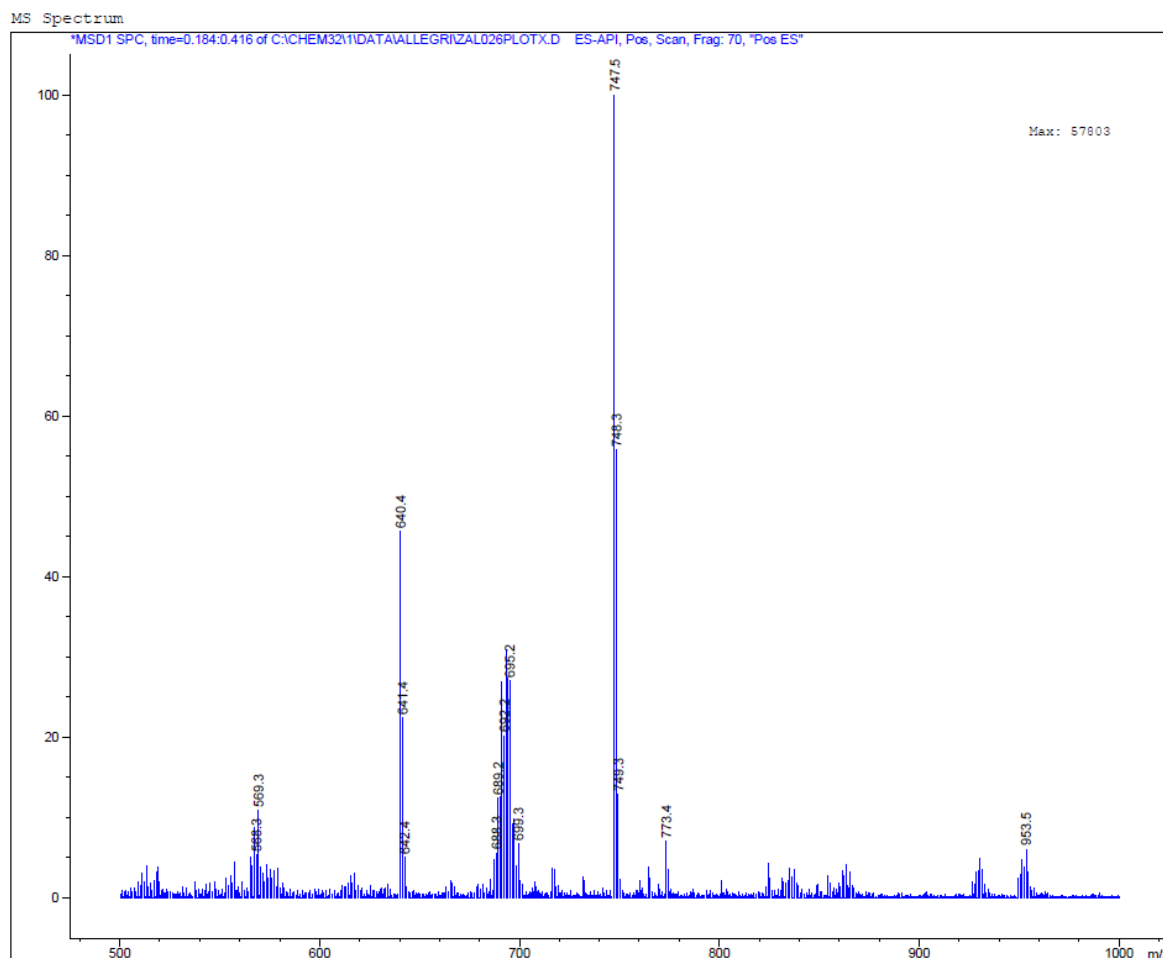
1,1'-(5-(tert-butyl)-1,3-phenylene)bis(4-(3-(tert-butyl)-5-iodophenyl)-1H-1,2,3-triazole) (20 mg, 0.0026 mmol), CsF (15.5 mg, 0.102 mmol), Pd(PPh<sub>3</sub>)<sub>4</sub> (3 mg, 0.0026 mmol) and the 2-methoxy-6-(tributylstannyl)pyridine (22.3 mg, 0.056 mmol) were dissolved in a minimum amount of CH<sub>3</sub>CN (2 ml). The reaction mixture was stirred at 90 °C o.n.. DMF dried was added (1 ml). The reaction was checked by TLC. The volatiles were removed in vacuum and the liquid obtained was filtered through a bed of celite, washed with brine and extracted with CH<sub>2</sub>Cl<sub>2</sub>, dried with MgSO<sub>4</sub> and concentrated under pressure. Purification by preparative TLC 8:2 (Hexane:AcOEt) to afford 7.8 mg of ZAL026 (Y= 52%).

**<sup>1</sup>H NMR (400 MHz, CDCl<sub>3</sub>):** δ 8.40 – 8.36 (m, 4H), 8.14 (dt, J = 8.7, 1.8 Hz, 3H), 8.03 (t, J = 1.7 Hz, 2H), 7.97 (d, J = 1.9 Hz, 2H), 7.71 – 7.65 (m, 2H), 7.47 – 7.44 (m, 2H), 6.74 (d, J = 8.1 Hz, 2H), 4.09 (s, 6H), 1.50 (s, 9H), 1.47 (s, 18H).

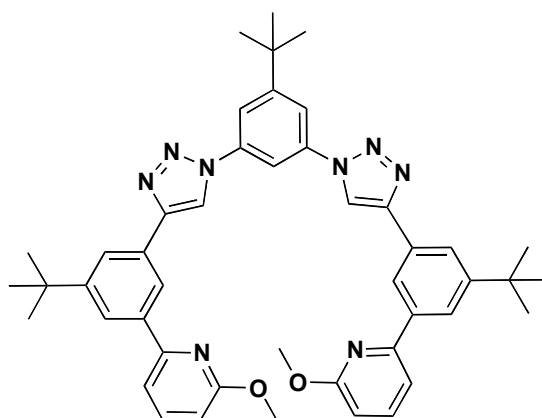
**<sup>13</sup>C NMR (100 MHz, CDCl<sub>3</sub>):** δ 163.83, 155.88, 154.82, 152.39, 149.23, 139.69, 139.25, 138.0, 130.02, 124.40, 123.64, 121.77, 117.88, 117.73, 113.27, 109.31, 53.32, 35.06, 31.43, 31.22, 29.70, 27.85, 26.85, 17.53, 13.61, 13.56.

**MS (ESI):** [M+H]<sup>+</sup> = 746.942





Finally this compound it was tested with EMSA like porphyrin.



#### c-Myc(Pu27) with different concentration of ZAL026

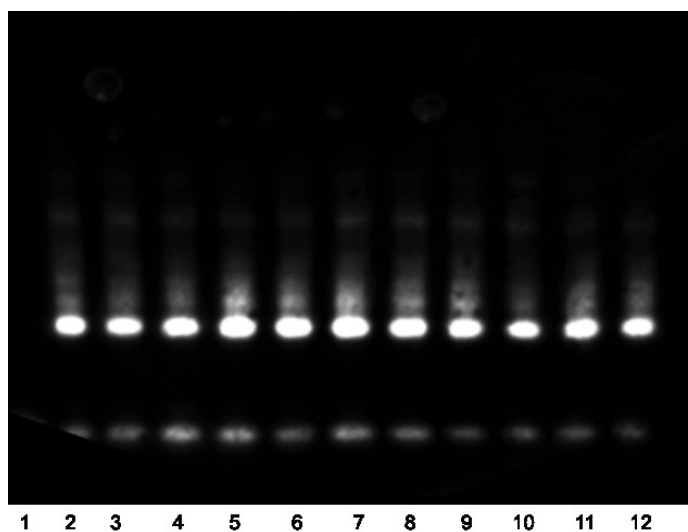


**Figure 40:** The EMSA intramolecular G-quadruplex structures of c-Myc with different concentration of chemical ZAL026. **1:** 1  $\mu$ l  $d_0H_2O$  + 1  $\mu$ l [10  $\eta$ M] c-Myc+ 8  $\mu$ l TE\*; **2:** 1  $\mu$ l  $d_0H_2O$  + 1  $\mu$ l [10  $\eta$ M] c-Myc+ 7  $\mu$ l TE + 1  $\mu$ l KCl; **3:** 1  $\mu$ l [0.001  $\mu$ M] ZAL026 + 1  $\mu$ l [10  $\eta$ M] c-Myc + 7  $\mu$ l TE + 1  $\mu$ l KCl; **4:** 1  $\mu$ l [0.005  $\mu$ M] ZAL026 + 1  $\mu$ l [10  $\eta$ M] c-Myc + 7  $\mu$ l TE + 1  $\mu$ l KCl; **5:** 1  $\mu$ l [0.01  $\mu$ M] ZAL026 + 1  $\mu$ l [10  $\eta$ M] c-Myc + 7  $\mu$ l TE + 1  $\mu$ l KCl; **6:** 1  $\mu$ l [0.05  $\mu$ M] ZAL026 + 1  $\mu$ l [10  $\eta$ M] c-Myc + 7  $\mu$ l TE + 1  $\mu$ l KCl; **7:** 1  $\mu$ l [0.1  $\mu$ M] ZAL026 + 1  $\mu$ l [10  $\eta$ M] c-Myc + 7  $\mu$ l TE + 1  $\mu$ l KCl; **8:** 1  $\mu$ l [0.25  $\mu$ M] ZAL026 + 1  $\mu$ l [10  $\eta$ M] c-Myc + 7  $\mu$ l TE + 1  $\mu$ l KCl; **9:** 1  $\mu$ l [0.5  $\mu$ M] ZAL026 + 1  $\mu$ l [10  $\eta$ M] c-Myc + 7  $\mu$ l TE + 1  $\mu$ l KCl; **10:** 1  $\mu$ l [1  $\mu$ M] ZAL026 + 1  $\mu$ l [10  $\eta$ M] c-Myc + 7  $\mu$ l TE + 1  $\mu$ l KCl; **11:** 1  $\mu$ l [2.5  $\mu$ M] ZAL026 + 1  $\mu$ l [10  $\eta$ M] c-Myc + 7  $\mu$ l TE + 1  $\mu$ l KCl; **12:** 1  $\mu$ l [5  $\mu$ M] ZAL026 + 1  $\mu$ l [10  $\eta$ M] c-Myc + 7  $\mu$ l TE + 1  $\mu$ l KCl  
\*: only heated at 95 degree for 5 minutes



## ILPR-1(1xG4) with different concentration of ZAL026

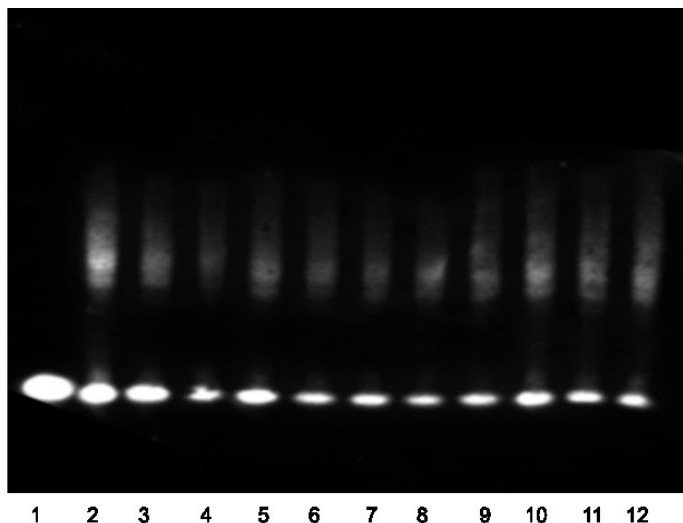


**Figure 41:** The EMSA intramolecular G-quadruplex structures of ILPR-1(1xG4) with different concentration of chemical ZAL026. 1: 1  $\mu$ l  $ddH_2O$  + 1  $\mu$ l [10  $\eta$ M] ILPR-1(1xG4) + 8  $\mu$ l TE\*; 2: 1  $\mu$ l  $ddH_2O$  + 1  $\mu$ l [10  $\eta$ M] ILPR-1(1xG4) + 7  $\mu$ l TE + 1  $\mu$ l KCl; 3: 1  $\mu$ l [0.001  $\mu$ M] ZAL026 + 1  $\mu$ l [10  $\eta$ M] ILPR-1(1xG4) + 7  $\mu$ l TE + 1  $\mu$ l KCl; 4: 1  $\mu$ l [0.005  $\mu$ M] ZAL026 + 1  $\mu$ l [10  $\eta$ M] ILPR-1(1xG4) + 7  $\mu$ l TE + 1  $\mu$ l KCl; 5: 1  $\mu$ l [0.01  $\mu$ M] ZAL026 + 1  $\mu$ l [10  $\eta$ M] ILPR-1(1xG4) + 7  $\mu$ l TE + 1  $\mu$ l KCl; 6: 1  $\mu$ l [0.05  $\mu$ M] ZAL026 + 1  $\mu$ l [10  $\eta$ M] ILPR-1(1xG4) + 7  $\mu$ l TE + 1  $\mu$ l KCl; 7: 1  $\mu$ l [0.1  $\mu$ M] ZAL026 + 1  $\mu$ l [10  $\eta$ M] ILPR-1(1xG4) + 7  $\mu$ l TE + 1  $\mu$ l KCl; 8: 1  $\mu$ l [0.25  $\mu$ M] ZAL026 + 1  $\mu$ l [10  $\eta$ M] ILPR-1(1xG4) + 7  $\mu$ l TE + 1  $\mu$ l KCl; 9: 1  $\mu$ l [0.5  $\mu$ M] ZAL026 + 1  $\mu$ l [10  $\eta$ M] ILPR-1(1xG4) + 7  $\mu$ l TE + 1  $\mu$ l KCl; 10: 1  $\mu$ l [1  $\mu$ M] ZAL026 + 1  $\mu$ l [10  $\eta$ M] ILPR-1(1xG4) + 7  $\mu$ l TE + 1  $\mu$ l KCl; 11: 1  $\mu$ l [2.5  $\mu$ M] ZAL026 + 1  $\mu$ l [10  $\eta$ M] ILPR-1(1xG4) + 7  $\mu$ l TE + 1  $\mu$ l KCl; 12: 1  $\mu$ l [5  $\mu$ M] ZAL026 + 1  $\mu$ l [10  $\eta$ M] ILPR-1(1xG4) + 7  $\mu$ l TE + 1  $\mu$ l KCl  
\*: only heated at 95 degree for 5 minutes

## ILPR-1(2xG4) with different concentration of ZAL026

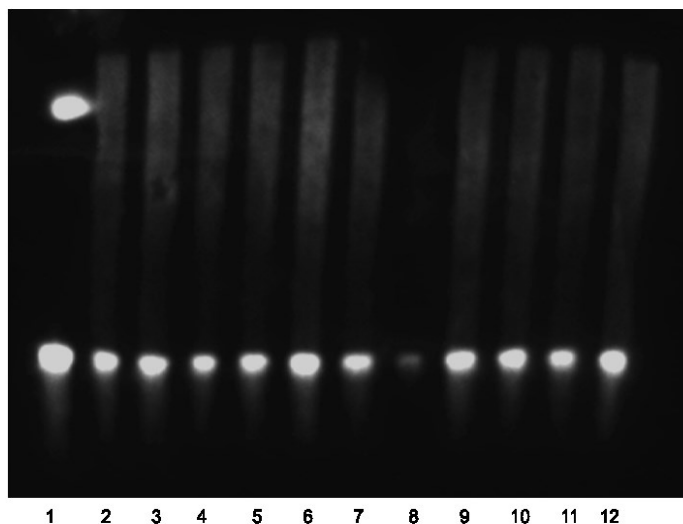


**Figure 42:** The EMSA intramolecular G-quadruplex structures of ILPR-1(2xG4) with different concentration of chemical ZAL026. 1: 1  $\mu$ l  $ddH_2O$  + 1  $\mu$ l [10  $\eta$ M] ILPR-1(2xG4) + 8  $\mu$ l TE\*; 2: 1  $\mu$ l  $ddH_2O$  + 1  $\mu$ l [10  $\eta$ M] ILPR-1(2xG4) + 7  $\mu$ l TE + 1  $\mu$ l KCl; 3: 1  $\mu$ l [0.001  $\mu$ M] ZAL026 + 1  $\mu$ l [10  $\eta$ M] ILPR-1(2xG4) + 7  $\mu$ l TE + 1  $\mu$ l KCl; 4: 1  $\mu$ l [0.005  $\mu$ M] ZAL026 + 1  $\mu$ l [10  $\eta$ M] ILPR-1(2xG4) + 7  $\mu$ l TE + 1  $\mu$ l KCl; 5: 1  $\mu$ l [0.01  $\mu$ M] ZAL026 + 1  $\mu$ l [10  $\eta$ M] ILPR-1(2xG4) + 7  $\mu$ l TE + 1  $\mu$ l KCl; 6: 1  $\mu$ l [0.05  $\mu$ M] ZAL026 + 1  $\mu$ l [10  $\eta$ M] ILPR-1(2xG4) + 7  $\mu$ l TE + 1  $\mu$ l KCl; 7: 1  $\mu$ l [0.1  $\mu$ M] ZAL026 + 1  $\mu$ l [10  $\eta$ M] ILPR-1(2xG4) + 7  $\mu$ l TE + 1  $\mu$ l KCl; 8: 1  $\mu$ l [0.25  $\mu$ M] ZAL026 + 1  $\mu$ l [10  $\eta$ M] ILPR-1(2xG4) + 7  $\mu$ l TE + 1  $\mu$ l KCl; 9: 1  $\mu$ l [0.5  $\mu$ M] ZAL026 + 1  $\mu$ l [10  $\eta$ M] ILPR-1(2xG4) + 7  $\mu$ l TE + 1  $\mu$ l KCl; 10: 1  $\mu$ l [1  $\mu$ M] ZAL026 + 1  $\mu$ l [10  $\eta$ M] ILPR-1(2xG4) + 7  $\mu$ l TE + 1  $\mu$ l KCl; 11: 1  $\mu$ l [2.5  $\mu$ M] ZAL026 + 1  $\mu$ l [10  $\eta$ M] ILPR-1(2xG4) + 7  $\mu$ l TE + 1  $\mu$ l KCl; 12: 1  $\mu$ l [5  $\mu$ M] ZAL026 + 1  $\mu$ l [10  $\eta$ M] ILPR-1(2xG4) + 7  $\mu$ l TE + 1  $\mu$ l KCl  
\*: only heated at 95 degree for 5 minutes

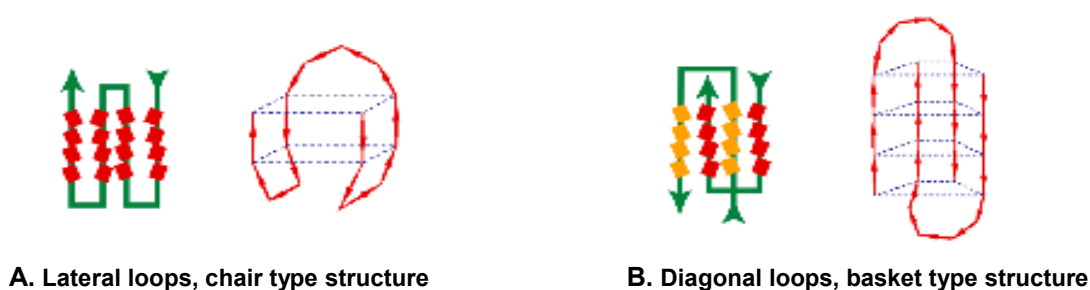
#### 4.6 Circular Dichroism

Circular dichroism (CD) refers to the differential absorption of left and right circularly polarized light. It is exhibited in the absorption bands of optically active chiral molecules. CD spectroscopy has a wide range of applications in many different fields. UV CD is used to investigate the secondary structure of proteins and to monitor the effects of chemical modification on quadruplex structure. The absorbance hypochromicity of quadruplex DNAs is inclined to be much smaller than that associated with duplex DNA<sup>65</sup>.

It seems in some type of DNA oligonucleotide that Na<sup>+</sup> induces an intramolecular basket-type G-quadruplex complex, while in presence of K<sup>+</sup> forms an intramolecular propeller-type G-quadruplex can be formed<sup>59</sup>.

There are four principal conformations of DNA quadruplex (Figure 42).

#### Anti-parallel structures



#### Parallel structures

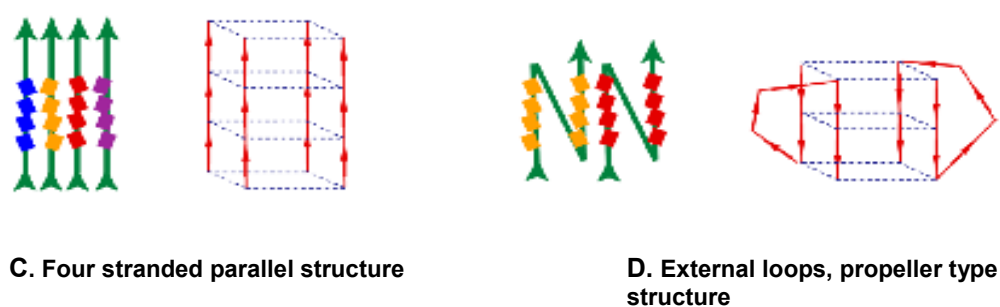


**Figure 43:** Possible structures of G quadruplex.

<sup>65</sup> S. Paramasivan, I. Rujan, P. H. Bolton, *Methods*, (2007), 43, 324-331.

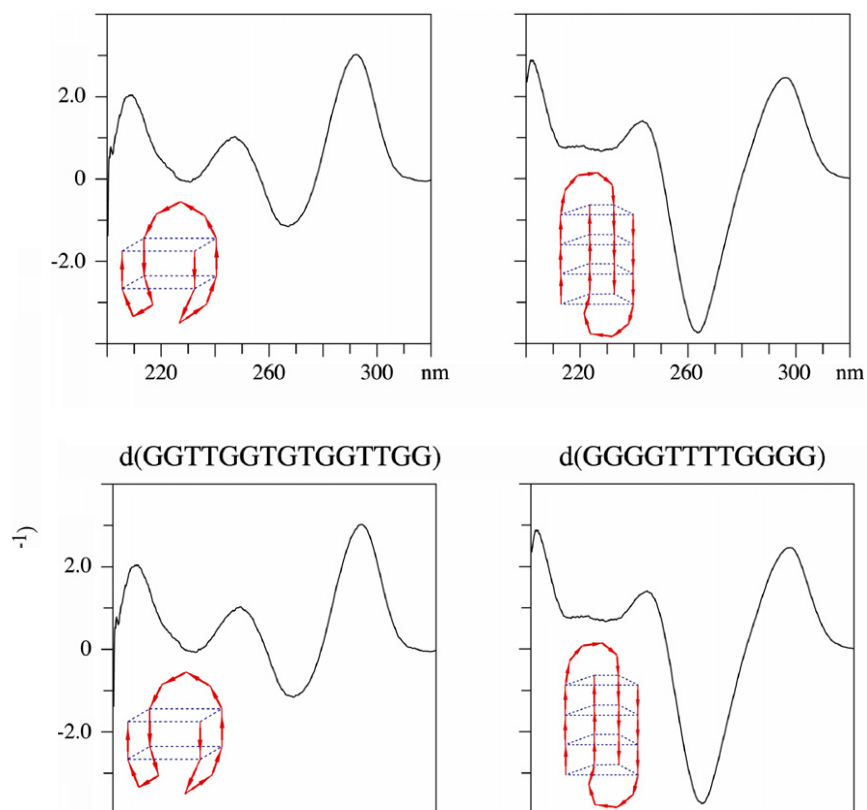


**Figure 44:** CD spectra of the four different types.

Structures	Characteristics wavelength	
	Positive(+)	Negative(-)
<b>A.</b> Lateral loops, chair type structure	210 nm, 240nm, 290nm	260 nm
<b>B.</b> Diagonal loops, basket type structure	210 nm (broad signal), 232nm, 245nm, 290nm	262 nm
<b>C.</b> Four stranded parallel structure	210 nm, 262 nm	240 nm
<b>D.</b> External loops, propeller type structure	260 nm, 290 nm	230 nm

**Table 2:** Wavelengths of different type of structures.

## REFERENCES

1. Pain Management Health Center, WebMD. <http://www.webmd.com/pain-management/>.
2. L. M. Harrison, A. J. Kastin, J. E. Zadina, *Peptides*, **(1998)**, 19, 1603–1630.
3. K. M. Standifer, G. W. Pasternak, *Cell. Signal.*, **(1997)**, 9, 237–248).
4. D. Bagnol, A. Mansour, H. Akil, S. J. Watson, *Neuroscience*, **(1997)**, 81, 579–591.
5. J. B. Wang, P. S. Johnson, Y. Imai, A. M. Persico, B. A. Ozenberger, C. M. Eppler, G. R. Uhl, *FEBS Letters*, **(1994)**, 348, 75-79.
6. J. E. Zadina, L. Hackler, L.-J. Ge, A. J. Kastin, *Nature*, **(1997)**, 386, 499-502.
7. C. W. Stevens, *Front Biosci*, **(2009)**, 14, 1247-1269.
8. J. E. Pope, T. R. Deer, *Expert Opinion on Pharmacotherapy*, **(2013)**, 14, 957-966.
9. D. R. Hillyard, V. D. Monje, I. M. Mintz, B. P. Bean, L. Nadasdi, J. Ramachandran, G. Miljanich, A. Azimi-Zoonooz, J. M. McIntosh, L. J. Cruz, J. S. Imperial, B. M. Olivera, *Neuron*, **(1992)**, 9, 69-77).
10. A. P. Lin, M.-C. Ko, *ACS Chem. Neurosci.*, **(2013)**, 4, 214–224.
11. E. Hu, G. Calò, R. Guerrini, M.-C. Ko, *Pain*, **(2010)**, 148, 107-113.
12. A. S. Yekkirala, A. E. Kalyuzhny, P. S. Portoghese, *ACS Chem. Biol.*, **(2010)**, 8, 1412–1416.
13. V. Casadó, A. Cortés, J. Mallol, K. Pérez-Capote, S. Ferré, C. Lluís, R. Franco, E. I. Canela, *Pharmacology & Therapeutics*, **(2009)**, 124, 248–257.
14. S. Bulenger, S. Marullo, M. BouvierTrends, *Pharmacol. Sci*, **(2005)**, 26, 131–137.
15. R. Rozenfeld, N. S. Abul-Husn, I. Gomez, L. A. Devi, *Sci World J.*, **(2007)**, 7, 64–73.
16. G. Calò, R. Guerrini, A. Rizzi, S. Salvadori, D. Regoli, *British Journal of Pharmacology*, **(2000)**, 129, 1261- 1283.
17. H.-L. Wang, C.-Y. Hsu, P.-C. Huang, Y.-L. Kuo, A. H. Li, T.-H. Yeh, A.-S. Tso, Y.-L. Chen, *Journal of Neurochemistry*, **(2005)**, 92, 1285-1294.
18. R. M. Evans, H. You, S. Hameed, C. Altier, A. Mezghrani, E. Bourinet, G. W. Zamponi, *J. Biol. Chem.*, **(2010)**, 285, 1032-1040.

19. Y. X. Pan, E. Bolan, G. W. Pasternak, *Biochem. Biophys. Res. Commun.*, **(2002)**, 297, 659–663.
20. J. Shonberg, P. J. Scammells, B. Capuano, *Chem. Med. Chem.*, **(2011)**, 6, 963-974.
21. D. P. Nair, M. Podgórski, S. Chatani, T. Gong, W. Xi, C. R. Fenoli, C. N. Bowman, *Chem. Mater.*, **(2014)**, 26, 724–744.
22. A. A. Aimetti, K. R. Feavera, K. S. Anseth, *Chem. Commun.*, **(2010)**, 46, 5781–5783.
23. A. Dondoni, A. Massi, P. Nanni, A. Roda, *Chem. Eur. J.*, **(2009)**, 15, 11444-11449.
24. C. E. Hoyle, C. N. Bowman, *Angew. Chem. Int. Ed.*, **(2010)**, 49, 1540-1573.
25. M. Li, P. De, S. R. Gondi, B. S. Sumerlin, *Polym. Sci., Part A: Polym. Chem.*, **(2008)**, 46, 5093-5100.
26. L. Negri, G. F. Erspamer, C. Severini, R. L. Potenza, P. Melchiorri, V. Erspamer, *Proc. Natl. Acad. Sci. USA*, **(1992)**, 89, 7203-7207.
27. R. Tomatis, M. Marastoni, G. Balboni, R. Guerrini, A. Capasso, L. Sorrentino, V. Santagada, G. Caltendo, L. H. Lazarus, S. Salvadori, *J. Med. Chem.*, **(1997)**, 40, 2948-2952.
28. W. X. Liu, R. Wang, *Med. Res. Rev.*, **(2012)**, 32, 536-580.
29. C.-L. Wang, C. Guo, Y.-Q. Wang, Y. Zhou, Q. Li, J.-M. Ni, R. Wang, *Peptides*, **(2011)**, 32, 293–299
30. C. E. Hoyle, *Polymer Preprints*, **(2008)**, 49, 155-156.
31. M. Kryger, *Chem. 535 Seminar*, **(2008)**.
32. C. Wiles, P. Watts, *Chem. Commun.*, **(2011)**, 47, 6512–6535.
33. N. W. Luedtke, *Chimia*, **(2009)**, 63, 134-139.
34. M. Gellert, M. N. Lipsett, D. R. Davies, *Proc. Natl. Acad. Sci. USA*, **(1962)**, 48, 2013-2018).
35. Y. Qin, L. H. Hurley, *Biochimie*, **(2008)**, 90, 1149-1171.
36. J. Cuesta, M. A. Read, S. Neidle, *Mini Rev. Med. Chem.*, **(2003)**, 3, 11-19.
37. S. Dhakal, J. Schonhoff, D. Koirala, Z. Yu, S. Basu, H. Mao, *J. Am. Chem. Soc.*, **(2010)**, 132, 8991-8997.
38. D. Monchaud, M.-P. Teulade-Fichou, *Org. Biomol. Chem.*, 6, **(2008)**, 627-636.
39. T.-M. Ou, Y.-J. Lu, J.-H. Tan, Z.-S. Huang, K.-Y. Wong, L.-Q. Gu, *ChemMedChem*, **(2008)**, 3, 690-713).

40. H. T. Le, M. C. Miller, R. Buscaglia, W. L. Dean, P. A. Holt, J. B. Chaires, J. O. Trent, *Org. Biomol. Chem.*, **(2012)**, 10, 9393-9404.
41. V. González, L. H. Hurley, *Annu. Rev. Pharmacol. Toxicol.*, **(2010)**, 50, 111-129.
42. A. C. Connor, K. A. Frederick, E. J. Morgan, L. B. McGown, *J. Am. Chem. Soc.*, **(2006)**, 128, 4986-4991.
43. M. C. U. Hammond-Kosack, K. Docherty, *FEBS Letters*, **(1992)**, 301, 79-82.
44. M. C. U. Hammond-Kosack, B. Dobrinski, R. Lurz, K. Docherty, M. W. Kilpatrick, *Nucleic Acids Research*, **(1992)**, 20, 231 -236.
- 45.<sup>1</sup> D. Sun, B. Thompson, B. E. Cathers, M. Salazar, S. M. Kerwin, J. O. Trent, T. C. Jenkins, S. Neidle, L. H. Hurley, *J. Med. Chem.*, **(1997)**, 40, 2113-2116.
46. H. Yaku, T. Murashima, D. Miyoshi, N. Sugimoto, *Chem. Commun.*, **(2010)**, 46, 5740-5742.
47. J. E. Reed, A. A. Arnal, S. Neidle, R. Vilar, *J. Am. Chem. Soc.*, **(2006)**, 128, 5992-5993.
48. G. S. Minhas, D. S. Pilch, J. E. Kerrigan, E. J. LaVoie, J. E. Rice, *Bioorg. Med. Chem. Lett.*, **(2006)**, 16, 3891-3895.
49. K. Guo, A. Pourpak, K. Beetz-Rogers, V. Gokhale, D. Sun, L. H. Hurley, *J. Am. Chem. Soc.*, **(2007)**, 129, 10220-10228.
50. R. T. Wheelhouse, D. Sun, H. Han, F. X. Han, L. H. Hurley, *J. Am. Chem. Soc.*, **(1998)**, 120, 3261-3262.
51. G. Catignani Kennedy, M. S. German, W. J. Rutter, *Nature Genetics*, **(1995)**, 9, 293-298.
52. D.-F. Shi, R. T. Wheelhouse, D. Sun, L. H. Hurley, *J. Med. Chem.*, **(2001)**, 44, 4509-4523.
53. M. A. Shamma, R. J. S. Reis, M. Akiyama, H. Koley, D. Chauhan, T. Hideshima, R.K. Goyal, L. H. Hurley, K. C. Anderson, N. C. Munshi, *Mol. Cancer. Ther.*, **(2003)**, 2, 825-833.
54. J. M. Nicoludis, S. P. Barrett, J.-L. Mergny, L. A. Yatsunyk, *Nucleic Acids Research*, **(2012)**, 40, 5432-5447.
55. T. Li, E. Wang, S. Dong, *Anal. Chem.*, **(2010)**, 82, 7576-758
56. A. D. Moorhouse, A. M. Santos, M. Gunaratnam, M. Moore, S. Neidle, J. E. Moses, *J. Am. Chem. Soc.*, **(2006)**, 128, 15972-15973.

57. PCT/US2005/001875.
58. Y. Li, A. H. Flood, *Angew. Chem.*, **(2008)**, 120, 2689-2692.
59. E. M. Rezler, J. Seenisamy, S. Bashyam, M.-Y. Kim, E. White, W. D. Wilson, L. H. Hurley, *J. Am. Chem. Soc.*, **(2005)**, 127, 9439-9447.
60. N. L. Benoiton, *Chemistry of Peptide Synthesis*. Taylor & Francis, **(2005)**, 125–154.
61. B. W. Bycroft, W. C. Chan, S. R. Chhabra, N. D. Hone, *J. Chem. Soc. Chem. Commun.*, **(1993)**, 778-779.
62. B.R. Conklin, Z. Farfel, K. D. Lustig, D. Julius, H.R. Bourne. *Nature*, **(1993)**, 363, 274-276.
63. L. A. Carpino, G. Y. Han, *J. Org. Chem.*, **(1972)**, 37, 3404-3409.
64. J. M. J. Tronchet, M. Zsély, M. Geoffroy, *Carbohydrate Research*, 275, **(1995)**, 245-258.
65. S. Paramasivan, I. Rujan, P. H. Bolton, *Methods*, **(2007)**, 43, 324-331.

## **PUBLICATION**

*“Racemic synthesis and solid phase peptide synthesis application of the chimeric Valine/Leucine derivative 2-amino-3,3,4-trimethyl-pentanoic acid.”*

M. Pelà, L. Del Zoppo, L. Allegri, E. Marzola, C. Trapella, C. Ruzza, G. Calo', E. Perissutti, F. Frecentese, S. Salvadori, R. Guerrini.

**Pharmazie**, In Press.

## **COMMUNICATION**

Oral communication **XI Day of Chemistry of EMILIA ROMAGNA** Modena 28-10-2011: *“Synthesis of 2-amino-3,3,4-trimethyl-pentanoic: VALINE/LEUCINE chimeric aminoacid.”*

Poster presentation at Congress of Berlin 02/06-09-2012 **EFMC-ISMC 2012 - 22nd International Symposium on Medicinal Chemistry** entitled *“Enantioselective Synthesis of the Non Proteinogenic Aminoacid 2,4 - diamino-3,3-dimethyl butyric acid (DDB) and ITS use in solid phase peptide synthesis.”*

*“Learn from yesterday, live for today, hope for tomorrow. The important thing is not to stop questioning”.*

A. Einsten



